Vehicle Handling Dynamics

Theory and Application

Masato Abe

For information on all Butterworth-Heinemann publications
visit our web site at books.elsevier.com

Working together to grow
libraries in developing countries

www.elsevier.com | www.bookaid.org | www.sabre.org

ELSEVIER   BOOK AID
International   Sabre Foundation

Preface

This book intends to give readers the fundamental theory and some applications of automotive vehicle dynamics. The book is suitable as a text book of vehicle dynamics for Undergraduate and Graduate courses in Automotive Engineering. It is also acceptable as a reference book for researchers and engineers in the field of R&D of vehicle dynamics and control, chassis design and development.

The vehicle motion dealt with in this book is generated by the tire forces, which are produced by the vehicle motion itself. The motion on the ground is possible in any direction by the driver's intention. This is a similar feature to flight dynamics and ship dynamics.

In Chapter 1, the vehicle motion studied in this book is defined. Chapter 2 examines the tire mechanics. The vehicle motion depends on the forces exerted upon tires and this chapter is the base of the book. However, if the reader experiences difficulties in the detailed description of the tire mechanics, they can skip to the next chapter, while still understanding the fundamentals of vehicle dynamics. In Chapter 3, the fundamental theory of vehicle dynamics is dealt with by using a two degree of freedom model. The vehicle motions to external disturbance forces are described using the two degree of freedom model from Chapter 4. This motion is inevitable for a vehicle that can move freely on the ground. In Chapter 5, the effect of the steering system on vehicle motion is studied. The vehicle-body roll effect on the vehicle dynamics is described in Chapter 6. Chapter 7 looks at the effect of the longitudinal motion on the lateral motion of the vehicle and the fundamental vehicle dynamics with active motion controls is described in Chapter 8. The vehicle motion is usually controlled by a human driver. The vehicle motion controlled by the human driver is dealt with in Chapter 9 and relations between the driver's evaluation of handling quality and vehicle dynamic characteristics are described in Chapter 10.

For readers who need only to understand fundamental aspects of vehicle dynamics and human driver, it is possible to skip to Chapter 9 after reading from Chapter 1 to Chapter 4. The readers who like to understand and are interested in more in detail of vehicle dynamics should continue to read through the book from Chapters 5 to 10, depending on their interests.

The original book is written by the author in Japanese and published in Japan. The book was once translated into English by Y. W. Chai when he was a Masters-course student of the author. The author has added new parts such as examples in each chapter and problems at the end of the chapters. W. Manning has revised the whole text for the English version.

The publication process started according to a suggestion by the author's old friend, D. A. Crolla. He has consistently continued to give us useful advice from the beginning to the final stage of the publication.

The author has to confess that without any support of the above mentioned three, the publication is not accomplished. The author would like to express his deep gratitude to their contributions to publishing the book.

The author is indebted as well to J. Ishio, a former master-course student of the author for his assistance in arranging the examples for each chapter. Also a special thank should go to Yokohama Rubber Co., Ltd. for the preparation of some tire data in the chapter 2.

Finally, author thanks the editorial and production staff of Elsevier Science & Technology Books for their efforts for the publication.

<div align="right">

Masato Abe
March 2009

</div>

Symbols

The following symbols are consistently used throughout Chapter 3 to Chapter 10 because they are fundamental symbols for representing the vehicle dynamics and it is rather convenient for the readers to be able to use them consistently. So these symbols are sometimes used without any explanation of the symbols. When it is impossible to avoid using these symbols for other meanings than below, some notice will be given at each part of the chapters where they are used.

m : vehicle mass
I : vehicle yaw moment inertia
l : wheel base
l_f : longitudinal position of front wheel(s) from vehicle center of gravity
l_r : longitudinal position of rear wheel(s) from vehicle center of gravity
K_f : cornering stiffness of front tire
K_r : cornering stiffness of rear tire
V : vehicle speed
δ : front wheel steer angle
β : side slip angle
r : yaw rate
θ : yaw angle
x : vehicle longitudinal direction
y : vehicle lateral direction and lateral displacement
t : time
s : Laplace transform variable

The symbols other than the above adopted in each chapter are defined at the first places where they are used in each chapter.

It should be notified that though, in general, $\ddot{x}$ and $\ddot{y}$ mean the second order time derivative of the variables x and y, they are expediently used in this book for the symbols to represent the vehicle longitudinal and lateral accelerations respectively. In addition, $\delta(s)$, for example, generally means δ as a function of variable, s. However, in this book it represents the Laplace transformation of variable, δ, and this representation is applied to all the variables used throughout this book.

Vehicle Dynamics and Control

1.1 DEFINITION OF THE VEHICLE

Ground vehicles can be divided into two main categories: vehicles that are restricted by a track set on the ground (e.g., the railway vehicles) and vehicles that are unrestricted by tracks, free to move in any direction on the ground by steering the wheels (e.g., road vehicles).

Aircraft are free to fly in the air, while ships can move freely on the water surface. In the same way, the road vehicle is free to move, by steering its wheels, and shares similarities with aircraft and ships, in the sense that its movements are unrestricted.

From the viewpoint of dynamic motion, the similarity lies in the fact that these three moving bodies receive forces generated by their own movement that are used to accomplish the desired movement. Aircraft depend on the lift force caused by the relative motion of its wings and the air; ships rely on the lift force brought by the relative motion of its body and the water; and ground vehicles rely on the wheel lateral force created by the relative motion of the wheels and the road.

In the above described manner, the dynamics and control of the three moving bodies are closely related to their natural function, whereby for an airplane, it is established as flight dynamics, a ship as ship dynamics, and a vehicle, similarly, as vehicle dynamics.

The vehicle studied in this book, is a vehicle, similar to the airplane and ship that is capable of independent motion on the ground, using the forces generated by its own motion.

1.2 VIRTUAL FOUR-WHEEL VEHICLE MODEL

For the study of vehicle dynamics and control, a typical vehicle mathematical model is assumed. This vehicle model has wheels that are steerable: two at the front and two at the rear, which are fitted to a rigid body. Passenger cars, trucks,

buses, and agricultural vehicles all fall into this category… At first sight, it may seem that there are no common dynamics among these vehicles, but by applying a simple four-wheeled vehicle model, as in Fig. 1.1, it is possible to obtain fundamental knowledge of the dynamics of all these vehicles.

In the vehicle mathematical model, which is presented in Fig. 1.1, the wheels are regarded as weightless, and the rigid body represents the total vehicle weight. The coordinate system is fixed to the vehicle, the x-axis in the longitudinal direction, the y-axis in the lateral direction, and the z-axis in the vertical direction, with the origin at the vehicle center of gravity.

With this coordinate system, the vehicle motion has six independent degrees of freedom:

1. vertical motion in z direction,
2. left and right motion in y direction,
3. longitudinal motion in x direction,
4. rolling motion around x-axis,
5. pitching motion around y-axis,
6. yawing motion around z-axis.

These can be divided into two main groups. One group consists of 1, 3, and 5 motions, which are the motions generated without direct relation to the steering. Motion 1 is the vertical motion caused by an uneven ground/road surface and is related to the vehicle ride. Motion 3 is the longitudinal, straight-line motion of the vehicle due to traction and braking during acceleration or braking. Motion 5 is the motion caused by either road unevenness, acceleration or braking and is also related to the vehicle ride.

Motions 2 and 6, the yaw and lateral movements, are generated initially by steering the vehicle. Motion 4 is generated mainly by motions 2 and 6 but could occur due to road unevenness as well.

As described earlier, the vehicle studied in this text can move freely in any direction on the ground, by steering the vehicle. The main behaviors studied here are motions 2, 4, and 6, which are caused by the steering of the vehicle.
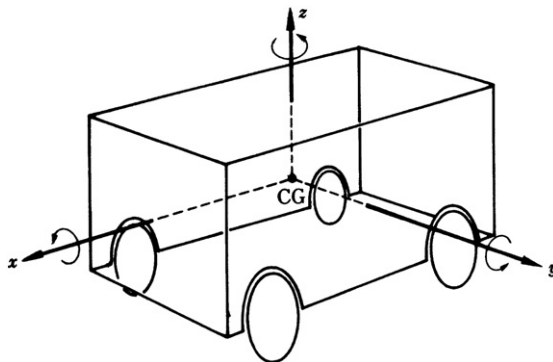
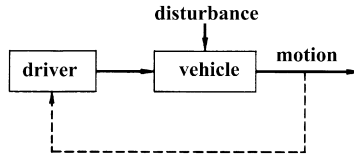

FIGURE 1.1 Vehicle dynamics model.

FIGURE 1.2 Vehicle and driver's control.

Motion 2 is the lateral motion, motion 6 is the yawing motion, and motion 4 is the rolling motion.

1.3 CONTROL OF MOTION

For normal vehicles, motions are controlled by the driver. The lateral, yaw, and roll motions of the vehicle are generated by the driver's steering and depend on its dynamic characteristics. This doesn't mean that the driver is steering the vehicle meaninglessly. The driver is continuously looking at the path in front, either following his target path, or setting a new target path to follow. The driver is observing many things, such as the current position of the vehicle with reference to the target path and the current vehicle motion. The driver is also predicting the imminent vehicle behavior. Based on this information, the driver decides and makes the suitable steer action. In this manner, the vehicle generates its motion in accordance to a target path that is a given or path set by the driver. Figure 1.2 shows the relation of vehicle motion and control in the block diagram.

The vehicle that is capable of free motion within a plane, without direct restrictions from preset tracks on the ground, only produces a meaningful motion when it is acted on by suitable steering control from the driver.

The primary interest now lies on the inherent dynamic characteristics of the vehicle itself. This becomes clear from the motion of the vehicle to a certain steering input. Next is to study this vehicle's characteristics when it is controlled by a human driver. Finally, the aim is to explore the vehicle dynamic characteristics that make it easier for the driver to control the vehicle.

Tire Mechanics

2.1 PREFACE

Chapter 1 discussed how this book deals with the independent motion of the vehicle, in the horizontal plane, without restrictions from a preset track on the ground. The force that makes this motion possible is generated by the relative motion of the vehicle to the ground.

The contact between the vehicle and the ground is at the wheels. If the wheel possesses a velocity component perpendicular to its rotation plane, it will receive a force perpendicular to its traveling direction. In other words, the wheel force that makes the vehicle motion possible is produced by the relative motion of the vehicle to the ground, and is generated at the ground. This is similar to the lift force acting vertically on the wing of a body in flight, and the lift force acting perpendicularly to the direction of movement of a rotating ship (for the ship, this becomes a force in the lateral direction).

The wheels fitted to the object vehicle, not only support the vehicle weight while rotating and produce traction/braking forces, but also play a major role in making the motion independent from the tracks or guide ways. This is the essential function of our vehicle.

In dealing with the dynamics and control of vehicle, it is essential to have knowledge of the forces that act on a wheel. Consequently, this chapter deals mainly with the mechanism for generating the force produced by the relative motion of the wheel to the ground, and explanation of its characteristics.

2.2 TIRE WHICH PRODUCES LATERAL FORCE

2.2.1 Tire and side-slip angle

Generally, when a vehicle is traveling in a straight line, the heading direction of the wheel coincides with the traveling direction. In other words, the wheel traveling direction is inline with the wheel rotational plane. However, when the vehicle has lateral motion and/or yaw motion, the traveling direction can be out of line with the rotational plane.

Figure 2.1 is the wheel looked at from the top, where (a) is when the traveling direction is inline with the rotation plane, and (b) is when it is not. The
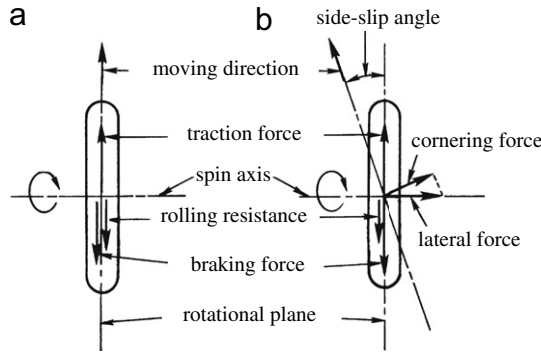
FIGURE 2.1 Vehicle tire in motion.

wheel in (b) is said to have side slip. The angle between the wheel traveling direction and the rotational plane, or its heading direction, is called the side-slip angle.

The wheel is also acted on by a traction force if the wheel is moving the vehicle in the traveling direction, or braking force if braking is applied. Also, a rolling resistance force is always at work. If the wheel has side slip, as in (b), a force that is perpendicular to its rotation plane is generated. This force could be regarded as a reaction force that prevents side slip when the wheel produces a side-slip angle. This is an important force that the vehicle depends on for its independent motion. Normally, this force is called the lateral force, while the component that is perpendicular to the wheel rotation plane, is called the cornering force. When the side-slip angle is small, these two are treated as the same.

This force corresponds to the lift force, explained in fluid dynamics, which acts on a body that travels in a fluid at an attack angle, as shown in Fig. 2.2.

There are many kinds of wheels, but all produce a force perpendicular to the rotation plane, when rotated with side slip. Figure 2.3 shows the schematic comparison of the lateral forces, at small side-slip angles, for a pneumatic tire wheel, a solid rubber-tire wheel, and an iron wheel.

From here, it is clear that the magnitude of the force produced depends on the type of wheel and is very different. In particular, the maximum possible force produced by an iron wheel is less than 1/3rd of that produced by a rubber-tire wheel. Compared to a solid rubber-tire wheel, a pneumatic tire wheel produces a larger force. For independent motion of the vehicle, the force that
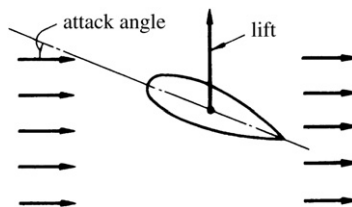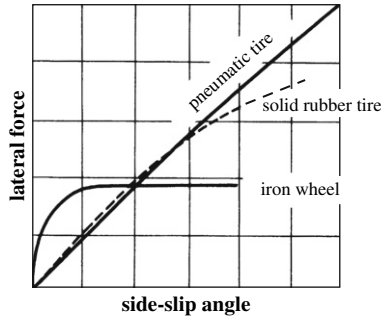

FIGURE 2.2 Lifting force.

FIGURE 2.3 Lateral forces for several wheels.

acts on a wheel with side slip is desired to be as large as possible. For this reason, the traveling vehicle that is free to move in the plane, without external restrictions, is usually fitted with pneumatic tires. These are fitted for both the purpose of vehicle ride, and for achieving a lateral force that is available for vehicle handling.

In the following chapter, the pneumatic tire is called the tire, and the mechanism for generating a lateral force that acts on a tire with side slip is explained.

2.2.2 Deformation of tire with side slip and lateral force

Generally, forces act through the contact surface between the tire and the road. A tire with lateral slip, as shown by Fig. 2.4, is expected to deform in the tire contact surface and its outer circumference: (a) shows the front and side views of the tire deformation; (b) shows the tire contact surface and outer circumference deformation viewed from the top.

At the front of the surface, the deformation direction is almost parallel to the tire's traveling direction. In this part, there is no relative slip to the ground.
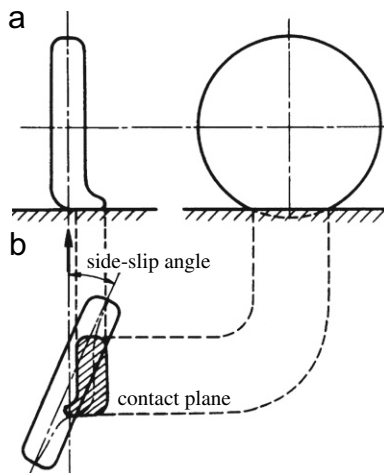

FIGURE 2.4 Tire deflection with side slip.

When the tire slip angle is small, the whole contact surface is similar to this and the rear end of the contact surface has the largest lateral deformation.

When the tire slip angle gets bigger, the front of the surface remains almost parallel to the tire traveling direction. The deformation reduces near the center of the contact patch, and the lateral deformation becomes largest at certain point between the front and rear of the surface. After this maximum, the tire contact surface slips away from the tire centerline and the lateral deformation does not increase.

As tire slip angle gets even larger, the point where lateral deformation becomes maximum moves rapidly toward the front. When the slip angle is around 10–12°, the contact surface that is parallel to the tire travel direction disappears. The contact surface deformation is nearly symmetric around the wheel center and consists of nearly all the slip regions.

The lateral deformation of the tire causes a lateral force to act through the contact surface, which is distributed according to the deformation. This lateral force is sometimes called the cornering force when the side-slip angle is small. By looking at the tire lateral deformation, the resultant lateral force may not be aligned with center of the contact surface. Thus, the lateral force creates a moment around the tire contact surface center. This moment is called the self-aligning torque and acts in the direction that reduces the tire slip angle.

2.2.3 Tire camber and lateral force

As shown in Fig. 2.5, the angle between the tire rotation plane and the vertical axis is called the camber angle. If a tire with a camber angle of ϕ is rotated freely on a horizontal plane, as shown in Fig. 2.5, the tire makes a circle with the radius of $R/\sin\phi$ and origin at O. If the circular motion is prohibited for a tire with camber angle, and the tire is forced to travel in a straight line only, a force will
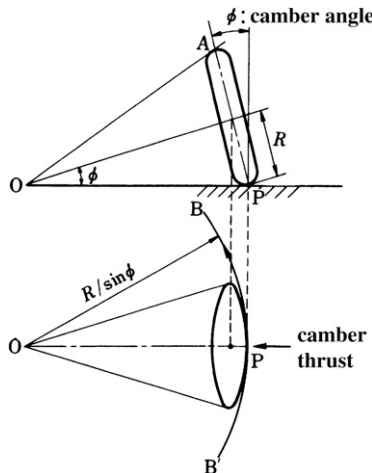

FIGURE 2.5 Tire with camber angle and camber thrust.

act on the tire as shown in the figure. This force, due to the camber between the tire and the ground, is called camber thrust.

2.3 TIRE CORNERING CHARACTERISTICS

The characteristics of the tire that produce lateral force and moment, as elaborated in Section 2.2, are defined as the **cornering characteristics**. In this section, the tire cornering characteristics will be examined in more detail.

2.3.1 Fiala's theory

The mathematical model proposed by Fiala [1] is widely accepted for the above analysis of the lateral force due to side slip of the tire. It is commonly called Fiala's theory and is related to the tire cornering characteristics. It is one of the fundamental theories used by many people for explaining tire cornering characteristics [2].

Here, based on Fiala's theory, the tire cornering characteristics will be studied theoretically. The tire structure is modeled as in Fig. 2.6. A is a stiff body equivalent to the rim. B is the pneumatic tube and sidewall that can deform elastically in both vertical and lateral directions. C is the equivalent thin tread base joined to the sidewall at both sides. D is equivalent to the tread rubber. The tread rubber is not a continuous circular body, but consists of large numbers of independent spring bodies around the tire circumference.

When a force acts in the lateral direction at the ground contact surface, the tire will deform in the lateral direction. The rim is stiff and it will not be deformed, but the tread base will have a bending deformation in the lateral direction. Moreover, the tread rubber will be deformed by the shear force between the tread base and ground surface. Figure 2.7 shows this kind of deformation in the lateral direction.

Assuming that the tread base deforms equally at the front and rear ends of the ground contact surface, the line that connects these points is the centerline for the tread base and is defined as the *x*-axis. The *y*-axis is perpendicular to the *x*-axis and positioned at the front end point. The *x*-axis is parallel to the tire rim centerline and also the tread base centerline before deformation. In these axes,
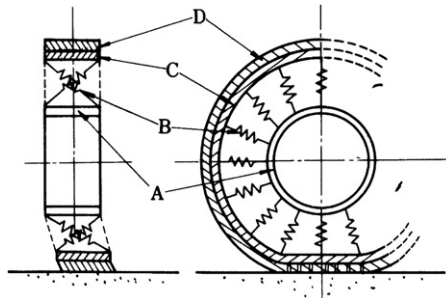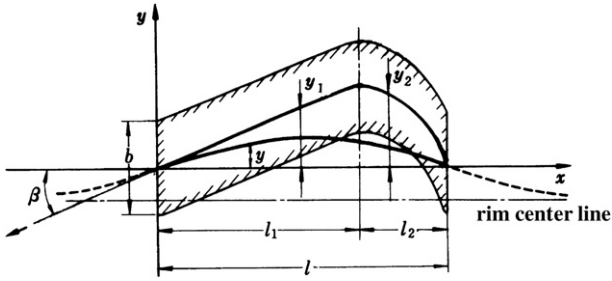

FIGURE 2.6 Tire structural model.

FIGURE 2.7 Tire deflection model.

the distance along the x-axis from the contact surface front end point is x, and the lateral displacement from the x-axis is y. y_1 is the lateral displacement from the x-axis for $0 \leq x \leq l_1$, and y_2 is the lateral displacement from the x-axis for $l_1 < x \leq l$. In the region $0 \leq x \leq l_1$, as described in subsection 2.2.2, there is no relative slip between the tire and the ground. The region $l_1 < x \leq l$ is where relative slip is produced. β is the side-slip angle of the tire, l is the contact surface length, and b is the contact surface width.

First we will consider the lateral deformation, y, of the tread base. If the tread base is extended along the tire circumference, it will look like Fig. 2.8. This is a beam with infinite length on top of a spring support that is built up by numerous springs, as B in Fig. 2.6.

The deformation of this beam is considered by taking the lateral force acting on the tire as F, the rim centerline as the x-axis and the y-axis passing through the tire center, perpendicular to the x-axis. If the force acts solely on the y-axis (i.e., $x = 0$) the equation below is obtained.

$$EI \frac{d^4 y}{dx^4} + ky = w(x) \tag{2.1}$$

Whereby if $x \neq 0$, then $w(x) = 0$, and if $x = 0$, then $w(x) = F$. E is the Young's modulus of the tread material, I is the moment of inertia of area of the tread base, and k is the spring constant per unit length of the spring
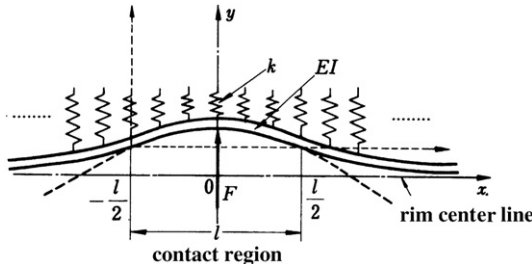

FIGURE 2.8 Tire rim deflection model.

support. Solving the above equation, the lateral displacement, y, is given by the following equation as a general solution.

$$y = \frac{\alpha F}{2k} e^{-ax}[\cos ax + \sin ax] \tag{2.2}$$

$$\alpha = \frac{1}{\sqrt{2}}\left(\frac{k}{EI}\right)^{\frac{1}{4}} \tag{2.3}$$

The tread base displacement within the ground contact region is assumed to be y at $|ax| \ll 1$. Assuming $\cos ax \approx 1$, $\sin ax \approx ax$, then y can be approximated to a second order equation of x.

$$y = \frac{\alpha F}{2k}(1 - \alpha^2 x^2) \tag{2.4}$$

Furthermore, expressing y with a transferred coordinate system such that $y = 0$ at $x = 0$ and $x = l$:

$$y = \frac{\alpha^3 l^2 F}{2k} \frac{x}{l}\left(1 - \frac{x}{l}\right) \tag{2.5}$$

This equation expresses the lateral displacement, y, of the tread base in Fig. 2.7. Next, the lateral displacements, y_1 and y_2, from the ground contact surface centerline are looked at. For the region $0 \leq x \leq l_1$, there is no relative slip between the tire and the ground. The contact surface deforms relatively in the opposite direction to the tire lateral traveling direction. The lateral displacement, y_1, for each point on the contact surface along the longitudinal direction can be written as:

$$y_1 = \tan \beta x \tag{2.6}$$

The tread base displacement is given by Eqn (2.5) and the tread rubber displacement by Eqn (2.6). As shown in Fig. 2.9, a shear strain of $(y_1 - y)/d$ occurs between the tread rubber and the tread base. A force per unit length in the lateral direction acts upon each point on the contact surface along the longitudinal direction.

$$f_1 = K_0(y_1 - y) = K_0\left[\tan \beta x - \frac{\alpha^3 l^2 F}{2k} \frac{x}{l}\left(1 - \frac{x}{l}\right)\right] \tag{2.7}$$
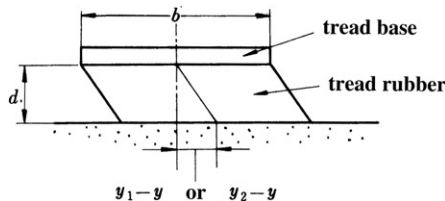

FIGURE 2.9 Shear deformation of tread rubber.

$$K_0 = G\frac{b}{d} = \frac{E}{2(1+v)}\frac{b}{d} \tag{2.8}$$

G is the shear modulus of the tread and v is the Poisson ratio.

As seen in Fig. 2.7, y_1-y becomes larger toward the rear end of the contact surface. If f_1 exceeds the friction force between the tread rubber and the ground, a relative slip will be produced between them. The slip region is denoted by $l_1 < x \le l$, and the shear strain of the tread rubber is $(y_2-y)/d$. The force that produces this strain, f_2, is the friction force between the tread rubber and the ground. For simplicity the tire load is taken as W, and the contact surface pressure distribution, p, along the x-direction is approximated by a second order equation with the peak pressure at the tire center, as in Fig. 2.10.

$$p = 4p_\mathrm{m}\frac{x}{l}\left(1 - \frac{x}{l}\right) \tag{2.9}$$

$$p_\mathrm{m} = \frac{3W}{2bl} \tag{2.10}$$

then f_2 becomes

$$f_2 = K_0(y_2 - y) = \mu pb = 4\mu p_\mathrm{m} b\frac{x}{l}\left(1 - \frac{x}{l}\right) \tag{2.11}$$

where μ is the friction coefficient between the tread rubber and the ground. l_1 is the value of x that satisfies $f_1 = f_2$

$$K_0\left[\tan \beta x - \frac{\alpha^3 l^2 F}{2k}\frac{x}{l}\left(1 - \frac{x}{l}\right)\right] = 4\mu p_\mathrm{m} b\frac{x}{l}\left(1 - \frac{x}{l}\right) \tag{2.12}$$
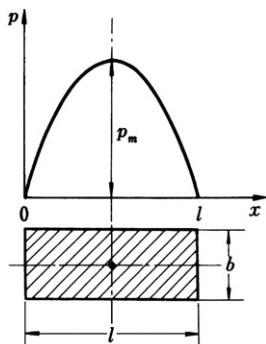

FIGURE 2.10 A contact pressure distribution.

thus, l_1 is given by solving this equation by x,

$$l_1 = l - \frac{K_0 l^2 \tan \beta}{\frac{K_0 \alpha^3 l^2}{2k} F + 4\mu p_m b} \tag{2.13}$$

The lateral force that acts on each point on the contact surface along the longitudinal direction, for a small increment of dx, is $f_1 dx$ for $0 \leq x \leq l_1$, and $f_2 dx$ for $l_1 < x \leq l$. The total force acting on the whole contact surface, which is the lateral force, F, is given by the following equation:

$$F = \int_0^{l_1} f_1 \, dx + \int_{l_1}^l f_2 \, dx = K_0 \int_0^{l_1} \left[\tan \beta x - \frac{\alpha^3 l^2 F}{2k} \frac{x}{l} \left(1 - \frac{x}{l} \right) \right] dx$$

$$+ \int_{l_1}^l 4\mu p_m b \frac{x}{l} \left(1 - \frac{x}{l} \right) dx \tag{2.14}$$

Substituting Eqn (2.13) into Eqn (2.14), and integrating it, results in F on both sides. This makes the equation complicated to solve. Fiala, thus, had approximated F in the following way.

$$F = \frac{K_1 l^2}{2} \tan \beta - \frac{1}{8} \frac{K_1^2 l^3}{\mu p_m b} \tan^2 \beta + \frac{1}{96} \frac{K_1^3 l^4}{\mu^2 p_m^2 b^2} \tan^3 \beta \tag{2.15}$$

$$K_1 = \frac{K_0}{1 + \frac{\alpha^3 l^3}{12k} K_0} \tag{2.16}$$

This is the fundamental method for expressing the relationship between the tire side-slip angle and the lateral force.

Figure 2.7 shows that the lateral force acting on the contact surface isn't symmetric across the contact surface center. This causes the lateral force to generate a moment around the vertical axis that passes through to contact surface center. This moment is the self-aligning torque. For a small increment of dx at each point on the contact surface, $(x-l/2)f_1 dx$ for $0 \leq x \leq l_1$, and $(x-l/2)f_2 dx$ for $l_1 < x \leq l$, it is

$$M = \int_0^{l_1} \left(x - \frac{l}{2} \right) f_1 \, dx + \int_{l_1}^l \left(x - \frac{l}{2} \right) f_2 \, dx$$

$$= K_0 \int_0^{l_1} \left(x - \frac{l}{2} \right) \left[\tan \beta x - \frac{\alpha^3 l^2 F}{2k} \frac{x}{l} \left(1 - \frac{x}{l} \right) \right] dx$$

$$+ \int_{l_1}^l \left(x - \frac{l}{2} \right) 4\mu p_m b \frac{x}{l} \left(1 - \frac{x}{l} \right) dx \tag{2.17}$$

Substituting Eqn (2.13) for l_1 into Eqn (2.17) gives an equation that is too complicated. Using the approximated equation of F as in Eqn (2.15), Fiala approximated M as below.

$$M = \frac{K_1 l^3}{12} \tan \beta - \frac{1}{16} \frac{K_1^2 l^4}{\mu p_{\mathrm{m}} b} \tan^2 \beta + \frac{1}{64} \frac{K_1^3 l^5}{\mu^2 p_{\mathrm{m}}^2 b^2} \tan^3 \beta$$
$$- \frac{1}{768} \frac{K_1^4 l^6}{\mu^3 p_{\mathrm{m}}^3 b^3} \tan^4 \beta \qquad (2.18)$$

This is the fundamental equation that expresses the relation between the tire side-slip angle and the self-aligning torque.

The lateral force per unit side-slip angle, when β is small, is called the cornering stiffness and is given by

$$K = \left(\frac{\mathrm{d}F}{\mathrm{d}\beta}\right)_{\beta = 0} = \frac{K_1 l^2}{2} \qquad (2.19)$$

The tire maximum friction force is found from Eqn (2.10)

$$\mu W = \frac{2}{3}\mu p_{\mathrm{m}} b l \qquad (2.20)$$

Defining ψ as

$$\psi = \frac{K}{\mu W} \tan \beta = \frac{3K_1 l}{4\mu p_{\mathrm{m}} b} \tan \beta \qquad (2.21)$$

Eqns (2.15) and (2.18) can be written as below.

$$\frac{F}{\mu W} = \psi - \frac{1}{3}\psi^2 + \frac{1}{27}\psi^3 \qquad (2.22)$$

$$\frac{M}{\mu W} = \frac{1}{6}\psi - \frac{1}{6}\psi^2 + \frac{1}{18}\psi^3 - \frac{1}{162}\psi^4 \qquad (2.23)$$

Differentiating Eqns (2.22) and (2.23) with respect to ψ, and putting them equal to 0, gives maximum $F/(\mu W)$ at $\psi = 3$, where $F/(\mu W) = 1$. $M/(\mu W)$ becomes largest at $\psi = 3/4$, where it is 27/512.

In other words, the lateral force, F, is largest when the side-slip angle is

$$\tan \beta = \frac{3\mu W}{K} \qquad (2.24)$$

and its maximum value, F_{max} is

$$F_{\mathrm{max}} = \mu W \qquad (2.25)$$

while the self-aligning torque is largest at a side-slip angle of

$$\tan \beta = \frac{3 \mu W}{4K} \tag{2.26}$$

and its maximum value, $M_{\max}$ is

$$M_{\max} = \frac{27}{512} l \mu W \tag{2.27}$$

Using Eqs (2.22) and (2.23), a dimensionless term of $F/(\mu W)$ for the lateral force and $M/(l\mu W)$ for the self-aligning torque can be derived in terms of the side-slip angle, $\psi = K \tan \beta/(\mu W)$ and are plotted in Figs 2.11 and 2.12.

As seen in Fig. 2.11, the lateral force, F, is almost proportional to $\tan \beta$ when the side-slip angle is small. After a certain value of β, the lateral force reaches saturation and doesn't increase further with increasing side-slip angle. From Fig. 2.12, the self-aligning torque is almost proportional to $\tan \beta$ when the side-slip angle is small. As β increases beyond a certain point, the self-aligning torque reaches saturation abruptly and decreases with the increase of side-slip angle. When β is small, $\tan \beta \approx \beta$, the lateral force and self-aligning torque can be treated as proportional to β. When β is large, the lateral force is no longer proportional to β, and has non-linear characteristics.

In the region where the side-slip angle is small, $\tan \beta \approx \beta$, terms with more than second orders of β can be ignored. The lateral force and self-aligning torque, in relation to β, are given by Eqns (2.15) and (2.18) as:

$$F \approx \frac{K_1 l^2}{2} \beta = K\beta \tag{2.28}$$

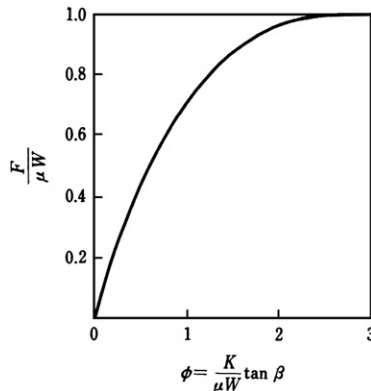$$M \approx \frac{K_1 l^3}{12} \beta = \xi_n K\beta \tag{2.29}$$

FIGURE 2.11 Lateral force to side-slip angle.
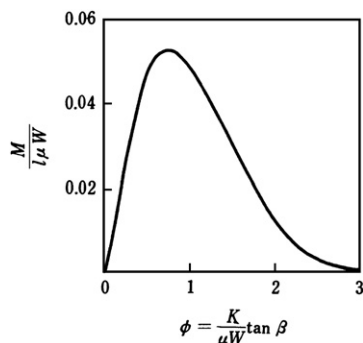
$$\phi = \frac{K}{\mu W}\tan \beta$$

FIGURE 2.12 Self-aligning torque to side-slip angle.

Here, K is generally the so-called cornering stiffness, which is given by Eqn (2.19). From Eqns (2.8) and (2.16), the cornering stiffness could be written as below.

$$K = \frac{\frac{l^2}{2}\frac{b}{d}G}{1 + \frac{\alpha^3 l^3}{12k}\frac{b}{d}G} \tag{2.30}$$

The distance of the acting point of the cornering force from the contact surface center, which is called the pneumatic trail, as shown by Fig. 2.13, is defined as below.

$$\xi_n = M/F \tag{2.31}$$

Based on Eqns (2.28) and (2.29), this value is $l/6$ when the value of β is small.

Until now, the force acting on a tire with side-slip angle has been examined. Following this, the force acting on a tire traveling on a straight line with a camber angle will be studied. This force is called the camber thrust. Fiala analyzed the tire with camber angle as below.

When tire camber is taken into consideration, as shown in Fig. 2.14, even without any side-slip angle, the tread base centerline isn't a straight line, but becomes a part of the arc.

When referred to the same coordinate system as in Fig. 2.7, and approximated to a parabolic, this part of the arc will become
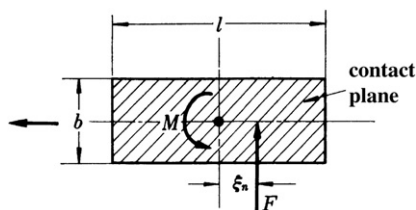

FIGURE 2.13 Pneumatic trail.
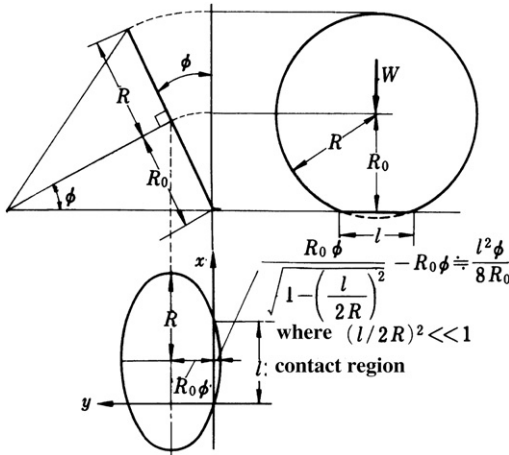
FIGURE 2.14 Tire tread base center with camber.

$$y_c = -\frac{l^2\phi}{2R_0}\frac{x}{l}\left(x - \frac{x}{l}\right) \tag{2.32}$$

where R_0 is the effective tread base radius, given by the equation below.

$$R_0 = R - \frac{W}{k_e} \tag{2.33}$$

R is the tread base radius at zero tire load, and k_e is the longitudinal spring constant of the tire.

This condition is shown in Fig. 2.15. If the tire moves freely, while having a camber angle, the contact surface center will follow the circular track as shown in Fig. 2.5. However, if the tire is to travel in a straight line only, the contact surface center should follow along the x-axis. Therefore, a shear strain between the tread base and the ground is produced at the tread rubber, and a lateral force, corresponding to this displacement acts at the contact surface.

This resultant force is the camber thrust, F_c. Assuming that the acting point of this force is concentrated to the contact surface center, the displacement of the tread base by this force is

$$y = \frac{\alpha^3 l^2 F_c}{2k}\frac{x}{l}\left(1 - \frac{x}{l}\right) \tag{2.34}$$

FIGURE 2.15 Tire deflection with camber.

Since the displacement from the x-axis at the contact surface is 0, the shear strain of the tread rubber at each point along the x-direction is $-(y_c + y)$. Therefore, the camber thrust that acts on the tire, F_c is
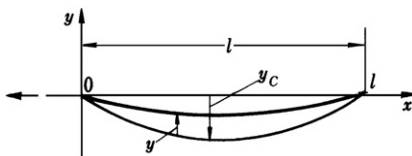
$$F_c = \int_0^l -K_0(y_c + y)dx = K_0\left[\frac{l^2\phi}{2R_0} - \frac{\alpha_3 l_2 F_c}{2k}\right]\int_0^l \frac{x}{l}\left(1 - \frac{x}{l}\right)dx \quad (2.35)$$

Integrating this equation to find F_c gives

$$F_c = \left(\frac{K_0}{1 + \frac{\alpha^3 l^3}{12k}K_0}\right)\frac{l_3}{12R_0}\phi = \frac{K_1 l^3}{12R_0}\phi \quad (2.36)$$

Equation (2.36) shows that the camber thrust is proportional to the camber angle. The proportional constant, K_c, is called the camber thrust coefficient, and by substituting Eqn (2.8), can be expressed as

$$K_c = \frac{K_1 l^3}{12R_0} = \left(\frac{\frac{l^2}{2}\frac{b}{d}G}{1 + \frac{\alpha^3 l^3}{12k}\frac{b}{d}G}\right)\frac{l}{6R_0} = \frac{l}{6R_0}K \quad (2.37)$$

From the above mathematical model and theoretical discussions, the characteristics of the lateral force and moment acting on the tire can be found. This means that the tire cornering characteristics are affected by E, v, I, b, d, k, l, μ, and W.

E and v are dependant on the tread material and construction; I, b, and d are decided by the tire shape; W is the tire vertical load; k is mainly dependant on the air pressure, and can be taken as proportional to air pressure; l is mainly decided by the tire shape, but also depends on the tire vertical load and tire air pressure; lastly, μ is dependant on the tread material and ground/road condition.

Consequently, the tire cornering characteristics are mainly affected by:

1. tire material, construction, and shape,
2. tire vertical load,
3. tire air pressure, and
4. ground/road condition.

The theoretical calculation of the influence of 1–4 on the various tire parameters/properties as summarized above is not easy. Neither is it straightforward to measure these effects experimentally. In contrast, the measurement of the lateral force and moment on the tire with side-slip angle or camber angle is relatively simple. Hence, it is common for the effects of 1–4 on tire cornering characteristics to be verified through direct experimental results.

Example 2.1

Estimate the tire side-slip angle at which the lateral force is saturated by considering the tire lateral deformation mechanism due to lateral force. Confirm that the side-slip angle estimated coincides with Eqn (2.24).

Solution
The lateral force at the saturation point is equal to μW, where μ is a friction coefficient between tire and road surface and W is a vertical load of the tire. Referring to Eqn (2.5), the lateral displacement of the tire tread base due to this force is expressed as

$$y = \frac{\alpha^3 l^2 \mu W}{2k} \frac{x}{l}\left(1 - \frac{x}{l}\right) \tag{E2.1}$$

At the saturation point, the lateral force distribution along the contact patch of the tire is equal to the multiplication of the vertical load distribution and the friction coefficient, μ:

$$\mu p = 4\mu p_m \frac{x}{l}\left(1 - \frac{x}{l}\right) \tag{E2.2}$$

As shown in Fig. E2.1, the shearing deformation of the tread rubber is expressed by $y' - y$, where y' is the lateral deformation of the contact patch of the tire, and the following relation is obtained

$$\mu p b = K_0(y' - y) \tag{E2.3}$$

From the three equations above, y' is obtained as

$$y' = \left(\frac{\alpha^3 l^2 F}{2k} + \frac{4\mu p_m b}{K_0}\right)\frac{x}{l}\left(1 - \frac{x}{l}\right) \tag{E2.4}$$
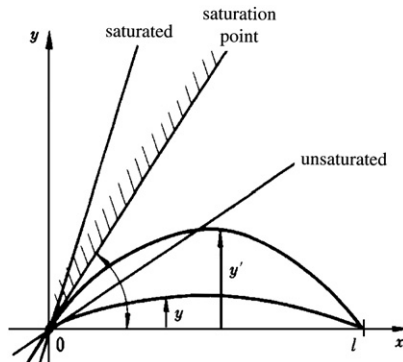

FIGURE E2.1.

This is a maximum lateral deformation of the each point of the tire contact patch. The tangential direction of y', dy'/dx, at $x = 0$ corresponds to the maximum side-slip angle at which the lateral force reaches the maximum value. Thus, the side-slip angle is described as

$$\tan \beta = \left(\frac{dy'}{dx}\right)_{x=0} = \left(\frac{\alpha^3 l^2 F}{2k} + \frac{4\mu p_m b}{K_0}\right)\frac{1}{l} \qquad \text{(E2.5)}$$

Using Eqns (2.8), (2.10), (2.16), and (2.19), the above equation is transformed to the same form as Eqn (2.24):

$$\tan \beta = \frac{3\mu W}{K}$$

2.3.2 Lateral force

In this section, the tire cornering characteristics verified experimentally so far, under given tire materials and constructions will be investigated and the lateral force and moment characteristics will be understood in more detail.

(1) COMMON CHARACTERISTICS

As expected from the mathematical model, the relation between the lateral force and the side-slip angle is almost a straight line when the side-slip angle is small. After the side-slip angle exceeds a certain value, the lateral force increases at a slower rate and finally saturates at $\tan \beta = 3\mu W/K$. Figure 2.16 is a typical example of the relation between cornering force and side-slip angle of the tire for passenger cars.

In this example, when β is less than around 4°, the lateral force increases in a straight line. Its increment becomes less and less after this value and finally saturates at around 8–10°. However, for a normal passenger car, its lateral motion usually occurs within the linear region. The slope of this line is the tire
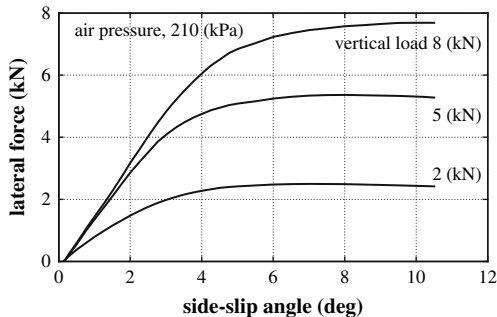

FIGURE 2.16 Tire lateral force to side-slip angle.

cornering stiffness, given by Eqn (2.30), and corresponds to the lateral force of the tire per unit side-slip angle. This is an important value in the evaluation of the tire cornering characteristics.

(2) EFFECTS OF VERTICAL LOAD AND ROAD CONDITION

The effect of tire vertical load on lateral force is also shown in Fig. 2.16. The tire vertical load has almost no effect on lateral force at very small side-slip angles. The different saturation levels of lateral force become more obvious with larger side-slip angles. The mathematical model shows that the tire load only affects lateral force in the region where there is relative slip between the tread rubber and the ground. When this region occupies the majority of the contact surface, i.e., side-slip angle is large, the lateral force approaches the product of μ and W, and so, the effect of W is remarkable. Figure 2.17 is an example that shows the effect of the tire vertical load effect on lateral force.
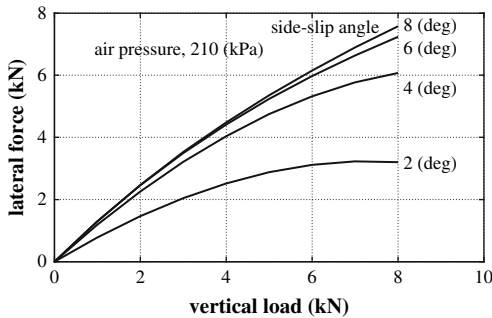
FIGURE 2.17 Lateral force to side-slip angle and vertical load.

Next is to study the effect of the tire vertical load on the tire cornering stiffness. From Fig. 2.16, when the tire load is small, the cornering stiffness increases together with the tire load, but after a certain limit, it seems to decrease.

The cornering stiffness, divided by the corresponding tire load, is called the cornering stiffness coefficient. This cornering stiffness coefficient decreases with tire load almost linearly, as shown in Fig. 2.18. Therefore, the dependence of the cornering stiffness the tire load is written as
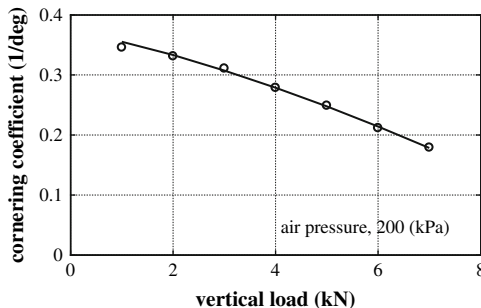
FIGURE 2.18 Effects of vertical load on cornering coefficient.
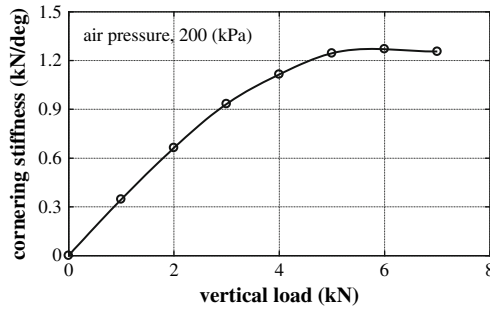
FIGURE 2.19 Effect of vertical load on cornering stiffness coefficient.

$$K = W(c - c_1 W) \tag{2.38}$$

here, c is the cornering stiffness coefficient near zero tire load, and c_1 is the tire load dependant coefficient.

In relation to tire load, cornering stiffness could be approximated as a parabolic that passes through the origin. Cornering stiffness increases with tire load to a peak value and beyond that it decreases. Tires are normally used in the region where cornering stiffness increases with vertical load.

Figure 2.19 shows the dependence of tire cornering stiffness on tire load for a real tire. The approximation to a parabolic is verified.

Usually, the effect of the tire vertical load is expressed in the form of μW. The friction coefficient between the tread rubber and ground, μ, is expected to have an effect similar to the tire vertical load. Figure 2.20 schematically shows the effects of the road surfaces on the cornering force as it changes with side-slip angle [2].

From the figure, it can be seen that the friction coefficient has almost no effect on lateral force at small side-slip angles, but has a more obvious effect as side-slip angles get larger. The effect of friction coefficient on the lateral force is very similar to the vertical.
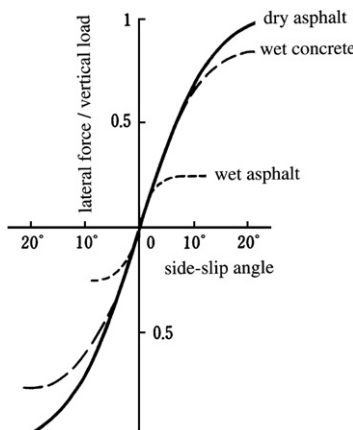
FIGURE 2.20 Effects of road surface on lateral force.
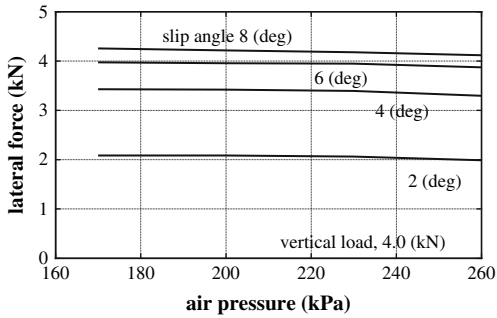
FIGURE 2.21 Effects of tire pressure on lateral force.

(3) TIRE PRESSURE EFFECT

From analysis of the mathematical model in subsection 2.3.1, it is clear that the tire lateral force becomes larger with a smaller tread base displacement under a constant force. From Eqn (2.5), y becomes smaller with smaller $\alpha^3 l^2/(2k)$. If k, the spring constant of the spring support, is large, and the tread base bending stiffness, EI, is also large, then the tread base displacement is small. Since spring constant, k, depends on tire air pressure, it is expected that cornering force also increases with tire pressure. However, the increase of tire pressure reduces the contact surface length, l, and Eqn (2.15) shows that the lateral force decreases with a decrease in contact length.

Figure 2.21 is a good example of the relationship between lateral force and tire pressure. The increase of tire pressure contributes to the increase of k and an increase in the lateral force is expected; however, the reduction of the contact length, l, due to the increase of the tire pressure decreases the lateral force. Eventually, it is interesting to see that the lateral force is almost constant with the variation in the tire pressure in this case.

The above point is shown in more detail by the relation of the cornering stiffness to the tire pressure in Fig. 2.22. If the vertical load is relatively low, the decrease in contact length contributes more than the increase of k as the tire pressure increases. In this case, the cornering stiffness decreases with an

FIGURE 2.22 Effects of tire pressure on cornering stiffness.

increase in tire pressure. On the other hand, if the vertical load is relatively high, the effect of the increasing k is dominant compared with the decrease in the contact length and the cornering stiffness increases with the tire pressure. However, with even higher vertical 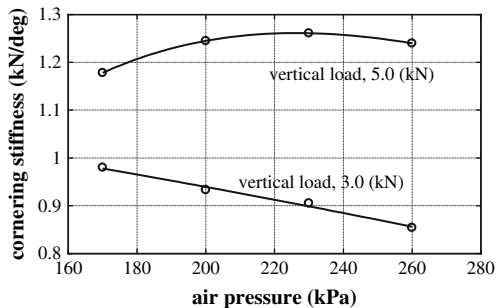loads, the excessive increase of the tire pressure has a greater effect on the contact length reduction and the cornering stiffness decreases with the increase of the tire pressure. The above points can be understood through Eqn (2.30).

(4) TIRE SHAPE EFFECT

The tread base bending stiffness, EI, is decided by the tire shape. If the tire material and the construction are given, the shape effect is dominated by the moment of inertia, I, of the tread base. This is generally larger for a larger tire. For tires with the same radius, it is larger for flatter tires with larger width. Therefore, low profile tires are desirable for obtaining larger cornering force.

From Eqn (2.30), the cornering stiffness increases when b is larger and d is smaller. Figure 2.23 is an example of the relationship between the cornering stiffness and the tread depth, which corresponds to the tread rubber thickness. From this figure, the increase in cornering stiffness is seen for a tire with smaller d, i.e., with worn tread.
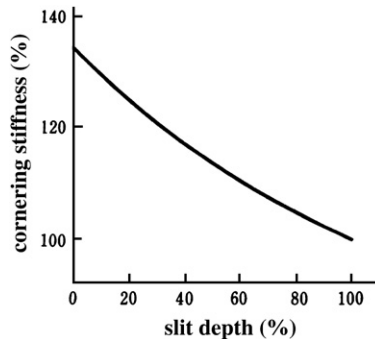
FIGURE 2.23 Effect of tire slit depth on cornering stiffness.

(5) BRAKING AND TRACTION FORCE EFFECT

The effects of tire parameters and vertical load on the lateral force have already been studied. During braking or traction, the tire is acted on by the vertical load that supports the vehicle weight and the longitudinal force at the contact surface that accelerates or stops the vehicle. These forces also affect the lateral force.

Based on the classical Law of Friction, and as shown in Fig. 2.24, the lateral force, F, and traction force (or braking force) T, acting on a tire, must always satisfy the following equation.

$$\sqrt{F^2 + T^2} \leq \mu W \qquad (2.39)$$
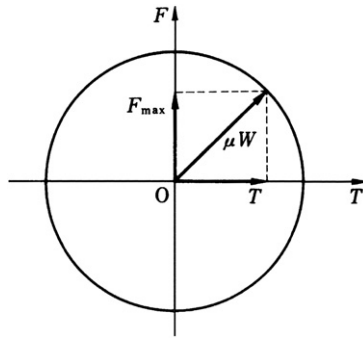
FIGURE 2.24 Friction circle.

In other words, the resultant of the horizontal, in-plane, forces that act on the contact surface between the tire and the ground cannot exceed the product of the tire load and the friction coefficient. This means that the resultant force vector is restricted to be inside a circle with radius μW. This circle is called the friction circle.

If there is a longitudinal force, either traction force or braking force, acting on the tire, the maximum cornering force, for a large side-slip angle, is given by,

$$F_{max} = \sqrt{\mu^2 W^2 - T^2} \qquad (2.40)$$

and, if $T = 0$, then the above is the same as in Eqn (2.25).

The relation of lateral force, F_0, to side-slip angle, when traction or braking force is zero, is given by the line O–A$_0$ in Fig. 2.25. The relation of lateral force to side-slip angle, when traction (or braking) force, T, is at work, is given by line O–A in the same figure. If the reduction ratio of lateral force due to traction (or braking) force is assumed to be the same at any side-slip angle, the following equation is true

$$\frac{F}{F_0} = \frac{\sqrt{\mu^2 W^2 - T^2}}{\mu W} \qquad (2.41)$$
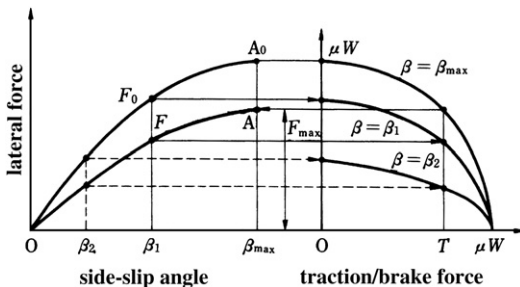
FIGURE 2.25 Effects of traction/brake force on lateral force.

or,

$$\left(\frac{T}{\mu W}\right)^2 + \left(\frac{F}{F_0}\right)^2 = 1 \tag{2.42}$$

which means, at any given side-slip angle, the lateral force, F, and traction (or braking) force, T, will form a circular relationship. This circle coincides with the friction circle shown previously when the side-slip angle produces the maximum lateral force. Figure 2.25 shows how the relationship between F and T is satisfied as a circle.

Much research has been carried out on the effect of traction force and braking force on lateral force. Figure 2.26 is an example of actual measurements that could be understood with the concept of the friction circle explained above.
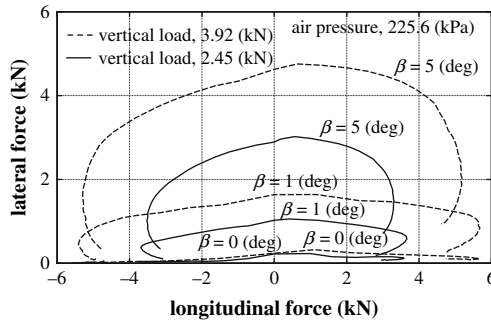
FIGURE 2.26 Lateral force with traction and braking forces.

2.3.3 Self-aligning torque

The theoretical analysis with the mathematical model shows that when the side-slip angle is small, the self-aligning torque increases linearly with side-slip angle, but when side-slip angle is large, the self-aligning torque approaches saturation and reaches its peak at a certain value. After this point, the self-aligning torque decreases with side-slip angle.

Figure 2.27 is a typical example of the relation between self-aligning torque and side-slip angle of a real tire.

In Fig. 2.27, the effect of tire load on self-aligning torque is shown together with the side slip. The effect of tire load on lateral force is small at small side-slip angles, and large at large side-slip angles. In comparison, the effect of tire load on self-aligning moment is large at any side-slip angle. One of the reasons for this is that the load effect occurs in the region where there is relative slip between the contact surface and the tread rubber, and self-aligning torque itself also has a greater contribution from the lateral force acting at both the ends of the contact surface. Another reason is that the contact surface length increases with tire load and the moment produced by the acting lateral force increases too. This could be verified from Eqn (2.18), where the third order or more term of l is included in the equation.
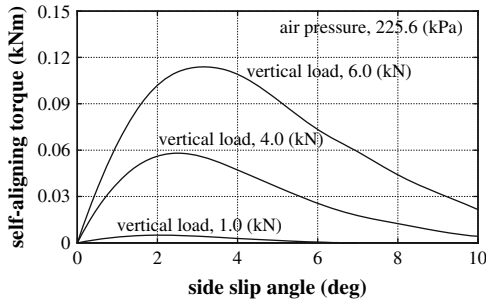
FIGURE 2.27 Self-aligning torque to side-slip angle.

If the tire pressure is increased, as seen from the previous discussion, the lateral force increases in some cases and the self-aligning torque also increases. However, on a real tire, self-aligning torque decreases if the tire pressure is increased. It is thought that while even though the lateral force increases with tire pressure, the contact surface length decreases with tire pressure. This has a large effect on self-aligning torque. Self-aligning torque increases if the tire pressure is decreased, but beyond a certain limit, the self-aligning torque does not increase with decreasing tire pressure. It is thought that if the tire pressure is too small, the decrease in lateral force has a larger effect than the effect of increasing the contact surface length.

Self-aligning torque is the moment of the lateral force around the vertical axis that passes through the contact surface center. Pneumatic trail is defined as in Fig. 2.13. Using Eqs (2.22) and (2.23), Fig. 2.28 shows the relationship between $\xi_n = M/F$ and ψ. The result shows that ξ_n decreases dramatically when side-slip angle becomes larger.
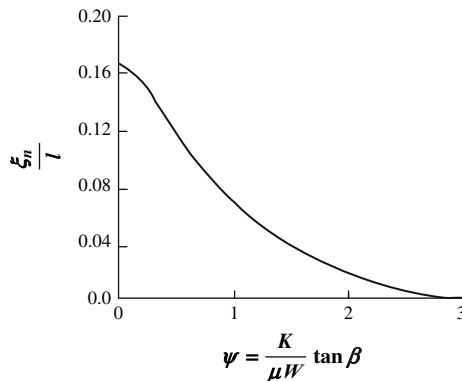
FIGURE 2.28 Pneumatic trail to side-slip angle.

2.3.4 Camber thrust

From Eqn (2.36), it is expected that the camber thrust of a tire is proportional to the camber angle when the side-slip angle is zero. Figure 2.29 is an example of
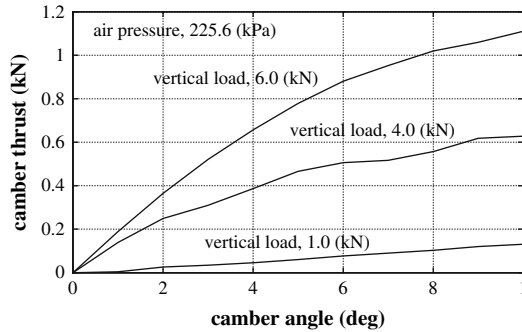
FIGURE 2.29 Camber thrust to camber angle.

the relationship between the camber angle and camber thrust of a normal tire. This example shows that the camber thrust is proportional to the camber angle. The effect of tire load is also noted in the same figure. As seen from the figure, the camber thrust coefficient, which is the camber thrust per unit camber angle, increases almost linearly with tire load. The tread base effective radius, R_0, is shown in Fig. 2.14 and depends on tire vertical load, W, as in Eqn (2.33). The contact surface length also increases with tire load. From Eqn (2.37), it is understood that camber thrust coefficient depends on tire vertical load, and increases with tire vertical load. Moreover, from the same equation, the camber thrust coefficient is equal to the product of the cornering stiffness and $l/(6R_0)$. It can now be assumed that the camber thrust coefficient has similar characteristics to the cornering stiffness. Since the ratio of contact surface length l to effective radius R_0, l/R_0, is generally about 0.3, the camber thrust coefficient is normally less than 1/10th of the cornering stiffness.

So far, the camber thrust and lateral force produced by side-slip angle have been considered. However, the normal tire that is fitted to a real vehicle usually has both side-slip angle and camber during its travel. In this case, the tire is simultaneously acted on by the lateral force and the camber thrust and it is regarded that they act independently.

Figure 2.30 is the example of the lateral force due to both side-slip angle and camber angle, as shown by Ellis [2]. The curves showing the relationship between camber angle and lateral force, at different side-slip angles, and the curves showing the relation of side-slip angle and lateral force, at different camber angles, are both parallel to each other. This shows that the lateral forces acting on the tire, produced by the camber angle and the side-slip angle, can be treated individually and independently.

In recent years, low profile tires have become more popular, especially among passenger cars. When this kind of tire cambers, the lateral distribution of the tire load in contact plane could easily give larger tire loads at the inner side, and smaller loads at the outer side. This kind of unequal distribution, compared to the case of equal distribution, causes a decrease in the generated lateral force at an axle. This is anticipated from the dependency of the lateral force and
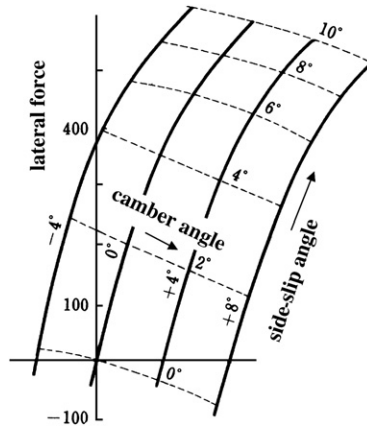
FIGURE 2.30 Effect of camber angle on tire lateral force.

cornering stiffness on the tire vertical load, which is shown by parabolic curves in Figs 2.17 and 2.19. The decrease of the lateral force due to a reduction in tire load is larger than the increase of the lateral force due to a tire load increase.

Consequently, even in cases where the camber angle is added so that the camber thrust and the lateral force caused by side-slip angle are in the same direction, the total lateral force produced by the tire with both side-slip angle and the camber angle may be reduced. This is due to the decrease of lateral force caused by tire load distribution changes, which in turn are caused by the camber angle.

To understand this phenomenon fully, the result using a low profile kart tire is plotted in Fig. 2.31.
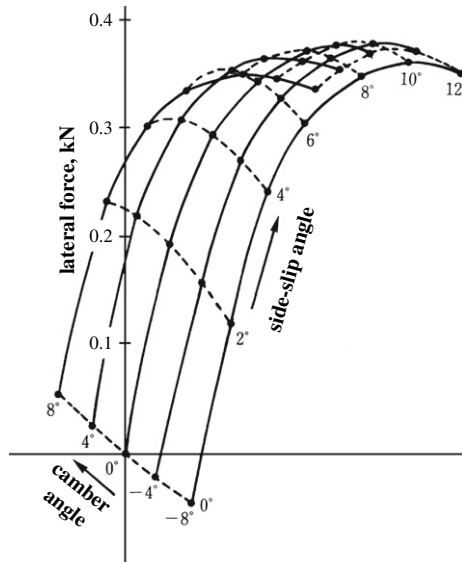
FIGURE 2.31 Effects of camber angle on lateral force of kart tire with small aspect ratio.

2.4 TRACTION, BRAKING, AND CORNERING CHARACTERISTICS

2.4.1 Mathematical model

The tire cornering characteristics from Fiala's theory have been explained in subsection 2.3.1. The mathematical model assumes that with side slip, the tire tread base deforms elastically in the lateral direction toward the tire rim and, at the same time, the tread rubber deforms elastically further more toward the tread base.

The effect of longitudinal force, such as traction and braking, could be considered using the same mathematical model, but the model would become too complex. Instead, Fig. 2.32 shows how the tread rubber is fitted circumferentially to the stiff rim, and the tread base is the only elastic part. This model allows elastic deformation in both the longitudinal and lateral directions. The tread rubber, similar to the previous model, is not a continuous circular body, but consists of a large number of independent springs around the tire circumference. This type of tire model is called the brush model.

This tire model will be used to understand theoretically the force generated by the tire in the longitudinal and lateral directions [3].
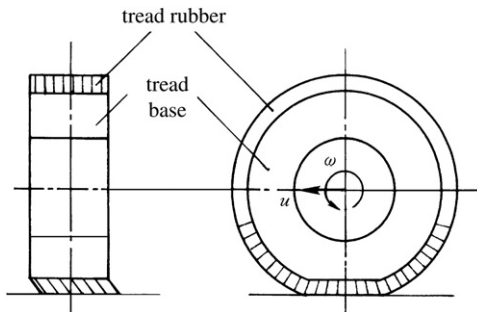
FIGURE 2.32 Tire deformable in lateral and longitudinal directions.

2.4.2 Tire lateral force during traction and braking

As shown in Fig. 2.33, the tire is rotating with an angular velocity, ω, while traveling in a direction that forms an angle of β to the rotation plane. The velocity component in the rotation plane is taken as u. Three forces act upon this tire, namely the longitudinal force, F_x, lateral force, F_y, and vertical force, F_z.

(1) BRAKING

Figure 2.34 shows how the front end point of the tire contact surface centerline is taken as the origin of the coordinate axes, with the x-axis in longitudinal direction, and the y-axis in lateral direction. The point on the tread base directly on top of point O is taken as point O′. After a fraction of time, Δt, the contact surface point moves from O to P, and the point O′ on the tread base moved to P′. The projected point P′ on x-axis is marked as P″.
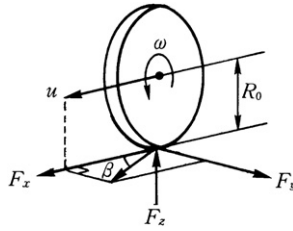
FIGURE 2.33 Tire forces in three directions.

During Δt, the distance in the x-direction of the contact point from point O is, the x-coordinate of point P:

$$x = u\Delta t \tag{2.43}$$

The x-coordinate of point P' from point O' is,

$$x' = R_0\omega\Delta t \tag{2.44}$$

Therefore, the relative displacement of point P and point P', i.e., the deformation of the tread rubber, is

$$\begin{aligned}
x - x' &= \frac{u - R_0\omega}{u}u\Delta t \\
&= sx \tag{2.45} \\
&= \frac{s}{1 - s}x'
\end{aligned}$$

whereby s is the tire slip ratio in the longitudinal direction.

$$s = \frac{u - R_0\omega}{u} \tag{2.46}$$

and the distance in y-direction of the contact point, from point O, i.e., the y-coordinate of point P, is

$$y = x \tan \beta = \frac{\tan \beta}{1 - s}x' \tag{2.47}$$
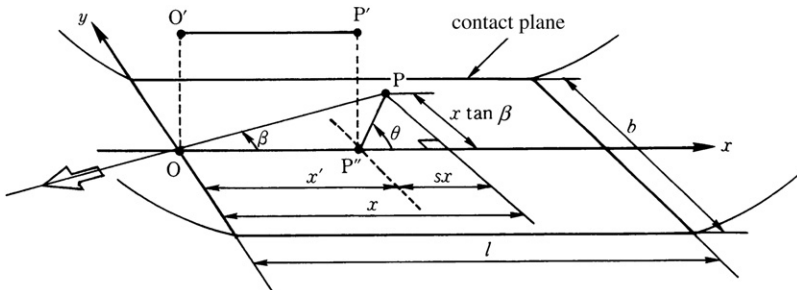
FIGURE 2.34 Tire deformation in contact plane.

Since there is no displacement of point P′ in the y-direction, the above is the deformation of tread rubber in the y-direction.

Therefore, the forces per unit length and width, acting on point P, in the x-direction and y-direction, respectively, are σ_x and σ_y

$$\sigma_x = -K_x(x - x') = -K_x \frac{s}{1-s} x' \tag{2.48}$$

$$\sigma_y = -K_y y = -K_y \frac{\tan \beta}{1-s} x' \tag{2.49}$$

The sign of these forces is taken as opposite to the axes direction. Furthermore, the resultant force magnitude is,

$$\begin{aligned} \sigma &= \sqrt{\sigma_x^2 + \sigma_y^2} \\ &= \sqrt{K_x^2 s^2 + K_y^2 \tan^2 \beta} \, \frac{x'}{1-s} \end{aligned} \tag{2.50}$$

Whereby K_x and K_y are the longitudinal and lateral tread rubber stiffnesses per unit width and unit length. When the tire longitudinal slip ratio and side-slip angle are produced, tire deformation occurs. As a result, a distribution of the contact surface force, proportional to x', is generated at the tire contact surface.

Assuming a tire pressure distribution that is the same as in subsection 2.3.1,

$$p = \frac{6F_z}{bl} \frac{x'}{l}\left(1 - \frac{x'}{l}\right) \tag{2.51}$$

As shown in Fig. 2.35, the tire contact surface force, as given by Eqn (2.50), is denoted by $0 \le x' \le x'_s$ in the adhesive region, and $x \ge x'_s$ in the slip region where the tire contact surface force is given by μp.

In the adhesive region, the forces acting at the contact surface, in x- and y-directions are σ_x and σ_y, respectively. In the slip region, the forces are $\mu p \cos \theta$ and $\mu p \sin \theta$. Here, θ determines the direction of the tire slip.
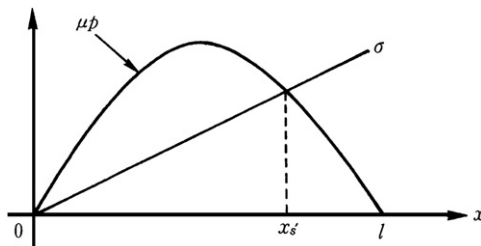
FIGURE 2.35 Force distributions in contact plane.

Substituting $\sigma = \mu p$ in Eqns (2.50) and (2.51), to find x'_s, and assuming a dimensionless variable, ξ_s as:

$$\xi_s = \frac{x'_s}{l} = 1 - \frac{K_s}{3\mu F_z} \frac{\lambda}{1 - s} \tag{2.52}$$

where,

$$\lambda = \sqrt{s^2 + \left(\frac{K_\beta}{K_s}\right)^2 \tan^2 \beta} \tag{2.53}$$

$$K_s = \frac{bl^2}{2} K_x, \ K_\beta = \frac{bl^2}{2} K_y \tag{2.54}$$

From the above, the overall forces acting on the whole tire contact surface, in x- and y-directions, are expressed as follows:

when $\xi_s > 0$, for a contact surface composed of adhesive and slip regions:

$$F_x = b\left(\int_0^{x'_s} \sigma_x \, dx' + \int_{x'_s}^l -\mu p \cos \theta \, dx'\right) \tag{2.55}$$

$$F_y = b\left(\int_0^{x'_s} \sigma_y \, dx' + \int_{x'_s}^l -\mu p \sin \theta \, dx'\right) \tag{2.56}$$

when $\xi_s \leq 0$, the contact surface consists only of a slip region,

$$F_x = b\int_0^l -\mu p \cos \theta \, dx' \tag{2.55'}$$

$$F_y = b\int_0^l -\mu p \sin \theta \, dx' \tag{2.56'}$$

Substituting Eqns (2.50)–(2.52) in Eqns (2.55)′–(2.56)′ gives F_x, F_y in the following forms:

When

$$\xi_s = 1 - \frac{K_s}{3\mu F_z} \frac{\lambda}{1 - s} > 0$$

then,

$$F_x = -\frac{K_s s}{1 - s}\xi_s^2 - 6\mu F_z \cos \theta \left(\frac{1}{6} - \frac{1}{2}\xi_s^2 + \frac{1}{3}\xi_s^3\right) \tag{2.57}$$

$$F_y = -\frac{K_\beta \tan \beta}{1 - s}\xi_s^2 - 6\mu F_z \sin \theta \left(\frac{1}{6} - \frac{1}{2}\xi_s^2 + \frac{1}{3}\xi_s^3\right) \tag{2.58}$$

when

$$\xi_s = 1 - \frac{K_s}{3\mu F_z} \frac{\lambda}{1-s} < 0$$

then,

$$F_x = -\mu F_z \cos\theta \qquad (2.57)'$$

$$F_y = -\mu F_z \sin\theta \qquad (2.58)'$$

The direction of the slip force, θ, is approximated by the slip direction at the slip start point.

$$\tan\theta = \frac{K_y \frac{\tan\beta}{1-s} x'}{K_x \frac{s}{1-s} x'} = \frac{K_\beta \tan\beta}{K_s s} \qquad (2.59)$$

Therefore,

$$\cos\theta = \frac{s}{\lambda} \qquad (2.60)$$

$$\sin\theta = \frac{K_\beta \tan\beta}{K_s \lambda} \qquad (2.61)$$

K_s, as defined by Eqn (2.54), is equivalent to the total longitudinal force per unit longitudinal slip ratio when $s \to 0$ at $\beta = 0$. K_β is equivalent to the total lateral force per unit side-slip angle when $\beta \to 0$ at $s = 0$. This can be derived from the definition of K_x and K_y by integrating the forces at the contact surface when they are very small and s or $\beta = 0$. Equations (2.57) and (2.58) confirm that $(\partial F_x/\partial s)_{s=0,\,\beta=0} = K_s$, and $(\partial F_y/\partial \beta)_{s=0,\,\beta=0} = K_\beta$. Hence, if F_x and F_y are used numerically, in simulations of the model described here, it is practical to determine experimentally the value of K_s and K_β, depending on the tire vertical load.

The friction coefficient, μ, is a function of F_z and the slip velocity, V_s, so an experimental equation that reflects the dependence of μ on tire load and slip velocity is desired. Here, V_s is defined as:

$$V_s = \sqrt{(u - R_0\omega)^2 + \mu^2 \tan^2\beta} = u\sqrt{s^2 + \tan^2\beta} \qquad (2.62)$$

As Eqn (2.63), the tire longitudinal and lateral forces can be obtained numerically as functions of the longitudinal slip ratio, s, slip angle, β, tire load, F_z, and tire traveling speed, u.

$$\begin{aligned} F_x &= F_x(s, \beta, F_z, u) \\ F_y &= F_y(s, \beta, F_z, u) \end{aligned} \qquad (2.63)$$

(2) ACCELERATING

As in the case of braking, the deformation of tread rubber to the tread base at the contact surface gives

$$x - x' = \frac{u - R_0\omega}{u} R_0\omega\Delta t = sx' \tag{2.64}$$

$$y = x \tan \beta = (1+s)\tan \beta x' \tag{2.65}$$

where s is tire longitudinal slip ratio during acceleration.

$$s = \frac{u - R_0\omega}{R_0\omega} \tag{2.66}$$

Then,

$$\sigma_x = -K_x s x' \tag{2.67}$$

$$\sigma_y = -K_y(1+s)\tan \beta x' \tag{2.68}$$

$$\sigma = \sqrt{K_x^2 s^2 + K_y^2(1+s)^2 \tan^2 \beta x'} \tag{2.69}$$

As with braking, the point the slip changes from the adhesive region to the slip region is found from

$$\xi_s = \frac{x'_s}{l} = 1 - \frac{K_s}{3\mu F_z}\lambda \tag{2.70}$$

$$\lambda = \sqrt{s^2 + \left(\frac{K_\beta}{K_s}\right)^2 (1+s)^2 \tan^2 \beta} \tag{2.71}$$

The forces acting in the x-direction and y-direction on the tire contact surface during acceleration are derived as below:
    When

$$\xi_s = 1 - \frac{K_s}{3\mu F_z}\lambda > 0$$

then,

$$F_x = -K_s s \xi_s^2 - 6\mu F_z \cos \theta \left(\frac{1}{6} - \frac{1}{2}\xi_s^2 + \frac{1}{3}\xi_s^3\right) \tag{2.72}$$

$$F_y = -K_\beta(1+s)\tan \beta \xi_s^2 - 6\mu F_z \sin \theta \left(\frac{1}{6} - \frac{1}{2}\xi_s^2 + \frac{1}{3}\xi_s^3\right) \tag{2.73}$$

When

$$\xi_s = 1 - \frac{K_s}{3\mu F_z}\lambda < 0$$

then,

$$F_x = -\mu F_z \cos\theta \qquad\qquad (2.72)'$$

$$F_y = -\mu F_z \sin\theta \qquad\qquad (2.73)'$$

Where,

$$\tan\theta = \frac{K_y(1+s)\tan\beta x'}{K_x s x'} = \frac{K_\beta \tan\beta(1+s)}{K_s s} \qquad (2.74)$$

$$\cos\theta = \frac{s}{\lambda} \qquad\qquad (2.75)$$
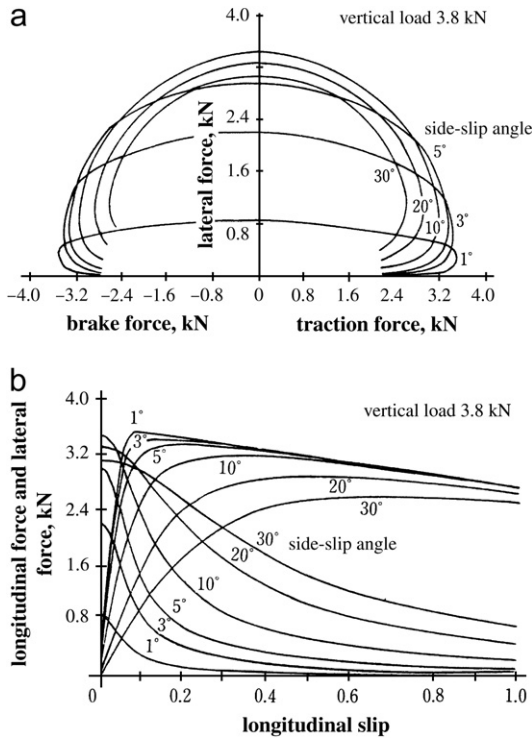
FIGURE 2.36 (a) Interaction between lateral and longitudinal forces. (b) Interaction between lateral and longitudinal forces.

$$\sin \theta = \frac{K_\beta \tan \beta (1 + s)}{K_s \lambda} \tag{2.76}$$

and the slip velocity, V_s is,

$$V_s = u \sqrt{\frac{s^2}{(1 + s)^2} + \tan^2 \beta} \tag{2.77}$$

The longitudinal and lateral forces that act on a tire with side slip, while under braking or acceleration, are shown in Fig. 2.36, which is plotted by using Eqns (2.57)–(2.58)' and (2.72)–(2.73)'. It is clear from the theoretical analysis here that, braking and acceleration affect the tire cornering characteristics, as explained in subsection 2.3.2 (5).

2.4.3 Self-aligning torque

As described in subsection 2.3.1, the lateral force acting on the contact surface is asymmetrical to the contact surface centerline, and this creates a moment around the vertical axis that passes through the tire contact center point. When the longitudinal force acts together with lateral force, the longitudinal force is offset from the tire centerline because of the lateral tire deformation. A self-aligning moment due to the longitudinal force is created in addition to that from the lateral force. The total of these moments is the self-aligning torque.

In Fig. 2.37, the force, per unit width and length, acting at a point on the contact plane, σ_x, σ_y is shown.

The self-aligning torque described above can be written as the total moment around point P as follows:

$$M = b \int_0^l \left[\left(x' - \frac{l}{2} \right) \sigma_y - y \sigma_x \right] dx' \tag{2.78}$$

Dividing the tire contact surface into adhesive and slip regions gives Eqn (2.78) as below:
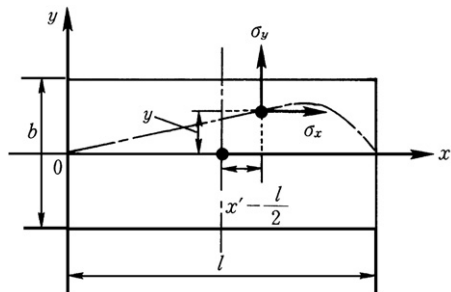
FIGURE 2.37 Lateral and longitudinal forces on contact plane.

$$M = b\left[\int_0^{x'_s}\left(x'-\frac{l}{2}\right)\sigma_y\,\mathrm{d}x' + \int_{x'_s}^l\left(x'-\frac{l}{2}\right)(-\mu p\sin\theta)\mathrm{d}x'\right]$$
$$-b\left[\int_0^{x'_s} y\sigma_x\,\mathrm{d}x' + \int_{x'_s}^l \frac{\mu p\sin\theta}{K_y}(-\mu p\cos\theta)\mathrm{d}x'\right] \tag{2.79}$$

The first and second integration terms in Eqn (2.79) are the self-aligning torques due to the lateral force, while the third and fourth integration terms represent the self-aligning torques due to the longitudinal force.

Using Eqns (2.47)–(2.49), or Eqns (2.65), (2.67), (2.68), and (2.51), the above integration can be carried out to give the self-aligning torque:

(1) BRAKING ($S > 0$)

When $\xi_s = \dfrac{x'_s}{l} = 1 - \dfrac{K_s}{3\mu F_z}\dfrac{\lambda}{1-s} \geq 0$

$$M = b\left[\int_0^{x'_s} -\frac{K_y\tan\beta}{1-s}\left(x'-\frac{l}{2}\right)x'\,\mathrm{d}x'\right.$$
$$\left. -\int_{x'_s}^l \frac{6\mu F_z\sin\theta}{bl}\left(x'-\frac{l}{2}\right)\frac{x'}{l}\left(1-\frac{x'}{l}\right)\mathrm{d}x'\right] - b\left[\int_0^{x'_s}\frac{K_xs\tan\beta}{(1-s)^2}x'2\,\mathrm{d}x'\right.$$
$$\left. +\int_{x'_s}^l \left(\frac{6\mu F_z}{bl}\right)^2\frac{\sin\theta\cos\theta}{K_y}\left(\frac{x'}{l}\right)^2\left(1-\frac{x'}{l}\right)^2\mathrm{d}x'\right]$$
$$= \frac{lK_\beta\tan\beta}{2(1-s)}\xi_s^2\left(1-\frac{4}{3}\xi_s\right) - \frac{3}{2}l\mu F_z\sin\theta\xi_s^2(1-\xi_s)^2 + \frac{2lK_ss\tan\beta}{3(1-s)^2}\xi_s^3$$
$$+\frac{3l(\mu F_z)^2\sin\theta\cos\theta}{5K_\beta}(1-10\xi_s^3+15\xi_s^4-6\xi_s^5) \tag{2.80}$$

When $\quad \xi_s = \dfrac{x'_s}{l} = 1 - \dfrac{K_s}{3\mu F_z}\dfrac{\lambda}{1-s} < 0$

$$M = -b\int_0^l \frac{6\mu F_z\sin\theta}{bl}\left(x'-\frac{l}{2}\right)\frac{x'}{l}\left(1-\frac{x'}{l}\right)\mathrm{d}x' + b\int_0^l \left(\frac{6\mu F_z}{bl}\right)^2$$
$$\times\frac{\sin\vartheta\cos\theta}{K_y}\left(\frac{x'}{l}\right)^2\left(1-\frac{x'}{l}\right)^2\mathrm{d}x'$$
$$= \frac{3l(\mu F_z)^2\sin\theta\cos\theta}{5K_\beta} \tag{2.81}$$

(2) ACCELERATING ($S < 0$)

When $\quad \xi_s = \dfrac{x'_s}{l} = 1 - \dfrac{K_s}{3\mu F_z}\lambda \geq 0$

$$
\begin{aligned}
M = b&\left[\int_0^{x'_s} -K_y(1+s)\tan\beta\left(x'-\frac{l}{2}\right)x'\,dx'\right.\\
&\left.-\int_{x'_s}^{l} \frac{6\mu F_z\sin\theta}{bl}\left(x'-\frac{l}{2}\right)\frac{x'}{l}(1-\frac{x'}{l})dx'\right]\\
-b&\left[\int_0^{x'_s} K_x(1+s)s\tan\beta x'2\,dx'\right.\\
&\left.+\int_{x'_s}^{l}\left(\frac{6\mu F_z}{bl}\right)^2\frac{\sin\theta\cos\theta}{K_y}\left(\frac{x'}{l}\right)^2\left(1-\frac{x'}{l}\right)^2 dx'\right]\\
= \frac{l}{2}&K_\beta(1+s)\tan\beta\xi_s^2\left(1-\frac{4}{3}\xi_s\right)-\frac{3}{2}l\mu F_z\sin\theta\xi_s^2(1-\xi_s)^2\\
+\frac{2}{3}&lk_s(1+s)s\tan\beta\xi_s^3+\frac{3l(\mu F_z)^2\sin\theta\cos\theta}{5K_\beta}(1-10\xi_s^3+15\xi_s^4-6\xi_s^5)
\end{aligned}
$$

$$\text{(2.82)}$$

When $\quad \xi_s = \dfrac{x'_s}{l} = 1 - \dfrac{K_s}{3\mu F_z}\lambda < 0$

$$
\begin{aligned}
M = -b&\int_0^{l}\frac{6\mu F_z\sin\theta}{bl}\left(x'-\frac{l}{2}\right)\frac{x'}{l}\left(1-\frac{x'}{l}\right)dx'+b\int_0^{l}\left(\frac{6\mu F_z}{bl}\right)^2\\
&\times\frac{\sin\vartheta\cos\theta}{K_y}\left(\frac{x'}{l}\right)^2\left(1-\frac{x'}{l}\right)^2 dx't\\
= &\frac{3l(\mu F_z)^2\sin\theta\cos\theta}{5K_\beta}
\end{aligned}
$$

$$\text{(2.83)}$$
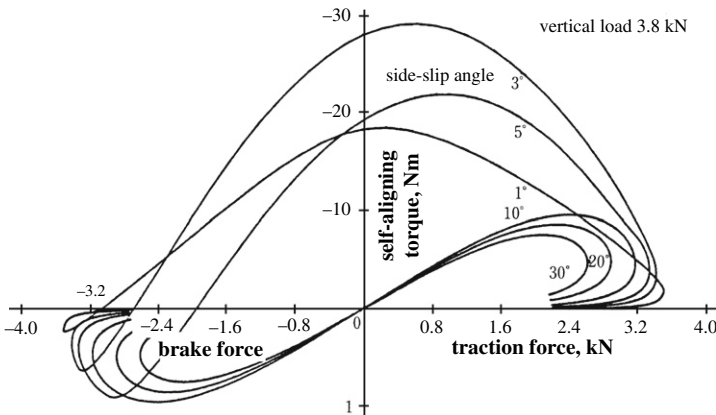
FIGURE 2.38 Effects of lateral and longitudinal forces on calculated self-aligning torque.

Figure 2.38 is plot of self-aligning torque against braking and traction forces, using Eqns (2.80)–(2.83). Unlike the lateral tire force, self-aligning torque changes tremendously during braking and acceleration. These changes are rather complex and depend on the braking or traction force and also the side-slip angle.

Example 2.2

Using the lateral force and the vertical load distribution diagrams, along the longitudinal direction on a tire contact plane with a small side-slip angle, try to explain, schematically, how the lateral force due to small side-slip angle is proportional to side-slip angle. Show this is basically independent of the vertical load and is determined by lateral stiffness of the tire.

Solution
Figure E2.2 is a schematic diagram of the distributions with small side-slip angle. A linear line is the lateral force due to the lateral deformation of the tread rubber. The parabolas are the distributions of the vertical loads multiplied by a friction coefficient. It is obvious from this diagram that as the side-slip angle is small, the tire lateral force expressed by the area surrounded by the linear line and one of the parabola lines is very robust to the vertical load variations. Also, as the side-slip angle is small, the surrounded plane is almost a triangle and so the area is almost proportional to the side-slip angle. The triangle is mostly determined by the lateral deformation of the tread rubber. The force produced by the lateral deformation depends directly on the lateral stiffness.
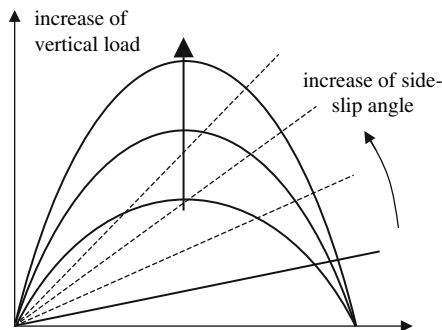
FIGURE E2.2.

Example 2.3

Derive the longitudinal and lateral forces, F_x and F_y, during braking when the vertical contact pressure load is distributed uniformly along the longitudinal direction in the contact plane.

Solution
For the uniform the vertical contact pressure load distribution, Eqn (2.51) is changed as follows:

$$p = \frac{F_z}{bl} \tag{E2.6}$$

As the point x' which satises $\sigma = \mu p$ is the point changing from adhesion to sliding, putting the above equation and Eqn (2.50) into $\sigma = \mu p$ gives us the following equations:

$$\sqrt{K_x^2 s^2 + K_y^2 \tan^2 \beta} \frac{x_s'}{1-s} = \mu \frac{F_z}{bl} \tag{E2.7}$$

As $K_s = bl^2 K_x/2$, $K_\beta = bl^2 K_y/2$, the above equation is transformed to:

$$2K_s \sqrt{s^2 + \left(\frac{K_\beta}{K_s}\right)^2 \tan^2 \beta} \frac{x_s'}{l} \frac{1}{1-s} = 2K_s \lambda \frac{x_s'}{l} \frac{1}{1-s} = \mu F_z \tag{E2.8}$$

Thus,

$$\xi_s = \frac{x_s'}{l} = \frac{\mu F_z}{2K_s} \frac{1-s}{\lambda} \tag{E2.9}$$

Following the same procedure as in subsection 2.4.2 (1), F_x and F_y are obtained as follows:

When $\xi_s \geq 1$, there is no slip region and:

$$F_x = b \int_0^l \sigma_x \, dx' = \frac{-K_s s}{1-s} \tag{E2.10}$$

$$F_y = b \int_0^l \sigma_y \, dx' = \frac{-K_\beta \tan \beta}{1-s} \tag{E2.11}$$

When $\xi_s \leq 1$, there are adhesion and slip regions and:

$$F_x = b\left(\int_0^{x_s'} \sigma_x \, dx' + \int_{x_s'}^{l} -\mu p \cos \theta \, dx' \right)$$

$$= -\frac{K_s s}{1-s} \xi_s^2 - \mu F_z \cos \theta (1 - \xi_s) \qquad \text{(E2.12)}$$

$$F_y = b\left(\int_0^{x_s'} \sigma_y \, dx' + \int_{x_s'}^{l} -\mu p \sin \theta \, dx' \right)$$

$$= -\frac{K_\beta \tan \beta}{1-s} \xi_s^2 - \mu F_z \sin \theta (1 - \xi_s) \qquad \text{(E2.13)}$$

2.5 DYNAMIC CHARACTERISTICS

The tire characteristics that have been observed until now are the steady state characteristics of the lateral force and self-aligning torque to a fixed side-slip angle. In this section, the transient lateral force and self-aligning torque, with changing side slip, are studied. These are the dynamic tire cornering characteristics.

In Sections 2.3 and 2.4, tire cornering characteristics were dealt with theoretically, using mathematical models that considered a micro-deformation at the tire contact surface. Dynamic cornering characteristics become too complicated when analyzed with these models. Instead, the transient response of lateral force and self-aligning torque to side-slip angle will be studied using a macro-tire model that deforms in the lateral direction, and is true for only small side-slip angles.

2.5.1 Lateral force dynamic characteristics

Figure 2.39 shows that when a sudden side-slip angle, β, occurs on a tire traveling in its rotating direction, then a lateral force is produced, and the contact surface deforms y in the lateral direction only. The lateral velocity of the contact surface is $\dot{y}$, and from Fig. 2.39, the contact surface side-slip angle is $\beta - \dot{y}/V$.

Taking F as the tire lateral force, and K as the cornering stiffness:

$$F = K\left(\beta - \frac{\dot{y}}{V} \right) \qquad \text{(2.84)}$$

if the tire lateral stiffness is defined as k_y,

$$F = k_y y \qquad \text{(2.85)}$$
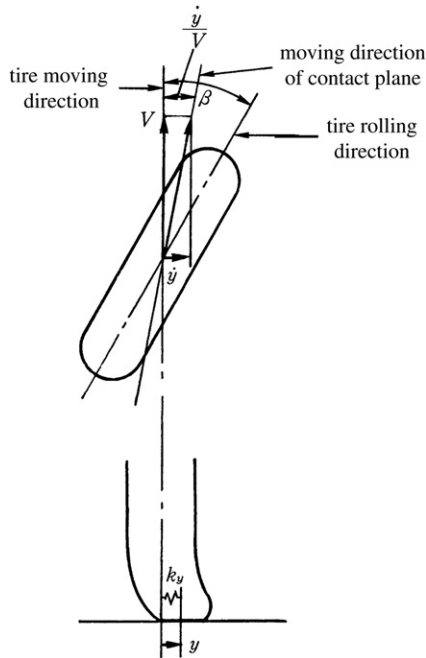
FIGURE 2.39 Tire deformation model for transient characteristics.

by eliminating y from these two equations

$$\frac{K}{k_y V}\frac{\mathrm{d}F}{\mathrm{d}t} + F = K\beta \tag{2.86}$$

Applying Laplace transforms to the above equation, the transfer function of the lateral force to side-slip angle is

$$\frac{F}{\beta}(s) = \frac{K}{1+\frac{K}{k_y V}s} = \frac{K}{1+T_1 s} \tag{2.87}$$

The response of lateral force to side-slip angle can be approximated by a first order lag element, with the time constant of $T_1 = K/k_y V$.

Using $j\omega$ instead of s in Eqn (2.87) gives the lateral force frequency response.

$$\frac{F}{\beta}\left(j\frac{\omega}{V}\right) = \frac{K}{1+j\frac{\omega}{V}\frac{K}{k_y}} \tag{2.88}$$

From Eqn (2.88), the frequency response of lateral force to side-slip angle, is with regard to a distance frequency, ω/V (rad/m), rather than a time
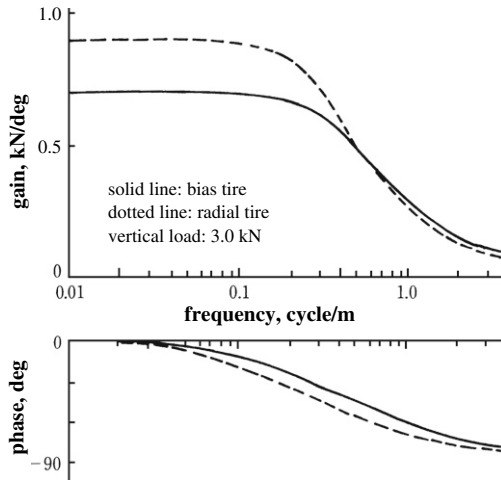
FIGURE 2.40 Frequency response of lateral force to side-slip angle.

frequency, ω (rad/s). Figure 2.40 is the example of real measurement of such a frequency response. As seen, the response could be accurately approximated by a first order lag element.

2.5.2 Self-aligning torque dynamic characteristics

The tire self-aligning torque in steady state is given by product of tire lateral force and pneumatic trail ξ. As stated in subsection 2.5.1, the transient response of lateral force to side-slip angle can be expressed as a first order delay element. The response of the self-aligning torque, M_s, by this lateral force, can also be approximated as a first order lag element. The time constant is taken as T_2,

$$\frac{M_s}{\beta}(s) = \frac{\xi K}{1 + T_2 s} \tag{2.89}$$

In this case, when a sudden side-slip angle occurs on a tire, the tire self-torsional deformation occurs. The torque due to the torsional deformation becomes part of the transient tire self-aligning torque. The tire torsional angle is largest at the instant when the side-slip angle, β, occurs, and its magnitude is the same as the side-slip angle, but after that, decreases with tire rotation and becomes 0 at steady state. Therefore, the response of the torque generated by tire torsion, M_t, to the side-slip angle, could be approximated by the following first order lead element.

$$\frac{M_t}{\beta}(s) = \frac{k_t T_3 s}{1 + T_3 s} \tag{2.90}$$

here, k_t is the tire torsional stiffness.
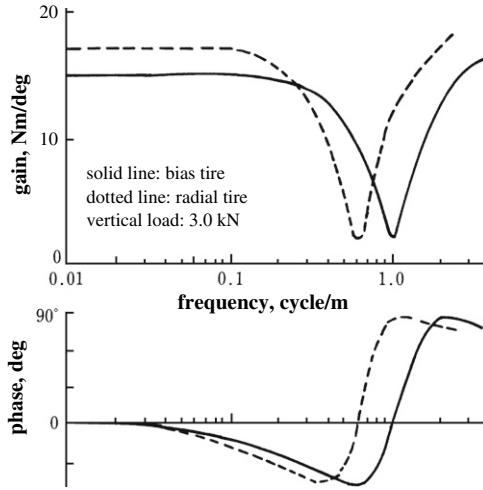
FIGURE 2.41 Frequency response of self-aligning torque to side-slip angle.

From the above, the tire self-aligning torque, M, is the sum of M_s and M_t, given by the following equation

$$\frac{M}{\beta}(s) = \frac{M_s}{\beta}(s) + \frac{M_t}{\beta}(s) = \frac{\xi K}{1 + T_2 s} + \frac{k_t T_3 s}{1 + T_3 s}$$

$$= \xi K \frac{1 + \left(1 + \frac{k_t}{\xi K}\right) T_3 s + \frac{k_t}{\xi K} T_2 T_3 s^2}{1 + (T_2 + T_3)s + T_2 T_3 s^2} \qquad (2.91)$$

and the frequency response is

$$\frac{M}{\beta}\left(j\frac{\omega}{V}\right) = \xi K \frac{1 - \frac{k_t V^2}{\xi K} T_2 T_3 \left(\frac{\omega}{V}\right)^2 + j\left(1 + \frac{k_t}{\xi K}\right) V T_3 \frac{\omega}{V}}{1 - V^2 T_2 T_3 \left(\frac{\omega}{V}\right)^2 + j V (T_2 + T_3)\frac{\omega}{V}} \qquad (2.92)$$

Figure 2.41 shows the measured data of the frequency response of self-aligning torque to ω/V. The shape confirms the suitability of the approximation by Eqn (2.92).

PROBLEMS

2.1 Find the approximate value of cornering stiffness using Eqn (2.24), when the lateral force is saturated at the side-slip angle equal to $10°$ with the vertical load, 4.0 kN, on a dry road surface, $\mu = 1.0$.

2.2 Estimate the side-slip angle at which the self-aligning torque becomes maximum, if the lateral force is saturated at $10°$, by referring to Eqns (2.24) and (2.26).

2.3 Confirm that the pneumatic trail is approximately equal to 1/6 of the contact length at small side-slip angles. Pay attention to the fact that the tire lateral deformation

distribution along the longitudinal direction on the contact plane is almost triangular, as explained in Example 2.2.

2.4 A centrifugal force of the vehicle is balanced with the sum of the four-tire lateral forces during turning. Calculate the side-slip angle of the tires when the four tires have an identical side-slip angle with the same cornering stiffness of 1.0 kN/deg. The vehicle mass, speed, and turning radius are 1500 kg, 60 km/h, and 140 m, respectively. Suppose that lateral force is proportional to side-slip angle and confirm it is less than $1.0°$.

2.5 Calculate the maximum lateral force available when a braking force of 3.0 kN is applied on the tire with 5.0 kN vertical load on a dry road surface, $\mu = 1.0$.

2.6 Calculate how much percent the lateral force is reduced when the traction force, T, which is equal to the 50% of the vertical load, is applied. Refer to Eqn (2.41) on a dry road surface, $\mu = 1.0$.

2.7 Confirm schematically the non-linear saturation property of the lateral force to the wide increase of side-slip angles, using the diagram used in Example 2.2 in which the lateral force is supposed to be expressed by the surrounded area by a linear lateral force distribution line and a parabola of the vertical load distribution multiplied by friction coefficient on the contact surface. The increase of the linear line gradient corresponds with the increase of the side-slip angle.

2.8 Confirm that the lateral force at some fixed side-slip angle has a non-linear relation to the increase of the vertical load using the same schematic method as in Problem 2.7.

2.9 Referring to Eqn (2.87), calculate the approximate time constant for the transient response of lateral force to side-slip angle where the cornering stiffness, the tire lateral stiffness, and the vehicle speed are 1.0 kN/deg, 200 kN/m, and 10m/s, respectively.

REFERENCES

[1] E. Fiala, Seitenkrafte am rollenden Luftreifen, VDI, Bd. 96, Nr. 29, 11, Okt., 1954.

[2] J. R. Ellis, Vehicle dynamics, London Business Book Ltd., London, 1969 (Chapter 1).

[3] J. E. Bernard et al., Tire shear force generation during combined steering and braking maneuvers, SAE Paper 770852.

Fundamentals of Vehicle Dynamics

3.1 PREFACE

This chapter will take the first look at the fundamentals of vehicle dynamics. As described earlier, in Chapter 1, the vehicle dynamics is the motion of the vehicle generated by the steering action, through which the vehicle is capable of independent motion.

The motion of the vehicle for a given steer input is studied and the mechanics of vehicle motion are explained. Only vehicle responses to a pre-determined steering action are studied in this chapter, steering in response to vehicle motion is studied later in the book.

There is an enormous amount of previous work that has studied the vehicle response to a predetermined steering action. These studies have established the fundamentals of vehicle dynamics. This chapter describes these fundamentals, which are necessary for understanding of the independent vehicle motion due to steering, i.e., the vehicle dynamics problem [1], [2].

3.2 VEHICLE EQUATIONS OF MOTION

The first chapter identified the vehicle motion degrees of freedom that should be considered as lateral, yaw, and roll. However, to understand the basic characteristics of vehicle motion, more simplicity is needed, provided the nature of the problem is not lost. The transient phenomena of the vehicle, such as sudden acceleration or deceleration are omitted, as is the case of a sudden large steer action. With these preconditions, the vehicle can be assumed to be traveling at a constant speed, and the roll motion can be neglected. If a vehicle travels at constant speed, and without roll, the vehicle vertical height can be neglected and only the lateral and yawing motions need to be considered. The vehicle is represented as a rigid body projected to the ground.

In describing the motion of the rigid body, the definition of a reference coordinate frame is necessary. Depending on particular body motion   47

characteristics, there could be many ways of defining the coordinates for describing the body motion. Clever definition of a coordinate frame can simplify the description of the body motion, so selection of suitable coordinates for a particular body is important. Considering this, it is sensible to first derive the fundamental vehicle equations of motion.

3.2.1 Equations of motion with fixed coordinates on the vehicle

Consider the vehicle moving in the horizontal plane. The vehicle longitudinal and lateral directions are continuously changing with reference to a fixed coordinate frame on the ground. If the vehicle is examined on-board, regardless of the direction of the vehicle, the motion constraints are basically unchangeable. It is more convenient to describe the vehicle motion by fixed coordinates on the vehicle rather than by fixed coordinates on the ground.

As shown in Fig. 3.1, X–Y are the fixed plane coordinates on the ground, and x–y are the fixed coordinates on the vehicle, with x in the vehicle longitudinal direction, and y in the lateral direction. The origin of the system is at the vehicle center of gravity, P. The yaw angle around the vertical axis is taken as positive in the anti-clockwise direction.

The vehicle is considered to be moving in plane with some speed. The position vector of point P, with reference to coordinate system X–Y, is defined as $\boldsymbol{R}$. The velocity vector $\dot{\boldsymbol{R}}$ can be written as:

$$\dot{\boldsymbol{R}} = u\boldsymbol{i} + v\boldsymbol{j} \tag{3.1}$$

here, $\boldsymbol{i}$ and $\boldsymbol{j}$ are the respective unit vectors in x and y directions. u and v are the velocity components of point P in the x and y directions. Differentiating Eqn (3.1) with time, the acceleration could be written as a vector of point P, as below. Here, '•' and '••' mean d/dt and d^2/dt^2.
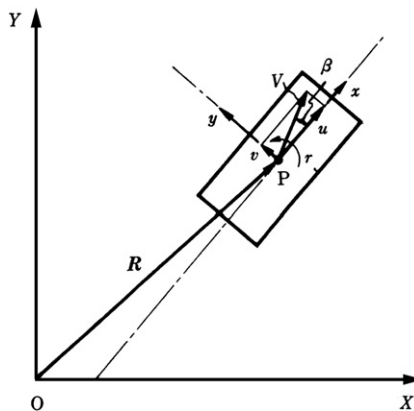
FIGURE 3.1 Coordinate axes for vehicle plane motion.
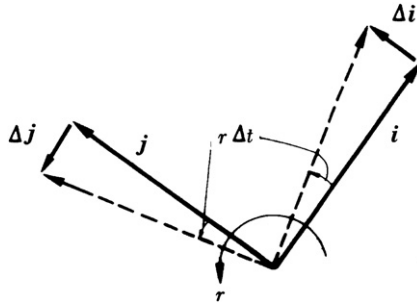
FIGURE 3.2 Time derivative of unit vectors.

$$\ddot{R} = \dot{u}i + u\dot{i} + \dot{v}j + v\dot{j} \tag{3.2}$$

The x–y-coordinate is fixed to the vehicle, and the vehicle has a yaw angular velocity of r around the vertical axis passing through point P, which is sometimes called yaw velocity or yaw rate.

The changes in i and j with time Δt, based on Fig. 3.2, are:

$$\Delta i = r\Delta t j$$

$$\Delta j = -r\Delta t i$$

thus,

$$\dot{i} = \lim_{\Delta t \to 0} \frac{\Delta i}{\Delta t} = rj$$

$$\dot{j} = \lim_{\Delta t \to 0} \frac{\Delta j}{\Delta t} = -ri$$

Example 3.1

Show an alternative way of expressing the time derivatives of unit vectors i and j.

Solution
As shown in Fig. E3.1, let i_F and j_F be the unit vectors fixed to the ground, then i and j are expressed as:
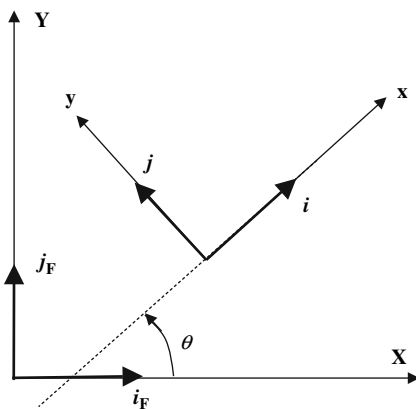
$$i = \cos\theta\, i_F + \sin\theta\, j_F$$
$$j = -\sin\theta\, i_F + \cos\theta\, j_F$$

FIGURE E3.1.

where θ is the angle between the unit vectors $\boldsymbol{i}$ and $\boldsymbol{i_F}$. Differentiating the above equations gives:

$$\dot{\boldsymbol{i}} = -\dot\theta \sin\theta\, \boldsymbol{i_F} + \dot\theta \cos\theta\, \boldsymbol{j_F} = r(-\sin\theta\, \boldsymbol{i_F} + \cos\theta\, \boldsymbol{j_F}) = r\boldsymbol{j}$$
$$\dot{\boldsymbol{j}} = -\dot\theta \cos\theta\, \boldsymbol{i_F} - \dot\theta \sin\theta\, \boldsymbol{j_F} = -r(\cos\theta\, \boldsymbol{i_F} + \sin\theta\, \boldsymbol{j_F}) = -r\boldsymbol{i}$$

The final acceleration vector of point P, $\ddot{\boldsymbol{R}}$ is

$$\ddot{\boldsymbol{R}} = (\dot{u} - vr)\boldsymbol{i} + (\dot{v} + ur)\boldsymbol{j} \tag{3.3}$$

The angle between the vehicle traveling direction and longitudinal direction, β, is expressed by $\tan^{-1}(v/u)$. This is called side-slip angle of the vehicle center of gravity. In normal cars, because $u \gg v$, $|\beta|$ is regarded to be very small. Also, if the vehicle speed is constant, $V = \sqrt{u^2 + v^2}$ is a constant too.

It is often more convenient to describe motion using β than the motion of point P by u and v. In other words, if β is small,

$$u = V\cos\beta \approx V, \quad v = V\sin\beta \approx V\beta,$$

$$\dot{u} = -V\sin\beta\dot\beta \approx -V\beta\dot\beta, \quad \dot{v} = V\cos\beta\dot\beta \approx V\dot\beta$$

Eqns (3.3) and (3.1) can be written as below:

$$\ddot{\boldsymbol{R}} = -V(\dot\beta + r)\beta\boldsymbol{i} + V(\dot\beta + r)\boldsymbol{j} \tag{3.3$'$}$$

$$\dot{\boldsymbol{R}} = V\boldsymbol{i} + V\beta\boldsymbol{j} \tag{3.1$'$}$$

Using Eqns (3.3)' and (3.1)', it can be shown that the dot product of vector $\ddot{\boldsymbol{R}}$ and vector $\dot{\boldsymbol{R}}$, $\ddot{\boldsymbol{R}} \cdot \dot{\boldsymbol{R}}$, is equal to 0. In other words, $\ddot{\boldsymbol{R}}$ is perpendicular to $\dot{\boldsymbol{R}}$, in the

traveling direction of point P. Equation (3.4)' shows that, if β is small, the acceleration of point P has a magnitude of $V(\dot{\beta} + r)$, and is perpendicular to the vehicle traveling direction, as shown in Fig. 3.3. When β is small, it can be assumed that the direction perpendicular to the traveling direction of the vehicle almost coincides with the lateral direction, y. Therefore, a vehicle moving in plane with a constant speed, regardless of motion with reference to the X–Y coordinates, will have an acceleration of $V(\dot{\beta} + r)$ in the lateral, or y-direction.

The lateral motion and yaw motion of the vehicle will generate slip angles at the tires. As described in Chapter 2, a lateral force will be produced at the tire in response to this side-slip angle. This lateral force produced by the vehicle motion becomes the force that controls the vehicle motion.

In Fig. 3.4(a), the angle of the front left and right wheels with respect to x direction is the actual steer angle, δ, and the tire side-slip angle at the front and rear wheels are β_{f1}, β_{f2}, β_{r1}, β_{r2}. The lateral forces acting on the tires are Y_{f1}, Y_{f2}, Y_{r1}, Y_{r2}. These forces are assumed to act in the direction perpendicular to the tire heading direction, i.e., the vehicle lateral direction, because $|\beta_{f1}|$, $|\beta_{f2}|$, $|\beta_{r1}|$, $|\beta_{r2}|$, $|\delta| \ll 1$. The lateral motion of the vehicle is described as below:

$$mV\left(\frac{d\beta}{dt} + r\right) = Y_{f1} + Y_{f2} + Y_{r1} + Y_{r2} \tag{3.4}$$

m is the vehicle inertia mass.

The lateral forces also result in a yaw moment around the center of gravity and the vehicle yaw motion is described as below:

$$I\frac{dr}{dt} = l_f(Y_{f1} + Y_{f2}) - l_r(Y_{r1} + Y_{r2}) \tag{3.5}$$

here, I is the yaw moment of inertia. l_f and l_r are the distances of the front and rear wheel axles from the center of gravity, and the lateral forces are assumed
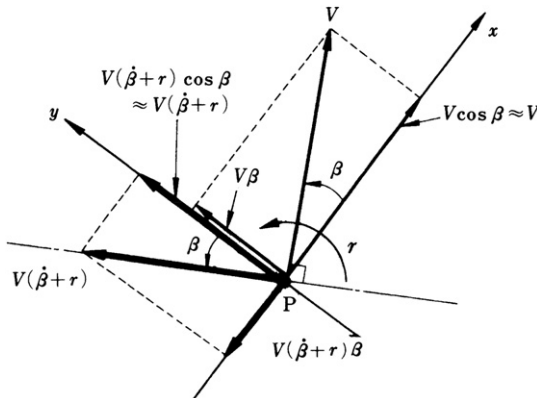
FIGURE 3.3 Acceleration and velocity at point P.
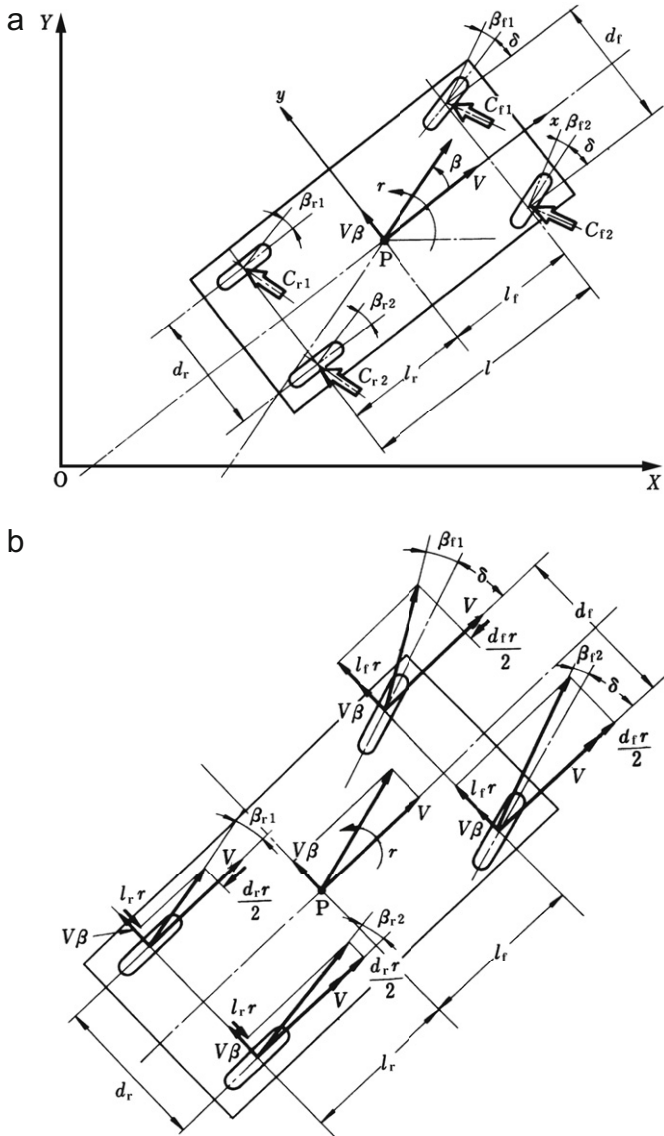
FIGURE 3.4 (a) Vehicle plane motion. (b) Side-slip angle of each tire.

to act along the axle. Equations (3.4) and (3.5) are the basic equations describing the plane motion of the vehicle traveling with a constant speed, and without roll motion.

To study the lateral forces, Y_{f1}, Y_{f2}, Y_{r1}, Y_{r2} acting on the tires in more detail, it is first necessary to examine the respective tire side-slip angle, β_{f1}, β_{f2}, β_{r1}, β_{r2}. Tire side-slip angle is defined as the angle between the tire traveling direction and the tire heading direction or the tire rotation plane. The rigid body vehicle has a velocity component of V in the longitudinal, x,

direction, and $V\beta$ in the lateral, y, direction. The vehicle also has an angular velocity of r around the center of gravity. Consequently, each tire will have the velocity component of the center of gravity, and velocity component due to rotation around the center of gravity. The velocity component in x- and y-direction for each tire is shown in Fig. 3.4(b). The heading direction of the front wheels has an angular displacement of δ with respect to the vehicle longitudinal direction, x. This is the actual steer angle of the front wheels. The heading direction of the rear wheels is the same as the vehicle longitudinal direction. Therefore, the side-slip angle for each tire could be written as below:

$$\beta_{f1} \approx \frac{V\beta + l_f r}{V - d_f r/2} - \delta \approx \beta + \frac{l_f r}{V} - \delta$$

$$\beta_{f2} \approx \frac{V\beta + l_f r}{V + d_f r/2} - \delta \approx \beta + \frac{l_f r}{V} - \delta$$

$$\beta_{r1} \approx \frac{V\beta - l_r r}{V - d_r r/2} \approx \beta - \frac{l_r r}{V}$$

$$\beta_{r2} \approx \frac{V\beta - l_r r}{V + d_r r/2} \approx \beta - \frac{l_r r}{V}$$

Whereby d_f and d_r are the vehicle front and rear treads, and second order terms of $|\beta|$, $|l_f r/V|$, $|l_r r/V|$, $|d_f r/2V|$, $|d_r r/2V| \ll 1$, can be ignored as negligible. Then the left and right tire side-slip angles for both front and rear wheels are equal, and taking these as β_f and β_r, respectively,

$$\beta_f = \beta_{f1} = \beta_{f2} = \beta + l_f r/V - \delta \tag{3.6}$$

$$\beta_r = \beta_{r1} = \beta_{r2} = \beta - l_r r/V \tag{3.7}$$

As the left and right tire side-slip angles are equal, the steer angle is small and there is a negligible roll motion, it is suitable to consider the left and right tires of the front and rear wheels to be concentrated at the intersecting point of the vehicle x-axis with the front and rear axles as shown in Fig. 3.5. In this way, a four-wheeled vehicle could be transformed to an equivalent two-wheeled vehicle, which makes the analysis of vehicle motion simpler.

Usually, if there is no difference in the characteristics in the left and right tires, the lateral forces of the left and right tires will be equal. Taking the front and rear lateral forces as Y_f and Y_r

$$2Y_f = Y_{f1} + Y_{f2}$$

$$2Y_r = Y_{r1} + Y_{r2}$$
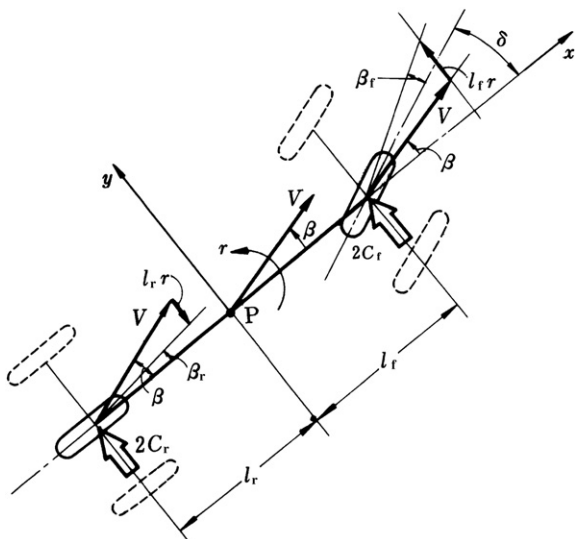
FIGURE 3.5 Equivalent bicycle model.

Since these forces act in the y-direction, Eqns (3.4) and (3.5) become:

$$mV\left(\frac{d\beta}{dt} + r\right) = 2Y_f + 2Y_r \tag{3.4}'$$

$$I\frac{dr}{dt} = 2l_f Y_f - 2l_r Y_r \tag{3.5}'$$

Defining the cornering stiffness of the front and rear wheels as K_f and K_r, Y_f and Y_r are proportional to β_f and β_r, respectively. In the x–y coordinates shown in Fig. 3.4(a), all angles are positive in the anti-clockwise direction. When a side-slip angle is positive, Y_f and Y_r act in the negative y-direction, and can be written as below:

$$Y_f = -K_f\beta_f = -K_f(\beta + l_f r/V - \delta) \tag{3.8}$$

$$Y_r = -K_r\beta_r = -K_r(\beta - l_r r/V) \tag{3.9}$$

From these equations, it is clear that the forces acting on the vehicle, Y_f and Y_r, are not dominated by the vehicle position, or attitude angle, in the fixed coordinate system. Instead, they are determined by the vehicle motion itself, namely by β, r, and steer angle, δ. Substituting Eqns (3.8) and (3.9) into the previous Eqns (3.4)' and (3.5)':

$$mV\left(\frac{d\beta}{dt} + r\right) = -2K_f\left(\beta + \frac{l_f}{V}r - \delta\right) - 2K_r\left(\beta - \frac{l_r}{V}r\right) \tag{3.10}$$

$$I\frac{dr}{dt} = -2K_f\left(\beta + \frac{l_f}{V}r - \delta\right)l_f + 2K_r\left(\beta - \frac{l_r}{V}r\right)l_r \tag{3.11}$$

And rearranging the above equations:

$$mV\frac{d\beta}{dt} + 2(K_f + K_r)\beta + \left\{mV + \frac{2}{V}(l_fK_f - l_rK_r)\right\}r = 2K_f\delta \qquad (3.12)$$

$$2(l_fK_f - l_rK_r)\beta + I\frac{dr}{dt} + \frac{2(l_f^2K_f + l_r^2K_r)}{V}r = 2l_fK_f\delta \qquad (3.13)$$

These equations now become the fundamental equations of motion describing the vehicle plane motion. The left hand side term of Eqns (3.12) and (3.13) describes the vehicle motion characteristics, in response to an arbitrary front wheel steer angle, δ, allocated at the right hand side of the equation. From these equations, it is clear too that the vehicle motion is not affected by the position of the vehicle or the heading direction of the vehicle with reference to the fixed coordinates on the ground.

Here, the Laplace-transformed Eqns (3.12) and (3.13) are rewritten as below, whereby s is the Laplace transform operator and $\beta(s)$, $r(s)$, $\delta(s)$ are the Laplace transforms for β, r, δ.

$$\begin{bmatrix} mVs + 2(K_f + K_r) & mV + \frac{2}{V}(l_fK_f - l_rK_r) \\ 2(l_fK_f - l_rK_r) & Is + \frac{2}{V}(l_f^2K_f + l_r^2K_r) \end{bmatrix} \begin{bmatrix} \beta(s) \\ r(s) \end{bmatrix} = \begin{bmatrix} 2K_f\delta(s) \\ 2l_fK_f\delta(s) \end{bmatrix}$$

Hence, the characteristics equation for vehicle motion is

$$\begin{vmatrix} mVs + 2(K_f + K_r) & mV + 2(l_fK_f - l_rK_r)/V \\ 2(l_fK_f - l_rK_r) & Is + 2(l_f^2K_f + l_r^2K_r)/V \end{vmatrix} = 0$$

Expanding and arranging this equation gives:

$$mIV\left[s^2 + \frac{2m(l_f^2K_f + l_r^2K_r) + 2I(K_f + K_r)}{mIV}s + \frac{4K_fK_rl^2}{mIV^2} - \frac{2(l_fK_f - l_rK_r)}{I}\right]$$
$$= 0$$

$$(3.14)$$

whereby l is the wheel base.

$$l = l_f + l_r$$

Examining the derived equations of motion (3.12) and (3.13), it is understood that they are simultaneous first order differential equations of β and r. In fact, this form of equation is not unique to vehicle motion only. The independent motion of ships, when steered, is expressed in the same form. In the case of a vehicle, front and rear lateral forces act because of the vehicle motion and, in turn, control the vehicle motion. In the case of ships, lift force (lateral force), is generated by the attack angle between the ships' longitudinal direction and traveling direction, and this force controls the ship motion. This

is how vehicle dynamics and ship dynamics have the same form of equations of motion. The aircraft is a typical example of motion that relies on lift force, where similarity with the motion dynamics stated above can also be seen, in particular in its longitudinal motion. This form of motion, as expressed in Eqns (3.12) and (3.13), is shared among the vehicles, ships, and aircraft as a general form of the equations of motion.

Looking at Eqns (3.12) and (3.13) in more detail, the coefficient $l_f K_f - l_r K_r$ has a big effect on vehicle motion. If this value is 0, in other words, $l_f K_f = l_r K_r$, then the coupling between lateral and yaw motions is incomplete, whereby r is no longer related to β at all, though β is still related to r. When $l_f K_f - l_r K_r \neq 0$, the sign of this term will have a big effect on the coupling of lateral and yaw motions. The relative magnitudes of $l_f K_f$ and $l_r K_r$ are directly related to the vehicle motion basic characteristics, and this will be explained in detail later.

3.2.2 Equations of motion with fixed coordinates on the ground

Previously, the vehicle motion has been expressed with respect to fixed coordinates on the vehicle, as this simplifies the analysis and understanding of the phenomena later on. However, in some cases, it can be convenient to express the vehicle motion with fixed coordinates on the ground. For example, when studying the motion of a vehicle traveling at constant speed on a straight road, expressing the motion with respect to the straight road is easier, and more convenient.

As shown in Fig. 3.6, the X–Y coordinates fixed on the ground are considered with the straight road direction as the X-axis, and the direction perpendicular to it as the Y-axis. The angle between the vehicle longitudinal direction and the X-axis, or the vehicle yaw angle is θ. The angle between the vehicle heading direction and the X-axis is γ, and the lateral displacement of the vehicle center of gravity, P, from the X-axis is y. Normally, when considering the motion of the vehicle moving in a straight line, $|\gamma| \ll 1$ and $|\theta| \ll 1$ are assumed. With these assumptions, and if the front steer angle, $|\delta| \ll 1$, then the direction of the lateral forces, Y_f, Y_r acting on the front and rear tires, almost coincides with Y-direction and the vehicle motion can be expressed as below. Firstly, the motion of the center of gravity in the Y-direction is:

$$m\frac{d^2 y}{dt^2} = 2Y_f + 2Y_r \qquad (3.15)$$

And the yaw motion is

$$I\frac{d^2 \theta}{dt^2} = 2l_f Y_f - 2l_r Y_r \qquad (3.16)$$

If $|\gamma|$ is small, the vehicle center of gravity has a velocity component of $V \cos \gamma \approx V$ in the X-direction and $V \sin \gamma \approx V\gamma = dy/dt$ in the Y-direction, and an angular velocity of $d\theta/dt$ around the center of gravity. The left and right
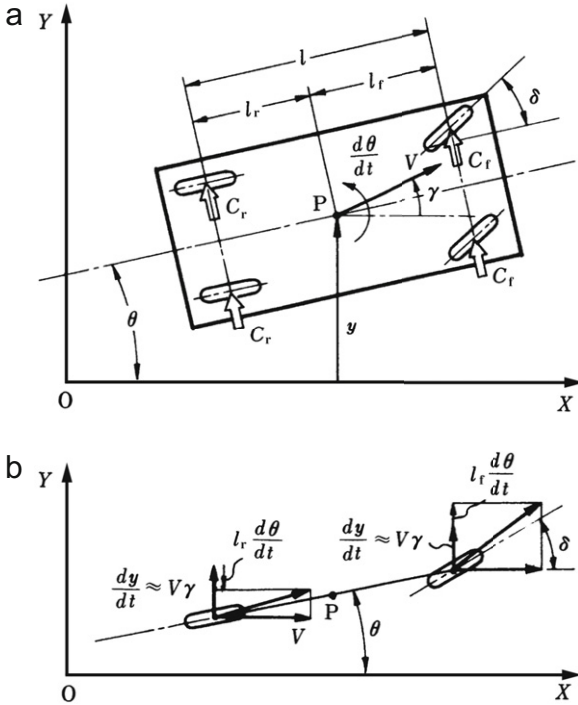
FIGURE 3.6 Vehicle motion with coordinate axis fixed on the ground.

wheels are considered to be concentrated to the vehicle axle centers, at the front and rear, and if $|\theta|$ is small, then the front and rear have additional velocity components of $l_f(d\theta/dt)$ and $l_r(d\theta/dt)$ in the Y-direction. Consequently, from Fig. 3.6(b), the angles between the front and rear wheels' traveling direction and the X-axis, γ_f, γ_r, are

$$\gamma_f = \frac{V\gamma + l_f(d\theta/dt)}{V} = \frac{1}{V}\frac{dy}{dt} + \frac{l_f}{V}\frac{d\theta}{dt}$$

$$\gamma_r = \frac{V\gamma - l_r(d\theta/dt)}{V} = \frac{1}{V}\frac{dy}{dt} - \frac{l_r}{V}\frac{d\theta}{dt}$$

The angles between the front and rear wheels' heading direction and the X-axis are $\theta_f = \theta + \delta$ and $\theta_r = \theta$, thus, the front and rear tire side-slip angles, β_f, β_r, are:

$$\beta_f = \gamma_f - \theta_f = \frac{1}{V}\frac{dy}{dt} + \frac{l_f}{V}\frac{d\theta}{dt} - \theta - \delta \tag{3.17}$$

$$\beta_r = \gamma_r - \theta_r = \frac{1}{V}\frac{dy}{dt} - \frac{l_r}{V}\frac{d\theta}{dt} - \theta \tag{3.18}$$

The lateral forces acting on the front and rear wheels, Y_f, Y_r, can be rewritten as:

$$Y_f = -K_f\beta_f = K_f\left(\delta + \theta - \frac{1}{V}\frac{dy}{dt} - \frac{l_f}{V}\frac{d\theta}{dt}\right) \tag{3.19}$$

$$Y_r = -K_r\beta_r = K_r\left(\theta - \frac{1}{V}\frac{dy}{dt} + \frac{l_r}{V}\frac{d\theta}{dt}\right) \tag{3.20}$$

Substituting these into Eqns (3.15) and (3.16):

$$m\frac{d^2y}{dt^2} = 2K_f\left(\delta + \theta - \frac{1}{V}\frac{dy}{dt} - \frac{l_f}{V}\frac{d\theta}{dt}\right) + 2K_r\left(\theta - \frac{1}{V}\frac{dy}{dt} + \frac{l_r}{V}\frac{d\theta}{dt}\right)$$

$$I\frac{d^2\theta}{dt^2} = 2K_f\left(\delta + \theta - \frac{1}{V}\frac{dy}{dt} - \frac{l_f}{V}\frac{d\theta}{dt}\right)l_f - 2K_r\left(\theta - \frac{1}{V}\frac{dy}{dt} + \frac{l_r}{V}\frac{d\theta}{dt}\right)l_r$$

and rearranging gives:

$$m\frac{d^2y}{dt^2} + \frac{2(K_f + K_r)}{V}\frac{dy}{dt} + \frac{2(l_fK_f - l_rK_r)}{V}\frac{d\theta}{dt} - 2(K_f + K_r)\theta = 2K_f\delta \tag{3.21}$$

$$\frac{2(l_fK_f - l_rK_r)}{V}\frac{dy}{dt} + I\frac{d^2\theta}{dt^2} + \frac{2(l_f^2K_f + l_r^2K_r)}{V}\frac{d\theta}{dt} - 2(l_fK_f - l_rK)\theta = 2l_fK_f\delta \tag{3.22}$$

These are the vehicle equations of motions with respect to the fixed coordinates on the ground.

The lateral and yaw motions of a vehicle traveling with constant speed, on an almost straight road, with small lateral velocity and yaw angle, can be expressed in a simpler form using fixed coordinates on the ground. The analysis and understanding of the phenomena become easier too. The left hand side of Eqns (3.21) and (3.22) describes the vehicle's lateral displacement, y, and yaw angle, θ, to the steer angle, δ. The term $l_fK_f - l_rK_r$ affects the coupling mode of y and θ, which means it is important in both ground and vehicle coordinate systems.

Next, the characteristic equation for Eqns (3.21) and (3.22) will be determined. The Laplace-transformed equations are written as below:

$$\begin{bmatrix} ms^2 + \frac{2(K_f + K_r)}{V}s & \frac{2(l_fK_f - l_rK_r)}{V}s - 2(K_f + K_r) \\ \frac{2(l_fK_f - l_rK_r)}{V}s & Is^2 + \frac{2(l_f^2K_f + l_r^2K_r)}{V}s - 2(l_fK_f - l_rK_r) \end{bmatrix} \begin{bmatrix} y(s) \\ \theta(s) \end{bmatrix}$$
$$= \begin{bmatrix} 2K_f\delta(s) \\ 2l_fK_f\delta(s) \end{bmatrix}$$

Whereby, $y(s)$ and $\theta(s)$ are the Laplace transforms for y and θ. Hence, the characteristic equation is:

$$\begin{vmatrix} ms^2 + \frac{2(K_f + K_r)}{V}s & \frac{2(l_fK_f - l_rK_r)}{V}s - 2(K_f + K_r) \\ \frac{2(l_fK_f - l_rK_r)}{V}s & Is^2 + \frac{2(l_f^2K_f + l_r^2K_r)}{V}s - 2(l_fK_f - l_rK_r) \end{vmatrix} = 0$$

Expanding and then rearranging these equations give:

$$mIs^2\left[s^2 + \frac{2m(l_f^2K_f + l_r^2K_r) + 2I(K_f + K_r)}{mIV}s + \frac{4K_fK_rl^2}{mIV^2} - \frac{2(l_fK_f - l_rK_r)}{I}\right] = 0$$

$$(3.23)$$

In this characteristic equation, if the term s^2 is omitted from the left hand side, it matches the characteristics of Eqn (3.14) for a vehicle using fixed coordinates. This guarantees that regardless of the fixation of the coordinates, on the vehicle or on the ground, the expressions for vehicle motion are fundamentally the same. The left hand side of Eqn (3.23) differs from Eqn (3.14) because of the s^2 term. The existence of this independent s^2 term inside the characteristics equation shows mathematically that the vehicle, at any location on the straight road, could move freely by steer. In practice, the vehicle could make lane changes or avoid the obstacles while traveling on the road. On the other hand, this s^2 term also shows that if suitable steer is not applied when the vehicle deviates laterally from the traveling path, by some disturbance, $|y|$, the deviation will get larger and larger and could result in the vehicle falling out of the path. (Refer to Chapter 9.)

Example 3.2

Describe the position of the moving vehicle center of gravity with respect to the axis fixed on the ground by using β and r in Eqns (3.12) and (3.13).

Solution
Let (X, Y) be the coordinate of vehicle center of gravity with respect to the axis fixed on the ground and θ, be the vehicle attitude angle with respect to X axis as shown in Fig. E3.2, then it is possible to have the following equations:
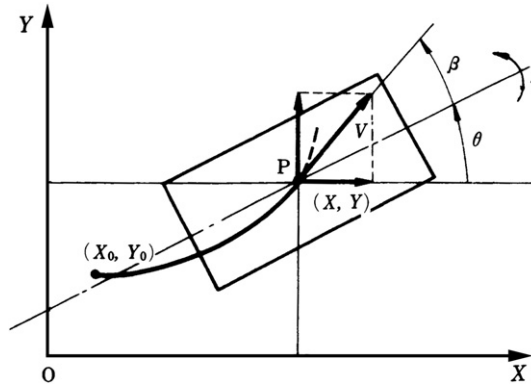
FIGURE E3.2.

$$\frac{dX}{dt} = V\cos(\beta + \theta) \tag{E3.1}$$

$$\frac{dY}{dt} = V\sin(\beta + \theta) \tag{E3.2}$$

Integration of the above equations gives us the equations to describe the position of the vehicle center of gravity as follows:

$$X = X_0 + V\int_0^t \cos(\beta + \theta)dt \tag{E3.3}$$

$$Y = Y_0 + V\int_0^t \sin(\beta + \theta)dt \tag{E3.4}$$

where

$$\theta = \theta_0 + \int_0^t r\,dt \tag{E3.5}$$

And X_0, Y_0, and θ_0 are the initial values of X, Y, and θ, respectively.

3.3 VEHICLE STEADY-STATE CORNERING

A theoretical understanding of a mechanical system is normally carried out by solving the equations of motion analytically, under suitable initial conditions. It may not be possible to solve the equations of motion analytically, and, even if an analytical solution is possible, the solution can be extremely complicated. This can make understanding the motion characteristics difficult. Equations of motion that are difficult to solve analytically could, by use of computers, be solved numerically, but the understanding of the basic motion characteristics is

almost impossible. There are several ways to understand the basic motion characteristics without the direct solution of a given equation of motion. One looks at the static characteristics by analyzing the steady-state condition of the mechanical system, and another studies the dynamic characteristics by examining the root of the characteristics equation and the response of the mechanical system to periodical external input.

Under normal conditions, a vehicle at constant speed and fixed front steer angle will make a steady circular motion with a constant radius of curvature. This is called steady-state cornering. By understanding the vehicle characteristics in steady-state cornering, the fundamental characteristics of vehicle motion can be understood.

3.3.1 Description of steady-state cornering

(1) DESCRIPTION BY EQUATIONS OF MOTION

The equations of motion derived in Section 3.2, using vehicle fixed coordinates, will be used to describe steady-state cornering. During steady-state cornering, there will be no changes in the side-slip angle and the yaw velocity. Here the steady-state conditions $d\beta/dt = 0$, $dr/dt = 0$ can be substituted into Eqns (3.12) and (3.13) giving:

$$2(K_f + K_r)\beta + \left\{mV + \frac{2}{V}(l_f K_f - l_r K_r)\right\}r = 2K_f\delta \qquad (3.24)$$

$$2(l_f K_f - l_r K_r)\beta + \frac{2(l_f^2 K_f + l_r^2 K_r)}{V}r = 2l_f K_f\delta \qquad (3.25)$$

The solutions for β and r are:

$$\beta = \begin{vmatrix} 2K_f & mV + \frac{2}{V}(l_f K_f - l_r K_r) \\ 2l_f K_f & \frac{2(l_f^2 K_f + l_r^2 K_r)}{V} \end{vmatrix} \begin{matrix} \delta \\ \overline{\Delta} \end{matrix} \qquad (3.26)$$

$$r = \begin{vmatrix} 2(K_f + K_r) & 2K_f \\ 2(l_f K_f - l_r K_r) & 2l_f K_f \end{vmatrix} \begin{matrix} \delta \\ \overline{\Delta} \end{matrix} \qquad (3.27)$$

whereby,

$$\Delta = \begin{vmatrix} 2(K_f + K_r) & mV + \frac{2}{V}(l_f K_f - l_r K_r) \\ 2(l_f K_f - l_r K_r) & \frac{2(l_f^2 K_f + l_r^2 K_r)}{V} \end{vmatrix} \qquad (3.28)$$

Expanding Eqns (3.26)–(3.28) and rearranging them, gives β and r as:

$$\beta = \left(\frac{1 - \frac{m}{2ll_r K_r} l_f V^2}{1 - \frac{m}{2l^2} \frac{l_f K_f - l_r K_r}{K_f K_r} V^2} \right) \frac{l_r}{l} \delta \tag{3.29}$$

$$r = \left(\frac{1}{1 - \frac{m}{2l^2} \frac{l_f K_f - l_r K_r}{K_f K_r} V^2} \right) \frac{V}{l} \delta \tag{3.30}$$

If the vehicle is traveling with a constant speed, V, and the yaw velocity is r, the radius of the steady-state cornering, ρ, is:

$$\rho = \frac{V}{r} = \left(1 - \frac{m}{2l^2} \frac{l_f K_f - l_r K_r}{K_f K_r} V^2 \right) \frac{l}{\delta} \tag{3.31}$$

Equations (3.29)–(3.31) describe the vehicle steady-state cornering with steer angle, δ, and constant traveling speed, V. They show physically how the side-slip angle, β, yaw velocity, r, cornering or turning radius, ρ, respond to steer angle at different traveling speeds.

Assuming that the vehicle is traveling at a very low speed ($V \approx 0$), the V^2 can be neglected in Eqns (3.29)–(3.31). β, r, and ρ can now be described as follows:

$$\beta_{(V \approx 0)} = \beta_s = \frac{l_r}{l} \delta$$
$$r_{(V \approx 0)} = r_s = \frac{V}{l} \delta \tag{3.32}$$
$$\rho_{(V \approx 0)} = \rho_s = \frac{l}{\delta}$$

Equations (3.29)–(3.31) can express the vehicle steady-state cornering as follows:

$$\frac{\beta}{\beta_s} = \frac{1 - \frac{m}{2l} \frac{l_f}{l_r K_r} V^2}{1 - \frac{m}{2l^2} \frac{l_f K_f - l_r K_r}{K_f K_r} V^2} \tag{3.29'}$$

$$\frac{r}{r_s} = \frac{1}{1 - \frac{m}{2l^2} \frac{l_f K_f - l_r K_r}{K_f K_r} V^2} \tag{3.30'}$$

$$\frac{\rho}{\rho_s} = 1 - \frac{m}{2l^2} \frac{l_f K_f - l_r K_r}{K_f K_r} V^2 \tag{3.31'}$$

The above equations show how the conditions for vehicle steady-state cornering change with the traveling speed, V. The state of vehicle circular motion at very low speeds, $V \approx 0$, can be used as reference.

(2) DESCRIPTION BY GEOMETRY

The study of vehicle steady-state cornering gave the response of β, r, and ρ to steer angle, δ, by simply putting steady-state conditions into the vehicle equations of motion derived from Section 3.2. Further derivations of Eqns (3.29)–(3.31), or $(3.29)'$–$(3.31)'$ show how they change with the traveling speed, V.

Next, the vehicle steady-state cornering will be studied geometrically to understand the vehicle motion more intuitively or in a more direct sense. Using geometry, the yaw angle, and yaw velocity isn't positive in the anti-clockwise direction, as in the equations of motions, but is taken as positive in the direction shown by Fig. 3.7(a).

First let us consider the steady-state cornering of the vehicle at very low speeds, $V \approx 0$. Under this circumstance, a centrifugal force doesn't act on the vehicle, lateral forces are not needed, and no side-slip angle is produced as both front and rear wheels travel in the heading direction of the vehicle and make a circular motion around O_s, as shown in Fig. 3.7(a). From this figure, the geometrical relations are formulated as:

$$\rho_s = \frac{l}{\delta}$$
$$r_s = \frac{V}{\rho_s} = \frac{V}{l}\delta \qquad (3.33)$$
$$\beta_s = \frac{l_r}{\rho_s} = \frac{l_r}{l}\delta$$

whereby $0 < \delta \ll 1$ and $l \ll \rho$. As seen from Fig. 3.8(a), the actual steer angle for the left and right front wheels is not δ, but is a little smaller for the left wheel, and a little larger for the right wheel. In practice, this is achieved by a steering link mechanism, but if $\delta \ll 1$ and $\rho_s \gg d$, then the difference is very small, and the left and right wheels can be considered as having the same steer angle, δ. Equation (3.33) agrees with the steady-state cornering Eqn (3.32), which is obtained from the equations of motion with $V \approx 0$. This geometrical relation is called the Ackermann steering geometry, and $\delta = l/\rho_s$ is called the Ackermann angle.

When the circular motion of the vehicle is considered at larger speeds, the centrifugal force becomes significant. The cornering forces at the front and rear wheels are needed to balance this centrifugal force and the side-slip angles are produced. When the centrifugal force acts at the vehicle center of gravity, the circular motion condition shown in Fig. 3.8(a) is no more accurate, and Eqn (3.33) is not accurate as well. Figure 3.7(b) shows the circular motion when the front and rear wheel side-slip angles, β_f, β_r, are produced by the centrifugal force.
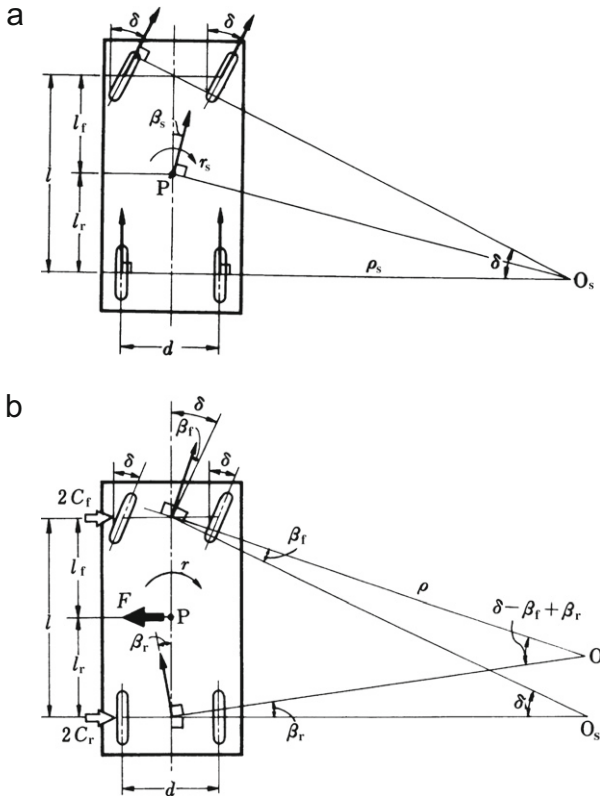
FIGURE 3.7 (a) Steady-state turning at low speed. (b) Steady-state turning with centrifugal force.

The center of the circular motion is the intersecting point of the two straight lines perpendicular to the front and rear wheels' traveling direction, denoted as O. The geometrical relations are formulated as follows:

$$\rho = \frac{l}{\delta - \beta_f + \beta_r} \tag{3.34}$$

assuming that $0 < \delta \ll 1, 0 < \beta_f, \beta_r \ll 1, \rho_s \gg l, d$.

Here, $r = V/\rho$, so

$$r = \frac{V(\delta - \beta_f + \beta_r)}{l} \tag{3.35}$$

Furthermore, from Fig. 3.8,

FIGURE 3.8 Side-slip angle during steady-state cornering.

$$\beta + \beta_r = \frac{l_r}{\rho}$$

Hence,

$$\beta = \frac{l_r}{\rho} - \beta_r = \frac{l_r}{l}\delta - \frac{l_r\beta_f + l_f\beta_r}{l} \qquad (3.36)$$

Equations (3.34)–(3.36) express the vehicle circular motion and are derived from the steady-state cornering geometrical relation. The front and rear wheel side-slip angles, β_f, β_r, can be found from the magnitude of the centrifugal force acting at the vehicle center of gravity. The centrifugal force is dependant on the vehicle speed, V, so ρ, r, β in Eqns (3.34)–(3.36) also change with V.

The steady-state cornering conditions with traveling speed have been determined by deriving Eqns (3.29)–(3.31). From the previous discussion, it is known that this occurs because the centrifugal force changes with speed. This causes the front and rear side-slip angles to change, which, in turn, changes the circular motion geometry and conditions of steady-state cornering.

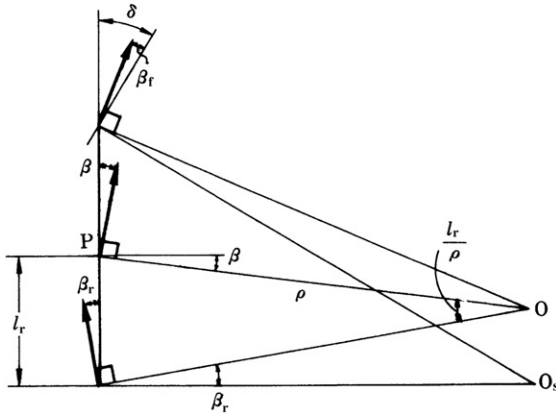Equations (3.34)–(3.36), which express the vehicle steady-state cornering, are derived from a geometrical relation. They are not influenced by the relationship between lateral forces and side-slip angles, β_f, β_r or any lateral forces acting on the front and rear wheels. As long as $|\delta| \ll 1$ and $\rho \gg l, d$, the equations are valid under any conditions. Contrary to this, it is important to note that Eqns (3.29)–(3.31) and (3.29)′–(3.31)′ are only valid when the lateral forces acting on the front and rear wheels are proportional to the side-slip angles β_f, β_r.

It is possible to introduce Eqns (3.29)–(3.31) from the geometrical descriptions of the steady-state turning. The centrifugal force is expressed by mV^2/ρ while the lateral forces exerted on the front and rear tires are proportional to the

side-slip angle and expressed by $-2K_f\beta_f$ and $-2K_r\beta_r$, respectively. If the vehicle is in steady-state turning, the following equilibrium equations arise:

$$mV^2/\rho - 2K_f\beta_f - 2K_r\beta_r = 0$$

$$-2l_fK_f\beta_f + 2l_rK_r\beta_r = 0$$

From the above two equations, the side-slip angles are obtained:

$$\beta_f = \frac{mV^2l_r}{2lK_f}\frac{1}{\rho}$$

$$\beta_r = \frac{mV^2l_f}{2lK_r}\frac{1}{\rho}$$

Substituting the above β_f and β_r into Eqns (3.34), (3.35), and (3.36) gives Eqns (3.31), (3.30), and (3.29) respectively.

3.3.2 Steady-state cornering and steer characteristics

(1) UNDERSTEER (US) AND OVERSTEER (OS) CHARACTERISTICS

This subsection will study in more detail how the vehicle steady-state cornering relationship with vehicle velocity is affected by the vehicle characteristics, using equations that express the vehicle steady-state cornering, as derived in subsection 3.3.1.

Firstly, look at the turning radius, ρ, given by Eqn (3.31). Taking the steer angle as δ_0

$$\rho = \left(1 - \frac{m}{2l^2}\frac{l_fK_f - l_rK_r}{K_fK_r}V^2\right)\frac{l}{\delta_0} \tag{3.37}$$

The above equation shows how the turning radius, ρ, changes with velocity V for a fixed steer angle of δ_0. Figure 3.9 shows how the relationship between ρ and V is affected by the sign of $l_fK_f - l_rK_r$.

As can be seen from Eqn (3.37) or Fig. 3.9, if the steer angle is constant, the radius of the vehicle path when $l_fK_f - l_rK_r = 0$ is not related to V. In other words, the radius has a constant value of l/δ_0 at any velocity. When $l_fK_f - l_rK_r < 0$, a vehicle turning radius increases with velocity. The radius decreases with velocity if $l_fK_f - l_rK_r > 0$. In the latter case, when $V = V_c$ then $\rho = 0$, i.e., no curvature (the value and meaning of V_c will be described in the following section). This means that if the velocity increases with a fixed steer angle, the vehicle with $l_fK_f - l_rK_r < 0$ will turn out from the original circular path, and make a circular path with an even larger radius. While the vehicle with $l_fK_f - l_rK_r > 0$ will, on the contrary, turn into the inner side of the original
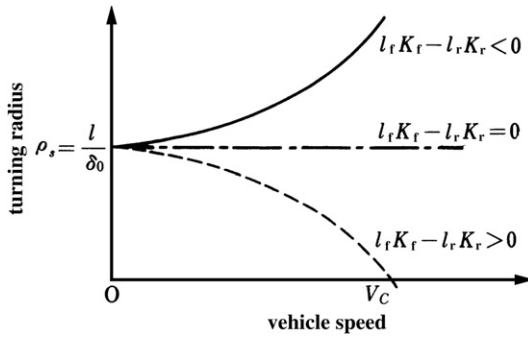
FIGURE 3.9 Relation of turning radius to vehicle speed with constant front wheel steer angle.

circular path, and make a circular path with an even smaller radius. These conditions are shown in Fig. 3.10.

When $l_f K_f - l_r K_r < 0$, if the steer angle is maintained, and the velocity increased, then there is insufficient steer angle to maintain the original circular path radius. This characteristic, where steer angle is insufficient with regards to increasing velocity, is called under-steer (below written as US). When $l_f K_f - l_r K_r > 0$, if the steer angle is maintained, and the velocity increased, there will be excessive steer angle to maintain the original circular path radius. This characteristic, where the steer angle is excessive with increasing velocity, is called over-steer (below written as OS). When $l_f K_f - l_r K_r = 0$, the radius is not dependant on velocity and the vehicle has neutral steer characteristics (below written as NS).

Next, let us study how the steer angle, δ, should be changed to maintain steady-state cornering, with a fixed radius, at different velocities. Taking $\rho = \rho_0$ (constant) in Eqn (3.29) gives:

$$\delta = \left(1 - \frac{m}{2l^2} \frac{l_f K_f - l_r K_r}{K_f K_r} V^2\right) \frac{l}{\rho_0} \qquad (3.38)$$

FIGURE 3.10 Change of turning radius with increase of vehicle speed.

This equation has exactly the same form as Eqn (3.37), and a typical relation between δ and V is shown in Fig. 3.11. For the vehicle to maintain a circular motion with a constant radius, a s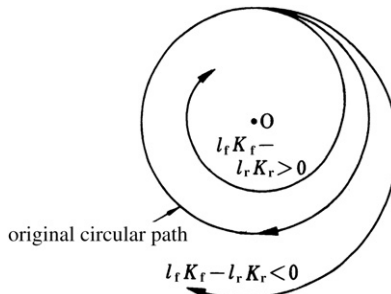teer angle, δ, must be added along with velocity if $l_f K_f - l_r K_r < 0$. When $l_f K_f - l_r K_r > 0$, the steer angle must be reduced with velocity and when $V = V_c$, $\delta = 0$. Furthermore, if $l_f K_f - l_r K_r = 0$, δ is not dependant on velocity.

When the forces, which are proportional to the side-slip angles, are the only lateral forces acting on the front and rear wheels, the vehicle circular motion is greatly influenced by $l_f K_f - l_r K_r$. The vehicle with $l_f K_f - l_r K_r < 0$ has US characteristics; the vehicle with $l_f K_f - l_r K_r = 0$ has NS characteristics, and the vehicle with $l_f K_f - l_r K_r > 0$ has OS characteristics. US, NS, and OS are generally called the steer characteristics.

Next is to study how the yaw velocity, r, of the steady-state cornering changes with vehicle steer characteristics. The yaw velocity is given by Eqn (3.30). From this equation, the relationship between r and V, for steady-state cornering with constant steer angle, is written as below:

$$r = \frac{1}{1 - \frac{m}{2l^2} \frac{l_f K_f - l_r K_r}{K_f K_r} V^2} \frac{V}{l} \delta_0 \tag{3.39}$$

Using this equation, the qualitative relation between r and V can be plotted, as in Fig. 3.12.

The yaw velocity of the vehicle with NS characteristics increases linearly with the vehicle velocity as shown in Fig. 3.12 and Eqn (3.39). If the vehicle had US characteristics, the yaw velocity also increases with the vehicle velocity, but
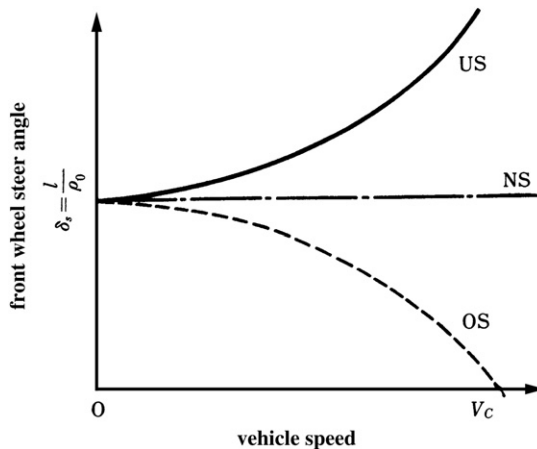
FIGURE 3.11 Front wheel steer angle due to vehicle speed with constant turning radius.
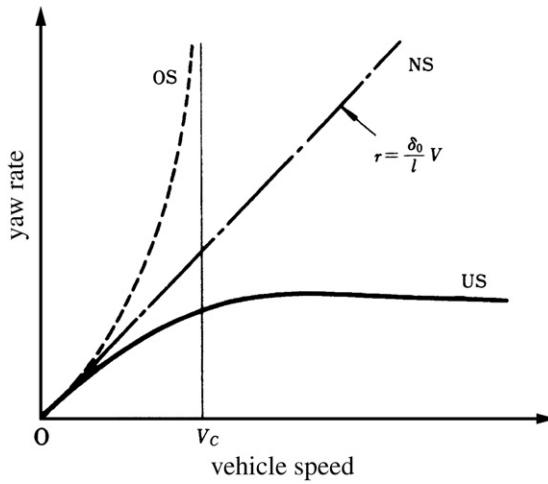
FIGURE 3.12 Steady-state yaw rate to vehicle speed.

saturates at a certain value. In the case of OS, the yaw velocity increases rapidly with the vehicle velocity and becomes infinite at $V = V_c$.

The next behavior to examine is how the side-slip angle, β, changes with velocity, V, for steady-state cornering. The side-slip angle β is given by Eqn (3.29). Taking $\delta = \delta_0$, the relationship between the side-slip angle and the velocity for steady-state cornering with constant steer angle is:

$$\beta = \left(\frac{1 - \frac{m}{2l} \frac{l_f}{l_r K_r} V^2}{1 - \frac{m}{2l^2} \frac{l_f K_f - l_r K_r}{K_f K_r} V^2} \right) \frac{l_r}{l} \delta_0 \tag{3.40}$$

The relationship between β and V, for different vehicle steer characteristics, is shown in Fig. 3.13.
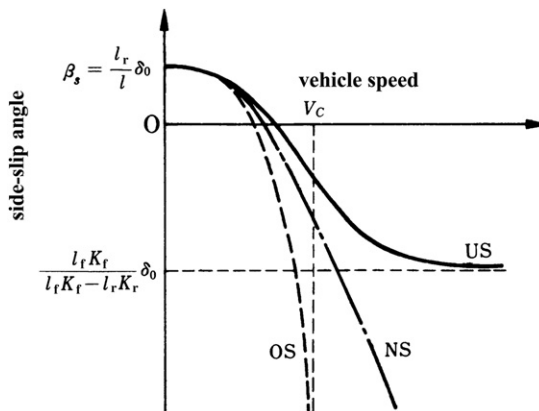
FIGURE 3.13 Steady-state side-slip angle due to vehicle speed.

Example 3.3

Calculate the steady-state cornering and draw the diagrams of $\rho - V$, $r - V$, and $\beta - V$ under vehicle parameters for a normal passenger car, given are: $m = 1500$ kg, $l_f = 1.1$ m, $l_r = 1.6$ m, $K_f = 55$ kN/rad, $K_r = 60$ kN/rad, and $\delta_0 = 0.04$ rad.

Solution

By using Eqns (3.37), (3.39), and (3.40) it is possible to draw the diagrams as shown in Fig. E3.3(a)–(c).
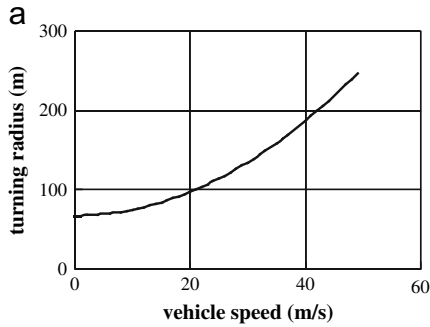
FIGURE E3.3(a).
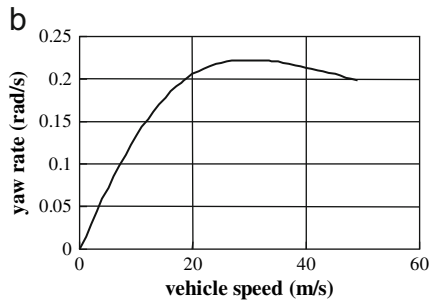
FIGURE E3.3(b).
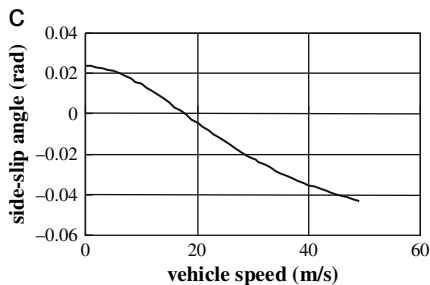
FIGURE E3.3(c).
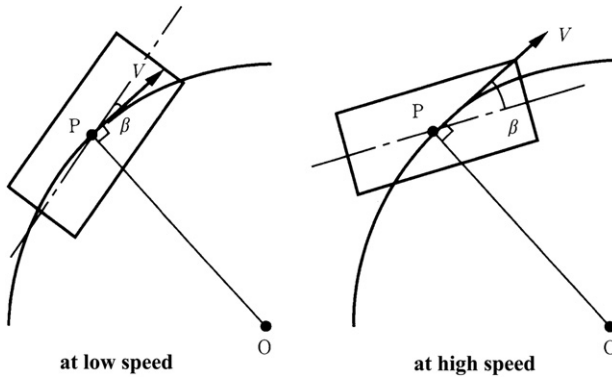
FIGURE 3.14 Vehicle attitude relative to circular path.

Figure 3.13 and Eqn (3.40) show that β decreases with vehicle velocity, regardless of the vehicle steer characteristics. After a certain velocity, β becomes negative and its absolute value increases continuously. If the vehicle exhibits US characteristics, β will reach a maximum value at larger velocities, and for OS characteristics, β becomes negative infinity at $V = V_c$. For vehicles with NS characteristics the quasi-static relations between the steer angle and the path radius or yaw velocity are maintained, regardless of velocity. The side-slip angle of the center of gravity, β, with NS, or $l_f K_f - l_r K_r = 0$, is:

$$\beta = \left(1 - \frac{ml_f}{2ll_r K_r}V^2\right)\frac{l_r}{l}\delta_0 \qquad (3.40)'$$

where β doesn't maintain a constant value of $(l_r/l)\delta_0$, but is proportional to V^2 and its absolute value increases. The vehicle side-slip angle, regardless of the vehicle steer characteristics, changes with velocity, due to the need of the lateral force to balance the centrifugal force. The vehicle side-slip angle is the angle between the vehicle longitudinal direction and the traveling direction of the vehicle center of gravity, i.e., the tangent line of the circular path. It shows the attitude of the vehicle in relation to the circular path during a steady-state cornering. The side-slip angle, β, becomes negative and its absolute magnitude increases with vehicle speed. This means that when the vehicle increases speed, the vehicle will point into the inner side of the circular path, as shown in Fig. 3.14. This tendency is even more obvious for vehicles with OS characteristics.

Example 3.4

Derive the equation, which describes the relation of side-slip angle to vehicle speed during steady-state turning with a constant turning radius. Draw the diagram of the relation qualitatively.
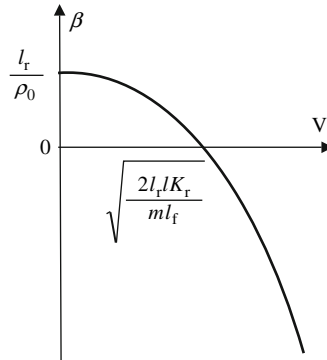
FIGURE E3.4.

Solution
The steer angle needed to turn with the constant radius, ρ_0, is expressed by Eqn (3.38). On the other hand, the side-slip angle during turning with the steer angle is given by Eqn (3.29). Eliminating δ from these two equations, the following equation is obtained:

$$\beta = \left(1 - \frac{ml_f}{2ll_rK_r}V^2\right)\frac{l_r}{\rho_0} \tag{E3.6}$$

This equation shows us how the side-slip angle changes with the vehicle speed during steady-state turning with constant turning radius, ρ_0. The qualitative relation is drawn in Fig. E3.4. It is interesting to see that there is no real difference in the side-slip angle due to the vehicle steer characteristics, US, OS, or NS.

(2) STABILITY LIMIT VELOCITY AND STABILITY FACTOR

When the vehicle has an OS characteristic, the circular turning radius, ρ, with regards to a constant steer angle becomes 0 when the vehicle velocity is $V = V_c$. Furthermore, the yaw angular velocity, r, and the side-slip angle, β, become infinity. When $V > V_c$, ρ, r, β are physically meaningless. V_c can be found from the following equation:

$$1 - \frac{m}{2l^2}\frac{l_fK_f - l_rK_r}{K_fK_r}V^2 = 0 \tag{3.41}$$

If $l_fK_f - l_rK_r > 0$, then the vehicle has an OS characteristic and a real value of the velocity that satisfies Eqn (3.41) exists

$$V_c = \sqrt{\frac{2lK_fK_r}{m(K_f + K_r)}\left(-\frac{1}{SM}\right)} \tag{3.42}$$

above this velocity, circular motion is no longer possible.

The critical velocity, V_c, becomes larger as $l_f K_f - l_r K_r$ reduces (as seen from Eqn (3.42)). It also increases with smaller vehicle mass, m, larger front and rear tire cornering stiffness, K_f, K_r, and a larger wheelbase, l.

When the vehicle has OS characteristics, it is important to note that the vehicle motion instability at $V \geq V_c$ depends on the front steer angle being fixed. It does not mean the vehicle cannot be driven above V_c, as this depends on the driver's ability. However, because the theoretical stability limit velocity exists, vehicle designers tend to avoid the OS characteristic, and it is rare to find a vehicle that is intentionally designed to have strong OS characteristic. If

$$A = -\frac{m}{2l^2} \frac{l_f K_f - l_r K_r}{K_f K_r} \tag{3.43}$$

Eqn (3.41) becomes:

$$1 + AV^2 = 0 \tag{3.41)'}$$

if $A < 0$, V_c can be written as:

$$V_c = \sqrt{-\frac{1}{A}} \tag{3.42)'}$$

Here, A is called the stability factor.

Using the stability factor, the relationship between β, r, ρ, and δ, during steady-state cornering, can be written as:

$$\beta = \frac{1 - \frac{m}{2l} \frac{l_f}{l_r K_r} V^2}{1 + AV^2} \frac{l_r}{l} \delta \tag{3.29)''}$$

$$r = \frac{1}{1 + AV^2} \frac{V}{l} \delta \tag{3.30)''}$$

$$\rho = (1 + AV^2) \frac{l}{\delta} \tag{3.31)''}$$

The sign of stability factor controls the vehicle steer characteristics. It is an important quantity that becomes the index of the degree of change in steady-state cornering due to vehicle velocity. In particular, the vehicle steady-state cornering is proportional to V^2, with the coefficient A. A is called the US/OS gradient.

As can be seen from Eqn (3.43), while the sign of $l_f K_f - l_r K_r$ influences the effect of velocity, a larger vehicle mass, m, smaller wheelbase, l, or smaller cornering stiffness, K_f, K_r, also increases the effect of V.

(3) STATIC MARGIN AND NEUTRAL STEER POINT

The vehicle steer characteristics, determined by the sign of $l_f K_f - l_r K_r$, have a fundamental influence on vehicle steady-state cornering. It is understood that the concept of US, NS, and OS is extremely important in the discussion of vehicle dynamic performance. More details about the physical meaning of the quantity of $l_f K_f - l_r K_r$ will be investigated.

Imagine the vehicle has the original condition $\delta = 0$, but for certain reasons, a side-slip angle at the vehicle center of gravity, β, is produced. The same side-slip angle is produced at the front and rear wheels, and lateral forces will be generated at the tires. These lateral forces produce a yaw moment around the center of gravity. The yaw motion due to this moment, based on Eqn (3.13), becomes:

$$I\frac{dr}{dt} + \frac{2(l_f^2 K_f + l_r^2 K_r)}{V}r = -2(l_f K_f - l_r K_r)\beta$$

If β is positive and $l_f K_f - l_r K_r$ is positive, a moment that produces negative r acts around the center of gravity. If $l_f K_f - l_r K_r = 0$, there is no moment acting, and if $l_f K_f - l_r K_r$ is negative, a moment that produces positive r acts around the center of gravity. In other words, if $l_f K_f - l_r K_r$ is positive, then the resultant force of the lateral forces at the front and rear wheels acts in front of the center of gravity, whereas if $l_f K_f - l_r K_r = 0$, then it acts at the center of gravity, and if $l_f K_f - l_r K_r$ is negative, it acts behind the center of gravity. This acting point of the resultant force is called the neutral steer point (below written as NSP).

If the center of gravity has a side-slip angle of β, the lateral force acting on the front and rear wheels will be $2K_f\beta$ and $2K_r\beta$. Taking the distance of NSP from the vehicle center of gravity as l_N, as shown in Fig. 3.15, the moment by $2K_f\beta$ and $2K_r\beta$ around NSP must be balanced.

$$(l_f + l_N)2K_f\beta = (l_r - l_N)2K_r\beta$$
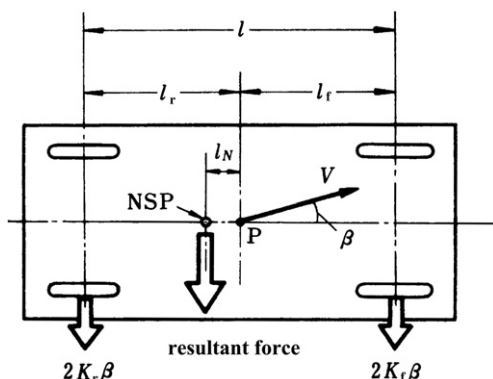
FIGURE 3.15 Resultant force of tire lateral forces due to vehicle side slip.

From this,

$$l_N = -\frac{l_f K_f - l_r K_r}{K_f + K_r} \tag{3.44}$$

NSP is in front of the center of gravity when $l_f K_f - l_r K_r$ is positive, and when $l_f K_f - l_r K_r$ is negative, it is behind the center of gravity. When $l_f K_f - l_r K_r = 0$, the NSP coincides with the center of gravity.

The dimensionless quantity of the ratio of l_N to wheelbase, l, is called the static margin (below written as SM).

$$SM = \frac{l_N}{l} = -\frac{l_f K_f - l_r K_r}{l(K_f + K_r)} \tag{3.45}$$

or transforming Eqn (3.45), it can also be written as:

$$SM = -\frac{l_f}{l} + \frac{K_r}{K_f + K_r} \tag{3.45}'$$

From the above, the quantity of $l_f K_f - l_r K_r$, which determines the vehicle steer characteristics, can be rewritten in the form of static margin, SM. The vehicle steer characteristic is defined as below using the SM.

when SM > 0, then US,
when SM = 0, then NS,   and
when SM < 0, then OS.

Moreover, if the stability limit velocity, V_c, is expressed using the term SM,

$$V_c = \sqrt{\frac{2l K_f K_r}{m(K_f + K_r)}\left(-\frac{1}{SM}\right)} \tag{3.42}''$$

And expressing stability factor, A, using SM,

$$A = \frac{m}{2l}\frac{K_f + K_r}{K_f K_r} SM \tag{3.43}'$$

(4) STEER CHARACTERISTICS AND GEOMETRY

The vehicle steady-state cornering characteristics have been studied by using equations that are derived from the fundamental equations of motion. These equations are introduced only for the case where the lateral tire forces are proportional to the side-slip angle.

Next, the vehicle steady-state cornering characteristics will be studied from a more practical viewpoint, using equations that express the steady-state cornering geometrically, without the constraints described above.

The relation between circular turning radius, ρ, to steer angle, β_f, β_r, is derived from the geometrical description of steady-state cornering and is given by Eqn (3.34)

$$\rho = \frac{l}{\delta - \beta_f + \beta_r} \qquad (3.34)$$

As seen from this equation, the relation between ρ and β_f, β_r depends on the magnitude of the wheel slip angles, β_f and β_r

When $\beta_f - \beta_r > 0$, then $\rho > \dfrac{l}{\delta}$, $\delta > \dfrac{l}{\rho}$.

When $\beta_f - \beta_r = 0$, then $\rho = \dfrac{l}{\delta}$, $\delta = \dfrac{l}{\rho}$.

When $\beta_f - \beta_r < 0$, then $\rho < \dfrac{l}{\delta}$, $\delta < \dfrac{l}{\rho}$.

In other words, if the relationship between the vehicle front and rear wheel side-slip angles is $\beta_f > \beta_r$, then the turning radius becomes larger in response to the vehicle speed with constant steer angle and more steer angle is needed to maintain the original radius. If $\beta_f = \beta_r$, then the turning radius and steer angle do not depend on vehicle speed. If $\beta_f < \beta_r$, then the radius becomes smaller as vehicle speed increases with the steer angle constant. The steer angle must be reduced to maintain the original radius. Therefore, the vehicle steer characteristic could be defined as:

When $\beta_f > \beta_r$, then US,
When $\beta_f = \beta_r$, then NS, and
When $\beta_f < \beta_r$, then OS.

This definition is not influenced by other lateral forces acting on the front and rear wheels than the tire lateral force due to side-slip, or if the lateral forces are proportional to the side-slip angle or not. Figure 3.16 shows how the vehicle circular motion, under constant steer action, changes with the relationship between β_f and β_r.
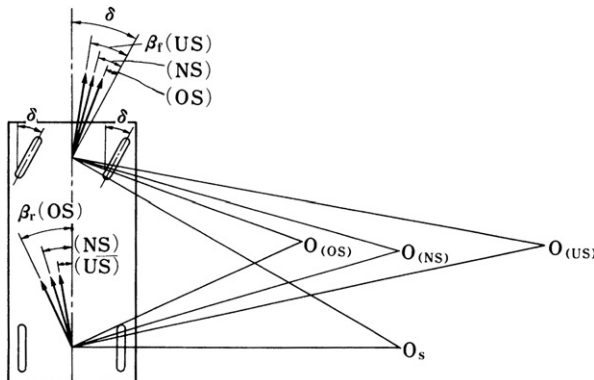

FIGURE 3.16 Side-slip angles of front and rear wheels in steady-state turning.

The figure also shows that the radius for a vehicle with US characteristics and $\beta_f > \beta_r$, is larger than l/δ, whereas for an NS characteristic, with $\beta_f = \beta_r$, the radius is equal to l/δ, and for an OS characteristic with $\beta_f < \beta_r$, it is smaller than l/δ. Furthermore, β_f and β_r increase with an increase in vehicle speed, regardless of the steer characteristics of the vehicle. This results in the circular motion center moving toward the front of the vehicle. Consequently, with increasing speed, the vehicle moves inward of the circular path. This tendency is even more obvious for the vehicle with OS characteristics.

Through the study of the vehicle US and OS by the sign of $\beta_f - \beta_r$, the physical meaning of vehicle steer characteristic by the sign of $l_f K_f - l_r K_r$ in Eqns (3.37) and (3.38) can be well understood. If the lateral force that acts on the front and rear wheels during the steady-state cornering is proportional to β_f, β_r, then from Eqns (3.31) and (3.34)

$$\frac{\rho}{l}(\beta_f - \beta_r) = -\frac{m}{2l^2}\frac{l_f K_f - l_r K_r}{K_f K_r}V^2 = AV^2 \qquad (3.46)$$

The definition of vehicle steer characteristic by $\beta_f - \beta_r$ and $l_f K_f - l_r K_r$ is consistent and $\rho(\beta_f - \beta_r)/(lV^2)$ is the quantity equivalent to stability factor, A.

Table 3.1 summarizes the relation between vehicle steer characteristics with the steady-state cornering.

3.3.3 Steady-state cornering and tire non-linear characteristics
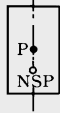
Subsection 3.3.2 studied the characteristics of vehicle steady-state cornering to give a basic understanding of the vehicle dynamics. It also looked at the vehicle steer characteristics, US, NS, and OS, as an important concept for describing a basic vehicle's dynamic characteristics. Previously, it was assumed that the lateral forces acting on the front and rear wheels are proportional to the side-slip angles. However, as seen in Chapter 2, the lateral force may not necessarily be proportional to the side-slip angle. In the case of larger side-slip angles and under certain other conditions, lateral forces may show non-linearity in its characteristics.

This subsection will examine the effect of non-linear tire characteristics on the vehicle steady-state cornering characteristics. If the vehicle is assumed to be in steady-state cornering with a lateral acceleration of

$$\ddot{y} = \frac{V^2}{\rho g} \qquad (3.47)$$

a centrifugal force of magnitude $m\ddot{y}g$ will act at the vehicle center of gravity, where g is the gravitational acceleration and $\ddot{y}$ has a gravitational unit for convenience sake. This has to be in equilibrium with the lateral forces acting

Table 3.1 Steer characteristics and steady-state turning.

$SM = \dfrac{-(l_f K_f - l_r K_r)}{l(K_f + K_r)}$		Relative position of NSP and CG	Effects of vehicle speed on steady-state turning				
			ρ (δ = const.)	δ (ρ = const.)	Yaw rate, r	Side-slip angles, β_f and β_r	Critical speed
US	>0	P• / NSP	Increases with speed	Increases with speed	Increases with speed to some extent and decreases	$\beta_f > \beta_r$	non
NS	=0	P / NSP	Constant $\rho = \dfrac{l}{\delta}$	Constant $\delta = \dfrac{l}{\rho}$	Proportional increase with speed	$\beta_f = \beta_r$	non
OS	<0	NSP / P•	Decreases with speed	Decreases with speed	Rapidly increases with speed	$\beta_f < \beta_r$	Constant $V_c = \sqrt{\dfrac{2K_f K_r l^2}{m(l_f K_f - l_r K_r)}}$

at the front and rear wheels, $2Y_f$, $2Y_r$ and the moment around the center of gravity should be zero. Thus,

$$m\ddot{y}g + 2Y_f + 2Y_r = 0$$
$$2l_f Y_f - 2l_r Y_r = 0$$

giving,

$$2Y_f = -mg\frac{l_r}{l}\ddot{y}$$

$$2Y_r = -mg\frac{l_f}{l}\ddot{y}$$

(3.48)

mgl_r/l and mgl_f/l are the vertical loads of the front and rear wheels. Taking the ratio of the lateral force to the vertical load at the front and rear wheels as μ_f, μ_r, respectively, from Eqn (3.48):

$$\mu_f = \frac{|2Y_f|}{mgl_r/l} = \ddot{y}, \; \mu_r = \frac{|2Y_r|}{mgl_f/l} = \ddot{y}$$

(3.49)

This means that during steady-state cornering, the lateral force at the front and rear wheels divided by their respective vertical loads is always equal to the lateral acceleration of the center of gravity, $\ddot{y}$.

Assuming the lateral force produced by the tire side-slip angles is the only lateral force, then μ_f, μ_r depend only on β_f, β_r. From Eqn (3.49), the tire cornering characteristics of the front and rear wheels ($\beta_f - \mu_f$ and $\beta_r - \mu_r$) become clear. If the lateral acceleration of the vehicle center of gravity, $\ddot{y}$, is known, the front and rear wheels' side-slip angles, β_f, β_r, at that instant can be found.

For vehicle steady-state cornering, regardless of whether lateral force acting at the front and rear wheels is proportional to the side-slip angle or not,

$$\rho = \frac{l}{\delta - \beta_f + \beta_r}$$

(3.50)

If the tire cornering characteristic is linear,

$$2Y_f = -2K_f\beta_f$$

$$2Y_r = -2K_r\beta_r$$

From Eqn (3.48)

$$\beta_f = \frac{mgl_r}{2K_f l}\ddot{y}$$

$$\beta_r = \frac{mgl_f}{2K_r l}\ddot{y}$$

This is the same discussion as at the end of subsection 3.3.1 (2). Substituting these into Eqn (3.50) gives:

$$\delta = \frac{l}{\rho} - \frac{mg(l_f K_f - l_r K_r)}{2K_f K_r l} \ddot{y} \tag{3.51}$$

Therefore, the relation between lateral acceleration, $\ddot{y}$, and the required steer angle for a given radius, $\rho = \rho_0$, of the circular motion, is:

$$\delta = \frac{l}{\rho_0} - \frac{mg(l_f K_f - l_r K_r)}{2K_f K_r l} \ddot{y} \tag{3.51'}$$

If the circular motion is at a constant speed of $V = V_0$, Eqn (3.47) yields:

$$\rho = \frac{V_0^2}{\ddot{y}g}$$

The relation between the lateral acceleration, $\ddot{y}$, and the required steer angle, δ, from Eqn (3.51)', is:

$$\delta = \left[\frac{gl}{V_0^2} - \frac{mg(l_f K_f - l_r K_r)}{2K_f K_r l} \right] \ddot{y} \tag{3.51''}$$

Using Eqns (3.51)' and (3.51)'', the qualitative relation between $\ddot{y}$ and δ during steady-state cornering, when the tire cornering characteristic is linear, will look like Fig. 3.17.

When the tire cornering characteristic is not linear, the front and rear tire cornering characteristics, $\beta_f - \mu_f$ and $\beta_r - \mu_r$, are shown in Fig. 3.18. As seen previously, if the vehicle is in steady-state cornering, the lateral acceleration, $\ddot{y}$, is equal to μ_f, μ_r. Thus, by knowing the lateral acceleration, $\ddot{y}$, the front and rear wheel side-slip angles, β_f, β_r, at that instant are known, and $\beta_f - \beta_r$ can be determined.
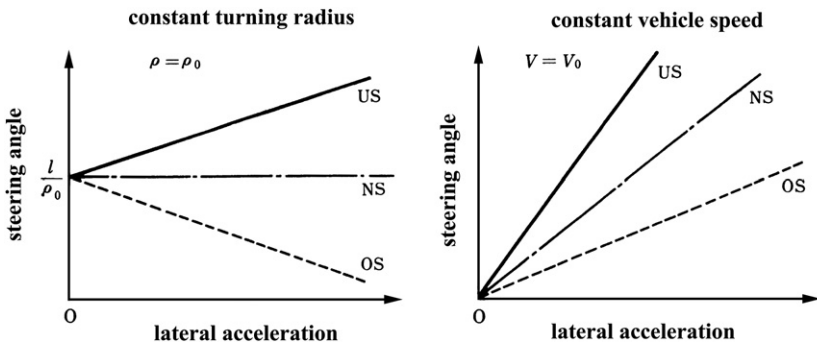
FIGURE 3.17 Required steering angle due to lateral acceleration for a linear tire vehicle.
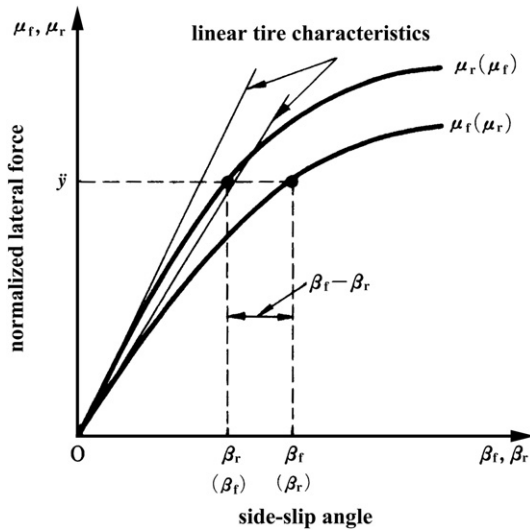
FIGURE 3.18 Non-linear tire characteristics of front and rear.

From Eqn (3.50), if the constant radius of the circular motion is ρ_0, then

$$\delta = \frac{l}{\rho_0} + \beta_f - \beta_r \tag{3.52}$$

By knowing $\ddot{y}$, and determining $\beta_f - \beta_r$ from Fig. 3.18, the relation between lateral acceleration, $\ddot{y}$, and steer angle, δ, can be plotted for constant radius circular motion, as in Fig. 3.19.

If $\mu_f < \mu_r$ with regard to tire side-slip angle, the vehicle shows US characteristics because $\beta_f > \beta_r$. If $\mu_f = \mu_r$ then $\beta_f = \beta_r$, the vehicle characteristic is
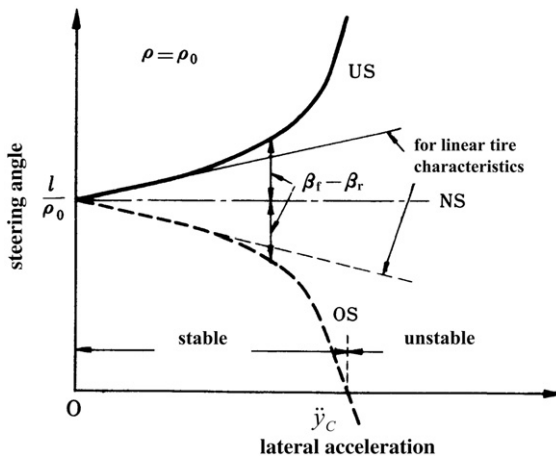
FIGURE 3.19 Steering angle due to lateral acceleration under constant turning radius.

therefore NS. Whereas if $\mu_f > \mu_r$ then $\beta_f < \beta_r$ and the vehicle characteristic becomes OS.

For the case when the vehicle characteristic is US in Fig. 3.18, if $\ddot{y}$ is small and the side-slip angles are small, $\beta_f - \beta_r$ is positive, and its value increases almost proportionally to $\ddot{y}$. Here, $\ddot{y}$ could also be assumed to be proportional to δ. When $\ddot{y}$ is greater than a certain value, $\beta_f - \beta_r$ is no longer proportional to $\ddot{y}$, and increases rapidly with $\ddot{y}$. Consequently, δ also increases rapidly with $\ddot{y}$, and the vehicle shows a strong US characteristic. On the contrary to this, for the case when vehicle characteristic is OS, when $\ddot{y}$ is small, $\beta_f - \beta_r$ is negative, and the value increases almost proportionally to $\ddot{y}$. Thus, δ also decreases proportionally to $\ddot{y}$. When $\ddot{y}$ is greater than a certain value, $\beta_f - \beta_r$ increases rapidly with $\ddot{y}$, and the vehicle shows a strong OS characteristic.

For the case of OS, δ decreases rapidly with large $\ddot{y}$. At $\ddot{y} = \ddot{y}_c$, $\delta = 0$. This point defines the limit where under steady-state cornering, with constant radius, ρ_0, it is not possible to increase the lateral acceleration by raising the velocity. This $\ddot{y}$ is considerably smaller than the case where the tire cornering characteristic is linear. The tire non-linear cornering characteristic further reduces the critical velocity for the OS vehicle. Chapter 2 showed that in practice, a lateral force saturates after a certain side-slip angle. It is important to note that the vehicle with OS characteristics becomes unstable at lower speeds than that with a linear characteristic. This velocity limit for circular motion is dependant on the radius of the circular motion, which is different from that for a linear tire characteristic.

Consider the case when the vehicle is making a circular motion with a constant speed of $V = V_0$. Here, $\rho = V_0^2/\ddot{y}g$, and the relation between lateral acceleration, $\ddot{y}$ and required steer angle δ, from Eqn (3.50), is:

$$\delta = \frac{gl}{V_0^2}\ddot{y} + \beta_f - \beta_r \qquad (3.53)$$

The value of $\beta_f - \beta_r$ can again be determined from Fig. 3.18, by knowing $\ddot{y}$. Using Eqn (3.53), the relationship between steer angle, δ, and lateral acceleration, $\ddot{y}$, during constant speed circular motion, is shown in Fig. 3.20.

This figure shows that an US vehicle, with $\ddot{y}$ small, has δ increasing almost proportionally to $\ddot{y}$. After $\ddot{y}$ reaches a certain value, δ increases rapidly with $\ddot{y}$ and the vehicle reveals a strong US characteristic.

On the contrary to this, for the case of OS, when $\ddot{y}$ is small, δ increases almost proportionally to $\ddot{y}$, but after $\ddot{y}$ reaches a certain value, the increase of δ with $\ddot{y}$ becomes weaker, and finally, when $\ddot{y} = \ddot{y}_c$, δ reaches its peak. When $\ddot{y}$ is greater than $\ddot{y}_c$, δ decreases. This reduction of δ decreases the turning radius at a constant speed. This means that when the vehicle is about to move to the right with regard to its current traveling direction, the steering should be turned to the left. This is impossible and has no physical meaning in practice. This point shows that circular motion with a radius that causes $\ddot{y} = \ddot{y}_c$ and the motion with smaller radius is not possible. For an OS vehicle there is always a lower limit to the cornering radius possible, regardless of vehicle speed. Furthermore, $\ddot{y}_c$ at
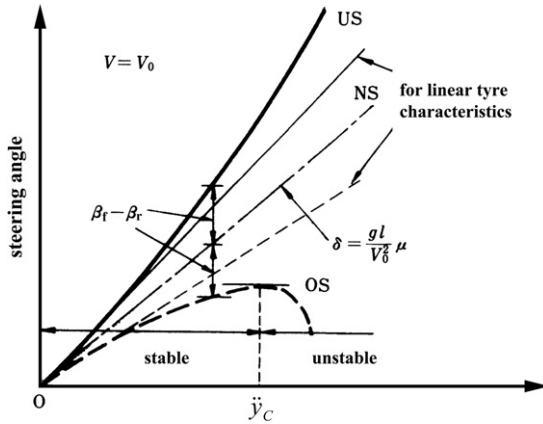
FIGURE 3.20 Steering angle due to lateral acceleration under constant vehicle speed.

constant turning radius, as shown in Fig. 3.19, has the same meaning as $\ddot{y}_c$ for the constant speed shown in Fig. 3.20.

The front and rear wheels' tire cornering characteristic shown in Fig. 3.18 is always either $\mu_f > \mu_r$ or $\mu_f < \mu_r$ for the whole range of side-slip angles. This is not always the case and depends on circumstances.

Consider the front and rear wheel tire cornering characteristics, $\beta_f - \mu_f$ and $\beta_r - \mu_r$, as shown in Fig. 3.21. (A) is the case where if β_f and β_r are smaller than β_p, then $\mu_f < \mu_r$; and if β_f and β_r are larger than β_p, then $\mu_f > \mu_r$. In contrast, (B) is the case where if β_f and β_r are smaller than β_p, then $\mu_f > \mu_r$; and if β_f and β_r are larger than β_p then $\mu_f < \mu_r$.

If the vehicle is making a circular motion of constant radius, ρ_0, Eqn (3.52) is formed as previously. By knowing the lateral acceleration, $\ddot{y}, \beta_f - \beta_r$ can be
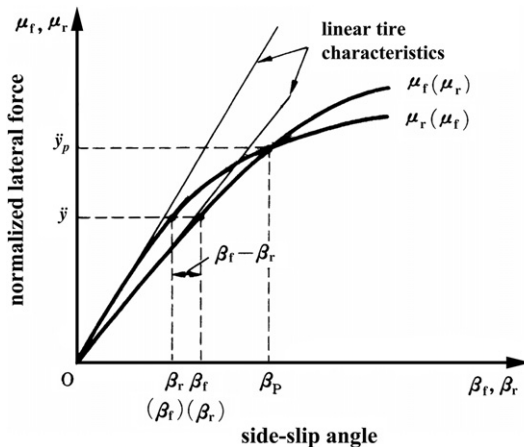
FIGURE 3.21 Non-linear tire characteristics of front and rear.

determined from Fig. 3.21 and using Eqn (3.52), the relationship between steer angle, δ, and lateral acceleration, $\ddot{y}$, during constant radius circular motion is seen in Fig. 3.22.

In the case of (A), when $\ddot{y}$ is small, $\beta_f - \beta_r$ increases with $\ddot{y}$, δ also increases and the vehicle shows an US characteristic. After $\ddot{y}$ reaches a certain value, with the increase of $\ddot{y}$, $\beta_f - \beta_r$ decreases, and at $\ddot{y} = \ddot{y}_p$, the value becomes 0. As $\ddot{y} > \ddot{y}_p$, $\beta_f - \beta_r$ decreases rapidly with $\ddot{y}$ and the vehicle reveals an OS characteristic. This tendency continues to increase with $\ddot{y}$, and at $\ddot{y} = \ddot{y}_c$, $\delta = 0$. This point, like in Fig. 3.19, shows that it is impossible to have circular motion with higher lateral acceleration with radius ρ_0.

In the case of (B), when $\ddot{y}$ is small, δ decreases with $\ddot{y}$, and the vehicle shows OS characteristic. After $\ddot{y}$ reaches a certain value, δ increases with $\ddot{y}$, and at $\ddot{y} = \ddot{y}_p$, the value returns to l/ρ_0. At $\ddot{y} > \ddot{y}_p$, δ increases rapidly, and the vehicle reveals a strong US characteristic.

If the vehicle is making a circular motion with a constant speed of $V = V_0$, Eqn (3.53) is formed. Therefore, by knowing the lateral acceleration, $\ddot{y}$, $\beta_f - \beta_r$ can be determined from Fig. 3.21 and using Eqn (3.53), the relationship between steer angle, δ, and lateral acceleration, $\ddot{y}$, during circular motion under constant speed is shown in Fig. 3.23.

In the case of (A), at small $\ddot{y}$, the vehicle shows an US characteristic, but at large $\ddot{y}$, the vehicle characteristic changes to OS. Circular motion with a radius that causes $\ddot{y} = \ddot{y}_c$ becomes impossible. (B) is opposite to (A), where $\ddot{y}$ becomes larger, and the vehicle shows an US characteristic.

As seen in case (A), the vehicle has an US characteristic at small lateral acceleration, $\ddot{y}$, but when $\ddot{y}$ gets large, the steer characteristic changes to OS due to the non-linear tire characteristic, and circular motion becomes impossible after a certain velocity. While there is no critical velocity based on the concept of linear tire, the stable vehicle might fall into a statically unstable condition during circular motion at larger lateral accelerations. As shown by Figs 3.22 and 3.23, the change of steer characteristic due to $\ddot{y}$ is called the reverse-steer.
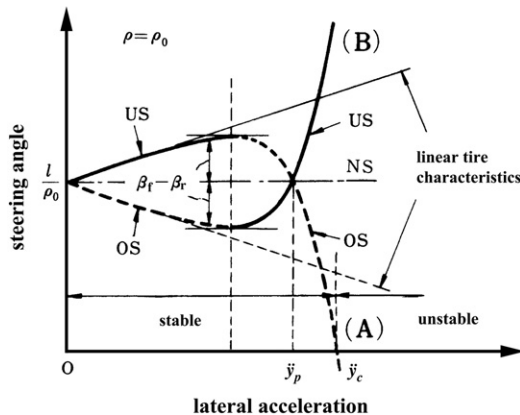
FIGURE 3.22 Steering angle due to lateral acceleration under constant turning radius.
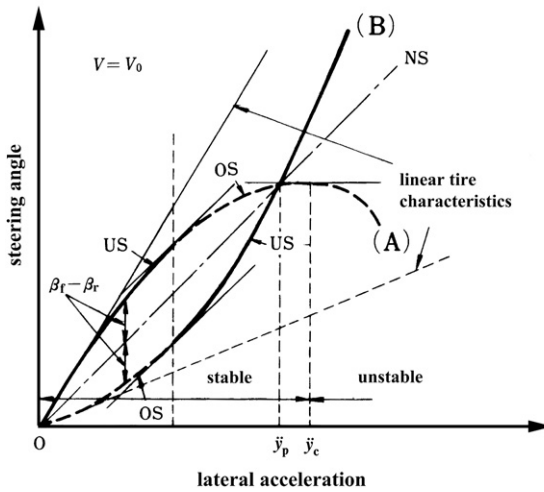
FIGURE 3.23 Steering angle due to lateral acceleration under constant vehicle speed.

Figures 3.22 and 3.23 also show that in case (B), when the lateral acceleration gets larger, the vehicle exhibits a strong US characteristic and, no matter how large the steer angle is, circular motion with lateral acceleration beyond a certain point is impossible. This condition is called vehicle drift. In the case of (A), the condition where the vehicle shows a strong OS characteristic and becomes statically unstable is called the vehicle spin.

3.4 VEHICLE DYNAMIC CHARACTERISTICS

Section 3.3 examined the basic characteristics of vehicle motion by looking at the vehicle steady-state cornering. The results obtained so far can only be classified as the static characteristics, in other words, the characteristics of the vehicle motion in steady state. To understand the characteristics of vehicle motion in more detail, the dynamic characteristics must be examined as well.

Thus, continuing from here, the vehicle's transient response to steer input will be analyzed from different points of view to further understand the fundamental characteristics of the vehicle motion.

3.4.1 Vehicle transient response to steer input [1]

(1) TRANSIENT RESPONSE AND DIRECTIONAL STABILITY

The basic equations that describe the vehicle motion are defined in Eqns (3.12) and (3.13), Section 3.2, as:

$$mV\frac{d\beta}{dt} + 2(K_f + K_r)\beta + \left\{mV + \frac{2}{V}(l_fK_f - l_rK_r)\right\}r = 2K_f\delta \qquad (3.12)$$

$$2(l_f K_f - l_r K_r)\beta + I\frac{dr}{dt} + \frac{2(l_f^2 K_f + l_r^2 K_r)}{V}r = 2l_f K_f \delta \qquad (3.13)$$

Once the equations of motion of a dynamic system, such as (3.12) and (3.13), are given, the vehicle response to δ can be obtained by solving the equations of motion under suitable conditions. If the system is linear, the transient behavior of the dynamic system can be understood by solving the equations of motion directly, or investigating the eigenvalues of the characteristic equation.

The characteristic equation of the dynamic system that is our subject of study is given by Eqn (3.14):

$$s^2 + \left[\frac{2m(l_f^2 K_f + l_r^2 K_r) + 2I(K_f + K_r)}{mIV}\right]s + \left[\frac{4K_f K_r l^2}{mIV^2} - \frac{2(l_f K_f - l_r K_r)}{I}\right] = 0$$
$$(3.54)$$

or,

$$s^2 + 2Ds + P^2 = 0 \qquad (3.55)$$

where

$$2D = \frac{2m(l_f^2 K_f + l_r^2 K_r) + 2I(K_f + K_r)}{mIV} \qquad (3.56)$$

$$P^2 = \frac{4K_f K_r l^2}{mIV^2} - \frac{2(l_f K_f - l_r K_r)}{I} \qquad (3.57)$$

And, the vehicle yaw inertia moment could be written as:

$$I = mk^2 \qquad (3.58)$$

here, k is called the vehicle yaw moment radius. Substituting Eqn (3.58) into Eqn (3.56), $2D$ could be written as following:

$$2D = \frac{2}{mV}\left[(K_f + K_r)\left(\frac{1 + k^2/l_f l_r}{k^2/l_f l_r}\right) + \frac{1}{k^2}(l_f - l_r)(l_f K_f - l_r K_r)\right] \qquad (3.56)'$$

and if $l_f \approx l_r$, $K_f \approx K_r$,

$$2D = \frac{2(K_f + K_r)}{mV}\left(\frac{1 + k^2/l_f l_r}{k^2/l_f l_r}\right) \qquad (3.56)''$$

then, substituting Eqn (3.58) into Eqn (3.57), P^2 could be written as following:

$$P^2 = \frac{4K_f K_r l^2}{m^2 k^2 V^2}\left(1 - \frac{m}{2l^2}\frac{l_f K_f - l_r K_r}{K_f K_r}V^2\right) \qquad (3.57)'$$

Now, the response of the system with the characteristic equation given by Eqn (3.55) is expressed by $C_1 e^{\lambda_1 t} + C_2 e^{\lambda_2 t}$, with λ_1 and λ_2 as the roots of the characteristic equation:

$$\lambda_{1,2} = -D \pm \sqrt{D^2 - P^2} \tag{3.59}$$

The transient response characteristics and stability of the system are dependant on whether λ_1 and λ_2 are integers or complex numbers, and the sign of λ_1, λ_2 if they are integers, or the sign of the real part of λ_1, λ_2 if they are complex numbers. Based on Eqn (3.59), the value of λ_1, λ_2 is dependant on D and P. From Eqn (3.55), it is apparent that $D > 0$ and the transient response characteristic and motion stability of the vehicle can be classified into the following categories based on D and P:

1. When $D^2 - P^2 \geq 0$, $P^2 > 0$ then λ_1, λ_2 are negative integers and motion converges without oscillation (stable).
2. When $D^2 - P^2 < 0$ then λ_1, λ_2 are complex numbers, the real part is negative and motion converges with oscillation (stable).
3. When $P^2 \leq 0$ then λ_1, λ_2 are positive and negative integers and motion diverges without oscillation (unstable).

This is under the premise that the steer of the vehicle is predetermined and not changeable in response to the vehicle behavior. It should be noted that the vehicle does not always show this behavior and the driver plays a key role in the vehicle stability. This situation not only applies to the vehicle motion, but also for ships and aircraft alike. The control of the motion by the driver (in some cases, control actuators) on board of the moving body itself is an important matter in studying the motion of the moving bodies (refer to Chapter 9 for a detailed approach).

Next, the response of the vehicle to steer input, which can be divided into three categories as above, is investigated. Also, the motion stability will be studied in more detail, and the type of vehicle, and of situation, that gives motion cases 1, 2, and 3 are investigated.

Firstly, case 3 is examined. From Eqn (3.57), the first term of P^2 is always positive, thus, for $P^2 \leq 0$, it is only the second term that can be negative, in other words, $l_f K_f - l_r K_r > 0$. Taking V_c as the velocity where $P^2 = 0$, from Eqn (3.57)':

$$1 - \frac{m}{2l^2} \frac{l_f K_f - l_r K_r}{K_f K_r} V_c^2 = 0 \tag{3.60}$$

hence,

$$V_c = \sqrt{\frac{2K_f K}{m(l_f K_f - l_r K_r)}} l = \sqrt{\frac{2l K_f K_r}{m(K_f + K_r)} \left(-\frac{1}{SM}\right)} \tag{3.61}$$
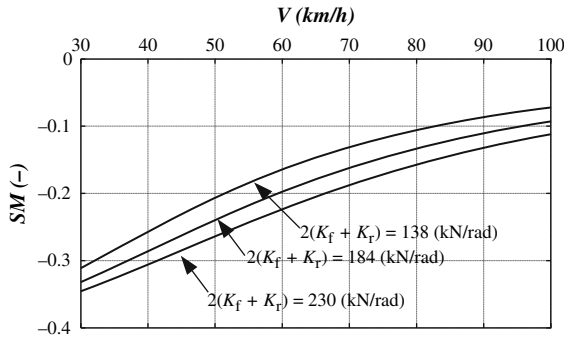
FIGURE 3.24 Relation of critical vehicle speed with SM.

Then, for all velocities greater than V_c, $P^2 \leq 0$. This is the condition for static instability of the mechanical system as described previously in subsection 3.3.2. When the vehicle shows OS characteristics, the vehicle lateral motion becomes unstable at velocity V_c, and diverges without oscillation in response to a fixed steer input. As could be seen clearly from Eqn (3.61), this stability limit is greatly dependant on the SM. Figure 3.24 shows the vehicle stability limit by SM and velocity, and shows that the smaller the absolute value of SM, and the larger the total cornering stiffness of the front and rear wheels is, the larger the stability limit velocity.

Example 3.5

It is obvious that the stability condition of the vehicle is described by:

$$1 - \frac{m}{2l^2} \frac{l_f K_f - l_r K_r}{K_f K_r} V^2 \geq 0$$

Show that there are upper and lower limits of the front and rear cornering stiffnesses, K_f and K_r, respectively, for the vehicle to be stable and draw the schematic diagram of the limits with respect to the vehicle speed.

Solution
The above inequality is rewritten as follows:

$$\frac{2l^2}{mV^2} - \frac{l_f}{K_r} + \frac{l_r}{K_f} \geq 0$$

It turns out to be a form of upper limit of the front cornering stiffness as:

$$K_f \leq \frac{l_r K_r}{l_f} \frac{V^2}{V^2 - \frac{2l^2 K_r}{m l_f}} \tag{E3.7}$$
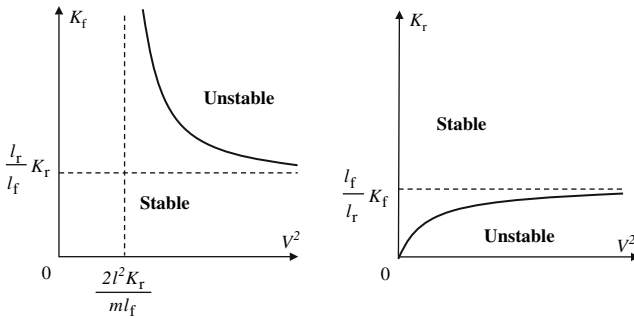
FIGURE E3.5.

and as the lower limit of the rear cornering stiffness, the following inequality is obtained:

$$K_r \geq \frac{l_f K_f}{l_r} \frac{V^2}{V^2 + \frac{2l^2 K_f}{m l_r}} \qquad \text{(E3.8)}$$

The schematic diagram of the upper and lower limits of the cornering stiffness with respect to vehicle speed is shown in Fig. E3.5.

Next, if $l_f K_f - l_r K_r < 0$, then the vehicle shows US characteristics, or if the vehicle reveals OS characteristic but $V < V_c$, then P^2 is always greater than 0 and the vehicle motion is stable. This corresponds to cases 1 and 2. Now, using Eqns (3.56) and (3.57), $D^2 - P^2$ is calculated as:

$$D^2 - P^2 = \frac{2(l_f K_f - l_r K_r)}{I} + \left[\left\{ \frac{m(l_f^2 K_f + l_r^2 K_r) + I(K_f + K_r)}{mI} \right\}^2 \right.$$

$$\left. - \frac{4 K_f K_r l^2}{mI} \right] \frac{1}{V^2} \qquad (3.62)$$

Transforming the coefficient of $1/V^2$ gives:

$$\left\{ \frac{m(l_f^2 K_f + l_r^2 K_r) - I(K_f + K_r)}{mI} \right\}^2 + \frac{4(l_f K_f - l_r K_r)^2}{mI} > 0 \qquad (3.63)$$

Since the coefficient of $1/V^2$ of Eqn (3.62) is always positive, if the first term $l_f K_f - l_r K_r$ is positive or 0, then, $D^2 - P^2$ is also positive or 0. Hence, if the vehicle steer characteristic is OS or NS, the vehicle transient steer response will always be without oscillation, stable or not. When $l_f K_f - l_r K_r$ is negative, the value of $D^2 - P^2$ is dependant on V, where above a certain value, $D^2 - P^2$ changes from positive to negative. In other words, when the vehicle shows US characteristics, the vehicle transient steer response is without oscillation at vehicle speed lower than a certain value, but beyond that, the response becomes oscillatory.

Using Eqns (3.45) and (3.58), and assuming that $l_f \approx l_r$ and $K_f \approx K_r$, then $D^2 - P^2$ can be calculated by transforming Eqn (3.62),

$$D^2 - P^2 = \frac{2(l_f K_f - l_r K_r)}{mk^2} + \left[\frac{(K_f + K_r)^2}{m^2}\left(\frac{1 - k^2/l_f l_r}{k^2/l_f l_r}\right)^2\right.$$

$$+ \left.\frac{4(l_f K_f - l_r K_r)^2}{m^2 k^2}\right]\frac{1}{V^2} \approx \frac{(K_f + K_r)^2}{m^2}\left[-\frac{l_f l_r}{k^2}\frac{8m}{l(K_f + K_r)}SM\right.$$

$$+ \left.\left\{\left(\frac{1 - k^2/l_f l_r}{k^2/l_f l_r}\right)^2 + \frac{16 l_f l_r}{k^2}SM^2\right\}\frac{1}{V^2}\right]$$

$$(3.62)'$$

From this equation, if SM > 0, i.e., the vehicle has US characteristics, the velocity, V_s, where vehicle transient steer response becomes oscillatory is:

$$V_s = \sqrt{\frac{2l(K_f + K_r)}{m}\left\{\frac{1}{16}\frac{(1 - k^2/l_f l_r)^2}{k^2/l_f l_r}\frac{1}{SM} + SM\right\}} \qquad (3.64)$$

In this equation V_s is affected by $k^2/l_f l_r$. From Eqn (3.64), when $k^2/l_f l_r = 1$, V_s is minimum and if $k^2/l_f l_r$ is greater or smaller than this, V_s always becomes larger. It is interesting to see that when the vehicle yaw moment inertia is larger or smaller than a certain value, the speed where vehicle transient steer response becomes oscillatory always becomes larger.

This analysis has shown that the characteristics of a vehicle's transient response to steer is particularly affected by the vehicle traveling speed and steer characteristics. This is shown in . The stability problem of the vehicle

Table 3.2 Vehicle steer characteristic and transient responses.

steer character-istics	transient response		
US	$0 \le V \le V_S$	② dumping with oscillation $V \ge V_S$	
NS	① dumping without oscillation		
OS	$0 \le V \le V_C$		③ diverge $V \ge V_C$
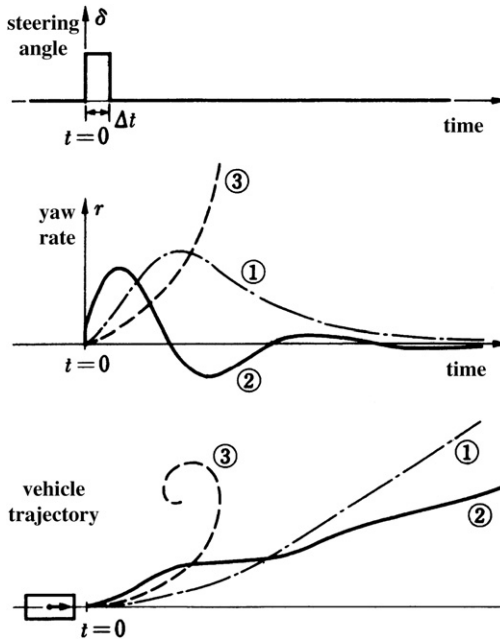
FIGURE 3.25 Qualitative understanding of vehicle transient responses.

motion, as shown in the table, is called the vehicle directional stability. The image of the vehicle response to a step steer input is shown in Fig. 3.25. The motion response characteristic corresponding to 1, 2, and 3 in Table 3.2 is clear.

(2) NATURAL FREQUENCY AND DAMPING RATIO

Here, the natural frequency and damping ratio of the vehicle response to steer input will be studied. Taking ω_n as the natural frequency, and ζ as the damping ratio, from the characteristic equation coefficients,

$$\omega_n^2 = P^2 \tag{3.65}$$

$$2\zeta\omega_n = 2D \tag{3.66}$$

using Eqns (3.56), (3.57), and (3.43), ω_n and ζ are:

$$\omega_n = P = \frac{2l}{V}\frac{\sqrt{K_f K_r}}{\sqrt{mI}}\sqrt{1 + AV^2} = \frac{2\sqrt{K_f K_r}l}{mk}\frac{\sqrt{1 + AV^2}}{V}$$

$$= \frac{2\sqrt{K_f K_r}l}{mk}\frac{1}{V}\sqrt{1 + \frac{m}{2l}\left(\frac{K_f + K_r}{K_f K_r}\right)SMV^2} \tag{3.67}$$

$$\zeta = \frac{D}{P} = \frac{m(l_f^2 K_f + l_r^2 K_r) + I(K_f + K_r)}{2l\sqrt{mIK_f K_r(1 + AV^2)}}$$

$$= \frac{K_f + K_r}{2\sqrt{K_f K_r}} \frac{k}{l} \frac{\left(\frac{1 + k^2/l_f l_r}{k^2/l_f l_r}\right) + \frac{1}{k^2}\frac{(l_f - l_r)(l_f K_f - l_r K_r)}{K_f + K_r}}{\sqrt{1 + AV^2}}$$

$$= \frac{K_f + K_r}{2\sqrt{K_f K_r}} \frac{k}{l} \frac{\left(\frac{1 + k^2/l_f l_r}{k^2/l_f l_r}\right) + \frac{1}{k^2}\frac{(l_f - l_r)(l_f K_f - l_r K_r)}{K_f + K_r}}{\sqrt{1 + \frac{m}{2l}\frac{K_f + K_r}{K_f K_r}SMV^2}} \qquad (3.68)$$

if $l_f \approx l_r$ and $K_f \approx K_r$, the approximation of ω_n and ζ could be written as:

$$\omega_n = \frac{2(K_f + K_r)}{mV}\sqrt{\frac{l_f l_r}{k^2}}\sqrt{1 + AV^2}$$

$$= \frac{2(K_f + K_r)}{mV}\sqrt{\frac{l_f l_r}{k^2}}\sqrt{1 + \frac{2m}{l(K_f + K_r)}SMV^2} \qquad (3.67)'$$

$$\zeta = \frac{1 + k^2/l_f l_r}{2\sqrt{k^2/l_f l_r}} \frac{1}{\sqrt{1 + AV^2}}$$

$$= \frac{1 + k^2/l_f l_r}{2\sqrt{k^2/l_f l_r}} \frac{1}{\sqrt{1 + \frac{2m}{l(K_f + K_r)}SMV^2}} \qquad (3.68)'$$

Next is to study how the vehicle natural frequency and damping ratio change in relation to vehicle steer characteristics and traveling speed.

Figure 3.26 is an example of the effect of SM and traveling speed, V, on ω_n, which corresponds to Eqn (3.67)'. From this figure, it can be seen that the natural frequency, ω_n, in particular, decreases with traveling speed V and only increases slightly with SM.

On the other hand, Fig. 3.27 shows the effect of SM and traveling speed, V, on the damping ratio, ζ, which corresponds to Eqn (3.68)'. From this figure, damping ratio, ζ, decreases with SM and the vehicle response to steer becomes more oscillatory. In the case of increasing V, when the vehicle exhibits US characteristics, ζ decreases, and so the vehicle motion becomes less damped and more oscillatory. When the vehicle exhibits OS characteristics, ζ increases and the vehicle response to steer is deteriorated. Furthermore, if $k^2/l_f l_r \approx 1$, when the vehicle exhibits NS characteristics, or when V is almost 0, regardless of the steer characteristics, ζ is almost equal to 1.0. In other words, it could be considered as a critically damped situation.
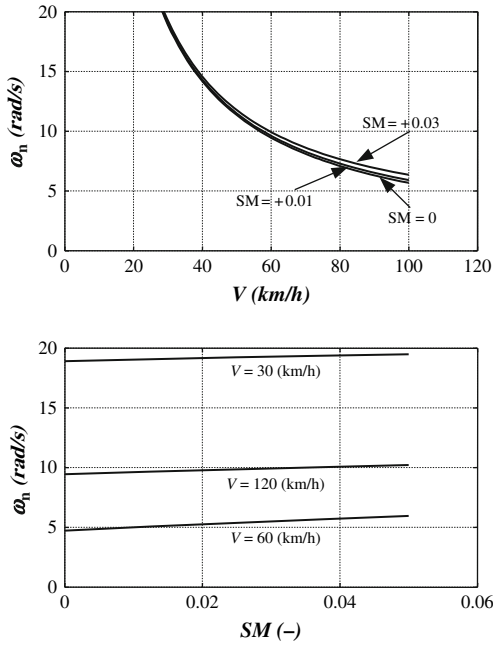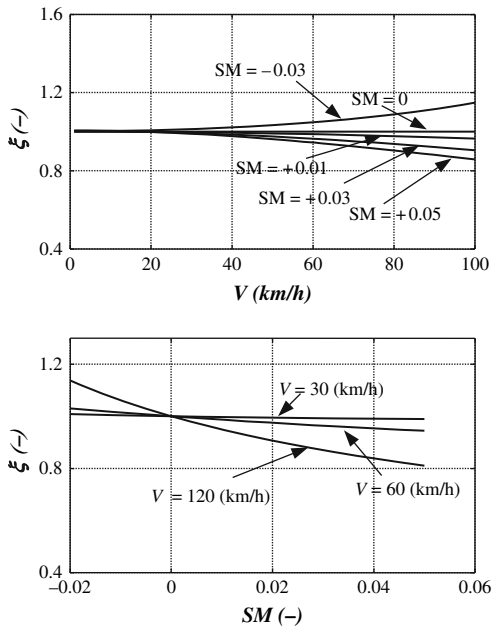
FIGURE 3.26 Effects of SM and vehicle speed on ω_n.

FIGURE 3.27 Effects of SM and vehicle speed on ζ.

At $\zeta < 1.0$, when the vehicle response is oscillating, if $l_f \approx l_r$, $K_f \approx K_r$, then the damped natural frequency could be determined by using Eqn (3.62)':

$$q = \sqrt{P^2 - D^2}$$

$$= \frac{4(K_f + K_r)}{m} \sqrt{\frac{l_f l_r}{k^2}} \sqrt{\frac{m}{2l(K_f + K_r)} SM - \left\{ \frac{1}{16} \frac{(1 - k^2/l_f l_r)^2}{k^2/l_f l_r} + SM^2 \right\} \frac{1}{V^2}}$$

(3.69)

and this is also equal to $\omega_n \sqrt{1 - \zeta^2}$.

(3) RESPONSIVENESS

Until here, the focus has been on whether the vehicle transient response to steer is without or with oscillation and stable. However, the responsiveness to steer input is also an important characteristic for the vehicle discussed here, as well as for ships and aircraft.

If λ is the real part of the root of the characteristic equation for a stable linear system, the response time, as defined in equation below, is a parameter that shows the response speed of the system.

$$t_R = -\frac{1}{\lambda}$$

(3.70)

Therefore, the t_R for the vehicle dealt with is, when $D^2 - P^2 \geq 0$,

$$t_R = \frac{1}{D \mp \sqrt{D^2 - P^2}}$$

(3.71)

and when $D^2 - P^2 < 0$,

$$t_R = \frac{1}{D}$$

(3.72)

if $l_f \approx l_r$ and $K_f \approx K_r$, using Eqns (3.56)'' and (3.62)', then the t_R for $D^2 - P^2 \geq 0$ and $D^2 - P^2 < 0$ is expressed as follows:

$$t_R = \frac{\frac{mV}{K_f + K_r}\left(\frac{k^2/l_f l_r}{1 + k^2/l_f l_r}\right)}{1 \mp \frac{4V\sqrt{k^2/l_f l_r}}{1 + k^2/l_f l_r} \sqrt{\left\{\frac{1}{16} \frac{(1 - k^2/l_f l_r)^2}{k^2/l_f l_r} + SM^2\right\}\frac{1}{V^2} - \frac{mSM}{2l(K_f + K_r)}}}$$

(when $D^2 - P^2 \geq 0$)   (3.73)

$$t_R = \frac{mV}{K_f + K_r} \frac{k^2/l_f l_r}{1 + k^2/l_f l_r} \quad \text{(when } D^2 - P^2 < 0\text{)}$$

(3.74)

Broadly speaking, it is more frequent to have the case, $D^2 - P^2 \approx 0$. In this case, the above two equations are equal, and the standard vehicle response time, t_R, could be taken as in Eqn (3.74).

From the above discussions, it is found that the basic nature of the vehicle dynamic characteristics (such as the vehicle natural frequency, ω_n, the damping ratio, ζ, and the response time, t_R) is dependant on the traveling speed and steer characteristics, namely SM. Also if $l_f \approx l_r$, and $K_f \approx K_r$, the transient response depends on the ratio of vehicle mass to cornering stiffness, $m/(K_f + K_r)$, wheelbase, l, and yaw inertia moment, $k^2/l_f l_r$ (which is decided by the wheelbase and center of gravity position). In particular, it should be noted that the yaw inertia moment actually affects the vehicle dynamic characteristics in the form of $k^2/l_f l_r$.

3.4.2 Steer response transfer function and response time history

Previously, a direct solving of Eqns (3.12) and (3.13), which are the basic equations of motion describing the vehicle motion, has been avoided. The characteristics of vehicle transient response to steer input has only been looked at by focusing on the characteristic equation and its roots.

Looking at the basic equations of motion (3.12) and (3.13) and transforming both sides of equations gives:

$$\{mVs + 2(K_f + K_r)\}\beta(s) + \left\{mV + \frac{2}{V}(l_f K_f - l_r K_r)\right\}r(s) = 2K_f\delta(s)$$

(3.75)

$$2(l_f K_f - l_r K_r)\beta(s) + \left\{Is + \frac{2(l_f^2 K_f + l_r^2 K_r)}{V}\right\}r(s) = 2l_f K_f\delta(s)$$ (3.76)

where $\beta(s), r(s)$, and $\delta(s)$ are the Laplace transformation of β, r, and δ. By solving the algebraic equation for $\beta(s)$ and $r(s)$, the following equations can be obtained:

$$\frac{\beta(s)}{\delta(s)} = \frac{\begin{vmatrix} 2K_f & mV + \frac{2}{V}(l_f K_f - l_r K_r) \\ l_f K_f & Is + \frac{2(l_f^2 K_f + l_r^2 K_r)}{V} \end{vmatrix}}{\begin{vmatrix} mVs + 2(K_f + K_r) & mV + \frac{2}{V}(l_f K_f - l_r K_r) \\ 2(l_f K_f - l_r K_r) & Is + \frac{2(l_f^2 K_f + l_r^2 K_r)}{V} \end{vmatrix}}$$ (3.77)

$$\frac{r(s)}{\delta(s)} = \frac{\begin{vmatrix} mVs + 2(K_f + K_r) & 2K_f \\ 2(l_f K_f - l_r K_r) & 2l_f K_f \end{vmatrix}}{\begin{vmatrix} mVs + 2(K_f + K_r) & mV + \frac{2}{V}(l_f K_f - l_r K_r) \\ 2(l_f K_f - l_r K_r) & Is + \frac{2(l_f^2 K_f + l_r^2 K_r)}{V} \end{vmatrix}}$$ (3.78)

Then, using ω_n and ζ derived earlier and rewriting Eqns (3.77) and (3.78):

$$\frac{\beta(s)}{\delta(s)} = G_\delta^\beta(0) \frac{1 + T_\beta s}{1 + \frac{2\zeta s}{\omega_n} + \frac{s^2}{\omega_n^2}} \tag{3.77'}$$

where

$$G_\delta^\beta(0) = \frac{1 - \frac{m}{2l} \frac{l_f}{l_r K_r} V^2}{1 + AV^2} \frac{l_r}{l} \tag{3.79}$$

$$T_\beta = \frac{IV}{2ll_r K_r} \frac{1}{1 - \frac{m}{2l} \frac{l_f}{l_r K_r} V^2} \tag{3.80}$$

$$\frac{r(s)}{\delta(s)} = G_\delta^r(0) \frac{1 + T_r s}{1 + \frac{2\zeta s}{\omega_n} + \frac{s^2}{\omega_n^2}} \tag{3.78'}$$

and

$$G_\delta^r(0) = \frac{1}{1 + AV^2} \frac{V}{l} \tag{3.81}$$

$$T_r = \frac{ml_f V}{2lK_r} \tag{3.82}$$

$G_\delta^\beta(0)$ is the side-slip angle gain constant, which is the value of β in response to δ during steady-state cornering and $G_\delta^r(0)$ is the yaw rate gain constant, which is the value of r in response to δ during steady-state cornering. Eqns (3.77)$'$ and (3.78)$'$ are the transfer functions of the response of side-slip angle, β, and yaw rate, r, to steer input, δ.

If the Laplace-transformed response of β and r to δ is given, as in Eqns (3.77) and (3.78) or (3.77)$'$ and (3.78)$'$, the response of β and r to a given δ could be obtained by inverse Laplace transformation. When a vehicle, traveling on a straight line, is suddenly given a step steer input, the vehicle response is as follows:

$$\beta(t) = L^{-1}[\beta(s)] = L^{-1}\left[G_\delta^\beta(0) \frac{1 + T_\beta s}{1 + \frac{2\zeta s}{\omega_n} + \frac{s^2}{\omega_n^2}} \frac{\delta_0}{s} \right] \tag{3.83}$$

$$r(t) = L^{-1}[r(s)] = L^{-1}\left[G_\delta^r(0) \frac{1 + T_r s}{1 + \frac{2\zeta s}{\omega_n} + \frac{s^2}{\omega_n^2}} \frac{\delta_0}{s} \right] \tag{3.84}$$

whereby L^{-1} means inverse Laplace transformation, and δ_0/s is the Laplace-transformed steer angle, $\delta(s)$ is a step input with a magnitude of δ_0. By applying the inverse Laplace transformation formula on the above equations, $\beta(t)$ and $r(t)$ become the following. Here, the initial value of β and r is 0. When the vehicle shows response without oscillation at $\zeta > 1$,

$$\beta(t) = G_\delta^\beta(0)\delta_0\left[1 + \frac{1 - \left(\zeta + \sqrt{\zeta^2 - 1}\right)\omega_n T_\beta}{2\left(\zeta + \sqrt{\zeta^2 - 1}\right)\sqrt{\zeta^2 - 1}}e^{(-\zeta - \sqrt{\zeta^2 - 1})\omega_n t}\right.$$

$$\left. - \frac{1 - (\zeta - \sqrt{\zeta^2 - 1})\omega_n T_\beta}{2\left(\zeta - \sqrt{\zeta^2 - 1}\right)\sqrt{\zeta^2 - 1}}e^{(-\zeta + \sqrt{\zeta^2 - 1})\omega_n t}\right]$$

$$(3.83)'$$

$$r(t) = G_\delta^r(0)\delta_0\left[1 + \frac{1 - (\zeta + \sqrt{\zeta^2 - 1})\omega_n T_r}{2(\zeta + \sqrt{\zeta^2 - 1})\sqrt{\zeta^2 - 1}}e^{(-\zeta - \sqrt{\zeta^2 - 1})\omega_n t}\right.$$

$$\left. - \frac{1 - (\zeta - \sqrt{\zeta^2 - 1})\omega_n T_r}{2(\zeta - \sqrt{\zeta^2 - 1})\sqrt{\zeta^2 - 1}}e^{(-\zeta + \sqrt{\zeta^2 - 1})\omega_n t}\right]$$

$$(3.84)'$$

when the response is without oscillation at $\zeta = 1$,

$$\beta(t) = G_\delta^\beta(0)\delta_0\left[1 + \left\{(\omega_n^2 T_\beta - \omega_n)t - 1\right\}e^{-\omega_n t}\right] \qquad (3.83)''$$

$$r(t) = G_\delta^r(0)\delta_0\left[1 + \left\{(\omega_n^2 T_r - \omega_n)t - 1\right\}e^{-\omega_n t}\right] \qquad (3.84)''$$

and when the response is with oscillation at $\zeta < 1$,

$$\beta(t) = G_\delta^\beta(0)\delta_0\left[1 + \frac{T_\beta}{\sqrt{1 - \zeta^2}}\right.$$

$$\left. \times \sqrt{(1/T_\beta - \zeta\omega_n)^2 + (1 - \zeta^2)\omega_n^2}\, e^{-\zeta\omega_n t}\sin\left(\sqrt{1 - \zeta^2}\omega_n t + \Psi_\beta\right)\right]$$

$$(3.83)'''$$

where $\quad \Psi_\beta = \tan^{-1}\left(\frac{\sqrt{1 - \zeta^2}\omega_n}{1/T_\beta - \zeta\omega_n}\right) - \tan^{-1}\left(\frac{\sqrt{1 - \zeta^2}}{-\zeta}\right)$

$$r(t) = G_\delta^r(0)\delta_0 \left[1 + \frac{T_r}{\sqrt{1-\zeta^2}} \right.$$

$$\left. \times \sqrt{(1/T_r - \zeta\omega_n)^2 + (1-\zeta^2)\omega_n^2} \; e^{-\zeta\omega_n t} \sin\left(\sqrt{1-\zeta^2}\omega_n t + \Psi_r\right) \right]$$

$$(3.83)'''$$

where $\Psi_r = \tan^{-1}\left(\dfrac{\sqrt{1-\zeta^2}\omega_n}{1/T_r - \zeta\omega_n}\right) - \tan^{-1}\left(\dfrac{\sqrt{1-\zeta^2}}{-\zeta}\right)$

The responsiveness to steer input, besides the response time that is described earlier, could also be expressed by the time to steady-state value, t_e, and the time to the first peak of the response oscillation, t_p, for the yaw rate response to step steer input. This is shown in Fig. 3.28.

Calculating t_e and t_p, gives the following terms:

$$t_e = \frac{1}{\omega_n^2 T_r} \tag{3.85}$$

$$t_p = \frac{1}{\omega_n \sqrt{1-\zeta^2}} \left\{ \pi - \tan^{-1}\left(\frac{\sqrt{1-\zeta^2}\omega_n T_r}{1 - \zeta\omega_n T_r}\right) \right\} \tag{3.86}$$

In particular, t_e could be defined as the approximated response time of yaw rate.

In order to see a time history of the vehicle responses to steer input, it is possible to use Eqns $(3.83)'$–$(3.84)'''$ however, recently there is an easier way to see the time history, which is a numerical simulation using a PC with some
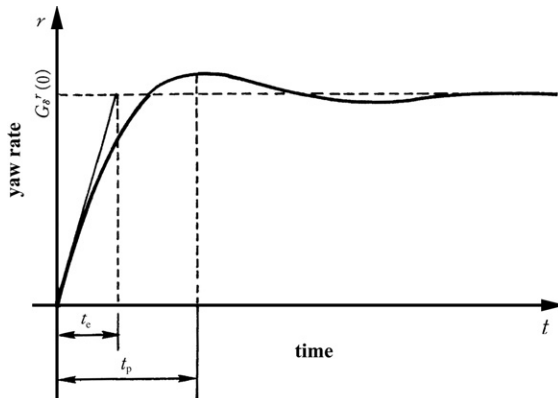

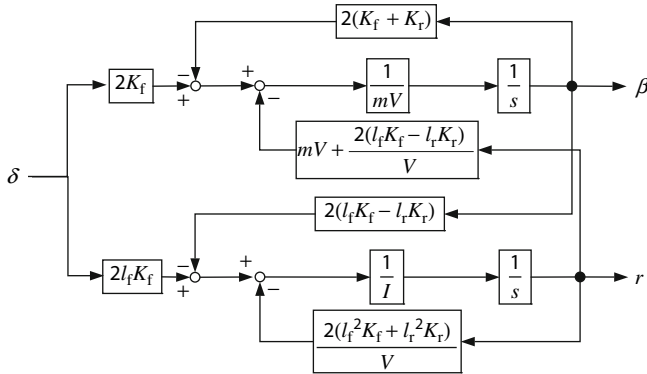FIGURE 3.28 Responsiveness of yaw rate.

FIGURE 3.29 Integral type block diagram of vehicle motion.

software, for example, Matlab-Simulink. Equations of vehicle motion (3.12) and (3.13) are rewritten as follows:

$$\frac{d\beta}{dt} = -\frac{2(K_f + K_r)}{mV}\beta - \left\{1 + \frac{2}{mV^2}(l_fK_f - l_rK_r)\right\}r + \frac{2K_f}{mV}\delta \qquad (3.12)'$$

$$\frac{dr}{dt} = -\frac{2(l_fK_f - l_rK_r)}{I}\beta - \frac{2(l_f^2K_f + l_r^2K_r)}{IV}r + \frac{2l_fK_f}{I}\delta \qquad (3.13)'$$

Side-slip angle and yaw rate are obtained by integrating the right hand side of the above equations. It is possible to have the integral type of block diagram of the vehicle motion to steer input as shown in Fig. 3.29. This is the basis of the simulation program using Matlab-Simulink software.

Example 3.6

Execute the simulation of the vehicle response to step steer input, $\delta = 0.04$ rad, by Matlab-Simulink at the vehicle speeds 60 km/h, 100 km/h, and 140 km/h with the vehicle parameters as $m = 1500$ kg, $I = 2500$ kg m^2, $l_f = 1.1$ m, $l_r = 1.6$ m, $K_f = 55$ kN/rad, and $K_r = 60$ kN/rad.

Solution

The vehicle parameters for the simulation are set as in Fig. E3.6(a). The simulation program is shown in Fig. E3.6(b) and Fig. E3.6(c) is a simulation condition. Figure E3.6(d) is a result of the simulation and all the results are summarized in Fig. E3.6(e).

```
🖳 Editor - C:¥Program Files¥MATLAB¥R2007a¥work¥chapter3¥v...  ▢ ▢ ✕
File  Edit  Text  Go  Cell  Tools  Debug  Desktop  Window  Help          ↘ ↗ ✕
 🗋 🖿 🖫  | ✂ 🗎 🗎  ⤺ ⤻ | 🖨 | 🏫 ← ➡ ƒ, | 🗐 🗗 | Ba... ▾     » | 🗖 ▾
 ✐ | ⤶🖳 ⤷🖳 ⤷🖳 | – 1.0  + | ÷ 1.1  × | ⁒ ⁒ 🟦
  1       % Vehicle parameters
  2 –      m = 1500;    % mass (kg)
  3 –       I = 2500;    % moment of inertia about z-axis:I (kgm^2)
  4 –      lf = 1.1;    % distance from C.O.G to front axle (m)
  5 –      lr = 1.6;    % distance from C.O.G to front axle (m)
  6 –       l = lf+lr;  % wheel base (m)
  7 –      Kf = 55000;   % front cornering stiffness (N/rad)
  8 –      Kr = 60000;   % rear cornering stiffness (N/rad)
  9       % Simulation parameters
 10 –      dt = 0.001;  % simulation rate (s)
 11 –      tf = 4.0;    % simulation time (s)
 12 –       V = 140/3.6;% velocity (m/s)
 13 –      Sf = 0.04;    % front tire steer angle (rad)
                        script              Ln  13    Col  44    OVR
```
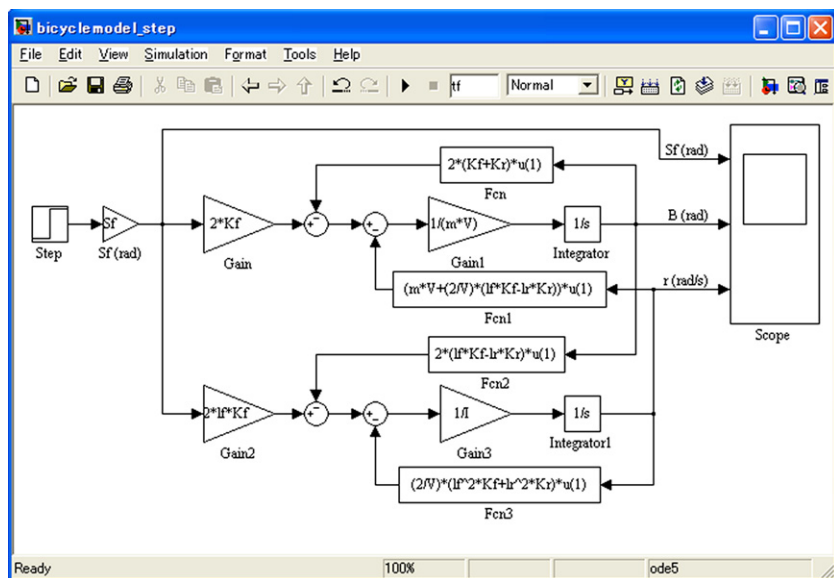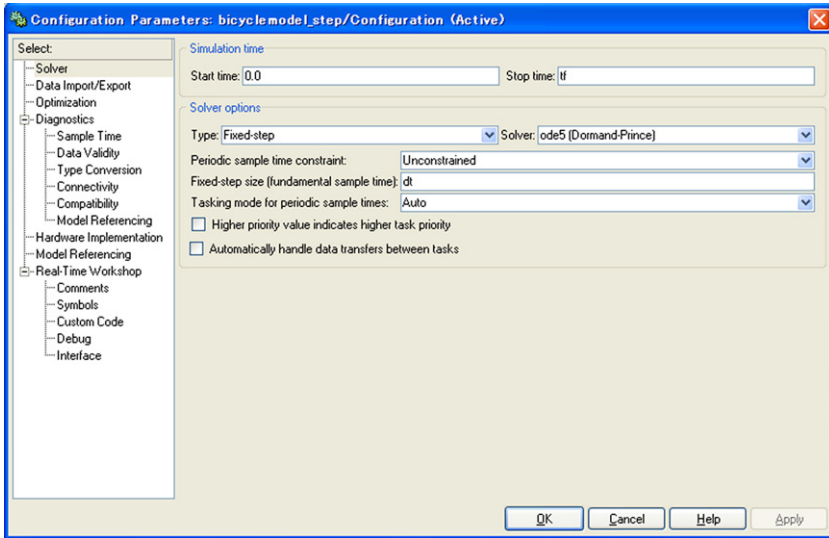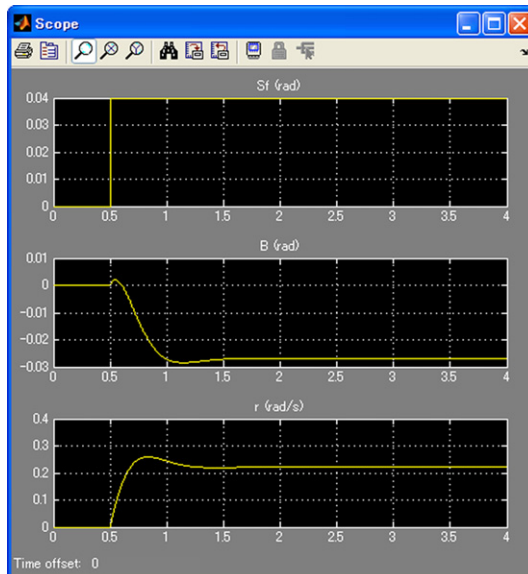
FIGURE E3.6(a).

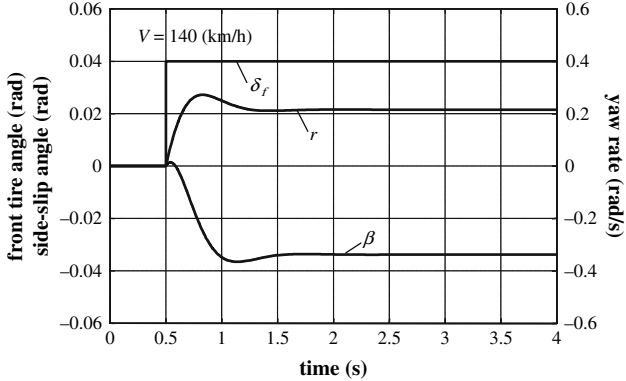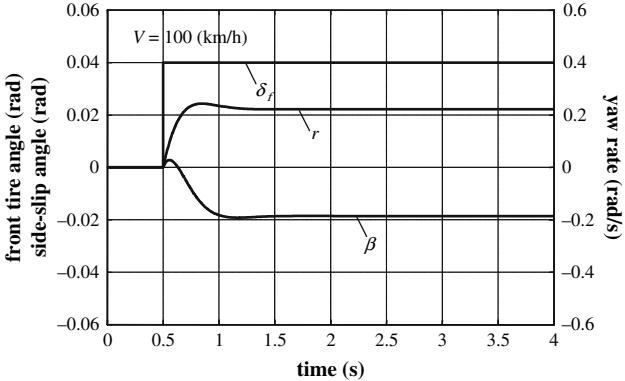FIGURE E3.6(b).

FIGURE E3.6(c).

FIGURE E3.6(d).
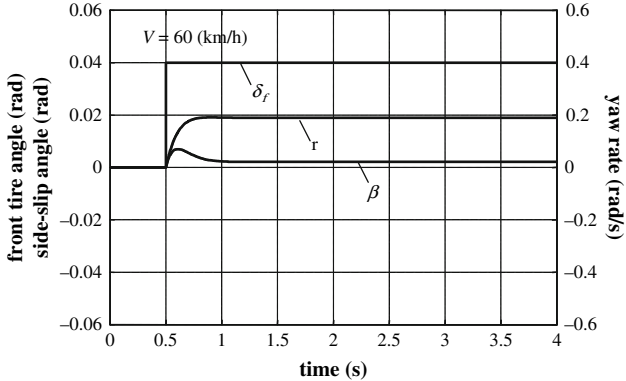
FIGURE E3.6(e).

If the vehicle motion is described with coordinates fixed on the ground, Eqns (3.21) and (3.22) will be achieved. By Laplace transforms:

$$\left\{ms^2 + \frac{2(K_f + K_r)}{V}s\right\}y(s) + \left\{\frac{2(l_fK_f - l_rK_r)}{V}s - 2(K_f + K_r)\right\}\theta(s)$$
$$= 2K_f\delta(s)$$

$$(3.21)'$$

$$\frac{2(l_fK_f - l_rK_r)}{V}sy(s) + \left\{Is^2 + \frac{2(l_f^2K_f + l_r^2K_r)}{V}s - 2(l_fK_f - l_rK_r)\right\}\theta(s)$$
$$= 2l_fK_f\delta(s)$$

$$(3.22)'$$

where $y(s)$ and $\theta(s)$ are the Laplace transforms of y and θ. Solving the algebraic equations of $y(s)$ and $\theta(s)$ gives:

$$\frac{y(s)}{\delta(s)} = \frac{\begin{vmatrix} 2K_f & \frac{2(l_fK_f - l_rK_r)}{V}s - 2(K_f + K_r) \\ l_fK_f & Is^2 + \frac{2(l_f^2K_f + l_r^2K_r)}{V}s - 2(l_fK_f - l_rK_r) \end{vmatrix}}{\begin{vmatrix} ms^2 + \frac{2(K_f + K_r)}{V}s & \frac{2(l_fK_f - l_rK_r)}{V}s - 2(K_f + K_r) \\ \frac{2(l_fK_f - l_rK_r)}{V}s & Is^2 + \frac{2(l_f^2K_f + l_r^2K_r)}{V}s - 2(l_fK_f - l_rK_r) \end{vmatrix}} \quad (3.87)$$

$$\frac{\theta(s)}{\delta(s)} = \frac{\begin{vmatrix} ms^2 + \frac{2(K_f + K_r)}{V}s & 2K_f \\ \frac{2(l_fK_f - l_rK_r)}{V}s & 2l_fK_f \end{vmatrix}}{\begin{vmatrix} ms^2 + \frac{2(K_f + K_r)}{V}s & \frac{2(l_fK_f - l_rK_r)}{V}s - 2(K_f + K_r) \\ \frac{2(l_fK_f - l_rK_r)}{V}s & Is^2 + \frac{2(l_f^2K_f + l_r^2K_r)}{V}s - 2(l_fK_f - l_rK_r) \end{vmatrix}} \quad (3.88)$$

Then, using ω_n and ζ derived earlier and rewriting equations, equation become:

$$\frac{y(s)}{\delta(s)} = G_\delta^{\ddot{y}}(0)\frac{1 + T_{y1}s + T_{y2}s^2}{s^2\left(1 + \frac{2\zeta s}{\omega_n} + \frac{s^2}{\omega_n^2}\right)} \quad (3.87)'$$

where

$$G_\delta^{\ddot{y}}(0) = \frac{1}{1 + AV^2}\frac{V^2}{l} = VG_\delta^r(0) \quad (3.89)$$

$$T_{y1} = \frac{l_{\mathrm{r}}}{V} \tag{3.90}$$

$$T_{y2} = \frac{I}{2lK_{\mathrm{r}}} \tag{3.91}$$

$G_{\delta}^{\ddot{y}}(0)$ is the lateral acceleration gain constant, which is the lateral acceleration value in response to δ during steady-state cornering and

$$\frac{\theta(s)}{\delta(s)} = G_{\delta}^{r}(0)\frac{1 + T_{\mathrm{r}}s}{s\left(1 + \frac{2\zeta s}{\omega_{\mathrm{n}}} + \frac{s^2}{\omega_{\mathrm{n}}^2}\right)} \tag{3.88$'$}$$

Eqns (3.87) and (3.88) or (3.87)' and (3.88)' are the transfer functions of the responses of lateral displacement and yaw angle to vehicle steer input. As previously shown, inverse Laplace transformations on $y(s)$ and $\theta(s)$ in the above equations can obtain the lateral displacement and yaw angle responses to a given steer input. Laplace transforms on the vehicle response to steer and expression of the vehicle motion in the form of transfer functions is convenient when the actual response to a given steer input is desired. It is also suitable in the case of taking the vehicle as the control target in the control system and studying the control of vehicle motions and the controllability of the vehicle.

Furthermore, ω_{n}, ζ, $G_{\delta}^{r}(0)$, $G_{\delta}^{\ddot{y}}(0)$, T_{r}, t_{e}, and t_{p}, which are the coefficients in the transfer functions are the parameters that determine the vehicle response characteristics to steer input and are called the response parameters.

3.4.3 Vehicle response to periodical steer input

Generally, among the methods for investigating dynamic characteristics of mechanical systems, the system response to periodical input is investigated. In vibration systems, this is called forced vibration, while in automatic control system, it is called the frequency response.

This method is widely used for understanding the dynamic characteristics of the vehicle, and the vehicle response to a periodical steer input is examined here. This is important, as an on-board driver can feel the vehicle lateral acceleration and yaw rate responses to steer input very well.

Firstly, the lateral acceleration of the vehicle's center of gravity to a periodical steer input, δ, can be written as below by multiplying by s^2 on both sides of Eqn (3.87)' and substituting $s = j2\pi f$.

$$G_{\delta}^{\ddot{y}}(j2\pi f) = G_{\delta}^{\ddot{y}}(0)\frac{1 - (2\pi f)^2 T_{y2} + j2\pi f T_{y1}}{1 - (2\pi f)^2/\omega_{\mathrm{n}}^2 + j2\pi f 2\zeta/\omega_{\mathrm{n}}} \tag{3.92}$$

where f is the frequency of the periodical steer, and $j = \sqrt{-1}$.

From this equation, the lateral acceleration gain $|G_\delta^{\ddot{y}}|$ and the phase angle $\angle G_\delta^{\ddot{y}}$ toward steer angle are as below:

$$\left|G_\delta^{\ddot{y}}\right| = \sqrt{\frac{P_y^2 + Q_y^2}{R_y^2 + S_y^2}}\, G_\delta^{\ddot{y}}(0) \tag{3.93}$$

$$\angle G_\delta^{\ddot{y}} = \tan^{-1}(Q_y/P_y) - \tan^{-1}(S_y/R_y) \tag{3.94}$$

where,

$$P_y = 1 - (2\pi f)^2 T_{y2}, \ Q_y = 2\pi f T_{y1}$$

$$R_y = 1 - (2\pi f)^2/\omega_n^2, \ S_y = 2\pi f 2\zeta/\omega_n$$

Next, the vehicle yaw rate response $G_\delta^r(j2\pi f)$ toward periodical steer δ can be written by substituting $s = j2\pi f$ into Eqn (3.78)$'$

$$G_\delta^r(j2\pi f) = G_\delta^r(0)\, \frac{1 + j2\pi f T_r}{1 - (2\pi f)^2/\omega_n^2 + j2\pi f 2\zeta/\omega_n} \tag{3.95}$$

From this equation, the yaw rate gain, $|G_\delta^r|$, and the phase angle, $\angle G_\delta^r$, to steer input are:

$$\left|G_\delta^r\right| = \sqrt{\frac{P_r^2 + Q_r^2}{R_r^2 + S_r^2}}\, G_\delta^r(0) \tag{3.96}$$

$$\angle G_\delta^r = \tan^{-1}(Q_r/P_r) - \tan^{-1}(S_r/R_r) \tag{3.97}$$

where,

$$P_r = 1, \ Q_r = 2\pi f T_r$$

$$R_r = 1 - (2\pi f)^2/\omega_n^2$$

$$S_r = 2\pi f 2\zeta/\omega_n$$

In particular, the investigation of the yaw rate response to a periodical steer is very common in the study of the vehicle inherent dynamic characteristics. The yaw rate response as expressed by Eqn (3.95) has a general form as shown in Fig. 3.30. When the steer frequency is small, the yaw rate to steer gain is almost constant. As the steer frequency becomes larger, the US vehicle gain reaches
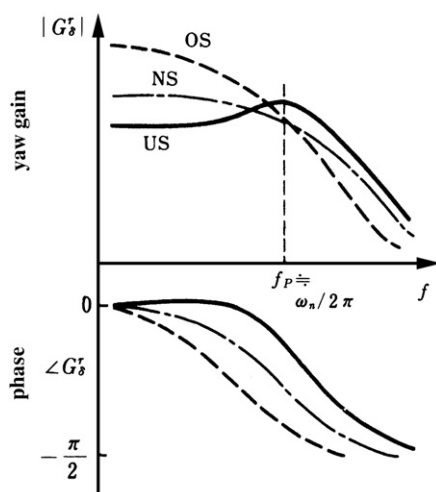
FIGURE 3.30 Conceptual diagram of yaw rate frequency response.

a peak at a certain frequency, and then decreases. The OS and NS vehicles do not have a peak, and their gain decreases with steer frequency. Furthermore, the phase lag is around 0 at low steer frequencies, but increases with frequency for all three steer characteristics. This tendency is more obvious for the vehicle with OS characteristics. For the US vehicle, the peak in the gain happens when the vehicle transient response to a fixed steer is oscillating. This peak becomes greater as the damping ratio, ζ, reduces. When the vehicle exhibits US characteristics, the peak will become larger with increasing traveling speed, V. The frequency where the peak occurs is nearly the same as the vehicle natural frequency, ω_n.

Figure 3.31 is a calculated example of the responses of yaw rate and lateral acceleration to a periodical steer for a small passenger car. From this figure, it is clear that with higher traveling speed, the motion phase lag, especially in the lateral acceleration response, becomes larger at higher frequencies. Furthermore, since the vehicle is US, a gain peak occurs at high traveling speed in the yaw rate response, and the vehicle transient response is oscillatory with insufficient damping.

Here, the relation between the frequency responses of lateral acceleration and yaw rate will be considered. The transfer function of the lateral acceleration to the steering input is derived in this section from equations of motion with fixed coordinates on the ground, Eqns $(3.21)'$ and $(3.22)'$. There is another way to derive the lateral acceleration transfer function using equations of motion with the fixed coordinates on the vehicle, Eqns (3.75) and (3.76). Based on these, the lateral acceleration is expressed by $V(\dot{\beta} + r)$. A side-slip rate intervenes between the lateral acceleration response and the yaw rate.

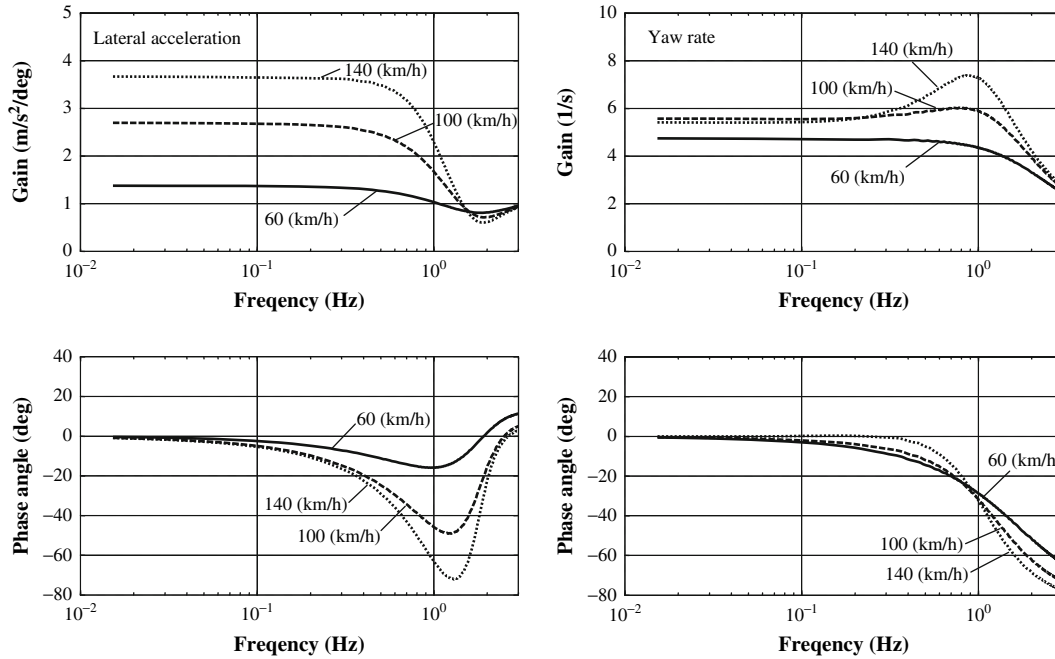FIGURE 3.31 Yaw rate and lateral acceleration frequency response.

Example 3.7

Calculate the yaw rate frequency responses of the vehicles with US, NS, and OS characteristics at the vehicle speed, $V = 120$ km/h using Matlab-Simulink and confirm the effects of the steer characteristics on the yaw rate frequency response shown previously in Fig. 3.30.
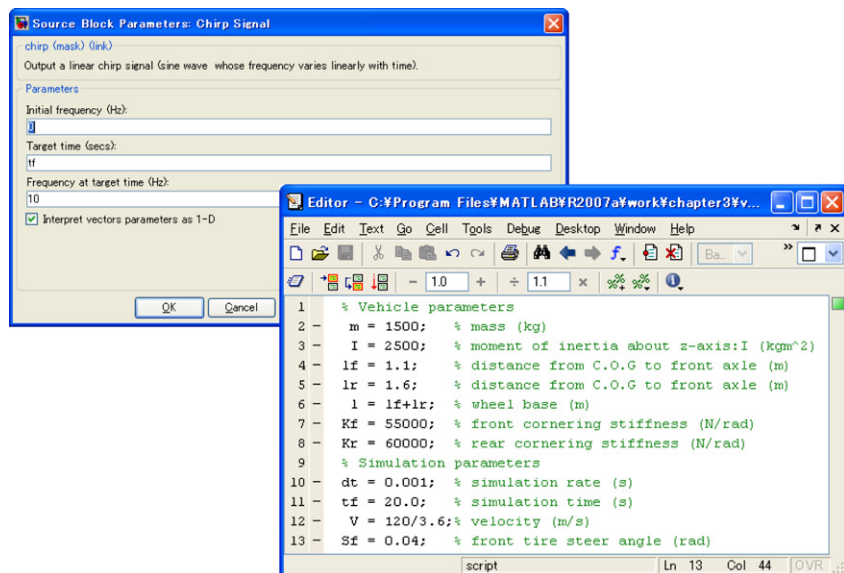
FIGURE E3.7(a).
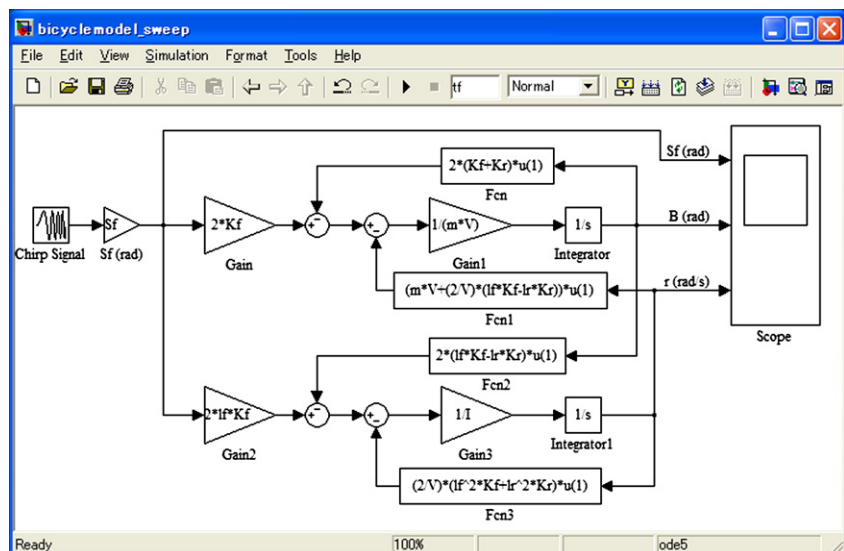
FIGURE E3.7(b).
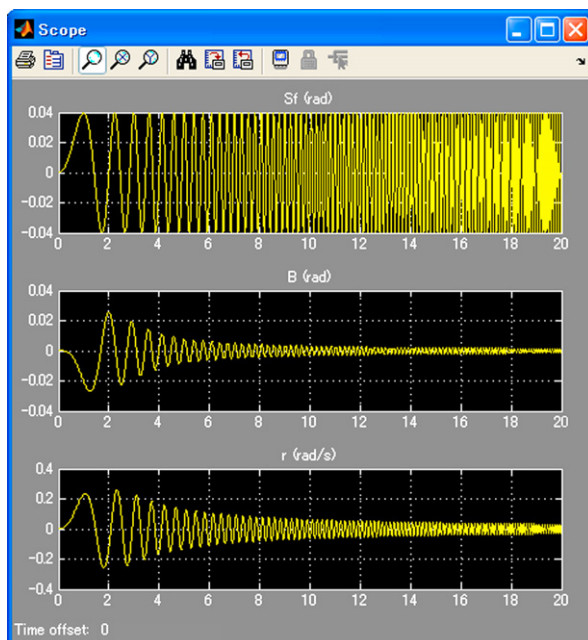
FIGURE E3.7(c).

FIGURE E3.7(d).
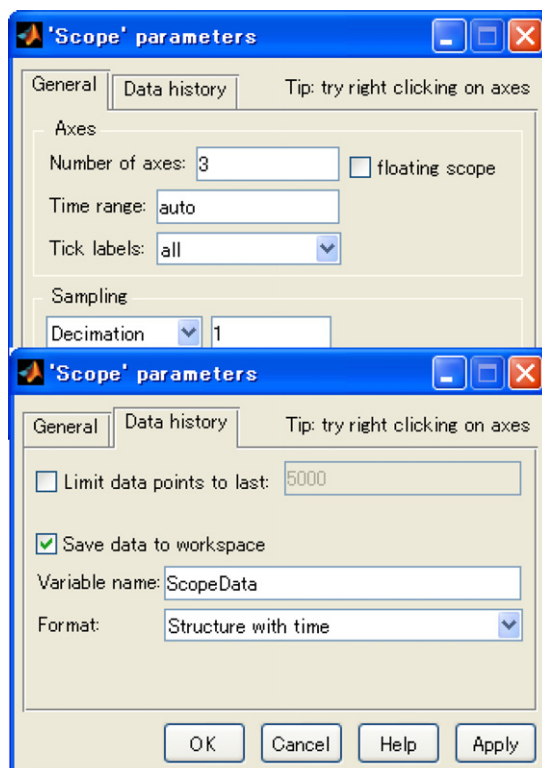
```
     Editor – C:¥Program Files¥MATLAB¥R2007a¥work¥program¥chapter3¥freqresponse.m
     File  Edit  Text  Go  Cell  Tools  Debug  Desktop  Window  Help

 1 -    Sf = ScopeData.signals(1,1).values(:,1);% front tire steer angle (rad)
 2 -     B = ScopeData.signals(1,2).values(:,1);% side slip Angle (rad)
 3 -     r = ScopeData.signals(1,3).values(:,1);% yaw rate (rad/s)
 4      %--------------------------------------------------------------------%
 5      % The frequency response is calculated by using Fourier trasform.
 6 -    gr = etfe([r,Sf],[],2^15,0.001);
 7      % The gain and the phase angle of the frequency response are calculated.
 8 -    [amp,phase,w] = bode(gr);
 9      % An extra dimension is deleted.
10 -    amp = squeeze(amp);
11 -    phase = squeeze(phase);
12      % Drawing gain-frequency relation.
13 -    figure;
14 -    a1 = subplot(2,1,1);
15 -    graph1 = semilogx(w/(2*pi),20*log10(amp));
16 -    set(get(a1,'XLabel'),'String','Frequency (Hz)');
17 -    set(get(a1,'YLabel'),'String','Gain (dB)');
18 -    axis([0.01 3 6 18]);
19 -    grid on;
20      % Drawing phase-frequency relation.
21 -    a2 = subplot(2,1,2);
22 -    graph2 = semilogx(w/(2*pi),phase);
23 -    set(get(a2,'XLabel'),'String','Frequency (Hz)');
24 -    set(get(a2,'YLabel'),'String','Phase angle (deg)');
25 -    axis([0.01 3 -80 40]);
26 -    grid on;

                                          script              Ln  1      Col  71    OVR
```

FIGURE E3.7(e).
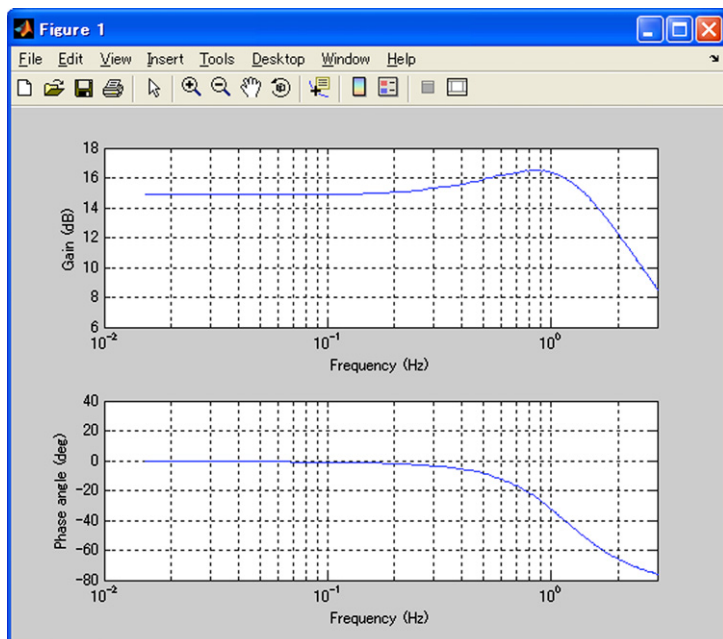
FIGURE E3.7(f).
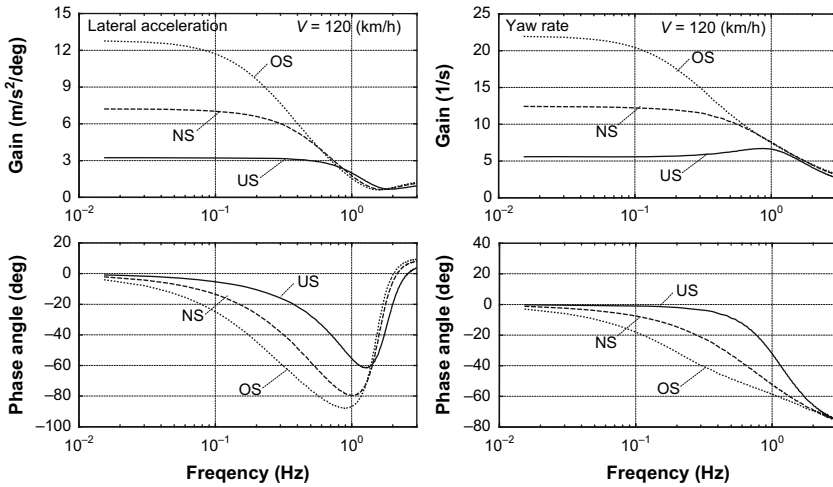
FIGURE E3.7(g).

Solution

The parameters of the US vehicle are the same as in Example 3.6 and the cornering stiffness for the NS vehicle is set as $K_f = 68.15$ kN/rad and $K_r = 46.85$ kN/rad, for the OS vehicle, $K_f = 72.5$ kN/rad and $K_r = 42.5$ kN/rad. The parameters of the vehicle and the sweep type sine wave are set as in Fig. E3.7(a). The simulation program of the vehicle response to the sweep type sine-wave steer input is shown in Fig. E3.7(b) and Fig. E3.7(c) is a result of the simulation. After finishing the vehicle response simulation to the sweep type of sine-wave steer input, the simulated data is saved as shown in Fig. E3.7(d) and the yaw rate frequency response to steer input is calculated applying the Fourier Transformation to the time histories simulated as shown in Fig. E3.7(e). A result is in Fig. E3.7(f) and Fig. E3.7(g) shows the summarized calculation results comparing the effects of the vehicle steer characteristics on the yaw rate frequency response.

Therefore, using Eqns $(3.77)'$ and $(3.78)'$, it is possible to describe the lateral acceleration transfer function as follows:

$$G_\delta^{\ddot{y}}(s) = V\frac{s\beta(s)}{\delta(s)} + V\frac{r(s)}{\delta(s)} = VG_\delta^\beta(0)\frac{s(1+T_\beta s)}{1+\frac{2\zeta s}{\omega_n}+\frac{s^2}{\omega_n^2}} + VG_\delta^r(0)\frac{1+T_r s}{1+\frac{2\zeta s}{\omega_n}+\frac{s^2}{\omega_n^2}}$$

$$= \frac{1}{1+AV^2}\frac{V^2}{l}\frac{\frac{l_r}{V}s - \frac{m}{2l}\frac{l_f V}{K_r}s + \frac{I}{2lK_r}s^2}{1+\frac{2\zeta s}{\omega_n}+\frac{s^2}{\omega_n^2}} + \frac{1}{1+AV^2}\frac{V^2}{l}\frac{1+\frac{m}{2l}\frac{l_f V}{K_r}s}{1+\frac{2\zeta s}{\omega_n}+\frac{s^2}{\omega_n^2}}$$

$$= \frac{1}{1+AV^2}\frac{V^2}{l}\frac{1+\frac{l_r}{V}s+\frac{I}{2lK_r}s^2}{1+\frac{2\zeta s}{\omega_n}+\frac{s^2}{\omega_n^2}} = G_\delta^{\ddot{y}}(0)\frac{1+T_{y1}s+T_{y2}s^2}{1+\frac{2\zeta s}{\omega_n}+\frac{s^2}{\omega_n^2}}$$

The coefficient of s in the numerator of the yaw rate transfer function, $ml_fV/(2lK_r)$, is eliminated by the same term, which is a negative part of steady-state response of side-slip angle to steer input in the numerator of the side-slip transfer function. Only the term, l_r/V, remains in the numerator of the lateral acceleration transfer function as a coefficient of s and this rapidly decreases with the vehicle speed.

The coefficient of s in the numerator of the transfer function, in general, has a lead effect and compensates for the response delay caused by the coefficient of s and s^2 in the denominator. The lateral acceleration response to steer has a smaller value of the coefficient of s in the numerator compared with that of the yaw rate, especially at high vehicle speed. This is partly why there is a significantly larger delay in the phase lag of the lateral acceleration compared with that of the yaw rate at high speed, as shown in Fig. 3.31. The larger delay in lateral acceleration is due to the side-slip response acting opposite to the steering angle at higher vehicle speeds. This is a very important part of the basic nature of the vehicle dynamics and is attributed to the intervention of vehicle side-slip motion between lateral acceleration and yaw rate.

3.4.4 Effect of non-linear tire characteristics

Previously, the vehicle dynamic characteristics have been studied with the assumption that the lateral force is proportional to the side-slip angles of the tires. It is important now to try to understand how the vehicle dynamics are affected when the lateral force is not proportional to the side-slip angles (e.g., at large tire slip angles).

The close relation between tire lateral force, F, and side-slip angles, β, has been discussed in subsections 2.3.1 and 2.4.2. For simplicity, take K as the cornering stiffness at $\beta = 0$, and a friction force, μW, as a saturated lateral force that can be approximated as a second order polynomial of β.

$$F = K\beta - \frac{K^2}{4\mu W}\beta^2 \qquad (3.98)$$

The relation is shown in Fig. 3.32.

When a vehicle, with weight W, is making a circular motion with lateral acceleration, $\ddot{y}$, as in Eqn (3.48), the lateral forces acting at the front and rear wheels are:

$$2Y_f(\beta_f) = \frac{l_r W}{l}\ddot{y} = 2K_f\beta_f - \frac{K_f^2}{\mu\frac{l_r W}{l}}\beta_f^2 \qquad (3.99)$$

$$2Y_r(\beta_r) = \frac{l_f W}{l}\ddot{y} = 2K_r\beta_r - \frac{K_r^2}{\mu\frac{l_f W}{l}}\beta_r^2 \qquad (3.100)$$
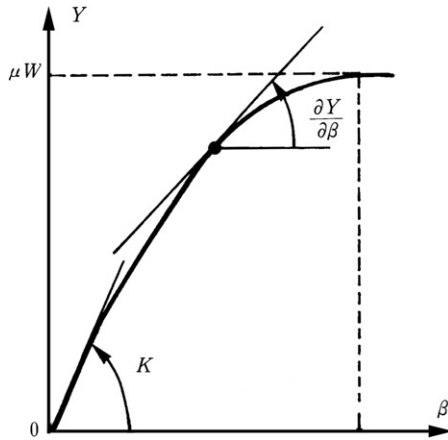
FIGURE 3.32 Approximation of tire non-linear characteristics.

where, β_f, β_r are the front and rear wheel side-slip angles.

Using these equations, the equivalent cornering stiffnesses, $\partial Y_f / \partial \beta_f$ and $\partial Y_r / \partial \beta_r$, are:

$$\frac{\partial Y_f}{\partial \beta_f} = K_f \left(1 - \frac{K_f}{\mu \frac{l_r W}{l}} \beta_f \right) = K_f \sqrt{1 - \frac{\ddot{y}}{\mu}} \tag{3.101}$$

$$\frac{\partial Y_r}{\partial \beta_r} = K_r \left(1 - \frac{K_r}{\mu \frac{l_f W}{l}} \beta_r \right) = K_r \sqrt{1 - \frac{\ddot{y}}{\mu}} \tag{3.102}$$

These are the gradients of the lateral forces to side-slip angle at the equilibrium point of circular motion with $\ddot{y}$. If $\ddot{y}/\mu \ll 1$,

$$\frac{\partial Y_f}{\partial \beta_f} = K_f \left(1 - \frac{\ddot{y}}{2\mu} \right) \tag{3.103}$$

$$\frac{\partial Y_r}{\partial \beta_r} = K_r \left(1 - \frac{\ddot{y}}{2\mu} \right) \tag{3.104}$$

The cornering stiffness of the vehicle during circular motion decreases with the lateral acceleration. When the lateral acceleration approaches the limit or the friction coefficient between the road and tire, it decreases abruptly. In the region where $\ddot{y}$ is small compared to μ, the cornering stiffness could be treated as decreasing linearly. The above condition is shown in Fig. 3.33.

Next, the characteristics of the vehicle motion in the region where the tire exhibits its non-linear characteristics will be looked at. Consider the very small motion of the vehicle in response to a very small steer input from the initial
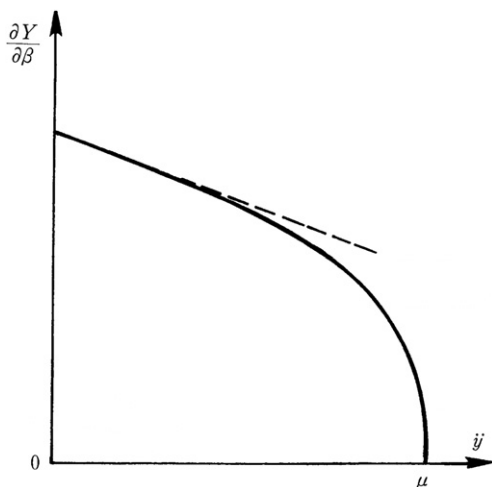
FIGURE 3.33 Change of equivalent cornering stiffness due to lateral acceleration.

condition of circular motion, with the lateral acceleration, $\ddot{y}$. Equations of motion at that time are expressed as below:

$$m\left\{ g\ddot{y} + V\left(\frac{d\beta}{dt} + r\right)\right\} = 2Y_f\left(\beta_f + \delta - \beta - \frac{l_f r}{V}\right) + 2Y_r\left(\beta_r - \beta + \frac{l_r r}{V}\right)$$

$$(3.105)$$

$$I\frac{dr}{dt} = 2l_f Y_f\left(\beta_f + \delta - \beta - \frac{l_f r}{V}\right) - 2l_r Y_r\left(\beta_r - \beta + \frac{l_r r}{V}\right) \qquad (3.106)$$

Because δ, β, and r are very small,

$$Y_f\left(\beta_f + \delta - \beta - \frac{l_f r}{V}\right) \cong Y_f(\beta_f) + \frac{\partial Y_f}{\partial \beta_f}\left(\delta - \beta - \frac{l_f r}{V}\right)$$

$$Y_r\left(\beta_r - \beta + \frac{l_r r}{V}\right) \cong Y_r(\beta_r) + \frac{\partial Y_r}{\partial \beta_r}\left(-\beta + \frac{l_r r}{V}\right)$$

and from the equilibrium,

$$mg\ddot{y} = 2Y_f(\beta_f) + 2Y_r(\beta_r)$$

$$2l_f Y_f(\beta_f) - 2l_r Y_r(\beta_r) = 0$$

Substituting these equations into Eqns (3.105) and (3.106) and rearranging them gives the following final equations:

$$mV\frac{d\beta}{dt} + 2\left(\frac{\partial Y_f}{\partial \beta_f} + \frac{\partial Y_r}{\partial \beta_r}\right)\beta + \left\{mV + \frac{2\left(l_f\frac{\partial Y_f}{\partial \beta_f} - l_r\frac{\partial Y_r}{\partial \beta_r}\right)}{V}\right\}r = 2\frac{\partial Y_f}{\partial \beta_f}\delta$$

(3.107)

$$2\left(l_f\frac{\partial Y_f}{\partial \beta_f} - l_r\frac{\partial Y_r}{\partial \beta_r}\right)\beta + I\frac{dr}{dt} + \frac{2\left(l_f^2\frac{\partial Y_f}{\partial \beta_f} + l_r^2\frac{\partial Y_r}{\partial \beta_r}\right)}{V}r = 2l_f\frac{\partial Y_f}{\partial \beta_f}\delta \qquad (3.108)$$

These are the linearized equations of motion for the region where tire characteristics are non-linear, based on the theory of small perturbation. In the region where tire characteristics are non-linear, the tire cornering stiffnesses of K_f, K_r are now replaced by the equivalent cornering stiffness of $\partial Y_f/\partial \beta_f$ and $\partial Y_r/\partial \beta_r$ in Eqns (3.101) and (3.102) or Eqns (3.103) and (3.104).

Here, when $\ddot{y}/\mu \ll 1$, the equivalent cornering stiffness is:

$$\frac{\partial Y_f}{\partial \beta_f} = K_f^* = K_f\left(1 - \frac{\ddot{y}}{2\mu}\right)$$

$$\frac{\partial Y_r}{\partial \beta_r} = K_r^* = K_r\left(1 - \frac{\ddot{y}}{2\mu}\right)$$

Several parameters that show the vehicle dynamic characteristics are obtained through the following equations. First of all, the stability factor is:

$$A^* = \frac{m}{2l^2}\frac{l_rK_r^* - l_fK_f^*}{K_f^*K_r^*} = \frac{m}{2l^2}\frac{l_rK_r - l_fK_f}{K_fK_r}\left(1 + \frac{\ddot{y}}{2\mu}\right) = A\left(1 + \frac{\ddot{y}}{2\mu}\right)$$

(3.109)

and the natural frequency now becomes:

$$\omega_n^* = \frac{2\sqrt{K_f^*K_r^*}l}{mk}\frac{\sqrt{1 + A^*V^2}}{V}$$

$$= \frac{2\sqrt{K_fK_r}l}{mk}\frac{\sqrt{1 + AV^2}}{V}\left[1 - \left(1 + \frac{1}{1 + AV^2}\right)\frac{\ddot{y}}{4\mu}\right]$$

$$= \omega_n\left[1 - \left(1 + \frac{1}{1 + AV^2}\right)\frac{\ddot{y}}{4\mu}\right] \qquad (3.110)$$
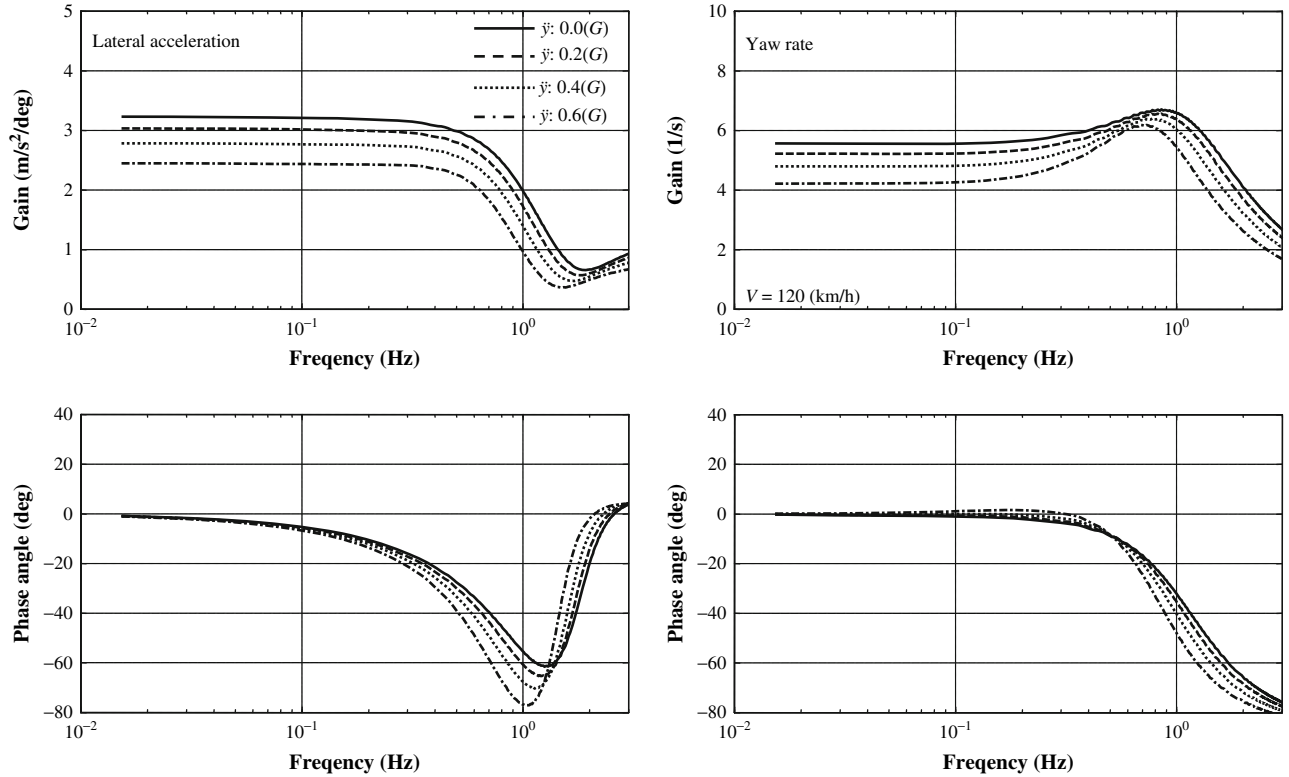
FIGURE 3.34 Effect of tire non-linear characteristics on frequency response.

and the approximated response time of yaw rate given by Eqn (3.85) is:

$$t_{\mathrm{e}}^{*} = \frac{1}{\omega_{\mathrm{n}}^{*2} T_{\mathrm{r}}} = \frac{1}{\omega_{\mathrm{n}}^{2} T_{\mathrm{r}}} \left(1 + \frac{1}{1 + AV^{2}} \frac{\ddot{y}}{2\mu} \right) = t_{\mathrm{e}} \left(1 + \frac{1}{1 + AV^{2}} \frac{\ddot{y}}{2\mu} \right)$$

$$(3.111)$$

These show the change of vehicle dynamic characteristics with respect to lateral acceleration, $\ddot{y}$, in the region where the tire characteristic is non-linear.

Figure 3.34 is an example of the vehicle yaw rate and lateral acceleration frequency response. It shows the vehicle dynamic characteristics during circular motion at different lateral acceleration values. This gives an idea of the effect of tire non-linear characteristics. The dynamic characteristics change substantially with the lateral acceleration due to the saturation property of tire characteristic to side-slip angle.

PROBLEMS

3.1 Referring to Fig. 3.4(b), confirm that it is acceptable to regard the side-slip angles of the right and left wheel as almost identical and using the bicycle vehicle model is reasonable when the vehicle speed is higher than 40 km/h, the yaw rate is less than 0.1 rad/s, and the vehicle track is 1.4 m.

3.2 Derive Eqns (3.29) and (3.30) from Eqns (3.26), (3.27), and (3.28).

3.3 Geometrically, show that the side-slip angle during steady-state cornering at low speed is described by the third equation in Eqn (3.33).

3.4 Give the geometrical proof of Eqn (3.34).

3.5 Find the vehicle speed at which steady-state yaw rate reaches the peak value, using Eqn (3.39).

3.6 Find the vehicle speed at which steady-state side-slip angle is equal to zero, using Eqn (3.40), and calculate the value under $m = 1500$ kg, $l_{\mathrm{f}} = 1.1$m, $l_{\mathrm{r}} = 1.6$m, and $K_{\mathrm{r}} = 60$ kN/rad.

3.7 Calculate the stability factor using Eqn (3.43) under $m = 1500$ kg, $l_{\mathrm{f}} = 1.1$m, $l_{\mathrm{r}} = 1.6$m, $K_{\mathrm{f}} = 55$ kN/rad, and $K_{\mathrm{r}} = 60$ kN/rad.

3.8 Calculate the static margin using Eqn (3.45) for the same vehicle parameters as used in 3.7.

3.9 Calculate the critical vehicle speed for the OS vehicle with the parameters used in Example 3.7.

3.10 Confirm that for the vehicle with static margin, SM, almost zero, the inverse of the vehicle natural frequency, $1/\omega_{\mathrm{n}}$, is nearly equal to the vehicle response time expressed by Eqn (3.74).

3.11 Using Eqn (3.110), estimate how many percent the vehicle natural frequency is reduced due to circular turning with the lateral acceleration, 2.0 m/s^2, on a dry road surface, $\mu = 1.0$.

3.12 Execute the vehicle response simulation to a single, 0.5 Hz, sine-wave steer input with an amplitude of 0.04 rads at vehicle speeds, 60, 100, and 140 km/h, using the Matlab-Simulink simulation software. Use the same vehicle parameters as in Example 3.6.

3.13 Find the steady-state side-slip angle caused by disturbance yaw rate Δr_{C} at steering angle equal to zero by using Eqn (3.24).

3.14 Using Eqn (3.25), find the steady-state yaw rate Δr_R caused by the restoring yaw moment, which is produced by the side-slip angle calculated in Problem 3.13, assume the steering angle is equal to zero.

3.15 From Problem 3.14, it is possible to obtain the ratio $\Delta r_R / \Delta r_C$. A ratio larger than 1.0 means that the result is larger than the cause and the result causes larger next results and so on, then the vehicle eventually becomes unstable. Find the vehicle speed, which satisfies $\Delta r_R / \Delta r_C = 1.0$ and confirm that the speed found is identical to the critical vehicle speed obtained by Eqn (3.42).

REFERENCES

[1] D. W. Whitcomb et al., Design implication of a general theory of automative stability and control, Proceedings of IMechE (AD), 1956.

[2] J. R. Ellis, VEHICLE DYNAMICS, LONDON BUSINESS BOOK LTD., London, 1969.

Vehicle Motion by Disturbances

4.1 PREFACE

The previous chapter studied the basic characteristics of the vehicle motion, particularly the steer input. It is clear that a vehicle moving freely in the horizontal plane, without any direct restrictions from tracks, can be disturbed laterally by some external force acting on the vehicle in the lateral direction. In other words, because the vehicle has the ability of free plane motion, it cannot avoid unwanted motion by a disturbance.

In this chapter, vehicle motion characteristics are further understood by examining the motion of the vehicle when subjected to lateral disturbances. In these studies, the vehicle steer angle is always kept zero, and there is no controlling steer action that responds to the vehicle motion.

4.2 MOTION BY LATERAL FORCE EXERTED ON THE CENTER OF GRAVITY

When the vehicle is traveling on a banked road for example, a component of the vehicle weight will act as a lateral force at the center of gravity, as shown in Fig. 4.1. This section will look at the vehicle motion when the lateral force, Y, acts at the center of gravity.

4.2.1 Vehicle motion due to a step change in lateral force

In order to study the vehicle motion due to the lateral force, Y, the vehicle response to an idealized form of lateral force will be looked at. Generally, one ideal form of lateral force in this kind of situation is a step change. Consider the lateral force shown in Fig. 4.2 acting on the center of gravity of a vehicle traveling on a straight line.

If this disturbance force acts for a long enough time, even if the Y_0 value is small, the vehicle will eventually deviate away from its original path. The
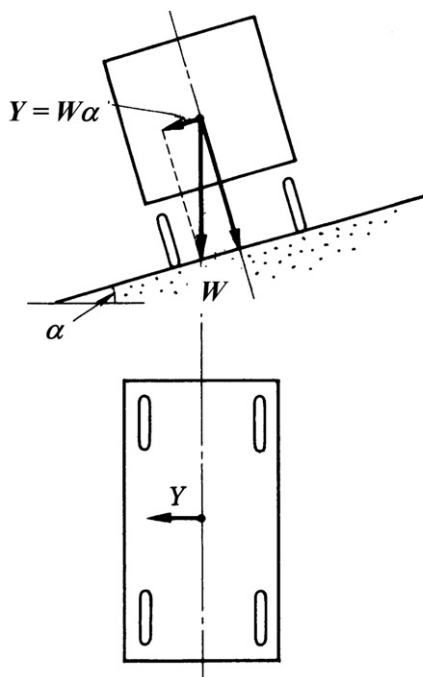
FIGURE 4.1 Lateral force exerted on CG.

vehicle motion in this case is more conveniently expressed with coordinates fixed on the vehicle itself, as discussed in subsection 3.2.1.

The vehicle equations of motion when the steer angle is zero and the lateral force acting at the center of gravity is Y, are found from Eqns (3.12) and (3.13) as below.

$$mV \frac{d\beta}{dt} + 2(K_f + K_r)\beta + \left\{ mV + \frac{2}{V}(l_f K_f - l_r K_r) \right\} r = Y \qquad (4.1)$$

$$2(l_f K_f - l_r K_r)\beta + I \frac{dr}{dt} + \frac{2(l_f^2 K_f + l_r^2 K_r)}{V} r = 0 \qquad (4.2)$$

where the magnitude of lateral force Y is not large, and the side-slip angle condition, $|\beta| \ll 1$, is always true, even during the vehicle motion.
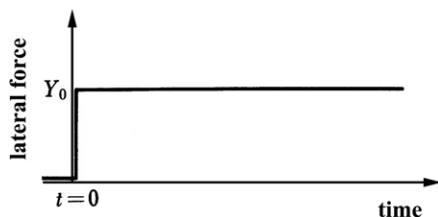
FIGURE 4.2 Step-form lateral force.

The side-slip and yaw rate response of the vehicle to Y can be obtained by Laplace transformation of Eqns (4.1) and (4.2). $\beta(s)$ and $r(s)$ are written as below.

$$\beta(s) = \frac{\begin{vmatrix} \frac{Y_0}{s} & mV + \frac{2}{V}(l_f K_f - l_r K_r) \\ 0 & Is + \frac{2(l_f^2 K_f + l_r^2 K_r)}{V} \end{vmatrix}}{\begin{vmatrix} mVs + 2(K_f + K_r) & mV + \frac{2}{V}(l_f K_f - l_r K_r) \\ 2(l_f K_f - l_r K_r) & Is + \frac{2(l_f^2 K_f + l_r^2 K_r)}{V} \end{vmatrix}}$$

$$= \frac{Y_0}{mV} \frac{s + a_\beta}{s(s^2 + 2\zeta\omega_n s + \omega_n^2)} \tag{4.3}$$

$$r(s) = \frac{\begin{vmatrix} mVs + 2(K_f + K_r) & \frac{Y_0}{s} \\ 2(l_f K_f - l_r K_r) & 0 \end{vmatrix}}{\begin{vmatrix} mVs + 2(K_f + K_r) & mV + \frac{2}{V}(l_f K_f - l_r K_r) \\ 2(l_f K_f - l_r K_r) & Is + \frac{2(l_f^2 K_f + l_r^2 K_r)}{V} \end{vmatrix}}$$

$$= \frac{Y_0}{mIV} \frac{a_r}{s(s^2 + 2\zeta\omega_n s + \omega_n^2)} \tag{4.4}$$

where

$$a_\beta = \frac{2(l_f^2 K_f + l_r^2 K_r)}{IV}, \qquad a_r = -2(l_f K_f - l_r K_r)$$

ω_n, ζ are the natural frequency and damping ratio given by Eqns (3.67) and (3.68) and Y_0/s is the Laplace transformation of Y.

(1) STEADY STATE CONDITION

First we will establish the final steady-state condition the vehicle reaches when acted on by a lateral force, as in Fig. 4.2.

Using Laplace transforms, the steady-state values of β and r become

$$\beta = \lim_{s \to 0} s\beta(s) = \frac{Y_0}{mV} \frac{a_\beta}{\omega_n^2} = \frac{l_f^2 K_f + l_r^2 K_r}{2l^2 K_f K_r \left[1 - \frac{m(l_f K_f - l_r K_r)}{2l^2 K_f K_r} V^2 \right]} Y_0 \tag{4.5}$$

$$r = \lim_{s \to 0} sr(s) = \frac{Y_0}{mIV} \frac{a_r}{\omega_n^2} = \frac{-(l_f K_f - l_r K_r)V}{2l^2 K_f K_r \left[1 - \frac{m(l_f K_f - l_r K_r)}{2l^2 K_f K_r} V^2 \right]} Y_0 \tag{4.6}$$

The above equation shows that β is always positive while r is positive when $l_f K_f < l_r K_r$ (US characteristic) and is negative when $l_f K_f > l_r K_r$ (OS characteristic) under $V < V_c$.

The physical meaning of Eqns (4.5) and (4.6) requires further discussion. For a vehicle with an US characteristic, the traveling condition and force equilibrium during steady state are shown in Fig. 4.3.

If the lateral disturbance, Y_0, acts on the vehicle, the center of gravity, P, will move and produce a side-slip angle of $\beta > 0$. Due to this β, the forces of $2K_f\beta$ and $2K_r\beta$ will be exerted on the front and rear tires. The resultant force of these two forces acts at the NSP, as explained in subsection 3.3.3 (3). The magnitude of the resultant force is $2(K_f + K_r)\beta$ and it acts in the opposite direction of Y_0. If the vehicle exhibits an US characteristic, the NSP is behind the center of gravity, P, and the resultant force produces an anti-clockwise yaw moment around the point P, as shown in Fig. 4.3.

If the vehicle motion is in steady state, a moment must act to balance this yawing moment. This moment can only be produced by a force acting on the tire, so there must be relative motion in lateral direction, other than β, between the tire and the road surface. Here, the anti-clockwise yaw motion around point P produces side-slip angles of $l_f r/V$ and $l_r r/V$ on the front and rear tires, respectively, as shown in Fig. 4.3. Two forces in an opposite direction to each other with the magnitude of $l_f K_f r/V$ and $l_r K_r r/V$ are exerted on the front and rear wheels to balance the yaw moment caused by the disturbance. This is why r in Eqn (4.6) is positive, and the vehicle makes an anti-clockwise circular motion when it exhibits US characteristic. The centrifugal force, mrV, also acts at the center of gravity in a direction opposite to Y_0. These forces are in the equilibrium so the vehicle is in steady-state cornering and heading outward from the circular path.

The vehicle with NS characteristic has the traveling condition and force equilibrium as shown in Fig. 4.4.

If the characteristic is NS, the NSP coincides with point P, and the resultant force of the tire forces, $2(K_f + K_r)\beta$, acts at the same position as Y_0. This resultant force does not produce any moment around the center of gravity and the vehicle has no yawing motion. There is no centrifugal force acting at the center of gravity. This is why r is zero in Eqn (4.6). The resultant force of the tire forces is in equilibrium with the external force, Y_0. Consequently, the vehicle continues its transverse motion while producing a side-slip angle.
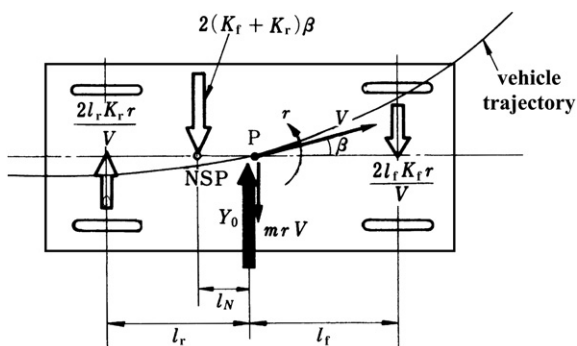

FIGURE 4.3 Steady state of US vehicle.

$$2(K_f + K_r)\beta$$
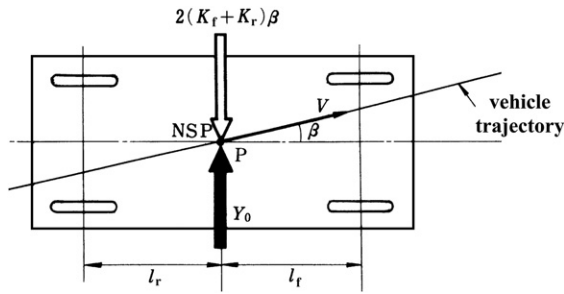
FIGURE 4.4 Steady state of NS vehicle.

Figure 4.5 shows the traveling condition and force equilibrium for an OS vehicle.

Here, the lateral force Y_0 moves the center of gravity to produce a side-slip angle. This side-slip angle generates forces of $2K_f\beta$ and $2K_r\beta$ at the front and rear wheels, and the resultant force acts at the NSP. If the vehicle characteristic is OS, the NSP is in front of P, and the resultant force $2(K_f + K_r)\beta$ produces a clockwise yaw moment around the vehicle center of gravity. In steady state, there must be a moment to balance this yawing moment. This moment is obtained from the front and rear lateral forces, $2K_f l_f r/V$ and $2K_r l_r r/V$, produced by the clockwise yawing motion of the vehicle. This is why r is negative in Eqn (4.6). Then, the centrifugal force, mrV, acts at the center of gravity in same direction as Y_0. When the vehicle exhibits an OS characteristic, the steady-state cornering is in the opposite direction to the case of US and the vehicle heads inwards of the circular path.

Figures 4.6(a) and (b) show how the vehicle side-slip angle, β, and yaw rate, r, change with traveling speed, during the steady-state cornering caused by lateral force, Y_0.

The figure shows that when the vehicle has an OS characteristic, it becomes more sensitive to disturbances as the vehicle speed increases.

$$2(K_f + K_r)\beta$$

FIGURE 4.5 Steady state of OS vehicle.
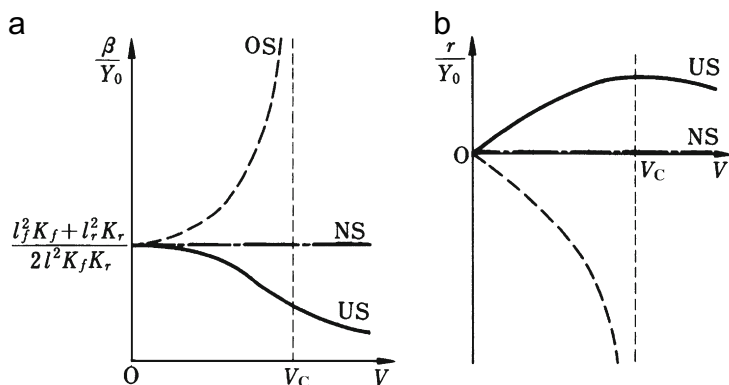
FIGURE 4.6 Steady-state cornering by lateral force Y_0.

(2) TRANSIENT CONDITION

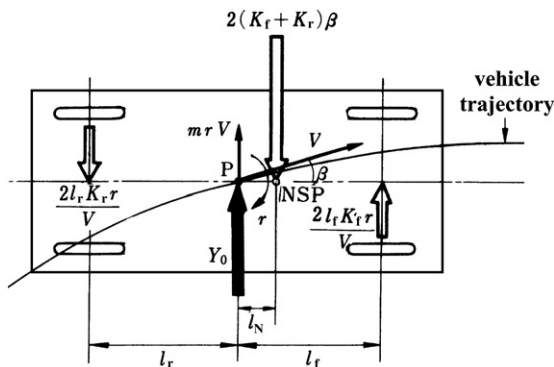The previous section examined the vehicle motion in-steady-state condition when subjected to a lateral disturbance, Y. Next we will study the transient response of the vehicle before reaching the steady state.

The transient response of the vehicle motion, with a lateral disturbance Y, can be obtained from Laplace transforms of Eqns (4.3) and (4.4). The equations will be studied for different levels of damping.

When $\zeta > 1$,

$$\beta(t) = \frac{Y_0}{mV}\left[\frac{a_\beta}{\omega_n^2} + \frac{a_\beta - (\zeta + \sqrt{\zeta^2 - 1})\omega_n}{2(\zeta + \sqrt{\zeta^2 - 1})\sqrt{\zeta^2 - 1}\omega_n^2}e^{(-\zeta - \sqrt{\zeta^2 - 1})\omega_n t}\right.$$
$$\left. - \frac{a_\beta - (\zeta - \sqrt{\zeta^2 - 1})\omega_n}{2(\zeta - \sqrt{\zeta^2 - 1})\sqrt{\zeta^2 - 1}\omega_n^2}e^{(-\zeta + \sqrt{\zeta^2 - 1})\omega_n t}\right] \tag{4.7}$$

$$r(t) = \frac{Y_0}{mIV}\left[\frac{a_r}{\omega_n^2} + \frac{a_r - (\zeta + \sqrt{\zeta^2 - 1})\omega_n}{2(\zeta + \sqrt{\zeta^2 - 1})\sqrt{\zeta^2 - 1}\omega_n^2}e^{(-\zeta - \sqrt{\zeta^2 - 1})\omega_n t}\right.$$
$$\left. - \frac{a_r - (\zeta - \sqrt{\zeta^2 - 1})\omega_n}{2(\zeta - \sqrt{\zeta^2 - 1})\sqrt{\zeta^2 - 1}\omega_n^2}e^{(-\zeta + \sqrt{\zeta^2 - 1})\omega_n t}\right] \tag{4.8}$$

when $\zeta = 1$,

$$\beta(t) = \frac{Y_0}{mV}\left[\frac{a_\beta}{\omega_n^2} + \left(\frac{\omega_n - a_\beta}{\omega_n}t - \frac{a_\beta}{\omega_n^2}\right)e^{-\omega_n t}\right] \tag{4.7'}$$

$$r(t) = \frac{Y_0}{mIV}\left[\frac{a_r}{\omega_n^2} + \left(\frac{\omega_n - a_r}{\omega_n}t - \frac{a_r}{\omega_n^2}\right)e^{-\omega_n t}\right] \tag{4.8'}$$

and when the transient response is oscillatory at $\zeta < 1$,

$$\beta(t) = \frac{Y_0}{mV}\left[\frac{a_\beta}{\omega_n^2} + \frac{1}{\omega_n^2\sqrt{1-\zeta^2}}\sqrt{(a_\beta - \zeta\omega_n)^2 + (1-\zeta^2)\omega_n^2}\, e^{-\zeta\omega_n t}\right.$$
$$\left. \times \sin\left(\sqrt{1-\zeta^2}\omega_n t + \Psi_\beta\right)\right]$$

$$(4.7)''$$

where

$$\Psi_\beta = \tan^{-1}\left(\frac{\sqrt{1-\zeta^2}\omega_n}{a_\beta - \zeta\omega}\right) - \tan^{-1}\left(\frac{\sqrt{1-\zeta^2}}{-\zeta}\right)$$

$$r(t) = \frac{Y_0}{mIV}\left[\frac{a_r}{\omega_n^2} + \frac{1}{\omega_n^2\sqrt{1-\zeta^2}}\sqrt{(a_r - \zeta\omega_n)^2 + (1-\zeta^2)\omega_n^2}\, e^{-\zeta\omega_n t}\right.$$
$$\left. \times \sin\left(\sqrt{1-\zeta^2}\omega_n t + \Psi_r\right)\right]$$

$$(4.8)''$$

where

$$\Psi_r = \tan^{-1}\left(\frac{\sqrt{1-\zeta^2}\omega_n}{a_r - \zeta\omega}\right) - \tan^{-1}\left(\frac{\sqrt{1-\zeta^2}}{-\zeta}\right)$$

It is rather difficult to gain a comprehensive understanding of the vehicle transient motion from the time histories of the vehicle response, so the transient motion is considered in a more realistic manner. First the case of US vehicle is considered. If a step lateral force is applied at the center of gravity of a vehicle traveling in straight line, the vehicle will, initially, produce a side-slip angle, β, at the center of gravity. At this instant, the vehicle has no other motion and the front and rear side slip angles are both equal to β. The above condition is shown in Fig. 4.7(a).

As the vehicle is US, the resultant force produces an anti-clockwise yaw moment around the vehicle center of gravity, and the vehicle begins its yaw motion. This yaw motion acts to reduce the side-slip angle produced initially at the center of gravity. It produces new side-slip angles at the front and rear wheels, which lead to lateral forces acting in opposite directions to each other. The moment produced by these forces is in the opposite direction to the moment caused by β. The centrifugal force acts at the center of gravity in a direction opposite to Y_0. This condition is shown in Fig. 4.7(b). The anti-clockwise yaw motion reduces the center of gravity side-slip angle. As the centrifugal force acts in the opposite direction to the lateral force, the resultant force of the tire forces required to maintain an equilibrium condition becomes smaller compared to (a). Moreover, the acting point moves from the original NSP towards point P, and the acting moment becomes smaller compared to (a).

In this way, the transient motion of the vehicle with US characteristic when acted on by the lateral disturbance, Y, reduces the effect of the lateral force. The
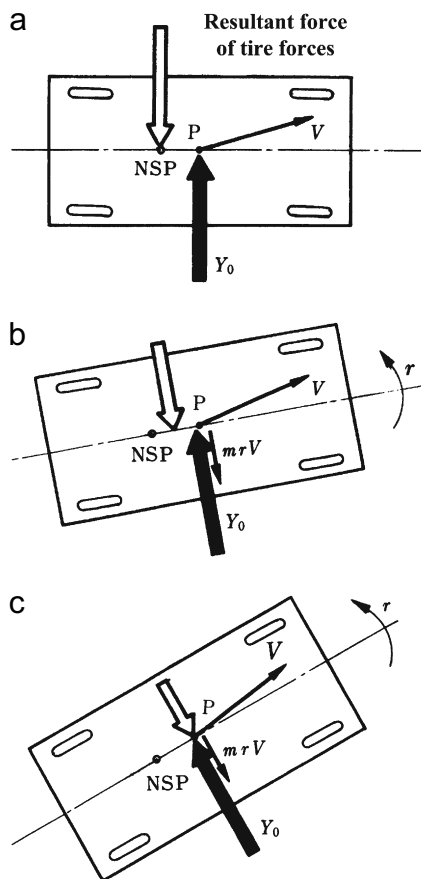
FIGURE 4.7 Transient motion of US vehicle due to lateral force Y_0.

effect of the lateral force, Y, becomes smaller due to the vehicle motion induced by the lateral force Y. Finally, the vehicle motion reaches a steady-state condition as shown in Fig. 4.7(c). If the vehicle exhibits an NS characteristic, the resultant force of the tire forces acts at the same point as the lateral force, P. As a result, there is no yaw moment acting on the vehicle. When $l_f K_f = l_r K_r$ in Eqns (4.1) and (4.2), r and β become uncoupled with each other. As long as the lateral force acts at the center of gravity, r is independent from any effects. In other words, for the case of NS, the vehicle response to the lateral force Y is only represented by side-slip motion.

Consider the case of an OS vehicle, as with the two previous cases, when a lateral force is added, the vehicle will produce a side-slip angle, β, at the center of gravity. At this instance, the front and rear side-slip angles are both equal to β, and the resultant force acts at the NSP. The above condition is shown in Fig. 4.8(a).

As the vehicle has an OS characteristic, the resultant force produces a clockwise yaw moment around the vehicle center of gravity. This yaw motion
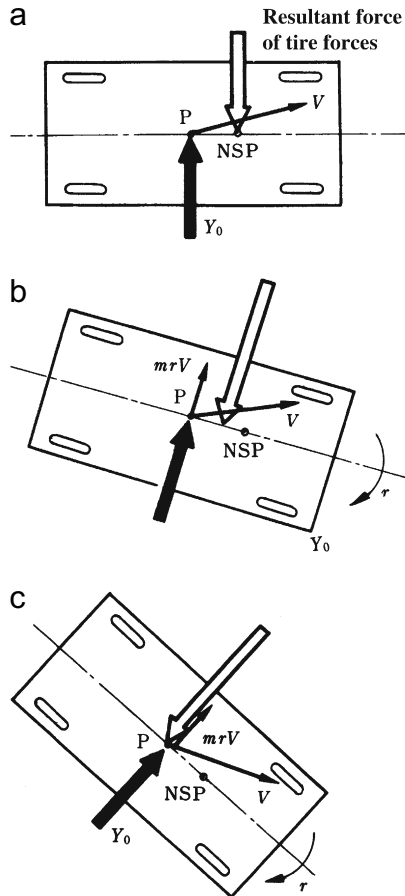
FIGURE 4.8 Transient motion of OS vehicle due to lateral force Y_0.

increases the side-slip angle produced initially at the center of gravity since a centrifugal force caused by the yaw motion acts at the center of gravity in the same direction as the lateral force Y_0. This condition is shown in Fig. 4.8(b). As the vehicle clockwise yaw motion increases, the center of gravity side-slip angle becomes larger and, because the centrifugal force acts in the same direction to the lateral force, the resultant force of the tire forces becomes larger than that in (a). Although the position of the resultant force moves from the original NSP towards the point P, the moment acting on the vehicle may not get smaller, as in the case of US, because resultant force magnitude increases.

When the vehicle exhibits an OS characteristic, the vehicle may not always reduce the effect of Y, as in the case of US. On the contrary, the vehicle motion might possibly excite the effect of Y on the vehicle. In particular, the centrifugal force increases dramatically with increasing vehicle speed. Beyond a certain speed, the centrifugal force due to the vehicle yaw motion becomes too large
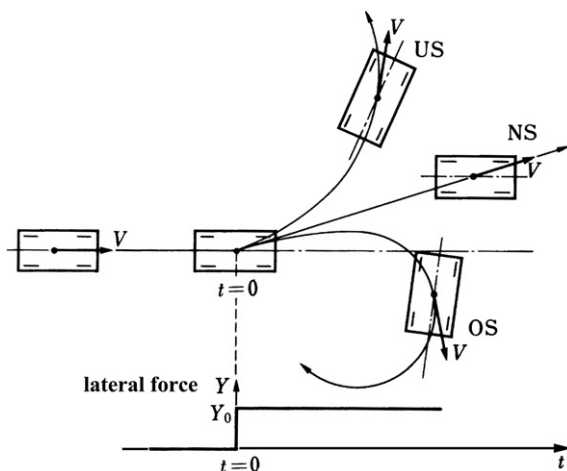
FIGURE 4.9 Vehicle motion to step-form lateral force on CG.

and the yaw moment acting on the vehicle becomes larger. Ultimately, the vehicle could fall into a spin motion. This velocity limit is the same as the stability limit velocity V_c derived in subsection 3.4.1 (1) and is the velocity that causes the denominator to be 0 in Eqns (4.5) and (4.6). If the vehicle traveling speed is below V_c, the resultant force acts at P, and the resultant force is in equilibrium with the centrifugal force and Y_0. The vehicle reaches its steady-state condition as shown in Fig. 4.8(c).

When the vehicle exhibits OS characteristics, even if there is no unstable condition, i.e., $V < V_c$, the vehicle motion caused by the lateral force acting at the center of gravity still excites the vehicle motion. When $V > V_c$, the vehicle dynamics fall into a mathematically unstable condition, and the steady condition cannot be reached. Figure 4.9 schematically shows the vehicle motion due to the lateral force Y in correspondence to different steer characteristics.

Example 4.1

In order to understand the vehicle response time history to the step disturbance force exerted on the vehicle CG more definitely and to confirm the schematic explanation of the effects of the steer characteristics on the vehicle response in Fig. 4.9, execute the vehicle response simulation to the disturbance of 4 kN exerted on CG with the Matlab–Simulink software. Regard the vehicle speed is 80 km/h and the steering angle is always fixed to zero. Calculate the vehicle track after the disturbance as well as the vehicle yaw rate and side-slip responses for the US, NS, and OS vehicles with the same vehicle parameters as in **Example 3.7**, respectively.
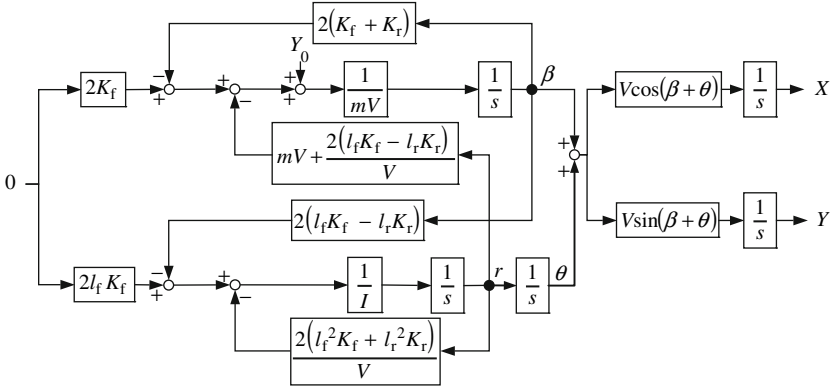
FIGURE E4.1(a).

Solution

The simulation is based on the same equations as the ones used in Example 3.6, just putting $\delta = 0$, which are as follows:

$$\frac{d\beta}{dt} = -\frac{2(K_f + K_r)}{mV}\beta - \left\{1 + \frac{2}{mV^2}(l_fK_f - l_rK_r)\right\}r + \frac{Y_0}{mV} \qquad \text{(E4.1)}$$

$$\frac{dr}{dt} = -\frac{2(l_fK_f - l_rK_r)}{I}\beta - \frac{2(l_f^2K_f + l_r^2K_r)}{IV}r \qquad \text{(E4.2)}$$


```
1      % Vehicle parameters
2 -      m = 1500;   % mass (kg)
3 -      I = 2500;   % moment of inertia about z-axis:I (kgm^2)
4 -      lf = 1.1;   % distance from C.O.G to front axle (m)
5 -      lr = 1.6;   % distance from C.O.G to front axle (m)
6 -      l = lf+lr;  % wheel base (m)
7 -      Kf = 55000; % front cornering stiffness (N/rad)
8 -      Kr = 60000; % rear cornering stiffness (N/rad)
9      % Simulation parameters
10 -     dt = 0.001; % simulation rate (s)
11 -     tf = 4.0;   % simulation time (s)
12 -     V = 80/3.6; % velocity (m/s)
13 -     Sf = 0.0;   % front tire steer angle (rad)
14 -     YO = 4000;  % side wind(N)
```
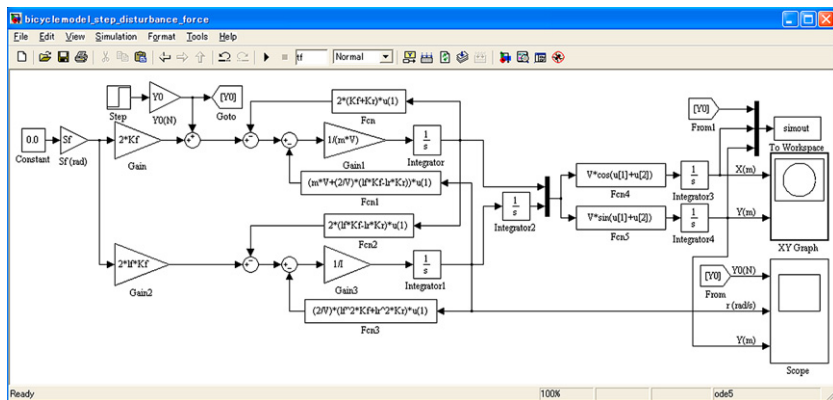
FIGURE E4.1(b).

FIGURE E4.1(c).
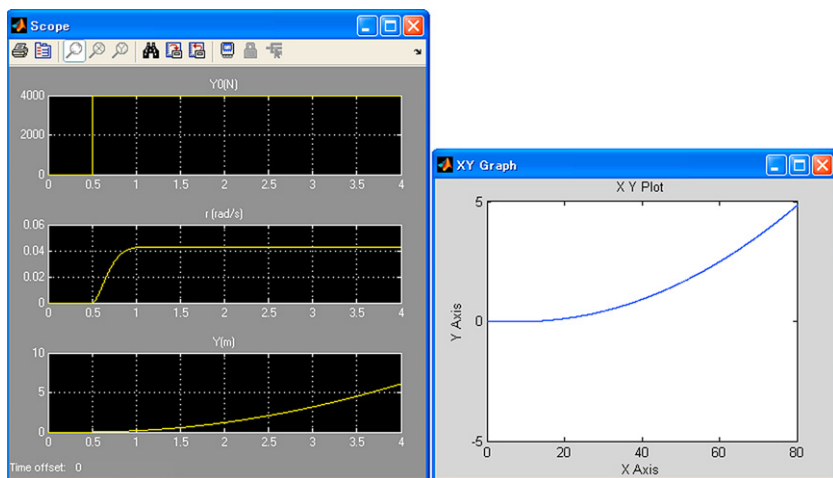
FIGURE E4.1(d).
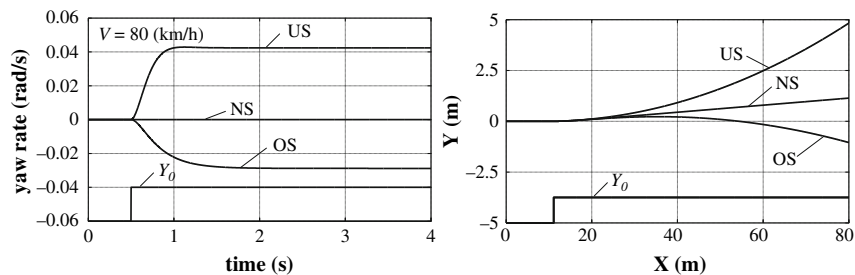
FIGURE E4.1(e).

In addition to the above, the equations introduced in Example 3.2 are needed for the calculation of the vehicle track:

$$\frac{dX}{dt} = V\cos(\beta + \theta) \tag{E3.1}$$

$$\frac{dY}{dt} = V\sin(\beta + \theta) \tag{E3.2}$$

$$\frac{d\theta}{dt} = r \tag{E4.3}$$

From the equations above, it is possible to have the integral type of block diagram of the vehicle motion due to the disturbance at CG as shown in Fig. E4.1(a). The vehicle parameters used in the simulation is shown in Fig. E4.1(b). Figure E4.1(c) shows the simulation program and Fig. E4.1(d) is a result of the simulation. The summarized effects of the steer characteristics on the vehicle behaviors are shown in Fig. E4.1(e).

4.2.2 Vehicle motion due to impulse lateral force

The vehicle motion due to an idealized form of lateral force at the center of gravity was studied in the previous section. For the actual vehicle, a lateral force acting at the center of gravity for a substantially long time is rare. Instead, a condition where the vehicle travels in a straight line, and part of the road banks, is more practical.

In this situation, vehicle motion is acted on by a lateral force as shown in Fig. 4.10. The impulse acting on the vehicle in the lateral direction, $Y_0\Delta t$, is not so large and the vehicle will not deviate largely from its original path. Under these circumstances, the vehicle motion is more conveniently expressed by coordinates fixed on the ground.

If the steer angle is zero, the vehicle equations of motion when acted on by the lateral force Y could be written as below, using Eqns (3.21) and (3.22), when $|\theta| \ll 1$:

$$m\frac{d^2y}{dt^2} + \frac{2(K_f + K_r)}{V}\frac{dy}{dt} + \frac{2(l_f K_f - l_r K_r)}{V}\frac{d\theta}{dt} - 2(K_f + K_r)\theta = Y \tag{4.9}$$
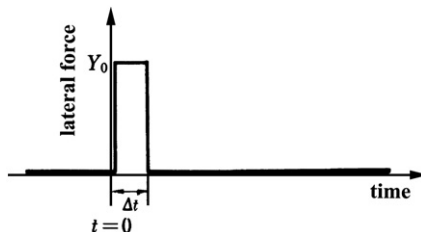
FIGURE 4.10 Pulse-form lateral force on CG.

$$\frac{2(l_f K_f - l_r K_r)}{V}\frac{dy}{dt} + I\frac{d^2\theta}{dt^2} + \frac{2(l_f^2 K_f + l_r^2 K_r)}{V}\frac{d\theta}{dt} - 2(l_f K_f - l_r K)\theta = 0$$

(4.10)

When Δt is very small compared to the period of the vehicle motion, the approximate Laplace transform of the lateral force Y, $Y(s)$, could be taken as $Y_0 \Delta t$. Consequently, the vehicle response to Y could be obtained by carrying out Laplace transforms on the above equations to find $y(s)$ and $\theta(s)$.

$$y(s) = \frac{\begin{vmatrix} Y_0\Delta t & \frac{2(l_f K_f - l_r K_r)}{V}s - 2(K_f + K_r) \\ 0 & Is^2 + \frac{2(l_f^2 K_f + l_r^2 K_r)}{V}s - 2(l_f K_f - l_r K_r) \end{vmatrix}}{\begin{vmatrix} ms^2 + \frac{2(K_f + K_r)}{V}s & \frac{2(l_f K_f - l_r K_r)}{V}s - 2(K_f + K_r) \\ \frac{2(l_f K_f - l_r K_r)}{V}s & Is^2 + \frac{2(l_f^2 K_f + l_r^2 K_r)}{V}s - 2(l_f K_f - l_r K_r) \end{vmatrix}}$$

$$= \frac{Y_0\Delta t}{m}\frac{s^2 + a_{y1}s + a_{y2}}{s^2(s^2 + 2\zeta\omega_n s + \omega_n^2)}$$

(4.11)

$$\theta(s) = \frac{\begin{vmatrix} ms^2 + \frac{2(K_f + K_r)}{V}s & Y_0\Delta t \\ \frac{2(l_f K_f - l_r K_r)}{V}s & 0 \end{vmatrix}}{\begin{vmatrix} ms^2 + \frac{2(K_f + K_r)}{V}s & \frac{2(l_f K_f - l_r K_r)}{V}s - 2(K_f + K_r) \\ \frac{2(l_f K_f - l_r K_r)}{V}s & Is^2 + \frac{2(l_f^2 K_f + l_r^2 K_r)}{V}s - 2(l_f K_f - l_r K_r) \end{vmatrix}}$$

$$= \frac{Y_0\Delta t}{mIV}\frac{a_r}{s(s^2 + 2\zeta\omega_n s + \omega_n^2)}$$

(4.12)

where

$$a_{y1} = \frac{2(l_f^2 K_f + l_r^2 K_r)}{IV}, \qquad a_{y2} = \frac{-2(l_f K_f - l_r K_r)}{I}$$

$$a_r = -2(l_f K_f - l_r K_r)$$

From these equations, the steady state reached by the vehicle is

$$y = \lim_{s \to 0} sy(s) = \pm\infty \quad (\text{when } l_f K_f \neq l_r K_r)$$

$$= \frac{l_f^2 K_f + l_r^2 K_r}{2l^2 K_f K_r}VY_0\Delta t \quad (\text{when } l_f K_f = l_r K_r)$$

(4.13)

$$\theta = \lim_{s \to 0} s\theta(s) = \frac{-(l_f K_f - l_r K_r)VY_0\Delta t}{2l^2 K_f K_r\left[1 - \frac{m(l_f K_f - l_r K_r)}{2l^2 K_f K_r}V^2\right]}$$

(4.14)

When $l_f K_f < l_r K_r$, and the vehicle has an US characteristic, $y = +\infty$; if $l_f K_f > l_r K_r$ and the vehicle has an OS characteristic, $y = -\infty$. Also, θ is positive for an US vehicle, negative for an OS vehicle and 0 for NS.

The vehicle has the same transient response for $Y = Y_0$ during $0 \le t \le \Delta t$, as the response to a step lateral force. At $t = \Delta t$, the lateral force Y becomes zero, and the vehicle center of gravity side-slip angle becomes small immediately. The lateral force acting at the tires due to the yaw motion becomes more predominant. These forces reduce the yaw motion and the vehicle maintains a constant yaw angle relative to the original traveling direction. This is positive for an US vehicle and negative for an OS vehicle. Consequently, the vehicle lateral displacement, y, relative to the coordinates fixed on the ground, increases in the positive direction for US and in negative direction for OS.

When the vehicle exhibits an NS characteristic, the yaw angle is not produced and the vehicle continues to travel straight, maintaining the original traveling direction after a constant lateral displacement.

Figure 4.11 shows the vehicle response to the lateral force, Y, for different steer characteristics.

4.2.3 Vehicle motion due to external disturbances and steer characteristics

As explained above, the vehicle motion due to the lateral forces acting at the center of gravity is greatly affected by the vehicle steer characteristics. Based on the studies until now, concerning the vehicle motions due to disturbances acting at the center of gravity in the lateral direction, the concept of steer characteristics could be rearranged as below.

When a traveling vehicle suddenly has a yaw velocity of r, then a centrifugal force of mrV acts at the vehicle center of gravity. As seen in the previous sections, lateral forces will act at the front and rear tires due to the side-slip angle of the center of gravity caused by the external force. The acting point of the resultant force is at the NSP. If the NSP is at the rear of the center of gravity, the resultant force will control the yawing motion caused by the yaw velocity, r. The US characteristic controls motions produced by the disturbances.
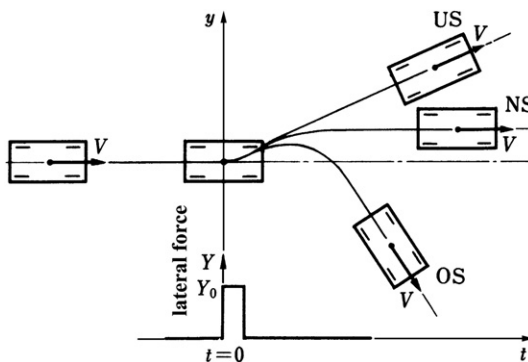
FIGURE 4.11 Vehicle motion due to pulse-form lateral force on CG.

If the NSP is in front of the center of gravity, the resultant force will excite the yaw motion. Here, the OS characteristic has a mechanism of exciting the motions produced by the disturbance through its own motion. From the motion mechanics point of view, this is why a vehicle with an OS characteristic is termed to be inferior in terms of directional stability. An NS characteristic means that the forces acting at the tires due to the side-slip angle of the center of gravity have no effect on the yawing motion.

The above discussions are shown in Fig. 4.12.

The vehicle steer characteristic not only describes the vehicle steady-state cornering characteristic, but also gives a strong indication of the vehicle's motion characteristics under external disturbances. It is understood here that the cross-coupling of vehicle side slip and yaw motions plays a principal role in determining the vehicle steer characteristics.

From subsection 4.2.1, if a constant lateral force, Y_0, acts at the center of gravity of a vehicle traveling with constant velocity, V, a yaw velocity of r given by Eqn (4.6) will be produced. The center of gravity acceleration, $\ddot{y}$, is

$$\ddot{y} = Vr = \frac{-\frac{m(l_f K_f - l_r K_r)}{2l^2 K_f K_r}V^2}{1 - \frac{m(l_f K_f - l_r K_r)}{2l^2 K_f K_r}V^2} \frac{Y_0}{m} \tag{4.15}$$

The lateral force of magnitude, Y_0, could be expressed as a unit of acceleration as below.
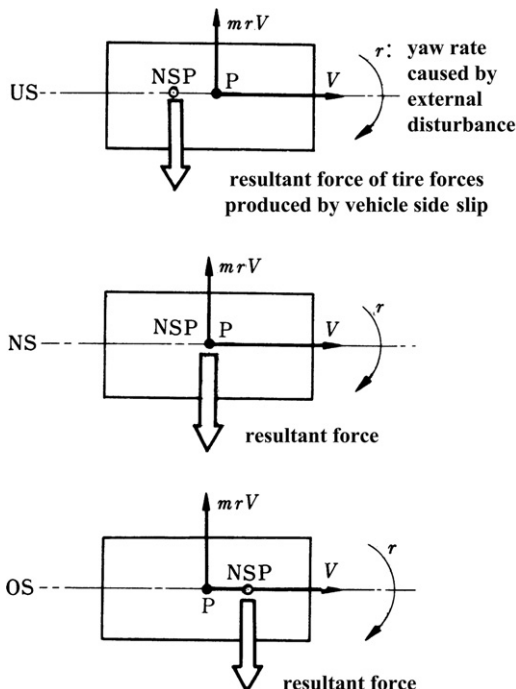
FIGURE 4.12 Vehicle motion due to external disturbance and steer characteristics.

$$\ddot{y}_0 = \frac{Y_0}{m} \tag{4.16}$$

The ratio of $\ddot{y}$ and $\ddot{y}_0$ is called the under-steer rate [1], U_R. The vehicle steer characteristic could also be based on this value.

$$U_R = \frac{\ddot{y}}{\ddot{y}_0} \tag{4.17}$$

A vehicle with U_R of 100% has a center of gravity acceleration, Y_0/m, and the circular motion radius is mV^2/Y_0. The vehicle with U_R of 0% is NS, and if U_R is negative, the vehicle is OS.

The vehicle steer characteristic is not only a characteristic of the vehicle steady-state cornering, but also a characteristic of the disturbance at its center of gravity, when the steer angle is zero. Substituting Eqns (4.15) and (4.16) into Eqn (4.17), the under-steer rate, U_R, could be written using the stability factor A from Eqn (3.43):

$$U_R = \frac{AV^2}{1 + AV^2} \tag{4.18}$$

When $A > 0$, U_R is positive and less than 1 for all velocities. In other words, when the vehicle has US characteristics and the external force of magnitude Y_0 is applied to the center of gravity, the lateral acceleration is always less than Y_0/m. On the contrary, when $A < 0$, U_R becomes negative, and at the velocity, which satisfies $AV^2 < -0.5$, the absolute value of U_R is greater than 1. When the vehicle has OS characteristics, the lateral acceleration is less than Y_0/m at the vehicle speed is lower than a certain value. It becomes greater than Y_0/m at higher speeds.

The vehicle response to a sudden yaw moment disturbance, as shown in Fig. 4.13, helps to understand more firmly that the OS vehicle is more sensitive to the external disturbance and less stable in terms of directional stability. The vehicle motion caused by the yaw moment is described by the following equations.

$$m\frac{d^2y}{dt^2} + \frac{2(K_f + K_r)}{V}\frac{dy}{dt} + \frac{2(l_fK_f - l_rK_r)}{V}\frac{d\theta}{dt} - 2(K_f + K_r)\theta = 0 \tag{4.9'}$$
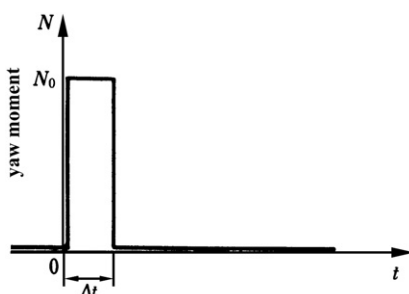
FIGURE 4.13 Disturbance yaw moment.

$$\frac{2(l_fK_f - l_rK_r)}{V}\frac{dy}{dt} + I\frac{d^2\theta}{dt^2} + \frac{2(l_f^2K_f + l_r^2K_r)}{V}\frac{d\theta}{dt} - 2(l_fK_f - l_rK)\theta = N$$

$$(4.10)'$$

Applying the Laplace transform to the above equations, the steady state yaw angle to the yaw moment input is obtained as follows.

$$\theta = \lim_{s \to 0} s\theta(s) = \frac{(K_f + K_r)VN_0\Delta t}{2l^2K_fK_r\left[1 - \frac{m(l_fK_f - l_rK_r)}{2l^2K_fK_r}V^2\right]}$$

Here, Δt is small enough that the yaw moment, N, is a pulse form with the magnitude N_0 of which the Laplace transformation is $N_0\Delta t$.

This equation shows the change of the vehicle attitude angle caused by the disturbance yaw moment with respect to the vehicle speed, as in Fig. 4.14. It is obvious that the stronger the vehicle OS aspect is, the larger the change of the attitude angle and the more sensitive it is to the disturbance.
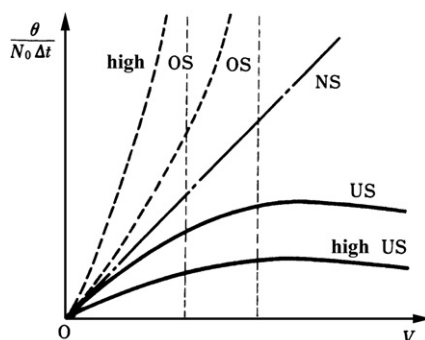
FIGURE 4.14 Change of vehicle attitude angle due to disturbance yaw moment.

4.3 VEHICLE MOTION DUE TO A LATERAL WIND DISTURBANCE

Vehicles traveling at high speeds encounter lateral wind disturbances, which result in lateral motion. This section will look at the basic motion characteristics of the vehicle traveling in a straight line, when it is acted on by a lateral wind disturbance.

4.3.1 Lateral wind disturbance force

If the vehicle traveling in a straight line at velocity, V, as shown in Fig. 4.15, is subjected to a lateral wind velocity of w, the lateral force, Y_w, and yaw moment, N_w, acting on the vehicle are expressed as

$$Y_w = C_y\frac{\rho}{2}S(V^2 + w^2) \qquad (4.19)$$
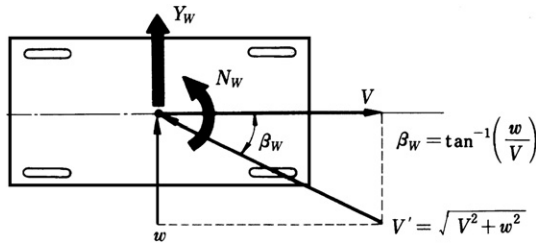
FIGURE 4.15 Disturbance force and yaw moment caused by side wind.

$$N_w = C_n \frac{\rho}{2} lS(V^2 + w^2) \tag{4.20}$$

Here, C_y is the lateral force coefficient, C_n is the yawing moment coefficient, and both are functions of the relative side-slip angle of the airflow, β_w. C_n is positive in the anti-clockwise direction, ρ is the air density, S is the vehicle frontal area, and l is the vehicle dimension normally taken as the wheelbase.

Figure 4.16 shows the lateral force coefficient and yawing moment coefficient related to the relative side-slip angle of the airflow, for a normal passenger car [2]. This figure shows that C_y and C_n increase with β_w and are significantly affected by the vehicle shape.

The acting point of the lateral force, Y_w, is called the aerodynamic center (AC). The distance between AC and the vehicle center of gravity is l_w, and is
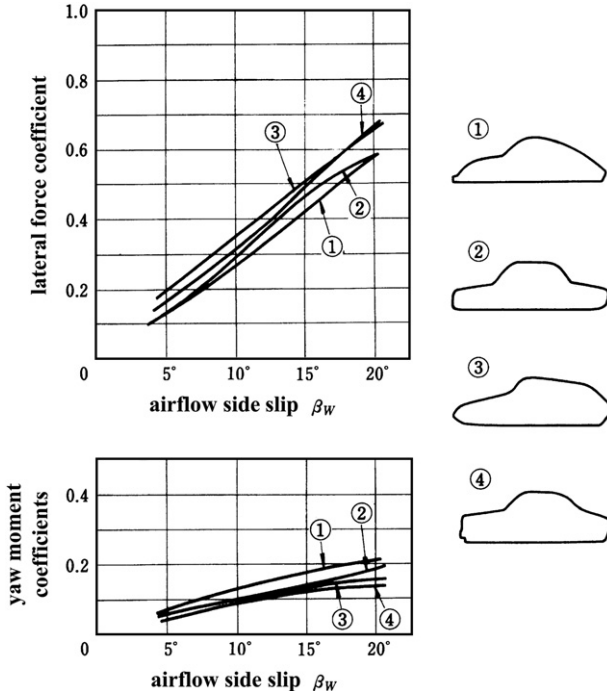
FIGURE 4.16 Lateral force and yaw moment coefficients of side wind.
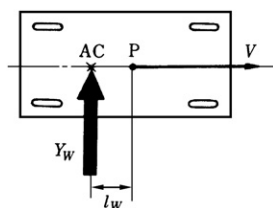
FIGURE 4.17 Lateral force by side wind.

positive if AC is behind the center of gravity. The yaw moment acting on the vehicle N_w can be written as

$$N_w = -l_w Y_w$$

The vehicle motion due to the lateral wind is caused by a lateral force, Y_w, acting at AC, a distance l_w from the center of gravity, as shown in Fig. 4.17.

Strictly speaking, C_y and C_n change with β_w, and β_w changes with vehicle motion. For example, if the vehicle is subjected to a constant lateral wind, Y_w and N_w are not constant but change with the vehicle motion. If the transient vehicle motion is not too long, Y_w and N_w can be viewed independently from the vehicle motion, which simplifies the analysis.

4.3.2 Vehicle motion due to lateral wind with constant speed

The vehicle motion when subjected to a constant speed lateral wind is shown in Fig. 4.18. At this time, the lateral force, Y_w, is assumed to be a step force that acts at the vehicle AC.

It is convenient to express the vehicle motion with coordinates fixed on the vehicle, as in subsection 4.2.1. By using Eqns (3.12) and (3.13), the equations of motion are derived as below.

$$mV \frac{d\beta}{dt} + 2(K_f + K_r)\beta + \left\{ mV + \frac{2}{V}(l_f K_f - l_r K_r) \right\} r = Y_w \qquad (4.21)$$

$$2(l_f K_f - l_r K_r)\beta + I\frac{dr}{dt} + \frac{2(l_f^2 K_f + l_r^2 K_r)}{V} r = -l_w Y_w \qquad (4.22)$$

The vehicle response to Y_w can be obtained by applying Laplace transforms to Eqns (4.21) and (4.22) as in subsection 4.2.1. $\beta(s)$ and $r(s)$ are obtained as follows:

$$\beta(s) = \frac{Y_{w0}}{mV} \frac{s + b_\beta}{s(s^2 + 2\zeta\omega_n s + \omega_n^2)} \qquad (4.23)$$

FIGURE 4.18 Side wind with constant speed.

$$r(s) = \frac{-l_w Y_{w0}}{I} \cdot \frac{s + b_r}{s(s^2 + 2\zeta\omega_n s + \omega_n^2)} \tag{4.24}$$

where

$$b_\beta = \frac{2(l_f^2 K_f + l_r^2 K_r) + 2l_w(l_f K_f - l_r K_r)}{IV} + \frac{ml_w V}{I}$$

$$= \frac{2}{IV}\left[l_f^2 K_f + l_r^2 K_r - l_w l_N(K_f + K_r)\right] + \frac{ml_w V}{I}$$

$$b_r = \frac{2(K_f + K_r)}{mV} + \frac{2(l_f K_f - l_r K_r)}{ml_w V} = \frac{2(l_w - l_N)}{ml_w V}(K_f + K_r)$$

Y_{w0} is the magnitude of the step lateral force. From these equations, the steady-state values of β and r are as follows:

$$\beta = \frac{\left[(l_f^2 K_f + l_r^2 K_r) - l_w l_N(K_f + K_r)\right] + \frac{ml_w}{2}V^2}{2l^2 K_f K_r\left[1 - \frac{m(l_f K_f - l_r K_r)}{2l^2 K_f K_r}V^2\right]}Y_{w0} \tag{4.25}$$

$$r = \frac{(l_N - l_w)(K_f + K_r)V}{2l^2 K_f K_r\left[1 - \frac{m(l_f K_f - l_r K_r)}{2l^2 K_f K_r}V^2\right]}Y_{w0} \tag{4.26}$$

where l_N is the distance between NSP and the center of gravity.

$$l_N = -\frac{(l_f K_f - l_r K_r)}{K_f + K_r} \tag{3.44}$$

From Eqn (4.26), when $l_N > l_w$, then $r > 0$; if $l_N = l_w$, $r = 0$; and when $l_N < l_w$, $r < 0$. l_N and l_w are taken as positive if the NSP and AC are behind the center of gravity. When $l_f K_f - l_r K_r > 0$, it is assumed that $V < V_c$.

The vehicle subjected continuously to lateral wind with constant speed, traveling in straight line, will ultimately enter into anti-clockwise circular motion if the aerodynamic center, AC, is in front of the NSP. It produces no circular motion except at transient period when the AC coincides with the NSP, and clockwise circular motion when the AC is behind the NSP. The relative position of the vehicle center of gravity to AC and NSP has no direct effect. Figure 4.19 shows the results of a computer simulation of the motion of a passenger car when it is acted on by the lateral wind disturbance.
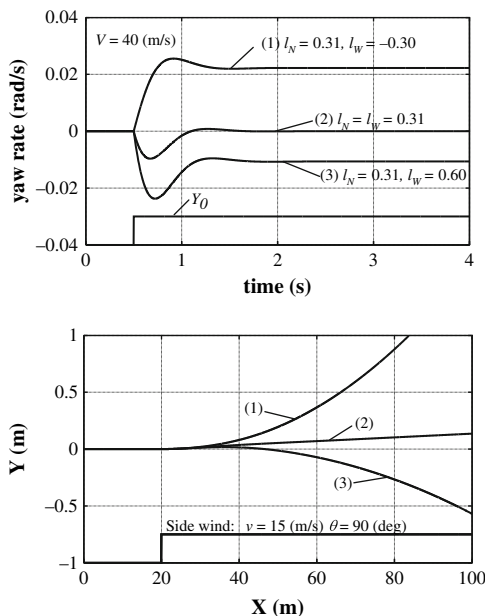
FIGURE 4.19 Vehicle motion subjected to side wind with constant speed.

The steady-state value of the lateral acceleration is Vr and, from Eqn (4.26), the steady-state value of the lateral acceleration per unit lateral wind force could be expressed as below.

$$S_w = \frac{Vr}{Y_{w0}} = \frac{(l_N - l_w)(K_f + K_r)V^2}{2l^2 K_f K_r \left[1 - \frac{m(l_f K_f - l_r K_r)}{2l^2 K_f K_r}V^2\right]} \tag{4.27}$$

This is termed the sensitivity coefficient of lateral wind and is suggested to be the index that shows the vehicle sensitivity to a lateral wind disturbance.

Example 4.2

Find the front wheel steer angle needed to keep the vehicle running on a straight path having a side wind with constant wind speed. Also, calculate the attitude angle of the vehicle with respect to the straight path during this period.

Solution

The steady-state yaw rate response to the constant side wind force is expressed by Eqn (4.26). On the other hand, the steady-state yaw rate response to the steering input is given by Eqn (3.39). If the sum of both yaw rates above is zero, it is regarded that the vehicle yaw motion caused by the side wind is eliminated by the yaw motion due to the front wheel

steering, i.e., the vehicle runs on a straight line having the side wind, which is described by:

$$\frac{(I_N - I_W)(K_f + K_r)V}{2I^2 K_f K_r \left[1 - \frac{m(I_f K_f - I_r K_r)}{2I^2 K_f K_r}V^2\right]} Y_{W0} + \frac{1}{2I^2 K_f K_r \left[1 - \frac{m(I_f K_f - I_r K_r)}{2I^2 K_f K_r}V^2\right]} \frac{V}{I}\delta_0 = 0$$

(E4.4)

From this equation, the steering angle is obtained as:

$$\delta_0 = \frac{I_W - I_N}{2I}\left(\frac{1}{K_f} + \frac{1}{K_r}\right)Y_{W0}$$

(E4.5)

It is understood that if I_N is greater than I_W, the steering angle in the counter direction to the wind is needed, on the other hand, greater I_W than I_N requires the steering angle in the following direction to the wind in order for the vehicle to keep the straight path under the side wind.

The attitude angle of the vehicle to the straight path is identical to the side-slip angle, β, of the vehicle. As the side wind force is balanced by the total lateral force of the front and rear tires:

$$-2K_f(\beta - \delta_0) - 2K_r\beta + Y_{W0} = 0$$

(E4.6)

Putting the above Eqn (E4.5) into this equation, the attitude angle is obtained as:

$$\beta = \frac{(I_f + I_W)Y_{W0}}{2I K_r} = \frac{(I_f + I_W)Y_{W0}}{2(I_f + I_N)(K_f + K_r)}$$

(E4.7)

In this process, pay attention to the relation, $I_N = -(I_f K_f - I_r K_r)/(K_f + K_r)$.

4.3.3 Vehicle motion due to a lateral wind gust

Consider the situation where the vehicle is subjected to a sudden lateral gust with the front steering angle fixed to zero. It is assumed that the lateral force Y_w as shown in Fig. 4.20 acts at the vehicle AC.
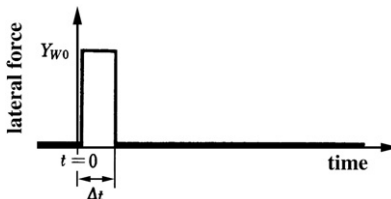
FIGURE 4.20 Lateral force by gust wind.

The vehicle motion is expressed in terms of absolute coordinates fixed on the ground for the same reason as in subsection 4.2.2. From Eqns (3.21) and (3.22), the equations of motion are derived as below.

$$m\frac{d^2y}{dt^2} + \frac{2(K_f + K_r)}{V}\frac{dy}{dt} + \frac{2(l_f K_f - l_r K_r)}{V}\frac{d\theta}{dt} - 2(K_f + K_r)\theta = Y_w \quad (4.28)$$

$$\frac{2(l_f K_f - l_r K_r)}{V}\frac{dy}{dt} + I\frac{d^2\theta}{dt^2} + \frac{2(l_f^2 K_f + l_r^2 K_r)}{V}\frac{d\theta}{dt} - 2(l_f K_f - l_r K)\theta = -l_w Y_w$$

$$(4.29)$$

If Δt is small enough, then by applying Laplace transforms to Eqns (4.28) and (4.29) as in subsection 4.2.2, $y(s)$ and $\theta(s)$ are:

$$y(s) = \frac{Y_{w0}\Delta t}{m}\frac{s^2 + b_{y1}s + b_{y2}}{s^2(s^2 + 2\zeta\omega_n s + \omega_n^2)} \quad (4.30)$$

$$\theta(s) = \frac{-l_w Y_{w0}\Delta t}{I}\frac{s + b_r}{s(s^2 + 2\zeta\omega_n s + \omega_n^2)} \quad (4.31)$$

where

$$b_{y1} = \frac{2(l_f^2 K_f + l_r^2 K_r) - 2l_w(l_f K_f - l_r K_r)}{IV}$$

$$= \frac{2(l_f^2 K_f + l_r^2 K_r) + 2l_N l_w(K_f + K_r)}{IV}$$

$$b_{y2} = -\frac{2(l_f K_f - l_r K_r) + 2l_w(K_f + K_r)}{I} = \frac{2(l_N - l_w)(K_f + K_r)}{I}$$

$$b_r = \frac{2(l_w - l_N)(K_f + K_r)}{l_w m V}$$

from these equations, the steady-state values are

$$y = \pm\infty \quad (\text{when } l_N \neq l_w)$$

$$= \frac{l_f^2 K_f + l_r^2 K_r}{2l^2 K_f K_r}VY_{w0}\Delta t \quad (\text{when } l_N = l_w) \quad (4.32)$$

$$\theta = \frac{(l_N - l_w)(K_f + K_r)V}{2l^2 K_f K_r\left[1 - \frac{m(l_f K_f - l_r K_r)}{2l^2 K_f K_r}V^2\right]}Y_{w0}\Delta t \quad (4.33)$$

The equations for vehicle steady-state motion are arranged as below, assuming $V < V_c$, when $l_f K_f - l_r K_r > 0$

when $l_N - l_w > 0$, then $y = +\infty$, $\theta = $ positive constant value;
when $l_N - l_w = 0$, then $y = $ positive constant value, $\theta = 0$;
when $l_N - l_w < 0$, then $y = -\infty$, $\theta = $ negative constant value.

The vehicle traveling in a straight line and subjected to a lateral gust, will change its direction towards the leeward and travel forward following the wind

gust if the AC is in front of the NSP. It will drift to the leeward temporarily and then regain its traveling direction if the AC and NSP coincide. If AC is in front of the NSP, the vehicle will drift to the leeward temporarily and then change its direction to the windward and travel forward against the wind gust direction.

Example 4.3

Execute a Matlab–Simulink simulation of the vehicle motion subjected to the wind gust, 25 m/s, for 0.4 s. The vehicle is running at $V = 40$ m/s and has the same parameters as in Example 3.6. Set the positions of NSP and AC, the same as in Fig. 4.19.

Solution
The wind force can be calculated by Eqn (4.19), where, C_y is estimated using Fig. 4.16 and $S = 1.5$ m^2, $\rho = 1.29$ kg/m^3. As a result of the calculation, $Y_w = 2.07$ kN.

The equations of motion of the vehicle subjected to the side wind gust are described by Eqns (4.28) and (4.29). The equations are rewritten in the following forms:

$$\frac{dv}{dt} = -\frac{2(K_f + K_r)}{mV}v - \frac{2(l_f K_f - l_r K_r)}{mV}r + \frac{2(K_f + K_r)}{m}\theta + \frac{Y_w}{m} \qquad (4.28)'$$

FIGURE E4.3(a).

FIGURE E4.3(b).

FIGURE E4.3(c).

FIGURE E4.3(d).

FIGURE E4.3(e).

$$\frac{dr}{dt} = -\frac{2(l_f K_f - l_r K_r)}{IV}v - \frac{2(l_f^2 K_f + l_r^2 K_r)}{IV}r + \frac{2(l_f K_f - l_r K)}{I}\theta + \frac{l_w Y_w}{I} \quad (4.29)'$$

$$\frac{dy}{dt} = v \quad\quad\quad\quad (E4.8)$$

$$\frac{d\theta}{dt} = r \quad\quad\quad\quad (E4.9)$$

It is possible to have the integral type of block diagram of the vehicle motion to the side wind gust as shown in Fig. E4.3(a). The vehicle parameters are set as in Fig. E4.3(b). Based on the above block diagram the simulation program is obtained as in Fig. E4.3(c). A simulation result is shown in Fig. E4.3(d) and the summarized results are in Fig. E4.3(e).

4.4 CONCLUSION

The vehicle motions when subjected to lateral external forces at the center of gravity are greatly affected by the positions of the center of gravity P and NSP, whereas the vehicle motions when subjected to lateral wind are greatly affected by the positions of the AC and NSP.

This is summarized and shown in .

The yaw rate reached by the vehicle, regardless of the type of disturbance, is either proportional to $1/(2l^2 K_f K_r)$ or $(K_f + K_r)/(2l^2 K_f K_r)$. Usually, vehicles with high cornering stiffnesses and large wheelbases are less sensitive, i.e., more robust to disturbances.

Table 4.1 Vehicle Motion Subjected to Lateral Disturbance.

	Vehicle Trajectory
Step-form lateral force on CG	
Pulse-form lateral force on CG	
Constant speed side wind	
Side wind gust	

● CGP   ○ NSP   ✕ AC

PROBLEMS

4.1 Calculate the steady-state side-slip angle and yaw rate for the vehicle running with the constant lateral force, $Y_0 = 2.0$ kN, exerted on the CG and then draw the $\beta - V$ and $r - V$ diagrams, respectively. Use the vehicle parameters as in Example 3.3.

4.2 Find the vehicle speed at which the yaw rate response in Problem 4.1 reaches the peak value.

4.3 Find the steering angle needed to keep straight running under a constant side force disturbance at CG.

4.4 Find the attitude angle of the vehicle due to the straight path in Problem 4.3.

4.5 Execute a Matlab–Simulink simulation of the vehicle response subjected to the disturbance force of 2.0 kN for 1.0 s at CG. Compare the effects of the vehicle speed with the responses. Use the same vehicle parameters as in Example 3.6.

4.6 Calculate the lateral force and yaw moment exerted on the vehicle running at 100 km/h with a side wind of 10 m/s. Refer to Fig. 4.16 for the lateral force and yaw moment coefficients of a specific vehicle and let ρ, l, and S be equal to 1.25 kg/m^3, 2.7 m and 1.5 m^2, respectively.

4.7 Confirm that in order to avoid the vehicle heading against the wind direction as a result of the side wind, more strong US characteristics are required for the vehicle with AC shifted to the rear ward direction relative to the CG position.

REFERENCES

[1] W. Bergman, Bergman gives new meaning to under-steer and over-steer, SAE Journal, Vol. 73, No. 12, 1965.

[2] H. Ichimura, Aerodynamic characteristics of passenger cars, JSAE Journal, Vol. 32, No. 4, 1978 (In Japanese).

Steering System and Vehicle Dynamics

5.1 PREFACE

The previous chapters looked at vehicle motion with the front steer angles fixed to a certain value. In reality, the front steer angle is controlled through the steering wheel and not directly. This mechanism, from the front wheel to the steering wheel, is called the steering system. In this chapter, the effect of the steering system characteristics on the vehicle dynamic performance will be studied. In order to do so, the equations of motion are derived for the steering system. These are used to examine the steering system characteristics due to the vehicle motion. Under normal traveling conditions of the vehicle, the steering wheel is controlled by the driver's hand. Thus, the effect of the driver's hand will be studied from a theoretical approach.

5.2 STEERING SYSTEM MODEL AND EQUATIONS OF MOTION

The steering system of normal vehicles is as constructed in Fig. 5.1. The steering wheel rotation is transferred through the steering wheel shaft and gearbox to the tie rod, and then through the knuckle arm, which allows the front wheel rotation around the kingpin.

   If all the steering system motion is converted to rotating motion around the kingpin, an equivalent modeling of the steering system can be assumed, as shown in Fig. 5.2.

   A rotating body equivalent to the steering wheel, with moment of inertia I_h is connected to another rotating body equivalent to the front wheels, with moment of inertia, I_s, through a rotating shaft equivalent to the steering wheel shaft and gearbox with spring constant K_s (I_h, I_s, and K_s are the moment of inertias and spring constant converted to around the kingpin). It is also considered that there
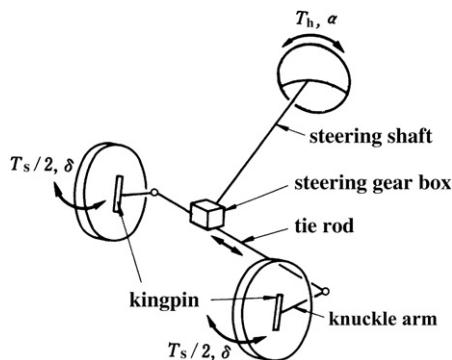
FIGURE 5.1 Vehicle steering system.

is a damping friction at the steering wheel shaft and kingpin, and these are defined as the damping coefficients C_h and C_s. If the rotational angle of the steering wheel, converted to around the kingpin, is taken as α, and actual front wheel steer angle is δ, the above equivalent steering system becomes a two degrees of freedom torsional vibration system. Here, I_s and C_s are the totals of the left and right wheels.

The torque, T_h, provided by the human driver at the steering wheel can be seen as an external force. On the other hand, when the vehicle is moving with a certain steering wheel angle, there is a torque acting to bring the steering wheel back to its original position. This is due to the moment around the kingpin produced by the lateral force that acts at the front wheels. This must also be taken into account as an external moment to the steering system. Chapter 2 showed that the acting point of the lateral force on the front wheel is shifted slightly behind the contact-surface centerline. It is common that the
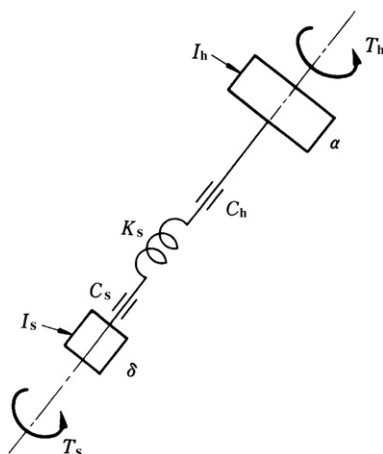
FIGURE 5.2 Steering system model.

intersecting point of the line extending from the kingpin shaft and the ground is always at the front of the contact-surface centerline. This condition is shown in Fig. 5.3.

This figure shows that if a side-slip angle in the anti-clockwise direction, β_f, is produced at the front wheel, the lateral force will act as a moment around the kingpin in the anti-clockwise direction. If the cornering stiffness of the front tire is K_f, the moment acting at the tire around the kingpin, $T_s/2$ is

$$\frac{T_s}{2} = (\xi_n + \xi_c)K_f\beta_f = \xi K_f\beta_f \tag{5.1}$$

whereby

$$\xi = \xi_n + \xi_c$$

ξ_n is the pneumatic trail and ξ_c is called the castor trail. $2\xi K_f$ is the restoring moment coefficient of the steering system.

If the front wheel side-slip angle is expressed by the vehicle motion variables, β_f becomes $\beta + l_f r/V - \delta$, as in Chapter 3, and the moment T_s can be written as:

$$T_s = 2\xi K_f\left(\beta + \frac{l_f r}{V} - \delta\right) \tag{5.2}$$

This moment is an external one acting at the front wheel of the steering system.
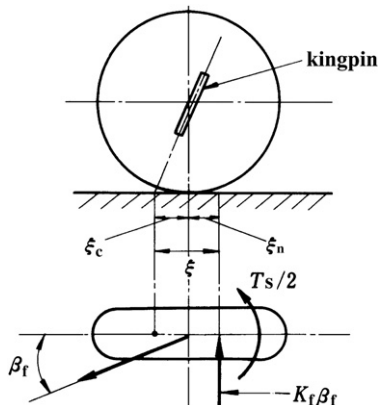
FIGURE 5.3 Self-aligning torque on front wheel.

Taking all these into account, the steering wheel rotation motion, which transferred around the kingpin, can be expressed as:

$$I_h \left(\frac{d^2\alpha}{dt^2} + \frac{dr}{dt} \right) + C_h \frac{d\alpha}{dt} + K_s(\alpha - \delta) = T_h \tag{5.3}$$

and similarly, for the front wheel rotational motion

$$I_s \left(\frac{d^2\delta}{dt^2} + \frac{dr}{dt} \right) + C_s \frac{d\delta}{dt} - K_s(\alpha - \delta) = 2\xi K_f \left(\beta + \frac{l_f r}{V} - \delta \right) \tag{5.4}$$

The reason why dr/dt is included in Eqns (5.3) and (5.4) is because the angular accelerations related to the absolute space are, respectively, $d^2\alpha/dt^2 + dr/dt$ and $d^2\delta/dt^2 + dr/dt$, which are due to the steering system attached to the traveling vehicle. In normal vehicle motion, it is assumed that $d^2\alpha/dt^2 \gg dr/dt$ and $d^2\delta/dt^2 \gg dr/dt$. Hence, the above steering system equations of motion could be written as below:

$$I_h \frac{d^2\alpha}{dt^2} + C_h \frac{d\alpha}{dt} + K_s(\alpha - \delta) = T_h \tag{5.5}$$

$$I_s \frac{d^2\delta}{dt^2} + C_s \frac{d\delta}{dt} + K_s(\delta - \alpha) = 2\xi K_f \left(\beta + \frac{l_f r}{V} - \delta \right) \tag{5.6}$$

5.3 EFFECTS OF STEERING SYSTEM CHARACTERISTICS ON VEHICLE MOTION

5.3.1 Effects of steering system characteristics on vehicle motion with fixed steering angle

The previous section showed that the steering system could be treated as a mechanical system with two degrees of freedoms, α and δ. This section will study the effect of steering system characteristics on the vehicle motion by treating the steering angle, α, as fixed and not as a state of motion of the mechanical system. In reality, this is when the steering wheel angle is maintained purposely at a fixed value regardless of the vehicle motion, or when the steering wheel angle is set with a fixed pattern regardless of steering wheel inertia, damping force, and restoring force. As mentioned earlier, until the previous chapters, the front wheel steer angle is given freely and is fixed. When the front wheel steer angle or the steering wheel angle is fixed, it is called fixed control.

Here, α is no longer treated as a state of motion, Eqn (5.5) becomes meaningless, and the steering system motion could be expressed by Eqn (5.6).

$$I_s \frac{d^2\delta}{dt^2} + C_s \frac{d\delta}{dt} + K_s(\delta - \alpha) = 2\xi K_f \left(\beta + \frac{l_f r}{V} - \delta \right) \tag{5.6}$$

And, α, here, is not a variable, but is known as an input. In relation to α, the front wheel steer angle, δ, is known from Eqn (5.6). The vehicle motion in relation to steer angle, δ, had been derived in Chapter 3.

$$mV \frac{d\beta}{dt} + 2(K_f + K_r)\beta + \left\{ mV + \frac{2}{V}(l_f K_f - l_r K_r) \right\} r = 2K_f \delta \tag{3.12}$$

$$2(l_f K_f - l_r K_r)\beta + I \frac{dr}{dt} + \frac{2\left(l_f^2 K_f + l_r^2 K_r\right)}{V} r = 2l_f K_f \delta \tag{3.13}$$

These cross-coupled Eqns (5.6), (3.12), and (3.13) are the equations of the vehicle motion due to a steering angle, α, taking the steering system into account.

To study the effect of static characteristics of the steering system, either the steering angle is fixed or rapid operation of the steering wheel is omitted, i.e., $d^2\delta/dt^2$ and $d\delta/dt$ are small. I_s and C_s are small too, thus, $I_s(d^2\delta/dt^2)$ and $C_s(d\delta/dt)$ can be neglected. The front wheel steer angle is determined by the following equation:

$$K_s(\delta - \alpha) = 2\xi K_f \left(\beta + \frac{l_f r}{V} - \delta \right) \tag{5.7}$$

δ is derived as

$$\delta = \frac{K_s}{K_s + 2\xi K_f} \alpha + \left(1 - \frac{K_s}{K_s + 2\xi K_f} \right) \left(\beta + \frac{l_f r}{V} \right)$$

By taking

$$e = \frac{K_s}{K_s + 2\xi K_f} = \frac{1}{1 + \frac{2\xi K_f}{K_s}} \tag{5.8}$$

$$\delta = e\alpha + (1 - e) \left(\beta + \frac{l_f}{V} r \right) \tag{5.9}$$

and substituting δ into Eqns (3.12) and (3.13) gives

$$mV \frac{d\beta}{dt} + 2(eK_f + K_r)\beta + \left\{ mV + \frac{2}{V}(l_f eK_f - l_r K_r) \right\} r = 2eK_f \alpha \tag{5.10}$$

$$2(l_f eK_f - l_r K_r)\beta + I \frac{dr}{dt} + \frac{2\left(l_f^2 eK_f + l_r^2 K_r\right)}{V} r = 2l_f eK_f \alpha \tag{5.11}$$

Equations (5.10) and (5.11) express the vehicle motion to steering angle, α, when considering the static characteristic of the steering system. Comparing these equations with Eqns (3.12) and (3.13) shows that the front wheel cornering stiffness, K_f, is replaced by eK_f in Eqns (5.10) and (5.11). In other words, the vehicle response to the steering wheel angle, α, has the characteristics of the vehicle response to front wheel steer angle with K_f replaced by eK_f. From Eqn (5.8), the value of e is smaller than 1 and the equivalent front wheel cornering stiffness is decreased. Larger restoring moment coefficients and smaller steering system stiffnesses increase this effect. If the front wheel cornering stiffness becomes smaller, the vehicle steer characteristics change toward US and the vehicle exhibits a larger tendency to US. It is true to say that a larger restoring moment coefficient and smaller steering system stiffness give stronger US characteristics and better directional stability to the vehicle.

It is difficult to fix the front wheel steer angle to a prior given value. Even if the vehicle shows some OS tendency from the theoretical study, the vehicle might actually have an US tendency when the steering system restoring moment coefficient and stiffness are considered. In other words, the vehicle actual US, OS steer characteristics not only depend on the tire characteristic and front and rear wheel positions, but also greatly depend on the steering system. The front wheel steer angle, $\alpha - \delta$, produced by the steering system restoring moment T_s is called the steering system compliance steer.

Example 5.1

Calculate the effect of the compliance steer on the equivalent reduction of the cornering stiffness when the cornering stiffness of the front tire itself, K_f, pneumatic trail + castor trail, ξ, and rigidity of the steering system, K_s, are equal to 80 kN/rad, 0.035 m, and 10.0 kNm/rad, respectively. Also confirm the effect of the equivalent reduction of the cornering stiffness on the steer characteristics of the vehicle with $m = 1500$ kg, $l_f = 1.1$, $l_r = 1.6$, and $K_r = 60.0$ kN/rad.

Solution
Using Eqn (5.8):

$$e = \frac{1}{1 + \frac{2\xi K_f}{K_s}} = \frac{1}{1 + \frac{2.0 \times 0.035 \times 80{,}000}{10{,}000}} = 0.64$$

So, the equivalent cornering stiffness of the front wheel is $0.64 \times 80.0 = 51.0$ kN/rad.

Using Eqn (3.43), the stability factor of the vehicle with the compliance steer taken into consideration is

$$A = -\frac{m}{2l^2}\frac{l_f K_f - l_r K_r}{K_f K_r} = -\frac{1500}{2 \times 2.7^2}\frac{1.1 \times 51,000 - 1.6 \times 60,000}{51,000 \times 60,000}$$

$$= 0.00134$$

and the stability factor of the vehicle with no consideration of the compliance steer is

$$A = -\frac{m}{2l^2}\frac{l_f K_f - l_r K_r}{K_f K_r} = -\frac{1500}{2 \times 2.7^2}\frac{1.1 \times 80,000 - 1.6 \times 60,000}{80,000 \times 60,000}$$

$$= 0.00017$$

As shown in Example 5.1, it is very important to understand that the compliance steer has a great effect on reducing the equivalent cornering stiffness of the front wheel and the vehicle steer characteristics. A normal value of the coefficient, e, is around 0.5–0.7, which means that once the tire is put on the front axle of the vehicle, the cornering stiffness of the front wheel is 50–70% of that of the original tire itself. It should be understood through out this book that the symbol, K_f, used for the cornering stiffness of the tire includes the effect of the compliance steer unless otherwise stated.

Previously, the steering angle, α, was either fixed or prevented from rapid changes so that $I_s(d^2\delta/dt^2)$, $C_s(d\delta/dt)$ in Eqn (5.6) could be neglected. This allowed study of the effect of static characteristics of the steering system. Strictly speaking, if the steering wheel can be operated more quickly, this should be considered. The equations of motion for the vehicle to steering angle, α, can be obtained by slightly modifying Eqns (5.6), (3.12), and (3.13).

$$mV\frac{d\beta}{dt} + 2(K_f + K_r)\beta + \left\{mV + \frac{2}{V}(l_f K_f - l_r K_r)\right\}r - 2K_f\delta = 0 \quad (5.12)$$

$$2(l_f K_f - l_r K_r)\beta + I\frac{dr}{dt} + \frac{2(l_f^2 K_f + l_r^2 K_r)}{V}r - 2l_f K_f\delta = 0 \quad (5.13)$$

$$-2\xi K_f\beta - \frac{2l_f\xi K_f}{V}r + I_s\frac{d^2\delta}{dt^2} + C_s\frac{d\delta}{dt} + (K_s + 2\xi K_f)\delta = K_s\alpha \quad (5.14)$$

Based on these equations, it is expected that the front wheel inertia and damping friction around the kingpin will cause a delay in the response of the front wheel steer angle, δ, to steering angle, α. The delay is also in the vehicle response to steering angle. The smaller the restoring moment coefficient and the stiffness of the steering system are, the greater this effect is. Figure 5.4 is an example of the response of vehicle yaw rate, r, to periodical steering
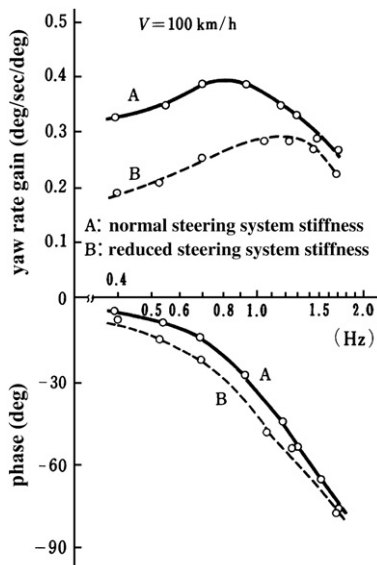
FIGURE 5.4 Effect of steering system stiffness.

angle, α, with different steering system stiffnesses [1]. As expected from Eqns (5.12) to (5.14), with the decrease of the steering system stiffness, the vehicle-response lag to steering angle becomes larger.

The previous discussion showed that the smaller the steering system stiffness is, the more liable the vehicle is to an US characteristic. Chapter 3 described how a vehicle with US characteristic has less delay in the response to actual steer angle. However, the US vehicle with low steering system stiffness has a larger delay to steering angle, particularly when the front wheel inertia and damping friction cannot be neglected. Therefore, excessively reducing the steering system stiffness is not something that is desired. In the case of restoring moment coefficient, the larger the coefficient, the more likely the vehicle will show US characteristics. Equations (5.12)–(5.14) show a larger restoring moment coefficient and will not cause any delay in the vehicle response to the steering angle. Therefore, the restoring moment coefficient, $2\xi K_f$, is desired to be as large as possible provided the steering force is not too heavy.

Example 5.2

Subsection 3.4.4 showed that it is possible to analyze the vehicle dynamics in the tire non-linear region by making the equivalent cornering stiffness decrease by increasing the lateral acceleration. In the subsection, however, only the saturation property of the tire to side-slip angle is dealt with and nothing is taken into consideration for the fact that the pneumatic trail decreases with increasing side-slip angle. As the pneumatic trail decreases with the side-slip angle, namely with the lateral acceleration, the aligning

torque decreases and the compliance steer is decreased, which has effects on the loss of the cornering stiffness due to the compliance steer.

Referring to subsections 2.3.3 and 3.4.4, the pneumatic trail, ξ', decreases proportionally to the side-slip angle and tends to be zero at the saturation point of the lateral force. The following equation is obtained.

$$\xi' = \xi\left(1 - \frac{K_f}{\mu'_{r/l}W}\beta_f\right) \tag{E5.1}$$

Taking the compliance steer in the steering system into account, find the equivalent cornering stiffness of the front tire at the large tire side-slip region.

Solution

The Eqn (3.101) suggests the following description for the pneumatic trail, ξ':

$$\xi' = \xi\left(1 - \frac{K_f}{\mu'_{r/l}W}\beta_f\right) = \xi\sqrt{1 - \frac{\ddot{y}}{\mu}} \tag{E5.2}$$

Also the cornering stiffness of the front wheel at large side-slip angle, K_f', is described as:

$$K_f' = K_f\sqrt{1 - \frac{\ddot{y}}{\mu}} \tag{E5.3}$$

So, referring to Eqn (5.8), the cornering stiffness reduction coefficient at large side-slip angle, e', is:

$$e' = \frac{1}{1 + \frac{2\xi'K_f'}{K_s}} = \frac{1}{1 + \frac{2\xi K_f}{K_s}\left(1 - \frac{\ddot{y}}{\mu}\right)} = \frac{e}{1 - \left(1 - e\right)\frac{\ddot{y}}{\mu}} \tag{E5.4}$$

From the above, the equivalent cornering stiffness at large side-slip angle considering the compliance steer is

$$e'K_f' = \frac{e}{1 - \left(1 - e\right)\frac{\ddot{y}}{\mu}}K_f\sqrt{1 - \frac{\ddot{y}}{\mu}} \approx eK_f\left\{1 - \left(e - \frac{1}{2}\right)\frac{\ddot{y}}{\mu}\right\} \tag{E5.5}$$

It is obvious that the reduction rate of the cornering stiffness due to the side-slip angle, namely to the lateral acceleration, in the above equation decreases compared with Eqns (3.101) and (3.102) or (3.103) and (3.104). This means that the equivalent cornering stiffness reduction due to the side-slip angle at the front wheel is smaller than that at the rear wheel, especially under large tire side-slip angle. It is interesting to see that

though the steering system compliance steer makes the vehicle US, there is a possibility to weaken this aspect at larger side slips and make the vehicle tend to OS. This is achieved by reducing the effects of compliance steer on the effective cornering stiffness of the front tire at large side slips.

5.3.2 Effects of steering system characteristics on vehicle motion with non-fixed steering angle

The previous section studied the effect of the steering system characteristics on the vehicle motion when the steering angle is assumed fixed at a given value. This section will look at the effect the steering system characteristics have on the vehicle motion when the steering angle, α, is not fixed, but has a degree of freedom. This is typical of when the driver takes his hand off from the steering wheel completely, or when the driver gives a torque to the steering wheel regardless of the steering angle. This situation is called free control.

The vehicle and steering system equations of motion during the free control are derived as follows:

$$mV\frac{\mathrm{d}\beta}{\mathrm{d}t} + 2(K_\mathrm{f} + K_\mathrm{r})\beta + \left\{mV + \frac{2}{V}(l_\mathrm{f}K_\mathrm{f} - l_\mathrm{r}K_\mathrm{r})\right\}r = 2K_\mathrm{f}\delta \qquad (3.12)$$

$$2(l_\mathrm{f}K_\mathrm{f} - l_\mathrm{r}K_\mathrm{r})\beta + I\frac{\mathrm{d}r}{\mathrm{d}t} + \frac{2\left(l_\mathrm{f}^2 K_\mathrm{f} + l_\mathrm{r}^2 K_\mathrm{r}\right)}{V}r = 2l_\mathrm{f}K_\mathrm{f}\delta \qquad (3.13)$$

$$I_\mathrm{h}\frac{\mathrm{d}^2\alpha}{\mathrm{d}t^2} + C_\mathrm{h}\frac{\mathrm{d}\alpha}{\mathrm{d}t} + K_\mathrm{s}(\alpha - \delta) = T_\mathrm{h} \qquad (5.5)$$

$$I_\mathrm{s}\frac{\mathrm{d}^2\delta}{\mathrm{d}t^2} + C_\mathrm{s}\frac{\mathrm{d}\delta}{\mathrm{d}t} + K_\mathrm{s}(\delta - \alpha) = 2\xi K_\mathrm{f}\left(\beta + \frac{l_\mathrm{f}r}{V} - \delta\right) \qquad (5.6)$$

Here, the front wheel moment of inertia around the kingpin, I_s, is small compared to the steering wheel moment of inertia, I_h, and can be neglected. If the damping coefficients, C_h and C_s, are neglected as small values, Eqns (5.5) and (5.6) become

$$I_\mathrm{h}\frac{\mathrm{d}^2\alpha}{\mathrm{d}t^2} + K_\mathrm{s}(\alpha - \delta) = T_\mathrm{h} \qquad (5.5)'$$

$$K_\mathrm{s}(\delta - \alpha) = 2\xi K_\mathrm{f}\left(\beta + \frac{l_\mathrm{f}r}{V} - \delta\right) \qquad (5.6)'$$

substituting Eqn (5.6)′ into Eqn (5.5)′

$$I_h \frac{d^2\alpha}{dt^2} - 2\xi K_f \left(\beta + \frac{l_f r}{V} - \delta \right) = T_h \qquad (5.5)''$$

Here, Eqn (5.6)′ is same as Eqn (5.7), and δ is obtained from this equation as in Eqn (5.9)

$$\delta = e\alpha + (1 - e)\left(\beta + \frac{l_f}{V}r \right)$$

If it is assumed that the steering system stiffness is large, which means $K_s = \infty$, Eqn (5.8) gives $e = 1$, and

$$\delta = \alpha \qquad (5.6)''$$

The vehicle equations of motion with the steering system during free control could be written in a simpler form, based on Eqns (3.12), (3.13), (5.5)″, and (5.6)″:

$$mV \frac{d\beta}{dt} + 2(K_f + K_r)\beta + \left\{ mV + \frac{2}{V}(l_f K_f - l_r K_r) \right\}r - 2K_f\alpha = 0 \quad (5.15)$$

$$2(l_f K_f - l_r K_r)\beta + I\frac{dr}{dt} + \frac{2\left(l_f^2 K_f + l_r^2 K_r \right)}{V}r - 2l_f K_f\alpha = 0 \qquad (5.16)$$

$$-2\xi K_f\beta - \frac{2l_f \xi K_f}{V}r + I_h\frac{d^2\alpha}{dt^2} + 2\xi K_f\alpha = T_h \qquad (5.17)$$

To further simplify the analysis in order to examine the effect of the steering system characteristics on the vehicle motion, the following assumptions are made:

$$K_f = K_r = K$$

$$l_f = l_r = l$$

$$I = mk^2 = ml_f l_r = m\left(\frac{l}{2} \right)^2$$

Substituting these equations into Eqns (5.15)–(5.17),

$$mV\frac{d\beta}{dt} + 4K\beta + mVr - 2K\alpha = 0 \qquad (5.15)'$$

$$m\left(\frac{l}{2}\right)^2\frac{dr}{dt} + \frac{l^2 K}{V}r - lK\alpha = 0 \tag{5.16}'$$

$$-\frac{2\xi K_f}{I_h}\beta - \frac{\xi l K_f}{I_h V}r + \frac{d^2\alpha}{dt^2} + \omega_s^2\alpha = \frac{T_h}{I_h} \tag{5.17}'$$

whereby

$$\omega_s^2 = \frac{2\xi K_f}{I_h} = \frac{2\xi K}{I_h} \tag{5.18}$$

ω_s^2 is the natural frequency of the steering system.

Applying Laplace transforms on the simplified Eqns (5.15)′, (5.16)′, and (5.17)′, gives the characteristic equations as follows:

$$\frac{4}{m^2 l^2 V}\begin{vmatrix} mVs & mV & -2K \\ 0 & m\left(\frac{l}{2}\right)^2 s + \frac{l^2 K}{V} & -lK \\ -\omega_s^2 & -\frac{l\omega_s^2}{2} & s^2 + \omega_s^2 \end{vmatrix} \tag{5.19}$$

$$= A_4 s^4 + A_3 s^3 + A_2 s^2 + A_1 s + A_0$$

where

$$A_0 = \frac{4K}{ml}\omega_s^2$$

$$A_1 = \frac{4K}{mV}\omega_s^2$$

$$A_2 = \omega_s^2 + \frac{16K^2}{m^2 V^2} \tag{5.20}$$

$$A_3 = \frac{8K}{mV}$$

$$A_4 = 1$$

For the motion to be stable, the coefficients of the characteristic Eqn (5.19) have to fulfill the Routh stability conditions as follows:

$$A_0, A_1, A_2, A_3, A_4 > 0 \tag{5.21}$$

$$\begin{vmatrix} A_1 & A_0 & 0 \\ A_3 & A_2 & A_1 \\ 0 & A_4 & A_3 \end{vmatrix} = A_1 A_2 A_3 - A_0 A_3^2 - A_1^2 A_4 > 0 \tag{5.22}$$

A_0 and A_1 are positive when $\xi > 0$ from Eqn (5.18), while A_2, A_3, and A_4 are always positive. Therefore, for the vehicle motion to be stable, trail ξ has to be always positive.

Substituting Eqn (5.20) into the condition (5.22) and rearranging it gives:

$$\frac{32K^2}{m^2V^2} + \omega_s^2 - \frac{16K}{ml} > 0 \tag{5.23}$$

By deriving this condition so that it is not related to traveling speed, V, then

$$\omega_s^2 - \frac{16K}{ml} > 0 \tag{5.24}$$

Here, substituting

$$\omega_y^2 = \frac{16K}{ml} = \frac{4lK}{m\left(\frac{l}{2}\right)^2} \tag{5.25}$$

the denominator at the right hand side of Eqn (5.25) is equivalent to the yaw moment of inertia, and the numerator is equivalent to the moment per unit yaw angle by the front and rear wheels' cornering stiffness (lateral stiffness). Hence, ω_y is a vehicle constant that could be viewed as the vehicle yaw natural frequency. Using this ω_y, Eqn (5.24) can be rewritten as:

$$\omega_s^2 - \omega_y^2 > 0 \tag{5.26}$$

For the vehicle motion to be stable during free control, regardless of the vehicle speed, the steering system natural frequency, ω_s, must be greater than the vehicle yaw natural frequency ω_y defined by Eqn (5.25).

If $\omega_s < \omega_y$, a stability limit velocity, V_{cr}, that causes the vehicle motion to be unstable will exist. This is obtained by calculating the V that makes the left hand side of Eqn (5.23) equal to 0.

$$V_{cr} = \sqrt{\frac{2lK}{m} \frac{1}{1 - (\omega_s/\omega_y)^2}} \tag{5.27}$$

If the vehicle traveling speed V is less than V_{cr}, then the vehicle is stable, but when $V > V_{cr}$ then the vehicle motion will be unstable [2].

Equation (5.18) shows that ω_s depends greatly on the trail ξ. Using Eqn (5.27), the relation between the trail ξ and the stability limit velocity, V_{cr}, for a normal passenger car is shown in Fig. 5.5.

It is clear that ξ is desired to be as large as possible within the region of smaller steering torques. As the steering system natural frequency, ω_s, is also desired to be as big as possible, a smaller I_h is better. Furthermore, the larger the K_s is, the larger the ω_s will be.

5.3.3 Effects of driver's hands and arms

In the previous chapters, the effect of the steering system characteristics on the vehicle motion was discussed with the assumptions that the steering wheel
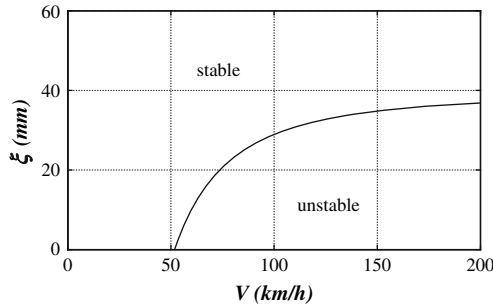
FIGURE 5.5 Relation of critical vehicle speed to trail ξ.

angle is either completely fixed or totally free. In a real vehicle situation, even when a driver isn't intentionally maneuvering the vehicle, the steering wheel is lightly supported by the driver's hand and arm. The steering wheel is neither completely fixed nor totally free.

The effect of a driver's hand and arm on the vehicle inherent motion will be looked at with some simple assumptions. The driver is not assumed to be a controller in controlling the vehicle motion (this matter is dealt with in Chapter 9).

The steering wheel is supported by the driver's hand and arm, which is assumed to play the role as an equivalent spring. Taking α_h as the steering wheel angle given by the human's hand, and α as the real steering wheel angle, a torque of T_h will act at the steering wheel by the human's hand.

$$T_h = K_h(\alpha_h - \alpha) \tag{5.28}$$

where K_h is the equivalent spring constant of the human's hand and arm.

As in subsection 5.3.2, the equations of motion of the vehicle and steering wheel, inclusive of the human's hand and arm effect, can be written as below by substituting Eqn (5.28) into Eqn (5.17).

$$mV\frac{d\beta}{dt} + 2(K_f + K_r)\beta + \left\{mV + \frac{2}{V}(l_f K_f - l_r K_r)\right\}r - 2K_f\alpha = 0 \tag{5.15}$$

$$2(l_f K_f - l_r K_r)\beta + I\frac{dr}{dt} + \frac{2\left(l_f^2 K_f + l_r^2 K_r\right)}{V}r - 2l_f K_f\alpha = 0 \tag{5.16}$$

$$-2\xi K_f\beta - \frac{2l_f\xi K_f}{V}r + I_h\frac{d^2\alpha}{dt^2} + (2\xi K_f + K_h)\alpha = K_h\alpha_h \tag{5.29}$$

from Eqn (5.29), the natural frequency of the steering system now becomes

$$\omega_s = \sqrt{\frac{2\xi K_f + K_h}{I_h}} \tag{5.30}$$

Consequently, the human's hand and arm have the effect of increasing the steering system natural frequency, ω_s. In subsection 5.3.2, it is shown that ω_s is desired to be as large as possible for the vehicle motion to be stable, and from this point of view, K_h is desired to be large.

For the vehicle motion where the steering system inertia could be neglected, Eqn (5.29) becomes

$$-2\xi K_f \beta - \frac{2l_f \xi K_f}{V} r + \left(2\xi K_f + K_h\right)\alpha = K_h \alpha_h \qquad (5.31)$$

From Eqn (5.31),

$$\alpha = \frac{K_h}{K_h + 2\xi K_f}\alpha_h + \left(1 - \frac{K_h}{K_h + 2\xi K_f}\right)\left(\beta + \frac{l_f}{V}r\right)$$

and

$$e_h = \frac{K_h}{K_h + 2\xi K_f} = \frac{1}{1 + \frac{2\xi K_f}{K_h}} \qquad (5.32)$$

$$\alpha = e_h \alpha_h + (1 - e_h)\left(\beta + \frac{l_f}{V}r\right) \qquad (5.33)$$

Substituting Eqn (5.33) into Eqns (5.15) and (5.16) and rearranging gives:

$$mV\frac{d\beta}{dt} + 2(e_h K_f + K_r)\beta + \left\{mV + \frac{2}{V}(l_f e_h K_f - l_r K_r)\right\}r = 2e_h K_f \alpha_h$$

$$(5.34)$$

$$2(e_h l_f K_f - l_r K_r)\beta + I\frac{dr}{dt} + \frac{2\left(l_f^2 e_h K_f + l_r^2 K_r\right)}{V}r = 2l_f e_h K_f \alpha_h \qquad (5.35)$$

Comparing these to the original equations, (5.15) and (5.16), the front wheel cornering stiffness has changed from K_f to $e_h K_f$ as before. In other words, when the effect of the human's hand and arm is taken into consideration, the front wheel cornering stiffness decreases since e_h is less than 1. The more the front wheel cornering stiffness decreases, the more the vehicle will be US, and the better the directional stability. Therefore, from this point of view, K_h is desired to be as small as possible.

There are now two contradictory requirements for K_h from the point of view of vehicle stability. This theoretical argument coincides with the reality. A human driver neither holds the steering wheel strongly (large K_h) such that it is fixed when driving at high speed, nor does the driver let the steering wheel free (K_h is zero) by leaving his hand off the wheel. The driver holds the steering wheel just light enough for practical driving.

Consequently, it could be said that the driver's hand and arm, supporting the steering wheel lightly, further stabilize the vehicle motion.

PROBLEMS

5.1 In order to understand that the compliance steer in the steering system has an equivalent effect on reducing the front tire cornering stiffness from K_f to eK_f in the fixed control of the vehicle, derive Eqns (5.10) and (5.11) by yourself using Eqns (5.9)–(3.12) and (3.13).

5.2 Calculate the natural frequency of the steering system when ξ, K, and I_h are 0.04 m, 60.0 kN/rad, and 20.0 kg m^2, respectively.

5.3 Calculate the upper limit of the inertia moment of the steering wheel equivalently around the kingpin for the free control vehicle stable at any vehicle speed under the given parameters: $\xi = 0.04$ m, $m = 1500$ kg, $l = 2.7$ m, and $K = 60$ kN/rad.

5.4 Show that the stability condition of the free control vehicle at any speed is approximately written as $I_h/I < \xi/2l$.

REFERENCES

[1] K. Nishii, et al., Effect of component factors on controllability and stability of vehicles, JSAE Journal, Vol. 26, No. 7, 1972 (In Japanese).

[2] T. Okada, Fundamental theory on automobile stability and control, JSAE Journal, Vol. 26, No. 7, 1972 (In Japanese).

Vehicle Body Roll and Vehicle Dynamics

6.1 PREFACE

The previous chapters have dealt with the vehicle motion under the assumption that the wheel is rigidly attached to the vehicle body, and there is no relative displacement between the body and the wheels. This is a good assumption, proven from practical experience, for understanding the basic vehicle motion characteristics. However, in the case of normal passenger cars, the vehicle body and wheels are connected to each other fby soft and elastic connections to improve the vehicle ride comfort. This mechanism is generally called the suspension system, and the vehicle body is called the sprung mass, while the wheels are called the unsprung mass. The suspension system between the vehicle body and the wheels allows a relative up–down displacement between the vehicle body and the wheels. When the vehicle moves laterally, a centrifugal force acts at the vehicle center of gravity, causing the vehicle to tilt to the direction of the centrifugal force. This 'tilt' is called the vehicle roll. If the suspension system is considered, the vehicle will have a roll degree of freedom that is produced together with vehicle lateral motion.

This chapter will look into the roll mechanism, derive the vehicle equations of motion including the roll motion, and study the effects of suspension system characteristics and vehicle roll on the vehicle motion.

6.2 ROLL GEOMETRY

Eberan's hypothesis of the roll center as the vehicle's geometrical instantaneous rotation center, and assumption that this roll center is always fixed [1], have long been taken as the standard approach. This hypothesis is generally used due to its simplicity. Based on this hypothesis, the roll mechanism of the

vehicle will be studied with a constant lateral acceleration, which is caused by a constant centrifugal force.

6.2.1 Roll center and roll axis

In general, there are various types of suspension systems, from the simple rigid axle type to the independent suspension that is common in passenger cars. The relative vertical displacement or angular displacement between the sprung and unsprung masses is dependant on the structure of the suspension system.

The front and rear wheel roll centers are also determined by the suspension system configuration. The line that connects the front and rear roll centers is called the roll axis. The roll center is the vehicle's instantaneous rotation center in the plane perpendicular to the vehicle's longitudinal direction, which contains the left and right wheels' ground contact point. The wheels are considered rigid in both up–down, left–right directions and the ground contact point is fixed.

Figure 6.1 shows the axle type suspension system. The vehicle body at points A_1 and B_1 can only have vertical displacement relative to the unsprung mass due to the springs. Even if the sprung mass rolls, the unsprung mass including the wheels is assumed rigid and thus, doesn't move, the roll center is at point O. In other words, when a rolling moment acts on the vehicle, the vehicle body will produce a roll angle, ϕ, relative to the wheels with respect to the point O.

Figure 6.2 shows a typical independent type of suspension – often called the double wishbone suspension. As its name implies, each wheel can move independently, relative to the vehicle body. If the vehicle body is fixed, the instantaneous rotation centers of the left and right unsprung mass relative to the vehicle body are the points O_1 and O_2, respectively. The point O_1 is the intersecting point of the extended lines of A_1–A_2 and A_3–A_4, while the point O_2 is the intersecting point of the extended lines of B_1–B_2 and B_3–B_4. Here, when the vehicle body rolls during cornering, the wheel contact points with the ground, A and B, are fixed and the unsprung masses must roll around them. The points O_1 and O_2 move in the direction perpendicular to O_1A and O_2B. O_1 and O_2 are the virtual points on the vehicle body as well as on the unsprung masses. Consequently, the vehicle body instantaneous rotating center, or the roll center is the intersection of the extended lines of O_1A and O_2B, which is the point O.
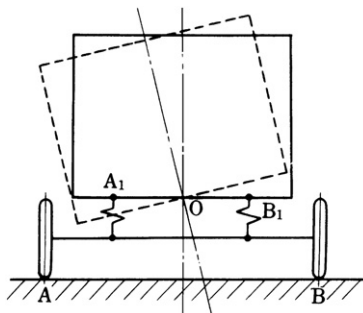
FIGURE 6.1 Roll center for rigid axle suspension.
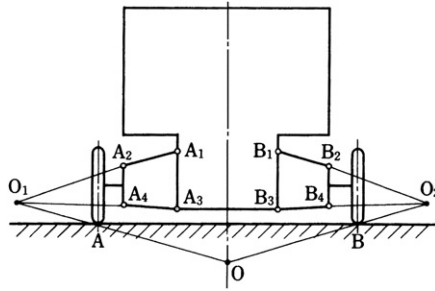
FIGURE 6.2 Roll center for wishbone suspension.

Based on this way of thinking, the roll center for other types of suspension system is shown in Fig. 6.3.

It is clear that the vehicle roll center position is dependant on the structure of the suspension system. Usually, the suspension system and the vehicle are symmetrical on the left and right, and the roll center is always on the symmetric axis. In this case, it is the height of the roll center that is dependant on the suspension system structure.

The roll center is the vehicle instantaneous rotation center, and its position can move during suspension movement. The point O shown here is the roll center when roll angle is zero; if the vehicle rolls, the roll center will also move. To understand

swing axle suspensions

Macpherson strut suspensions
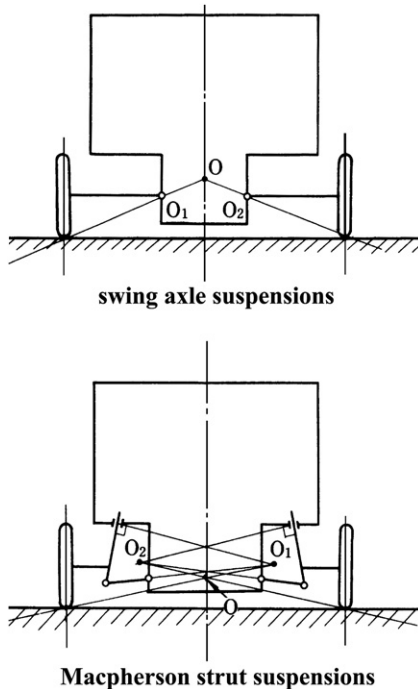
FIGURE 6.3 Roll center for independent suspensions.
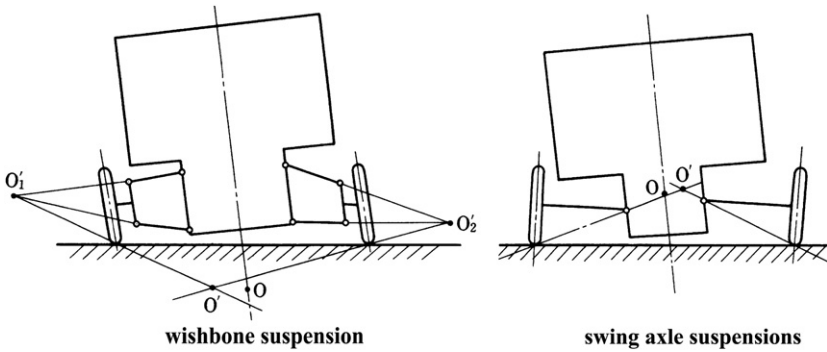
FIGURE 6.4 Change of roll center position due to body roll.

this, the roll center O' during body roll is shown for two types of suspension system – the wishbone and the swing axle suspension systems, in Fig. 6.4.

If the roll angle is not large, the movement of the roll center is small, and it is possible to assume that the roll centers are fixed at point O. It is still possible to understand the vehicle roll mechanism, even with a moving roll center. But the fixed roll center concept is easier to understand and gives a good understanding of the basic vehicle dynamics. Based on Eberan's roll center hypothesis, the front and rear roll centers are determined, and if the vehicle body is rigid, the vehicle's fixed roll axis is determined as shown in Fig. 6.5. The roll center at the front and rear may not have the same height above the ground and the roll axis is not necessarily parallel to the vehicle longitudinal axis.

Furthermore, when vehicle motion is accompanied by large roll angles, the fixed roll center and roll axis concepts are not suitable anymore. In such cases, vehicle roll is usually dealt with as the indeterminate problem of the vehicle's four wheels.

6.2.2 Roll stiffness and load transfer

Now, the vehicle is assumed to have a constant lateral acceleration and centrifugal force acting at the vehicle center of gravity. The center of gravity

FIGURE 6.5 Roll axis.

FIGURE 6.6 Roll center and CG heights.

doesn't normally coincide with the vehicle roll axis, but is usually above the roll axis, as shown in Fig. 6.6. The centrifugal force acting at the center of gravity produces a rolling moment around the roll axis resulting in a constant roll angle. If the vehicle body ro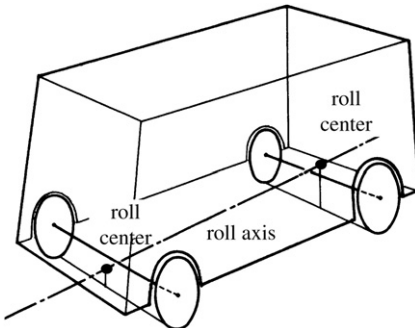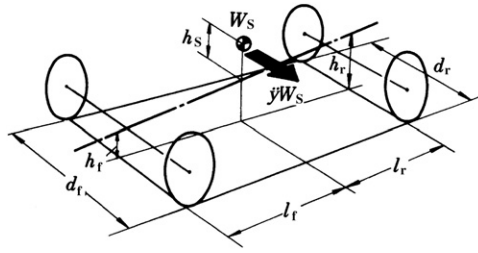lls, the left and right vertical springs of the suspension system will be stretched at one side and be compressed on the other side. This produces an equilibrium moment to the rolling moment due to the centrifugal force. The magnitude of the moment produced by the stretch and the compression of the spring per unit roll angle is called the roll stiffness.

Here, the respective roll stiffness for the front and rear suspension systems is defined as $K_{\phi f}$, $K_{\phi r}$, the roll center height from the ground as h_f, h_r, the front and rear tread as d_f, d_r, the distance between the vehicle center of gravity and the roll axis as h_s, and the distance between the front and rear axles to the center of gravity as l_f, l_r. The weight of the unsprung mass is small compared to the weight of the sprung mass and could be neglected. In this case, the vehicle weight is taken to be equal to the vehicle body weight, and written as W_s. The vehicle lateral acceleration is taken as $\ddot{y}$ (same as in subsection 3.3.3) and the centrifugal force acting on the vehicle is $\ddot{y}W_s$. Assuming that the vehicle is rigid, and the roll angle is small, the rolling moment by the centrifugal force is $\ddot{y}W_s h_s$ and the roll moment by the vehicle weight due to tilting of the vehicle body is $W_s h_s \phi$, the vehicle roll angle becomes

$$(K_{\phi f} + K_{\phi r})\phi = \ddot{y}W_s h_s + W_s h_s \phi \text{ or } \phi = \frac{\ddot{y}W_s h_s}{K_{\phi f} + K_{\phi r} - W_s h_s} \qquad (6.1)$$

The centrifugal force, $\ddot{y}W_s$, acting on the vehicle requires tire cornering forces to achieve equilibrium. Distributing the $\ddot{y}W_s$ force acting at the center of gravity to the front and rear wheels, the forces $\ddot{y}W_s l_r/l$ and $\ddot{y}W_s l_f/l$ could be considered to act on the front and rear wheels, respectively, where $l = l_f + l_r$. These forces are equal to the front and rear wheel lateral forces.

If the vehicle body rolls, the left and right wheels at both front and rear axles will increase in load at one side and decrease at the other side. This is called the load transfer due to roll. Defining the load transfer for the front and rear as ΔW_f and ΔW_r, respectively, the roll moment around the roll center at the front and rear wheels in the plane perpendicular to the vehicle longitudinal direction has to be in equilibrium, as shown in Fig. 6.7. The following equations are derived:
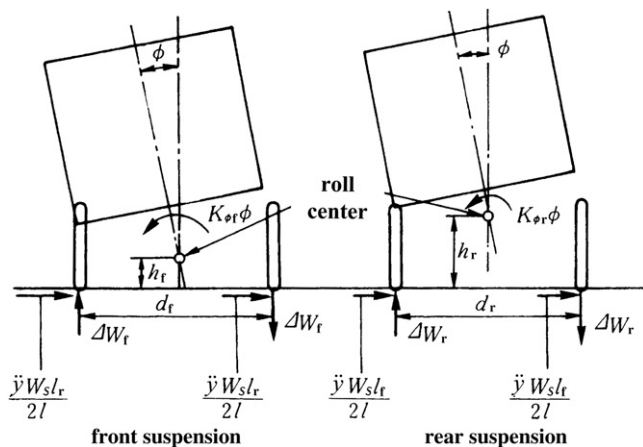
FIGURE 6.7 Transversal load transfer due to body roll.

$$K_{\phi f}\phi = \Delta W_f d_f - \frac{\ddot{y}W_s l_r}{l}h_f \tag{6.2}$$

$$K_{\phi r}\phi = \Delta W_r d_r - \frac{\ddot{y}W_s l_f}{l}h_r \tag{6.3}$$

At this time, it is assumed that there is no load transfer between the front and the rear. Substituting Eqn (6.1) into Eqns (6.2) and (6.3) to find ΔW_f and ΔW_r, gives the following equations:

$$\Delta W_f = \frac{\ddot{y}W_s}{d_f}\left[\frac{K_{\phi f}h_s}{K_{\phi f} + K_{\phi r} - W_s h_s} + \frac{l_r}{l}h_f\right] \tag{6.4}$$

$$\Delta W_r = \frac{\ddot{y}W_s}{d_r}\left[\frac{K_{\phi r}h_s}{K_{\phi f} + K_{\phi r} - W_s h_s} + \frac{l_f}{l}h_r\right] \tag{6.5}$$

These equations give the load transfer between the left and right wheels due to a constant lateral acceleration. The equations show that a higher vehicle center of gravity distance from the roll axis, h_s, results in a larger load transfer at the front and rear wheels. Furthermore, a load transfer at the front and rear wheels is basically proportional to the front and rear roll stiffness ratios to the total roll stiffness, respectively.

The last term in Eqns (6.4) and (6.5) depends on the height of the roll axis from the ground, h_f and h_r, and causes the jack-up effect.

6.2.3 Camber change and roll steer

If the ground contact point of the wheels is fixed, as the vehicle body rolls, the unsprung mass, including the wheels, tilts relative to the ground. This gives the

camber change of the wheel, which is measured relative to the ground and is due to body roll. The vehicle roll also gives the wheels an up-and-down displacement relative to the vehicle body. At such time, depending on the structure of the suspension system, the wheels may produce some angular displacement in the horizontal plane along with the up-and-down movement relative to the vehicle body. This is called the roll steer.

The camber change and roll steer are dependant on the structure of the suspension system. The suspension system is designed with keen consideration of these characteristics, often using them to affect the vehicle dynamics or sometimes trying to avoid them completely. This chapter will skip the detailed explanation of camber change and roll steer mechanism for various suspension systems, and only look at the basic characteristics of camber change and roll steer. The collective term for camber change and roll steer is sometimes called the alignment change due to roll.

In axle type suspensions, the wheel doesn't produce any camber change due to vehicle roll. The camber change due to roll only occurs for independent suspension systems, where depending on the suspension structure, there could be one of two cases: camber change in the same direction as roll, which is called positive camber, or in the opposite direction, negative camber. This is shown in Fig. 6.8.

Independent suspension systems are constructed by a linkage mechanism, and the vehicle roll angle and camber change can be determined from geometrical analysis of the linkage. Figure 6.9 shows the actual measured value and calculated value of the camber change for a wishbone type suspension system. This relationship varies substantially with the arrangement of the links, even for suspension systems of the same type. From the figure, if the roll angle is not large, the camber change can be considered as nearly proportional to the roll angle. As the roll angle becomes large, this linear relation is lost, and non-linearity appears. This is generally for other types of suspension systems. The non-linear characteristic of the camber change is one of the main factors that
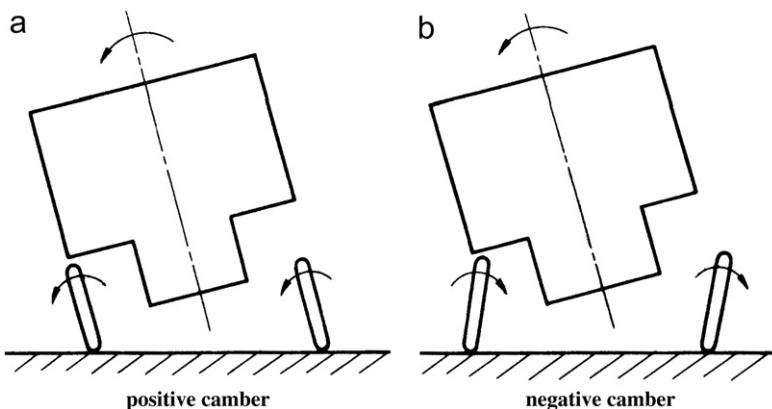
FIGURE 6.8 Camber change due to body roll.
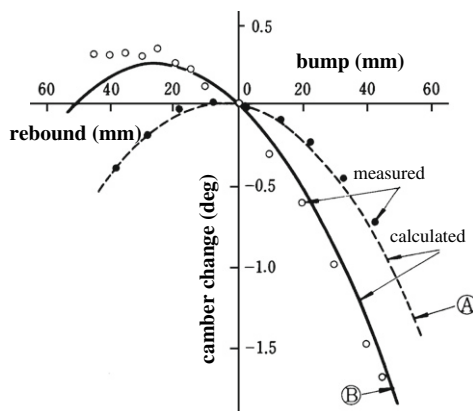
FIGURE 6.9 Chamber changes to suspension stroke.

influences the vehicle motion at large lateral accelerations. For lower lateral accelerations, the camber change could be considered to be proportional to the roll angle, in the directions shown in either Fig. 6.8(a) or (b).

Example 6.1

Investigate the geometrical condition of the suspension mechanism such as in Figs 6.2 or 6.3, which basically determines the positive or negative camber to the body roll.

Solution

Any part of the left half of the vehicle body is going downward and the right half upward due to the body roll. While the unsprung mass rolls around the tire contact point, for example, point A in Fig. 6.2, which is a camber change. So any point of the left side of the unsprung mass relative to the center line of the left wheel is going downward and the right side to upward due to the positive camber of the unsprung mass. Due to the negative camber, the left side is going upward and the right side is going to downward.

As the virtual point, O_1, is the common point fixed to the vehicle body and the left hand side unsprung mass, it must move in the same direction as the body roll and the camber change during roll motion. If point O_1 is to the left of the body center and the right of the wheel centerline, then the suspension has negative camber. If the point O_1 is to the left of the body and to the right of the wheel centerline, or to the right of the body center and the wheel centerline, then the suspension has to show the positive camber.

The roll steer due to the roll of the vehicle body is also dependant on the suspension system structure. For an axle type suspension, the sprung mass and unsprung mass are often connected using leaf springs. The mounting point of the spring at the vehicle axle moves in the rear-and-forward direction and causes the axle to produce an angular displacement relative to the vehicle body in the horizontal plane. This is roll steer for an axle type suspension, which is sometimes called axle steer due to roll.

For independent suspension systems, the amount of roll steer can be determined from geometrical analysis of the linkage. Similar to camber change, the roll steer direction and magnitude, relative to the roll angle, can vary substantially with the arrangement of the links. The suspension systems are usually designed to control the amount of steer by careful arrangement of the links. For independent suspensions, if the roll angle is small, the roll steer can be considered to be proportional to the roll angle. The direction of the roll steer can sometimes be in either positive or negative direction, depending on the suspension system structure.

The roll steer for an independent type suspension is sometimes called the toe change due to the vertical stroke of the suspension. Figure 6.10 shows an example of toe change due to suspension stroke. Roll steer in the direction toward the inner side of the vehicle is called toe-in and the one in the opposite direction is called toe-out.

6.3 BODY ROLL AND VEHICLE DYNAMICS

By examining the vehicle in steady-state cornering, the vehicle steer characteristics that fundamentally influence the vehicle dynamic performance have
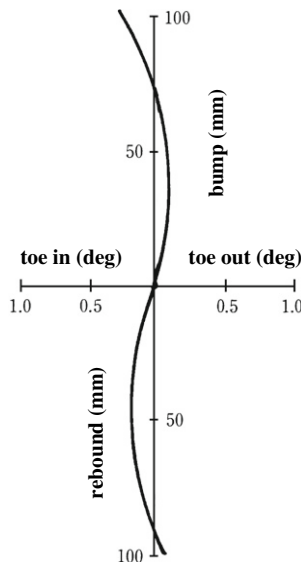

FIGURE 6.10 Roll steer (toe change due to suspension stroke).

been understood. During steady-state cornering, a constant centrifugal force acts at the vehicle center of gravity and if the suspension system is considered, the vehicle will produce a constant roll angle. The previous sections explained body roll geometrically. This section will try to study the effect of vehicle roll on the steer characteristics by considering vehicle steady-state cornering with body roll. The effect of suspension lateral stiffness on vehicle steer characteristics will also be looked at.

6.3.1 Load transfer effect

As described in Chapter 2, the tire lateral force changes with tire load in the form of a saturating curve. When there is a load transfer between the left and the right wheels, the sum of their lateral forces will be lower than when load transfer is not considered. The larger the load transfer, the greater the reduction in total lateral force.

Figure 6.11 shows a typical relationship between the load transfer and the lateral force. For an axle with two wheels and weight W, a load transfer of ΔW occurs between the left and right sides. This yields lateral forces of $\overline{P_1A_1}$ and $\overline{P_2A_2}$, and their sum is $2\overline{BA}$. In contrast, the lateral force when there is no load transfer is $2\overline{PA}$. The reduction of the lateral force at this axle, due to roll, is exactly equal to $2\overline{PB}$.

During vehicle body roll, the lateral load transfer occurs at the front and rear axles, as described by Eqns (6.4) and (6.5). Consequently, the front and rear wheel cornering stiffnesses will decrease according to the magnitude of ΔW_f and ΔW_r. In order to undergo steady-state cornering, at the same radius as without load transfer, with the same magnitude of centrifugal force, the front and rear wheel side-slip angles must increase according to the magnitude of ΔW_f and ΔW_r. This will produce the lateral forces for equilibrium.

The vehicle steer characteristic is determined by the relative magnitude of the front and rear wheel side-slip angles. If $\Delta W_f > \Delta W_r$, the vehicle steer

FIGURE 6.11 Load transfer and lateral force.

characteristic will tend to US, while if $\Delta W_f < \Delta W_r$, the steer characteristic will change to OS.

The load transfer for the front and rear wheels, as shown by Eqns (6.4) and (6.5) is dependant on:

- the front and rear roll center heights, h_f and h_r,
- the ratio of front and rear roll stiffnesses, $K_{\phi f}/K_{\phi r}$, and
- the front and rear tracks, d_f and d_r.

If the following conditions are true: $h_f \rightarrow$ large, $h_r \rightarrow$ small, $K_{\phi f}/K_{\phi r} \rightarrow$ large, $d_f \rightarrow$ small, and $d_r \rightarrow$ large, then ΔW_f will become larger than ΔW_r, and the vehicle steer characteristic changes to US. In contrast, the vehicle steer characteristic will change to OS if $h_f \rightarrow$ small, $h_r \rightarrow$ large, $K_{\phi f}/K_{\phi r} \rightarrow$ small, $d_f \rightarrow$ large, and $d_r \rightarrow$ small.

Below is a further examination of the reduction in the axle equivalent cornering characteristics due to the load transfer between the left and right wheels.

Curve OP in Fig. 6.12 is the relationship between the lateral force and tire side-slip angle for a tire with the weight W. The lateral force for the tire with the extra weight of ΔW is shown by curve OP_1, and the lateral force for the tire with less weight of ΔW is shown by curve OP_2. The sum of these two curves is the lateral force for the axle when there is a load difference of ΔW between the left and right wheels. This is equal to two times of the curve OB.

If there is no load difference, the lateral force for that axle is shown by the curve OP, which is larger than the curve OB. These two curves are the axle lateral force divided by the axle weight.

At lateral accelerations of $\ddot{y}_1, \ddot{y}_2$, and $\ddot{y}_3$, there are load transfers of ΔW_1, ΔW_2, and ΔW_3, respectively, at the vehicle axle. The curves of the axle force divided by the axle weight to side-slip angle for each load transfer are seen in Fig. 6.13. As described in subsection 3.3.3, the vertical axis in Fig. 6.13 is identical to the vehicle lateral acceleration. Projecting points $\ddot{y}_1, \ddot{y}_2$, and $\ddot{y}_3$ from the vertical axis of Fig. 6.13 onto the curve for load differences ΔW_1, ΔW_2, and ΔW_3, respectively, and connecting all the points on the curves, give a new curve of equivalent cornering force of the axle when lateral load transfer occurs according to the lateral acceleration.
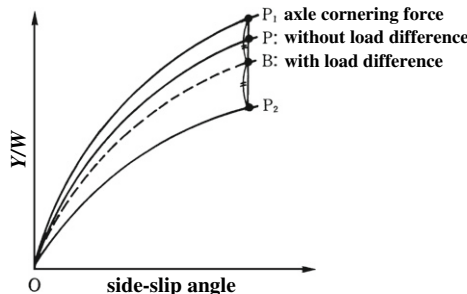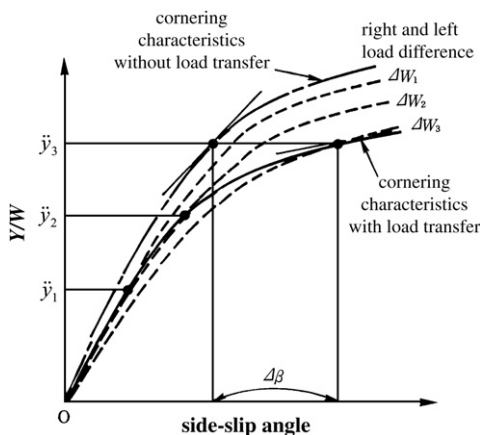

FIGURE 6.12 Axle lateral force and vertical load.

FIGURE 6.13 Effect of load transfer on axle lateral force.

The above investigation infers that a change of tire characteristics due to load transfer is expected and the change of vehicle motion characteristics due to this will become more obvious at large lateral accelerations because of the non-linear tire characteristics.

6.3.2 Camber change effect

The wheel camber could occur in either the same or the opposite direction to the roll direction, as described in subsection 6.2.3. Here, it is assumed that the first case gives positive camber change, and the second gives a negative camber change. In either case, the camber change results in a force that acts in the lateral direction (camber thrust). This is proportional to the camber angle, as described in Chapter 2. In steady-state cornering, the camber thrust becomes one of the forces that balance the centrifugal force at the CG. Positive camber angles produce a camber thrust that acts in the same direction as the centrifugal force. In this case, larger wheel side-slip angles are needed to achieve steady-state cornering at the same radius and speed as when camber change is not considered. In contrast, negative camber angles produce a camber thrust that acts in the opposite direction to the centrifugal force. Here the cornering force and the wheel side-slip angles can become smaller.

The vehicle steer characteristics are determined by the relative magnitude of the front and rear wheel side-slip angles. Consequently, the positive camber change alters the vehicle steer characteristic to US at the front wheels and OS at the rear wheels. Negative camber changes have an opposite effect and change the vehicle steer characteristic to OS at the front wheels and US at the rear wheels.

6.3.3 Roll steer effect

The angular displacement of the wheel due to roll is defined as roll steer. A positive roll steer acts in the same direction as the actual steer angle while a negative roll steer acts in the opposite direction.

Figure 6.14 shows the geometry of a steady-state cornering vehicle with roll steer. Here, α_f and α_r are the front and rear roll steers. The geometrical relation of steady-state cornering excluding roll steer is given by Eqn (3.34). With roll steer as in Fig. 6.14, the equation becomes

$$\rho = \frac{l}{\delta - \beta_f + \beta_r + \alpha_f - \alpha_r} \tag{6.6}$$

Equation 6.6 shows that the vehicle steer characteristic is determined by the front and rear roll steer angles, α_f and α_r as well as the front and rear wheel side-slip angles, β_f and β_r. When a cornering radius at a constant steer angle increases with speed or lateral acceleration, the steer characteristics is termed as US. If the radius decreases, the steer characteristic is called OS. If the front roll steer, α_f, is positive, it will change the vehicle steer characteristics to OS and if it is negative, the vehicle will tend to US. On the contrary, if the rear roll steer, α_r, is positive, it will change the vehicle steer characteristics to US, and a negative roll steer will result in an OS vehicle. Figure 6.15 shows the effect of roll steer on the vehicle steer characteristic. Rewriting Eqn (6.6) gives:

$$\delta = \frac{l}{\rho} + \beta_f - \beta_r + \alpha_r - \alpha_f \tag{6.6'}$$

As described in subsection 3.3.3, $\beta_f - \beta_r$ is determined in relation to the lateral acceleration, $\ddot{y}$, during cornering. Also, the front and rear roll steers, α_f and α_r, are found from the roll angle (or the suspension stroke), which is proportional to the lateral acceleration, $\ddot{y}$.

Based upon the above, Eqn (6.6)' can be used to investigate the vehicle steer characteristics in the relationship between the steady-state steer angle, δ, and the lateral acceleration, $\ddot{y}$, when roll steer is considered.
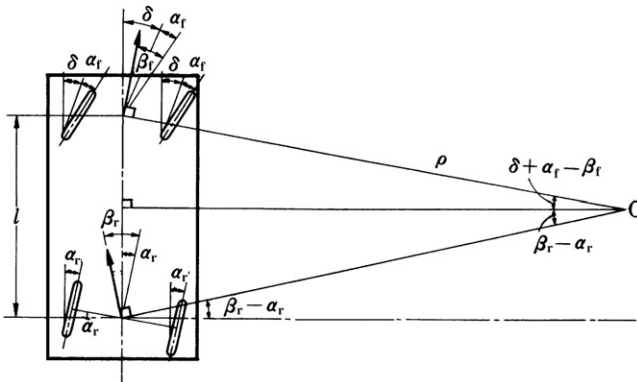

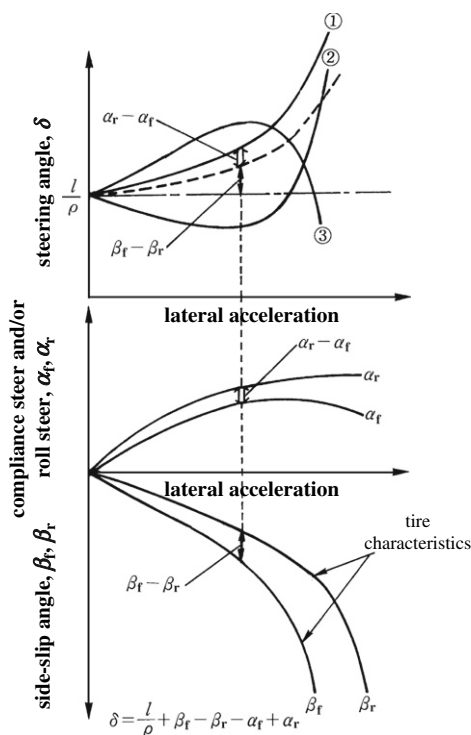FIGURE 6.14 Steady-state cornering with roll steer.

FIGURE 6.15 Vehicle steer characteristics with roll steer.

Example 6.2

Derive the equation to show the effect of the roll steer on the steady-state turning radius when the front and rear suspensions both have the roll steer proportional to the roll angle.

Solution
As is described at the end of subsection 3.3.1 (2), the side-slip angles of the front and rear tires during steady-state turning with the lateral acceleration, mV^2/ρ, are described as:

$$\beta_f = \frac{mV^2 l_r}{2lK_f} \frac{1}{\rho}$$

$$\beta_r = \frac{mV^2 l_f}{2lK_r} \frac{1}{\rho}$$

From Eqn (6.1), the roll angle in the steady-state turning is

$$\phi = \frac{\ddot{y}W_s h_s}{K_\phi} = \frac{m_s V^2 h_s}{K_\phi}\frac{1}{\rho}$$

where $K_\phi = K_{\phi f} + K_{\phi r} - W_s h_s$.

The roll steer angles of the front and rear wheels proportional to the roll angle are described as:

$$\alpha_f = \frac{\partial \alpha_f}{\partial \phi}\phi = \frac{\partial \alpha_f}{\partial \phi}\frac{m_s V^2 h_s}{K_\phi}\frac{1}{\rho} \tag{E6.1}$$

$$\alpha_r = \frac{\partial \alpha_r}{\partial \phi}\phi = \frac{\partial \alpha_r}{\partial \phi}\frac{m_s V^2 h_s}{K_\phi}\frac{1}{\rho} \tag{E6.2}$$

Substituting the above β_f, β_r, α_f, and α_r into Eqn (6.6):

$$\rho = \left[1 + \left\{-\frac{m(l_f K_f - l_r K_r)}{2l^2 K_f K_r} - \frac{m_s h_s}{lK_\phi}\frac{\partial \alpha_f}{\partial \phi} + \frac{m_s h_s}{lK_\phi}\frac{\partial \alpha_r}{\partial \phi}\right\}V^2\right]\frac{l}{\delta} \tag{E6.3}$$

6.3.4 Suspension lateral stiffness and its effect

Section 6.1 described how the vehicle body and the wheels are connected elastically by the suspension. This suspension system gives the vehicle wheels a displacement relative to the vehicle body mainly in the vertical direction; however, the vehicle body and the wheels are not completely connected rigidly in the lateral direction.

This section will look at the effect of this suspension system lateral stiffness on the vehicle steer characteristics.

Figure 6.16 shows the connection of the vehicle body with the wheel in the horizontal plane. The lateral force doesn't usually act through the lateral stiffness center of the suspension system. Therefore, it produces an angular displacement of the wheel in the horizontal plane. This is called the compliance steer and influences the vehicle steer characteristic.

The compliance steer is generated by the lateral tire force, which depends on the lateral acceleration. Consequently, the suspension system compliance steer is due to the lateral acceleration during cornering. If α_f and α_r in Fig. 6.15 are considered as the compliance steers, the effect of the compliance steer on the vehicle steer characteristic can be studied in exactly the same way as the roll steer effect.

The compliance steer can be assumed to be proportional to the lateral force acting on the tire within a relatively small lateral acceleration range. If the cornering stiffness is K, and the lateral force is proportional to the side-slip angle, then
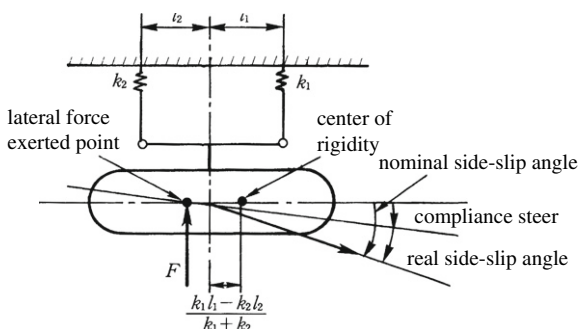
FIGURE 6.16 Suspension plane model.

$$\alpha = cF = cK(\beta - \alpha)$$

Here, c is a compliance coefficient of the suspension system.

Eliminating α in the above equation gives:

$$F = \frac{K}{1 + cK}\beta = eK\beta$$

whereby $e = 1/(1 + cK)$. In other words, the compliance steer has the effect of changing the tire equivalent cornering stiffness from K to eK. This effect is similar to the effect of the steering system stiffness as described in subsection 5.3.1.

The above concept can be extended beyond the region where the compliance steer is proportional to the lateral force, to the non-linear region where the lateral force is not proportional to the side-slip angle. Figure 6.17 shows how the tire cornering characteristics considering both the suspension system lateral stiffness and the steering system stiffness equivalently vary from the original tire cornering characteristics by the compliance steers.

A tire with real side-slip angle, β, suspension system compliance steer, α_1, and steering system compliance steer, α_2, has a nominal side-slip angle of $\beta + \alpha_1 + \alpha_2$. This lateral force at side-slip angle equal to β is equivalently regarded as the lateral force when the side-slip angle is equal to $\beta + \alpha_1 + \alpha_2$. In this manner, the equivalent tire cornering characteristics with consideration of the compliance steers are obtained, and their effect on the vehicle steer characteristics can be investigated.

6.4 EQUATIONS OF MOTION INCLUSIVE OF ROLL

Until here, the vehicle roll mechanism has only been dealt geometrically, or from a static point of view, where the roll is produced by a constant lateral acceleration.

Next, this knowledge will be used to derive the vehicle equations of motion that include rolling motion. This will enable us to investigate the vehicle motion further. These equations of motion are based on those proposed by Segel, using the fixed roll axis concept [2].
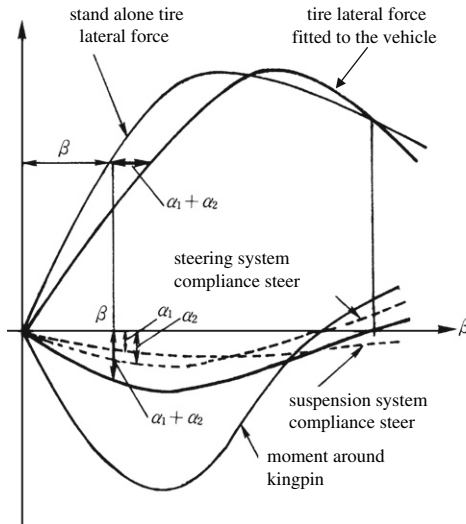
FIGURE 6.17 Tire cornering characteristics considering compliance steer.

The choice of the coordinate system for dealing with the motion is not necessarily standardized, and can vary. Here, the coordinate system that the author thinks is most easily understood is used.

6.4.1 Coordinate system and dynamic model

A coordinate system with the X–Y plane parallel to the ground is fixed in absolute space as shown in Fig. 6.18.

Point P in Fig. 6.18 is where a vertical line through the CG crosses the roll axis. This is the origin of a coordinate system x–y–z that is fixed to the vehicle body, i.e., the sprung mass. The vehicle longitudinal direction, parallel to the ground, is taken as the x-axis (the forward direction is positive), the lateral
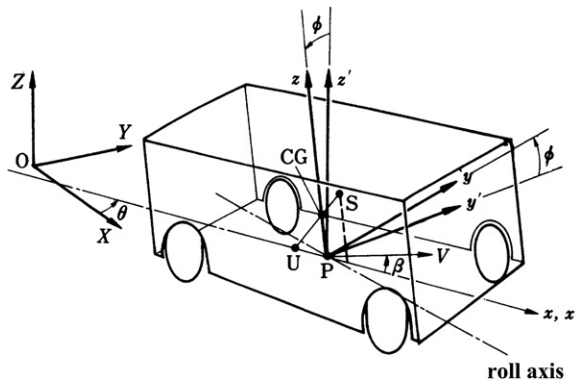

FIGURE 6.18 Coordinate system.

direction perpendicular to this is taken as the y-axis (the left hand side when the vehicle is facing to the front as positive), and the vertical direction as the z-axis (up direction as positive).

A coordinate system of $x'-y'-z'$ is fixed to the unsprung mass with the same origin P. The vehicle longitudinal direction is the x'-axis, the lateral direction perpendicular to this is the y'-axis, and the vertical direction is the z'-axis.

The vehicle roll axis doesn't always coincide with the x-axis, as mentioned in subsection 6.2.1. For simplicity, the vehicle body is assumed to roll around the x-axis. Furthermore, the roll angle is assumed to be small and the vehicle is assumed to yaw around the z-axis. The unsprung mass roll motion is neglected, and the unsprung mass is assumed to produce the same yawing motion as the vehicle body around the z'-axis (therefore, the x-axis and the x'-axis always coincide). All the angular displacements and angular accelerations are taken as positive in the direction shown in Fig. 6.18.

Figure 6.19 shows the equivalent mechanic model for the sprung mass and the unsprung mass. The mass of the vehicle body, or the sprung mass, is assumed to be distributed symmetrically to the x–z plane and the center of gravity is taken as the point S in the x–z plane. The height of the unsprung mass in the z'-direction is neglected, and its mass is assumed to be distributed in the y'–z' plane with the center of gravity at point U on the x'-axis.

Here, m_S is the mass of the sprung mass, m_U is the mass of the unsprung mass and m is the mass of the whole vehicle. h_s is the distance between the sprung mass center of gravity to the x-axis, c and e are the distances of the sprung mass and the unsprung mass center of gravity to the z-axis, respectively, while r and p are the vehicle yaw angular velocity and roll angular velocity, respectively. ϕ is the vehicle roll angle.
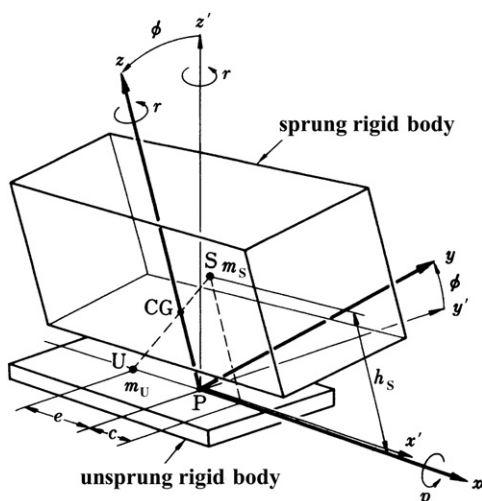

FIGURE 6.19 Equivalent dynamic model.

6.4.2 Inertias

Rigid body motion can be divided into both the translational motion of the center of gravity and the rotational motion around the center of gravity. Here, these motions will be considered for the sprung mass and the unsprung mass, which are both rigid bodies.

(1) TRANSLATIONAL MOTION

The translational motion of the center of gravity of a rigid body is equal to the motion of the point where the entire body mass is concentrated at the center of gravity.

The coordinate system X–Y–Z is fixed in the absolute space and the coordinate system x–y–z fixed on the moving rigid body as shown in Fig. 6.20.

The position vector of the center of gravity C relative to the x–y–z coordinates is taken as ρ. If points P and C are described by position vectors r, R, relative to the X–Y–Z system, then

$$r = R + \rho$$

The x–y–z-coordinate system has a translational velocity, $\dot{R}$, relative to the X–Y–Z coordinates, and also a rotational motion with an angular velocity of ω. Thus,

$$\dot{r} = \dot{R} + \dot{\rho}_r + \omega \times \rho$$

Here, $\dot{\rho}_r$ is the relative velocity of the point C to the point P and if the point C is fixed on the x–y–z coordinate, then $\dot{\rho}_r = 0$, so

$$\dot{r} = \dot{R} + \omega \times \rho \tag{6.7}$$

The translational motions of the sprung and unsprung mass centers of gravity, S and U in the X–Y–Z-coordinate system are r_S and r_U. The position vectors of the point S and the point U relative to the x–y–z system are ρ_S and ρ_U, and the angular velocities of x–y–z and x'-y'-z' coordinates are ω_S and ω_U. The unit
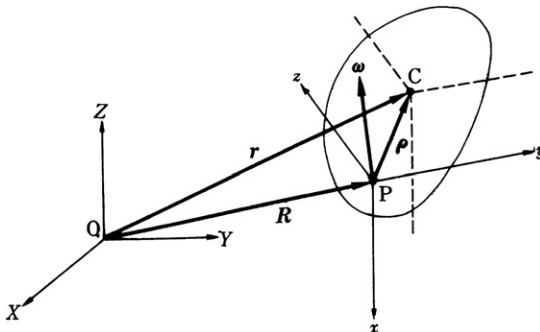
FIGURE 6.20 General motion description of rigid body.

vectors in the x–y–z direction are $\boldsymbol{i}, \boldsymbol{j}$, and $\boldsymbol{k}$ and the unit vectors in the x'-y'-z' direction are $\boldsymbol{i'}, \boldsymbol{j'}$, and $\boldsymbol{k'}$. These are shown in Fig. 6.21.

The points S and U are fixed on the x–y–z and x'-y'-z' coordinates, respectively, and the following equations are formed based on Eqn (6.7):

$$\dot{r}_S = \dot{R} + \omega_S \times \rho_S \tag{6.8}$$

$$\dot{r}_U = \dot{R} + \omega_U \times \rho_U \tag{6.9}$$

Assuming that point P has a velocity component of u in the x-direction and v in the y- or y'-direction when ϕ is small, then

$$\dot{R} = u\boldsymbol{i} + v\boldsymbol{j} = u\boldsymbol{i'} + v\boldsymbol{j'} \tag{6.10}$$

The x–y–z coordinates that move with the sprung mass has a roll velocity of p around the x-axis and a yaw velocity of r around the z-axis, hence,

$$\omega_S = p\boldsymbol{i} + r\boldsymbol{k} \tag{6.11}$$

the x'–y'–z' coordinates, which move together with the unsprung mass have a yaw velocity of r around the z'-axis, so

$$\omega_U = r\boldsymbol{k'} \tag{6.12}$$

and, ρ_S, ρ_U can be written as follows:

$$\rho_S = c\boldsymbol{i} + h_s\boldsymbol{k} \tag{6.13}$$
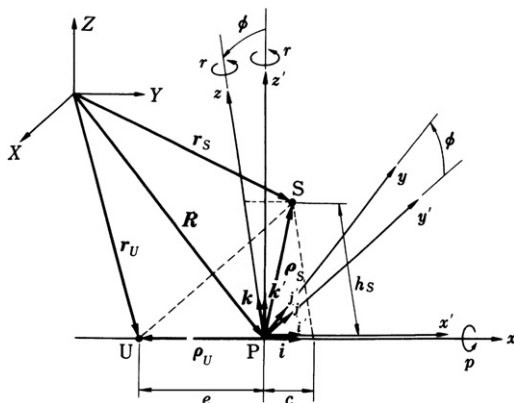
$$\rho_U = -e\boldsymbol{i'} \tag{6.14}$$

FIGURE 6.21 Motion of points S and P.

Substituting Eqns (6.10), (6.11), and (6.13) into Eqn (6.8) and Eqns (6.10), (6.12), and (6.14) into Eqn (6.9) gives $\dot{r}_S$ and $\dot{r}_U$ as follows:

$$\dot{r}_S = u\mathbf{i} + (v - h_s p + cr)\mathbf{j} \tag{6.15}$$

$$\dot{r}_U = u\mathbf{i}' + (v - er)\mathbf{j}' \tag{6.16}$$

Differentiating Eqns (6.15) and (6.16) gives the acceleration vector of the point S and the point U:

$$\ddot{r}_S = (\dot{u} - vr + h_s pr - cr^2)\mathbf{i} + (\dot{v} + ur - h_s\dot{p} + c\dot{r})\mathbf{j} + (vp + h_s p^2 + cpr)\mathbf{k} \tag{6.17}$$

$$\ddot{r}_U = (\dot{u} - vr + er^2)\mathbf{i}' + (\dot{v} + ur - e\dot{r})\mathbf{j}' \tag{6.18}$$

From Eqns (6.17) and (6.18), the lateral acceleration, in other words, the acceleration in the y- and y'-direction, the lateral direction, for the sprung mass and the unsprung mass, α_S and α_U, is

$$\alpha_S = \dot{v} + ur - h_s\dot{p} + c\dot{r}$$

$$\alpha_U = \dot{v} + ur - e\dot{r}$$

If the side-slip angle of the point P, β, is $|\beta| \ll 1$ and the velocity magnitude of the point P, V, is always constant, then $u \approx V$, $v \approx V\beta$, and

$$\alpha_S = V\dot{\beta} + Vr - h_s\dot{p} + c\dot{r}$$

$$\alpha_U = V\dot{\beta} + Vr - e\dot{r}$$

The masses for the sprung mass and the unsprung mass are m_S and m_U, respectively. The inertia forces in lateral direction, Y_S and Y_U, of the sprung mass and the unsprung mass are:

$$Y_S = m_S\alpha_S = m_S V(\dot{\beta} + r) - m_S h_s\dot{p} + m_S c\dot{r}$$

$$Y_U = m_U\alpha_U = m_U V(\dot{\beta} + r) - m_U e\dot{r}$$

Consequently, the total vehicle inertia force in lateral direction ΣY is

$$\Sigma Y = Y_S + Y_U = (m_S + m_U)V(\dot{\beta} + r) - m_S h_s\dot{p} + (m_S c - m_U e)\dot{r}$$

Here, $m_S + m_U = m$, and CG is the entire vehicle center of gravity, therefore, $m_S c - m_U e = 0$. Thus,

$$\Sigma Y = mV(\dot{\beta} + r) - m_S h_S \dot{p} \tag{6.19}$$

Example 6.3

Differentiate Eqns (6.15) and (6.16) and derive Eqns (6.17) and (6.18).

Solution
From Eqns (6.15) and (6.16):

$$\ddot{\boldsymbol{r}}_S = \dot{u}\boldsymbol{i} + u\dot{\boldsymbol{i}} + (\dot{v} - h_S\dot{p} + c\dot{r})\boldsymbol{j} + (v - h_S p + cr)\dot{\boldsymbol{j}} \tag{E6.4}$$

$$\ddot{\boldsymbol{r}}_U = \dot{u}\boldsymbol{i}' + u\dot{\boldsymbol{i}}' + (\dot{v} - e\dot{r})\boldsymbol{j}' + (v - er)\dot{\boldsymbol{j}}' \tag{E6.5}$$

It is known that:

$$\dot{\boldsymbol{i}} = \boldsymbol{\omega}_S \times \boldsymbol{i}, \ \dot{\boldsymbol{j}} = \boldsymbol{\omega}_S \times \boldsymbol{j}$$

$$\dot{\boldsymbol{i}}' = \boldsymbol{\omega}_U \times \boldsymbol{i}', \ \dot{\boldsymbol{j}}' = \boldsymbol{\omega}_U \times \boldsymbol{j}'$$

Substituting Eqns (6.11) and (6.12) into the above gives

$$\dot{\boldsymbol{i}} = (p\boldsymbol{i} + r\boldsymbol{k}) \times \boldsymbol{i} = r\boldsymbol{j}$$

$$\dot{\boldsymbol{j}} = (p\boldsymbol{i} + r\boldsymbol{k}) \times \boldsymbol{j} = p\boldsymbol{k} - r\boldsymbol{i}$$

$$\dot{\boldsymbol{i}}' = r\boldsymbol{k}' \times \boldsymbol{i}' = r\boldsymbol{j}'$$

$$\dot{\boldsymbol{j}}' = r\boldsymbol{k}' \times \boldsymbol{j}' = -r\boldsymbol{i}'$$

Using the above, Eqns (E6.4) and (E6.5) can be rewritten as follows:

$$\ddot{\boldsymbol{r}}_S = (\dot{u} - vr + h_S pr - cr^2)\boldsymbol{i} + (\dot{v} + ur - h_S\dot{p} + c\dot{r})\boldsymbol{j} + (vp + h_S p^2 + cpr)\boldsymbol{k} \tag{6.17}$$

$$\ddot{\boldsymbol{r}}_U = (\dot{u} - vr + er^2)\boldsymbol{i}' + (\dot{v} + ur - e\dot{r})\boldsymbol{j}' \tag{6.18}$$

(2) ROTATIONAL MOTION

Generally, the moment of momentum, H_C, around center of gravity, C, of a rigid body could be written as follows:

$$
\begin{aligned}
H_C &= \boldsymbol{I} \times \boldsymbol{\omega} \\
&= (I_{xx}\omega_x - I_{xy}\omega_y - I_{xz}\omega_z)\boldsymbol{i} + (-I_{yx}\omega_x + I_{yy}\omega_y - I_{yz}\omega_z)\boldsymbol{j} \\
&\quad + (-I_{zx}\omega_x - I_{zy}\omega_y + I_{zz}\omega_z)\boldsymbol{k}
\end{aligned}
$$

whereby $\boldsymbol{I}$ is the inertia tensor of the rigid body around point C. The elements I_{xx}, I_{xy}, ... are the inertia moments, or inertia products, around the axis passing through point C parallel to the x-, y-, z-axis. ω_x, ω_y, ω_z are the components of the angular velocity $\boldsymbol{\omega}$ in the x-, y-, z-direction.

The moment of momentum of the sprung mass centre of gravity, H_S, with angular velocity, ω_S, given by Eqn (6.11) is

$$
H_S = \boldsymbol{I}_S \times \boldsymbol{\omega}_S = (I_{xxS}p - I_{xzS}r)\boldsymbol{i} + (-I_{zzS}p + I_{zzS}r)\boldsymbol{k} \tag{6.20}
$$

Here, $\boldsymbol{I}_S$ is the inertia tensor of the sprung mass around the point S. Considering that the sprung mass is symmetrical in the xz plane, $I_{yxS} = I_{yzS} = 0$.

Similarly, with the angular velocity, ω_U, given by Eqn (6.12), the moment of momentum, H_U, around the unsprung mass center of gravity, U, is

$$
H_U = I_{zzU}r\boldsymbol{k}' \tag{6.21}
$$

Here, I_{zzU} is the moment of inertia around the axis passing through the point U and parallel to the z'-axis. If the unsprung mass is symmetrical to the x'-axis, then the height is neglected and the mass is assumed to be distributed in the x'–y' plane; all the inertia products are zero.

The time variation of moment of momentum of the moving body is caused by the external moment. Differentiating Eqns (6.20) and (6.21) with respect to time gives

$$
\begin{aligned}
\dot{H}_S &= (I_{xxS}\dot{p} - I_{xzS}\dot{r})\boldsymbol{i} + [I_{xzS}p^2 + (I_{xxS} - I_{zzS})pr - I_{xzS}r^2]\boldsymbol{j} \\
&\quad + (-I_{zzS}\dot{p} + I_{zzS}\dot{r})\boldsymbol{k}
\end{aligned} \tag{6.22}
$$

$$
\dot{H}_U = I_{zzU}\dot{r}\boldsymbol{k}' \tag{6.23}
$$

From these equations, the yaw and rolling moments, N_S and L_S, of the sprung mass around the axis parallel to the x- and z-axis and passing through the point S are

$$
N_S = -I_{zzS}\dot{p} + I_{zzS}\dot{r}
$$

$$
L_S = I_{xxS}\dot{p} - I_{xzS}\dot{r}
$$

The yawing moment, N_U, around the axis passing through the point U parallel to the z'-axis for the unsprung mass is:

$$N_U = I_{zzU}\dot{r}$$

From the above, the total vehicle yawing moment, ΣN, around the z- or z'-axis and the total rolling moment, ΣL, around the x- or x'-axis are given in Eqns (6.24) and (6.25), where Y_S and Y_U act at the sprung and unsprung mass centers of gravity, S and U, respectively:

$$
\begin{aligned}
\Sigma N &= N_S + N_U + cY_S - eY_U \\
&= (I_{zzS} + I_{zzU} + m_S c^2 + m_U e^2)\dot{r} - (I_{zxS} + m_S h_s c)\dot{p} \\
&\quad + (m_S c - m_U e)V(\dot{\beta} + r) \\
&= I_z \dot{r} - I_{zx}\dot{p}
\end{aligned}
\tag{6.24}
$$

$$
\begin{aligned}
\Sigma L &= L_s - h_s Y_S \\
&= (I_{xxS} + m_S h_s^2)\dot{p} - (I_{xzS} + m_S h_s c)\dot{r} \\
&\quad + m_S h_s V(\dot{\beta} + r) \\
&= I_x \dot{p} - I_{xz}\dot{r} - m_S h_s V(\dot{\beta} + r)
\end{aligned}
\tag{6.25}
$$

whereby $|\phi| \ll 1$

$$I_z = I_{zzS} + I_{zzU} + m_S c^2 + m_U e^2$$

$$I_{zx} = I_{xz} = I_{xzS} + m_S h_s c$$

$$I_x = I_{xxS} + m_S h_s^2$$

I_z is the total yaw moment of inertia around the vertical axis passing through the vehicle center of gravity, and I_x is the rolling moment of inertia of the sprung mass around the x-axis.

6.4.3 External force

The external forces that act on the vehicle are the lateral tire forces. As described in Section 3.2, lateral forces, which are proportional to the tire side-slip angles, act at the front and rear tires of a moving vehicle. Where roll is considered, camber thrusts also act at the tires. When the vehicle equations of motion include roll motion, these forces must be included in the external forces acting on the entire vehicle.

The front and rear roll steers are α_f and α_r. If they are assumed to be proportional to the roll angle, then

$$\alpha_f = \frac{\partial \alpha_f}{\partial \phi}\phi,$$

$$\alpha_r = \frac{\partial \alpha_r}{\partial \phi} \phi$$

where $\partial \alpha_f / \partial \phi$ and $\partial \alpha_r / \partial \phi$ are the front and rear wheel roll steer angles per unit roll angle. These are positive when the roll angle is positive, in other words, positive when the steer angle is in the anti-clockwise direction.

The front wheel steered angle is now changed by α_f from the steer angle δ. Similarly, a change of α_r is generated at the rear wheel. Using the same assumptions as in Section 3.2 and Eqns (3.6) and (3.7), the front and rear wheel tire side-slip angles are

$$\beta_f = \beta + \frac{l_f}{V}r - \delta - \alpha_f = \beta + \frac{l_f}{V}r - \delta - \frac{\partial \alpha_f}{\partial \phi} \phi$$

$$\beta_r = \beta - \frac{l_r}{V}r - \alpha_r = \beta - \frac{l_r}{V}r - \frac{\partial \alpha_r}{\partial \phi} \phi$$

Therefore, the lateral forces, $2Y_f$ and $2Y_r$, acting at the front and rear wheels are

$$2Y_f = -2K_f \beta_f = 2K_f \left(\delta + \frac{\partial \alpha_f}{\partial \phi} \phi - \beta - \frac{l_f}{V}r \right)$$

$$2Y_r = -2K_r \beta_r = 2K_r \left(\frac{\partial \alpha_r}{\partial \phi} \phi - \beta + \frac{l_r}{V}r \right)$$

where the lateral force changes caused by load transfer are neglected.

Assuming that the camber angle produced by the vehicle body roll is proportional to the roll angle, the camber thrust, $2Y_{cf}$ and $2Y_{cr}$, acting at the front and rear wheels, respectively, is:

$$2Y_{cf} = -2K_{cf} \frac{\partial \phi_f}{\partial \phi} \phi$$

$$2Y_{cr} = -2K_{cr} \frac{\partial \phi_r}{\partial \phi} \phi$$

where K_{cf} and K_{cr} are the front and rear wheel tire camber thrust coefficients. $\partial \phi_f / \partial \phi$ and $\partial \phi_r / \partial \phi$ are the front and rear wheel camber angles per unit roll angle. These are positive if the camber angle is in the same direction as the roll. It is also assumed that a camber thrust of the same magnitude and in the same direction is produced at the left and right wheels.

The total external forces acting on the entire vehicle in the lateral direction, in other words, the y-direction, are shown in Fig. 6.22.

$$\Sigma F_y = 2Y_f + 2Y_r + 2Y_{cf} + 2Y_{cr}$$
$$= 2K_f\left(\delta + \frac{\partial\alpha_f}{\partial\phi}\phi - \beta - \frac{l_f}{V}r\right) + 2K_r\left(\frac{\partial\alpha_r}{\partial\phi}\phi - \beta + \frac{l_r}{V}r\right)$$
$$-2K_{cf}\frac{\partial\phi_f}{\partial\phi}\phi - 2K_{cr}\frac{\partial\phi_r}{\partial\phi}\phi \quad (6.26)$$

The total yaw moment around the z-axis produced by the external forces acting on the entire vehicle, ΣM_z, is:

$$\Sigma M_z = 2l_f Y_f - 2l_r Y_r + 2l_f Y_{cf} - 2l_r Y_{cr}$$
$$= 2l_f K_f\left(\delta + \frac{\partial\alpha_f}{\partial\phi}\phi - \beta - \frac{l_f}{V}r\right) - 2l_r K_r\left(\frac{\partial\alpha_r}{\partial\phi}\phi - \beta + \frac{l_r}{V}r\right)$$
$$-2l_f K_{cf}\frac{\partial\phi_f}{\partial\phi}\phi + 2l_r K_{cr}\frac{\partial\phi_r}{\partial\phi}\phi \quad (6.27)$$

When the vehicle body rolls, it will be subjected to the reaction force by the suspension system spring and shock absorber. These reaction forces produce the rolling moment to the vehicle body around the roll axis, in other words, the x-axis. From subsection 6.2.2, the rolling moment, which comes from the spring is $-K_\phi\phi$. Assuming that the reaction force produced by the shock absorber is proportional to the roll angular velocity, the rolling moment produced by this reaction force is written as $-C_\phi p$. Here, C_ϕ is the equivalent damping coefficient of the rolling motion, which is the sum of the rolling moment per unit roll angular velocity at the front and rear shock absorbers.

A rolling moment around the x-axis by the weight $m_S g$ also acts on the vehicle as shown in Fig. 6.23. If roll angle ϕ is small, this can be approximated by $m_S g h_s \phi$.

The total rolling moment around the x-axis by the external forces acting on the entire vehicle, ΣM_x, is expressed as:

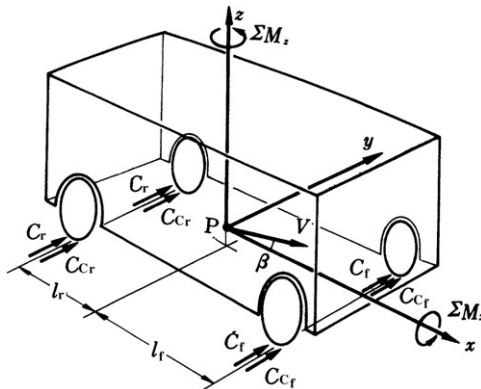$$\Sigma M_x = (-K_\phi + m_S g h_s)\phi - C_\phi p \quad (6.28)$$

FIGURE 6.22 External forces exerted on vehicle tires.

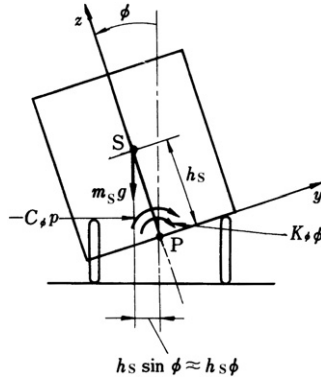$$h_s \sin \phi \approx h_s \phi$$

FIGURE 6.23 Roll moments exerted on vehicle body.

6.4.4 Equations of motion

The external forces and inertia forces of the vehicle motion inclusive of vehicle body roll can now be used in the equilibrium equations to derive the equations of motion:

$$\Sigma Y - \Sigma F_y = 0 \text{ (equilibrium of lateral forces)},$$
$$\Sigma N - \Sigma M_z = 0 \text{ (equilibrium of yawing moment), and}$$
$$\Sigma L - \Sigma M_x = 0 \text{ (equilibrium of rolling moment).}$$

Substituting Eqns (6.19) and (6.24)–(6.28) into the above equations, derives the vehicle equations of motion inclusive of roll motion as below. Here, $d\phi/dt = p$, and I and I_ϕ are used in replacement of I_z and I_{xx}. I is the entire vehicle yaw moment of inertia, while I_ϕ is the roll moment of inertia around the roll axis when the roll axis is assumed to coincide with the x-axis.

$$mV\left(\frac{d\beta}{dt} + r\right) - m_s h_s \frac{d^2\phi}{dt^2} = 2K_f\left(\delta + \frac{\partial \alpha_f}{\partial \phi}\phi - \beta - \frac{l_f}{V}r\right) + 2K_r\left(\frac{\partial \alpha_r}{\partial \phi}\phi - \beta\right.$$
$$\left. + \frac{l_r}{V}r\right) - 2\left(K_{cf}\frac{\partial \phi_f}{\partial \phi}\phi + K_{cr}\frac{\partial \phi_r}{\partial \phi}\phi\right)$$

$$(6.29)$$

$$I\frac{dr}{dt} - I_{xz}\frac{d^2\phi}{dt^2} = 2K_f\left(\delta + \frac{\partial \alpha_f}{\partial \phi}\phi - \beta - \frac{l_f}{V}r\right)l_f - 2K_r\left(\frac{\partial \alpha_r}{\partial \phi}\phi - \beta + \frac{l_r}{V}r\right)l_r$$
$$- 2\left(l_f K_{cf}\frac{\partial \phi_f}{\partial \phi}\phi - l_r K_{cr}\frac{\partial \phi_r}{\partial \phi}\phi\right)$$

$$(6.30)$$

$$I_\phi\frac{d^2\phi}{dt^2} - I_{xz}\frac{dr}{dt} - m_s h_s V\left(\frac{d\beta}{dt} + r\right) = (-K_\phi + m_s g h_s)\phi - C_\phi\frac{d\phi}{dt} \quad (6.31)$$

rearranging the above equations gives

$$
mV\frac{\mathrm{d}\beta}{\mathrm{d}t} + 2\left(K_{\mathrm{f}} + K_{\mathrm{r}}\right)\beta + \left[mV + \frac{2(l_{\mathrm{f}}K_{\mathrm{f}} - l_{\mathrm{r}}K_{\mathrm{r}})}{V}\right]r - m_{\mathrm{S}}h_{\mathrm{s}}\frac{\mathrm{d}^2\phi}{\mathrm{d}t^2} - 2Y_\phi\phi
$$
$$
= 2K_{\mathrm{f}}\delta
$$

$$(6.29)'$$

$$
2(l_{\mathrm{f}}K_{\mathrm{f}} - l_{\mathrm{r}}K_{\mathrm{r}})\beta + I\frac{\mathrm{d}r}{\mathrm{d}t} + \frac{2(l_{\mathrm{f}}^2 K_{\mathrm{f}} + l_{\mathrm{r}}^2 K_{\mathrm{r}})}{V}r - I_{xz}\frac{\mathrm{d}^2\phi}{\mathrm{d}t^2} - 2N_\phi\phi = 2l_{\mathrm{f}}K_{\mathrm{f}}\delta
$$

$$(6.30)'$$

$$
-m_{\mathrm{S}}h_{\mathrm{s}}V\frac{\mathrm{d}\beta}{\mathrm{d}t} - I_{xz}\frac{\mathrm{d}r}{\mathrm{d}t} - m_{\mathrm{S}}h_{\mathrm{s}}Vr + I_\phi\frac{\mathrm{d}^2\phi}{\mathrm{d}t^2} + C_\phi\frac{\mathrm{d}\phi}{\mathrm{d}t} + (K_\phi - m_{\mathrm{S}}gh_{\mathrm{s}})\phi = 0
$$

$$(6.31)'$$

where

$$
Y_\phi = \left(\frac{\partial\alpha_{\mathrm{f}}}{\partial\phi}K_{\mathrm{f}} + \frac{\partial\alpha_{\mathrm{r}}}{\partial\phi}K_{\mathrm{r}}\right) - \left(\frac{\partial\phi_{\mathrm{f}}}{\partial\phi}K_{\mathrm{cf}} + \frac{\partial\phi_{\mathrm{r}}}{\partial\phi}K_{\mathrm{cr}}\right) \tag{6.32}
$$

$$
N_\phi = \left(\frac{\partial\alpha_{\mathrm{f}}}{\partial\phi}l_{\mathrm{f}}K_{\mathrm{f}} - \frac{\partial\alpha_{\mathrm{r}}}{\partial\phi}l_{\mathrm{r}}K_{\mathrm{r}}\right) - \left(\frac{\partial\phi_{\mathrm{f}}}{\partial\phi}l_{\mathrm{f}}K_{\mathrm{cf}} - \frac{\partial\phi_{\mathrm{r}}}{\partial\phi}l_{\mathrm{r}}K_{\mathrm{cr}}\right) \tag{6.33}
$$

These are the equations of motion of the vehicle with body roll. Here, the change of rolling resistance due to the load transfer between the left and right wheels is neglected as its effect on the vehicle yaw motion is assumed to be small.

Applying Laplace transformation to Eqns (6.29)′–(6.31)′, the vehicle characteristic equation is obtained as follows:

$$
\begin{vmatrix}
mVs + 2(K_{\mathrm{f}} + K_{\mathrm{r}}) & mV + \frac{2(l_{\mathrm{f}}K_{\mathrm{f}} - l_{\mathrm{r}}K_{\mathrm{r}})}{V} & -m_{\mathrm{S}}h_{\mathrm{s}}s^2 - 2Y_\phi \\
2(l_{\mathrm{f}}K_{\mathrm{f}} - l_{\mathrm{r}}K_{\mathrm{r}}) & Is + \frac{2(l_{\mathrm{f}}^2 K_{\mathrm{f}} + l_{\mathrm{r}}^2 K_{\mathrm{r}})}{V} & -I_{xz}s^2 - 2N_\phi \\
-m_{\mathrm{S}}h_{\mathrm{s}}Vs & -I_{xz}s - m_{\mathrm{S}}h_{\mathrm{s}}V & I_\phi s^2 + C_\phi s + (K_\phi - m_{\mathrm{S}}gh_{\mathrm{s}})
\end{vmatrix} = 0
$$

$$(6.34)$$

The above characteristic equation is a little complicated in this form, thus, assuming

$$
K_{\mathrm{f}} \approx K_{\mathrm{r}} \approx K
$$

$$
l_{\mathrm{f}} \approx l_{\mathrm{r}} \approx \frac{l}{2}
$$

$$I \approx m l_f l_r \approx m \left(\frac{l}{2} \right)^2$$

and neglecting the inertia products:

$$K_\phi - m_S g h_s \approx K_\phi$$

$$I_{xz} \approx 0$$

the characteristic equation becomes

$$\begin{vmatrix} mVs + 4K & mV & -m_S h_s s^2 - 2Y_\phi \\ 0 & m\left(\frac{l}{2}\right)^2 s + \frac{Kl^2}{V} & -2N_\phi \\ -m_S h_s V s & -m_S h_s V & I_\phi s^2 + C_\phi s + K_\phi \end{vmatrix} = 0 \qquad (6.34)'$$

Expanding this and rearranging gives

$$A_4 s^4 + A_3 s^3 + A_2 s^2 + A_1 s + A_0 = 0$$

where

$$\left. \begin{aligned} A_0 &= \frac{16 K^2 K_\phi}{mV} - \frac{32 m_S h_s K N_\phi}{m l^2} V \\ A_1 &= 8K \left(K_\phi - \frac{m_S h_s Y_\phi}{m} \right) + \frac{16 K^2 C_\phi}{mV} \\ A_2 &= (m K_\phi - 2 m_S h_s Y_\phi) V + 8 K C_\phi + \frac{16 K^2 I_\phi}{mV} \\ A_3 &= m C_\phi V + 4K \left(2 I_\phi - \frac{m_S^2 h_s^2}{m} \right) \\ A_4 &= m \left(I_\phi - \frac{m_S^2 h_s^2}{m} \right) V \end{aligned} \right\} \qquad (6.35)$$

6.5 EFFECT OF BODY ROLL ON VEHICLE DYNAMICS

In the last section, the vehicle equations of motion with vehicle body roll were derived. The equation of motion is still too complicated for analysis of the vehicle motion characteristics. In order to analyze the basic effects of vehicle body roll on vehicle motion, a two degrees of freedom equation of motion (vehicle lateral side slip and yaw motion) that includes an equivalent roll effect will be derived referring to Ellis [3]. This is done by considering vehicle body roll due to constant lateral acceleration.

The steady-state vehicle body roll angle, from Eqn (6.31), is derived by assuming

$$\frac{d\beta}{dt} = \frac{dr}{dt} = \frac{d^2\phi}{dt^2} = \frac{d\phi}{dt} = 0$$

and the result is

$$\phi = \frac{m_S h_s V}{K_\phi - m_S g h_s} r \tag{6.36}$$

Rewriting the right hand side of Eqns (6.29) and (6.30) with a steady-state roll angle gives

$$mV\left(\frac{d\beta}{dt} + r\right) = 2K_f\left\{\delta - \beta - \frac{l_f}{V}r + \left(\frac{\partial\alpha_f}{\partial\phi} - \frac{K_{cf}}{K_f}\frac{\partial\phi_f}{\partial\phi}\right)\phi\right\} + 2K_r\left\{-\beta\right.$$
$$\left. + \frac{l_r}{V}r + \left(\frac{\partial\alpha_r}{\partial\phi} - \frac{K_{cr}}{K_r}\frac{\partial\phi_r}{\partial\phi}\right)\phi\right\}$$

$$I\frac{dr}{dt} = 2K_f\left\{\delta - \beta - \frac{l_f}{V}r + \left(\frac{\partial\alpha_f}{\partial\phi} - \frac{K_{cf}}{K_f}\frac{\partial\phi_f}{\partial\phi}\right)\phi\right\}l_f - 2K_r\left\{-\beta + \frac{l_r}{V}r\right.$$
$$\left. + \left(\frac{\partial\alpha_r}{\partial\phi} - \frac{K_{cr}}{K_r}\frac{\partial\phi_r}{\partial\phi}\right)\phi\right\}l_r$$

ϕ in these equations is proportional to r, as given by Eqn (6.36), and the above equations are equivalent to the following equations:

$$mV\left(\frac{d\beta}{dt} + r\right) = 2K_f\left(\delta - \beta - \frac{l'_f}{V}r\right) + 2K_r\left(-\beta + \frac{l'_r}{V}r\right) \tag{6.37}$$

$$I\frac{dr}{dt} = 2K_f\left(\delta - \beta - \frac{l'_f}{V}r\right)l_f + 2K_r\left(-\beta + \frac{l'_r}{V}r\right)l_r \tag{6.38}$$

where

$$l'_f = l_f(1 + B_f V^2) \tag{6.39}$$

$$l'_r = l_r(1 + B_r V^2) \tag{6.40}$$

$$B_f = \frac{-m_S h_s\left(\frac{\partial\alpha_f}{\partial\phi} - \frac{K_{cf}}{K_f}\frac{\partial\phi_f}{\partial\phi}\right)}{l_f(K_\phi - m_S g h_s)}$$

$$B_r = \frac{m_S h_s \left(\frac{\partial \alpha_r}{\partial \phi} - \frac{K_{cr}}{K_r} \frac{\partial \phi_r}{\partial \phi} \right)}{l_r (K_\phi - m_S g h_s)}$$

When Eqns (6.37) and (6.38) are compared with Eqns (3.10) and (3.11), it is easily understood that the equivalent vehicle lateral side-slip motion and yawing motion with body roll are found by replacing the front and rear wheel distances from the vehicle center of gravity l_f and l_r with equivalent l'_f and l'_r.

Rewriting Eqns (6.37) and (6.38), the equivalent vehicle two degrees of freedom equations of motion with roll can be expressed as follows:

$$mV\frac{d\beta}{dt} + 2(K_f + K_r)\beta + \left[mV + \frac{2(l'_f K_f - l'_r K_r)}{V} \right] r = 2K_f \delta \qquad (6.37)'$$

$$2(l_f K_f - l_r K_r)\beta + I\frac{dr}{dt} + \frac{2(l'_f l_f K_f + l'_r l_r K_r)}{V} r = 2l_f K_f \delta \qquad (6.38)'$$

In steady-state cornering, $d\beta/dt = dr/dt = 0$ can be substituted into Eqns $(6.37)'$ and $(6.38)'$. The yaw velocity, r, in response to a constant steer angle is:

$$r = \frac{1}{1 - \frac{ml_f K_f - l_r K_r}{2l(l'_f + l'_r)K_f K_r}V^2} \frac{V}{(l'_f + l'_r)} \delta \qquad (6.42)$$

from Eqns (6.39) and (6.40),

$$l'_f + l'_r = l(1 + BV^2) \qquad (6.43)$$

where

$$B = \frac{l_f B_f + l_r B_r}{l} = \frac{m_S h_s}{l(K_\phi - m_S g h_s)} \left[\frac{\partial \alpha_r}{\partial \phi} - \frac{\partial \alpha_f}{\partial \phi} + \frac{K_{cf}}{K_f} \frac{\partial \phi_f}{\partial \phi} - \frac{K_{cr}}{K_r} \frac{\partial \phi_r}{\partial \phi} \right]$$

$$(6.44)$$

Substituting Eqns (3.43), (6.43), and (6.44) into Eqn (6.42) gives

$$r = \frac{1}{1 + \frac{AV^2}{1 + BV^2}} \frac{1}{1 + BV^2} \frac{V}{l} \delta = \frac{1}{1 + A'V^2} \frac{V}{l} \delta \qquad (6.45)$$

Here, A' is the equivalent stability factor when roll is being considered.

$$A' = A + B$$
$$= -\frac{m(l_f K_f - l_r K_r)}{2l^2 K_f K_r} + \frac{m_S h_s}{l(K_\phi - m_S g h_s)}\left[\frac{\partial \alpha_r}{\partial \phi} - \frac{\partial \alpha_f}{\partial \phi} + \frac{K_{cf}}{K_f}\frac{\partial \phi_f}{\partial \phi}\right.$$
$$\left. - \frac{K_{cr}}{K_r}\frac{\partial \phi_r}{\partial \phi}\right] \tag{6.46}$$

from the above, if $B > 0$ namely:

$$\left[\frac{\partial \alpha_r}{\partial \phi} - \frac{\partial \alpha_f}{\partial \phi} + \frac{K_{cf}}{K_f}\frac{\partial \phi_f}{\partial \phi} - \frac{K_{cr}}{K_r}\frac{\partial \phi_r}{\partial \phi}\right] > 0$$

the vehicle body roll changes the vehicle steer characteristics to US. More precisely, positive roll steer at the rear wheel and positive camber change at the front wheel, or negative roll steer at the front wheel and negative camber change at the rear wheel, have the effect of changing the vehicle steer characteristics toward US.

Figure 6.24 is an example of how the relation between yaw velocity, r, and the traveling speed, V, changes with the distance of the front axle from the vehicle center of gravity. The results are for steady-state cornering, for a normal passenger car, with rear wheel roll steer. The rear wheel roll steer is set so that it always changes the vehicle steer characteristic to either NS or US, regardless of the distance of the front axle from the vehicle center of gravity.

In the same figure, the relationship between the yaw velocity and the traveling speed for a two degrees of freedom model without vehicle roll is also shown. The figure shows that with the introduction of rear wheel roll steer, not only the vehicle steer characteristic is changed to US, but also the change in the vehicle steer characteristic due to the distance between front axle and the center of gravity also becomes less prominent.

Applying Laplace transforms to Eqns (6.37)' and (6.38)', the vehicle characteristic equation is obtained, which has a general form of:

$$s^2 + 2D's + P'^2 = 0 \tag{6.47}$$
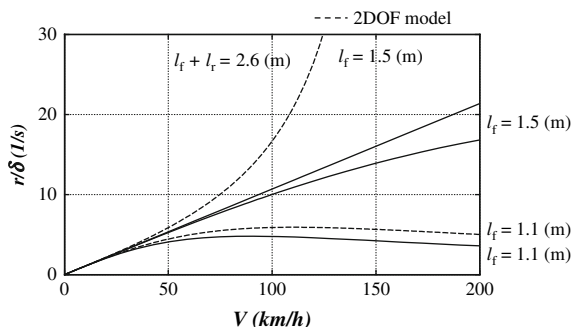
FIGURE 6.24 Effect of roll steer on steady-state cornering.

where

$$2D' = \frac{2m(l'_f l_f K_f + l'_r l_r K_r) + 2I(K_f + K_r)}{mIV} = 2D + \frac{2(l_f^2 K_f B_f + l_r^2 K_r B_r)V}{I}$$

(6.48)

$$P'^2 = \frac{4K_f K_r l(l'_f + l'_r)}{mIV^2} - \frac{2(l_f K_f - l_r K_r)}{I} = P^2 + \frac{4K_f K_r l^2}{mI}B$$

(6.49)

$2D$ and P^2 are the coefficients of the characteristic equation given by Eqns (3.56) and (3.57) when the roll is not being considered. Consequently, taking $I = mk^2$ and by Eqn (3.67), the vehicle natural frequency ω'_n when the roll is being considered is

$$
\begin{aligned}
\omega'_n = P' &= \sqrt{P + \frac{4K_f K_r l^2}{mI}B} \\
&= \sqrt{\frac{4K_f K_r l^2}{m^2 k^2}\left(\frac{1 + AV^2}{V^2}\right) + \frac{4K_f K_r l^2}{m^2 k^2}B} \\
&= \frac{2\sqrt{K_f K_r}l}{mk}\frac{\sqrt{1 + A'V^2}}{V}
\end{aligned}
$$

(6.50)

Assuming $l_f \approx l_r$, $K_f \approx K_r$, the damping ratio ζ' when the roll is being considered is

$$\zeta' = \frac{D'}{P'} = \left[\frac{1 + k^2/l_f l_r}{2\sqrt{k^2/l_f l_r}} + \frac{1}{2\sqrt{k^2/l_f l_r}}BV^2\right]\frac{1}{\sqrt{1 + A'V^2}}$$

(6.51)

PROBLEMS

6.1 Sometimes the roll angle of the vehicle subjected to the 0.5-g steady lateral acceleration is defined as the roll rate. Calculate the roll rate of the vehicle with the mass of the vehicle body $m_S = 1400$ kg, the body CG height from the ground $h_S = 0.52$ m, the front roll stiffness $K_{\phi f} = 65.0$ kNm/rad, and the rear roll stiffness $K_{\phi r} = 35.0$ kNm/rad.

6.2 Calculate the lateral load transfer at the front and rear suspensions, respectively, for the vehicle in Problem 6.1. Use the following vehicle parameters in addition to those in 6.1: the position of the front wheels from the CG $l_f = 1.1$ m, the position of the rear wheels $l_r = 1.6$ m, the front tread $d_f = 1.5$ m, and the rear tread $d_r = 1.5$ m.

6.3 Calculate how much percent of the cornering stiffness is equivalently reduced by the suspension compliance steer if the cornering stiffness of the original tire is 60 kN/rad and the compliance steer to a unit lateral force is 0.00185 rad/kN.

6.4 Investigate the relative value of the camber change rate and the roll steer rate, which gives us almost the same effects on the steer characteristics of the vehicle.

6.5 Find the roll steer rate at the rear suspension, which is needed to make the OS vehicle in Fig. 6.24 NS.

REFERENCES

[1] R. Eberan, ROLL ANGLES, The calculation of wheel loads and angular move-
    ment on curves, Automobile Engineers, October, 1951.

[2] L. Segel, Theoretical prediction and experimental substantiation of the response of
    the automobile to steering control, Proceedings of IMechE (AD), 1956–1957.

[3] J.R. Ellis, Vehicle dynamics, London Business Book Ltd., London, 1969.

Vehicle Motion with Traction and Braking

7.1 PREFACE

Until now, the discussion of vehicle motion has been limited to the case of constant forward speed only, without consideration of the traction and braking of the vehicle. However, the ground vehicle that is the subject of study in this book accelerates and decelerates in the longitudinal direction more frequently than other modes of transportation.

Therefore, in this chapter, the basic characteristics of vehicle motion will be reconsidered to include traction/braking. In particular, it is shown that the analysis of the vehicle motion with traction/braking becomes possible if the change of vehicle speed due to traction/braking is small when the vehicle is traveling at high speed.

7.2 EQUATIONS OF MOTION INCLUSIVE OF LONGITUDINAL MOTION

From subsection 3.2.1, the acceleration vector of the vehicle center of gravity P in the horizontal plane motion is given by Eqn (3.3):

$$\ddot{\boldsymbol{R}} = (\dot{u} - vr)\boldsymbol{i} + (\dot{v} + ur)\boldsymbol{j} \tag{3.3}$$

Although v is small in comparison to u, as described previously, u isn't necessarily always constant. Therefore, the use of β in the description of the vehicle motion isn't always convenient. The vehicle longitudinal and lateral accelerations are better expressed by $\dot{u} - vr$ and $\dot{v} + ur$, respectively.

Using the same assumptions as in subsection 3.2.1, the vehicle equations of motion in basic plane motion inclusive of the motion in longitudinal direction can be expressed by the following equations:

$$m\left(\frac{du}{dt} - vr\right) = 2X_f + 2X_r \tag{7.1}$$

$$m\left(\frac{dv}{dt} + ur\right) = 2Y_f + 2Y_r \tag{7.2}$$

$$I\frac{dr}{dt} = 2(l_f Y_f - l_r Y_r) \tag{3.5''}$$

Here, X_f, X_r are the longitudinal forces acting on the tires. These are mainly dependant on the tire longitudinal slip ratio as discussed in Section 2.4, and can be considered to be independent of the vehicle plane motion. Y_f, Y_r are dependant on the tire side-slip angle, and when the side-slip angle is small, these forces are given by Eqns (3.8) and (3.9). The side-slip angle at this instance is $\beta \approx v/u$, when $u \gg v$. Furthermore, the lateral forces acting on the tires Y_f and Y_r depend on the longitudinal forces X_f and X_r as described in Sections 2.3 or 2.4.

It is understood that the study of the basic characteristics of vehicle motion inclusive of longitudinal motion through direct solving and analysis of Eqns (7.1), (7.2), and (3.5)′ by their original forms is impossible.

7.3 VEHICLE QUASI-STEADY STATE CORNERING

As mentioned in the previous section, the analytical study of the basic characteristics of vehicle motion with longitudinal motion based on the equations of the motion is difficult and some modification is needed.

When a vehicle undergoes steady-state cornering and constant traction/braking, the vehicle speed changes and a steady-state condition isn't fulfilled. If a very short period of time is considered, where the changes of the speed due to traction/braking can be neglected, e.g., when the vehicle is traveling at high speed, the assumption of steady-state cornering at constant longitudinal and lateral acceleration is possible. This is called quasi-steady-state cornering.

This kind of cornering condition does exist in reality. When the vehicle corners at a constant speed, on a curved road with a slope, while subjected to traction/braking is an example. In this case, the vehicle is capable of steady-state cornering with traction/braking.

7.3.1 Expansion of the stability factor for traction/braking

(1) TIRE SIDE-SLIP ANGLE DURING CORNERING

The cornering lateral acceleration of a vehicle with weight W, when accompanied by traction/braking, is defined as $\ddot{y}$, same as in previous chapters. The equilibrium equations are:

$$W\ddot{y} = (K_{f1} + K_{f2})\beta_f + (K_{r1} + K_{r2})\beta_r \tag{7.3}$$

$$l_f\left(K_{f1} + K_{f2}\right)\beta_f - l_r\left(K_{r1} + K_{r2}\right)\beta_r = 0 \tag{7.4}$$

Here, β_f and β_r are the front and rear tire side-slip angles, K_{f1} and K_{f2} are the front left and right tire cornering stiffnesses, and K_{r1} and K_{r2} are the rear left and right cornering stiffnesses. In the following discussion, subscript 1 will be used for the left wheel and subscript 2 for the right wheel, in order to discriminate the characteristic difference between left and right tires.

The tire cornering stiffness depends on the tire load and the effect of the load transfer on the cornering stiffness can be considered up to the first order term, if its effect is small. The relationship between the lateral force and the traction/braking force can be approximated using Eqn (2.40). Also, if the traction/braking force is small compared to the tire load, it can be modeled by a simple parabolic function. With these simplifications in mind, the cornering stiffness at small side-slip angle, could be written as below, in this case for the front wheel

$$K_{f1} \approx \left\{K_{f0} + \frac{\partial K_f}{\partial W}\left(-\Delta W_f - \frac{\Delta W}{2}\right)\right\}\left\{1 - \frac{1}{2}\left(\frac{2X_f}{\mu W_f}\right)^2\right\}$$

where ΔW_f is the load transfer across the front axle during cornering, ΔW is the load transfer between the front and rear due to traction/braking, W_f is the front axle vertical load, and μ is the friction coefficient between the tire and the road surface.

For small longitudinal and lateral accelerations,

$$\frac{\partial K_f}{\partial W}\frac{\Delta W_f}{K_{f0}}, \frac{\partial K_f}{\partial W}\frac{\Delta W}{K_{f0}}, \left(\frac{2X_f}{\mu W_f}\right)^2$$

These are considered as small values of the same order, giving

$$K_{f1} = K_{f0}\left\{1 - \frac{\partial K_f}{\partial W}\frac{\Delta W_f}{K_{f0}} - \frac{\partial K_f}{\partial W}\frac{\Delta W}{2K_{f0}} - \frac{1}{2}\left(\frac{2X_f}{\mu W_f}\right)^2\right\} \tag{7.5}$$

$$K_{f2} = K_{f0}\left\{1 + \frac{\partial K_f}{\partial W}\frac{\Delta W_f}{K_{f0}} - \frac{\partial K_f}{\partial W}\frac{\Delta W}{2K_{f0}} - \frac{1}{2}\left(\frac{2X_f}{\mu W_f}\right)^2\right\} \tag{7.6}$$

$$K_{r1} = K_{r0}\left\{1 - \frac{\partial K_r}{\partial W}\frac{\Delta W_r}{K_{r0}} + \frac{\partial K_r}{\partial W}\frac{\Delta W}{2K_{r0}} - \frac{1}{2}\left(\frac{2X_r}{\mu W_r}\right)^2\right\} \tag{7.7}$$

$$K_{r2} = K_{r0}\left\{1 + \frac{\partial K_r}{\partial W}\frac{\Delta W_r}{K_{r0}} + \frac{\partial K_r}{\partial W}\frac{\Delta W}{2K_{r0}} - \frac{1}{2}\left(\frac{2X_r}{\mu W_r}\right)^2\right\} \tag{7.8}$$

where ΔW_r is the load transfer across the rear axle and W_r is the rear axle vertical load.

From the above, the equivalent cornering stiffnesses of the front and rear axles are obtained by summing up the left and right wheel cornering stiffnesses, respectively:

$$2K_f^* = K_{f1} + K_{f2} = 2K_{f0}\left\{1 - \frac{\partial K_f}{\partial W}\frac{\Delta W}{2K_{f0}} - \frac{1}{2}\left(\frac{2X_f}{\mu W_f}\right)^2\right\} \quad (7.9)$$

$$2K_r^* = K_{r1} + K_{r2} = 2K_{r0}\left\{1 + \frac{\partial K_r}{\partial W}\frac{\Delta W}{2K_{r0}} - \frac{1}{2}\left(\frac{2X_r}{\mu W_r}\right)^2\right\} \quad (7.10)$$

Obtaining β_f and β_r from Eqns (7.3) and (7.4) and using Eqns (7.9) and (7.10), by the same assumption of small values as above gives:

$$\beta_f \approx \frac{l_r W}{2lK_{f0}}\left\{1 + \frac{\partial K_f}{\partial W}\frac{\Delta W}{2K_{f0}} + \frac{1}{2}\left(\frac{2X_f}{\mu W_f}\right)^2\right\}\ddot{y} \quad (7.11)$$

$$\beta_r \approx \frac{l_f W}{2lK_{r0}}\left\{1 - \frac{\partial K_r}{\partial W}\frac{\Delta W}{2K_{r0}} + \frac{1}{2}\left(\frac{2X_r}{\mu W_r}\right)^2\right\}\ddot{y} \quad (7.12)$$

Here $W_f = l_r W/l$, $W_r = l_f W/l$, $\Delta W = hW\ddot{x}/l$, $X_f = \alpha_c W\ddot{x}/2$, $X_r = (1 - \alpha_c)W\ddot{x}/2$. α_c is the traction/braking force distribution ratio between the front and rear, $\ddot{x}$ is the longitudinal acceleration by traction/braking (in gravitational units), and h is the height of the center of gravity from the ground. Substituting these into Eqns (7.11) and (7.12) gives:

$$\beta_f \approx \frac{l_r W}{2lK_{f0}}\left\{1 + \frac{hW}{2lK_{f0}}\frac{\partial K_f}{\partial W}\ddot{x} + \frac{1}{2}\left(\frac{\alpha_c l}{\mu l_r}\right)^2\ddot{x}^2\right\}\ddot{y} \quad (7.13)$$

$$\beta_r \approx \frac{l_f W}{2lK_{r0}}\left\{1 - \frac{hW}{2lK_{r0}}\frac{\partial K_r}{\partial W}\ddot{x} + \frac{1}{2}\left(\frac{(1 - \alpha_c)l}{\mu l_f}\right)^2\ddot{x}^2\right\}\ddot{y} \quad (7.14)$$

Moreover, expressing the equivalent cornering stiffnesses in Eqns (7.9) and (7.10) by $\ddot{x}$, gives:

$$2K_f^* \approx 2K_{f0}\left[1 + \frac{hW}{2lK_{f0}}\frac{\partial K_f}{\partial W}\ddot{x} + \frac{1}{2}\left(\frac{\alpha_c l}{\mu l_r}\right)^2\ddot{x}^2\right] \quad (7.9)'$$

$$2K_r^* \approx 2K_{r0}\left[1 - \frac{hW}{2lK_{r0}}\frac{\partial K_r}{\partial W}\ddot{x} + \frac{1}{2}\left(\frac{(1 - \alpha_c)l}{\mu l_f}\right)^2\ddot{x}^2\right] \quad (7.10)'$$

(2) TOE ANGLE CHANGE AND COMPLIANCE STEER DURING CORNERING

Sections 5.3 and 6.3 studied the effect of the tire toe angle change and compliance steer on vehicle plane motion. These effects are now included for cornering with traction/braking.

If the vehicle has longitudinal and lateral accelerations of $\ddot{x}$ and $\ddot{y}$, the vehicle will pitch and roll. This will result in changes in the suspension stroke. Assuming that the pitch and the roll axes are on the ground, the toe angle change at the front wheel, due to the pitching motion, is $(\partial\alpha_f/\partial z)(l_f hW\ddot{x}/K_\theta)$. Similarly, the toe angle change due to roll is $(\partial\alpha_f/\partial z)(d_f hW\ddot{y}/2K_\phi)$. Here, $\partial\alpha_f/\partial z$ is the tire toe angle change per unit suspension stroke, d_f is the tread, K_θ is the pitch stiffness, and K_ϕ is the roll stiffness of the vehicle.

Furthermore, the torque T_s exerted on the steering system by the tire lateral force, $2Y_f = l_r W\ddot{y}$, and the longitudinal force, $X_f = \alpha_c W\ddot{x}$, acting on the front wheels is:

$$T_s = 2\xi Y_f + \frac{Y_f}{K_y}2X_f = \left(\xi + \frac{\alpha_c W}{2K_y}\ddot{x}\right)\frac{l_r W}{l}\ddot{y} \qquad (7.15)$$

This is shown in Fig. 7.1.

K_y is the tire lateral stiffness and ξ is the sum of a pneumatic trail and a castor trail.

From the above, the sum of the toe angle change and the compliance steer for each tire can be written as:

$$\alpha_{f1} = \frac{\partial\alpha_f}{\partial z}\frac{l_f hW}{K_\theta}\ddot{x} + \frac{\partial\alpha_f}{\partial z}\frac{d_f hW}{2K_\phi}\ddot{y} - \frac{\partial\alpha_f}{\partial X}\frac{\alpha_c W}{2}\ddot{x} - \frac{\partial\alpha_f}{\partial T}\left(\xi + \frac{\alpha_c W}{2K_y}\ddot{x}\right)\frac{l_r W}{l}\ddot{y}$$

$$(7.16)$$
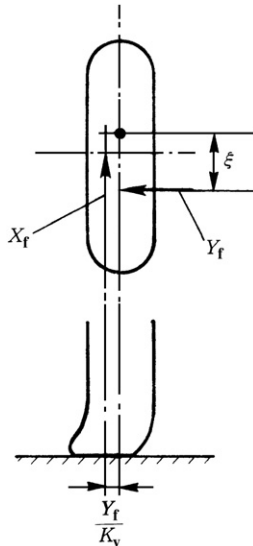
FIGURE 7.1 Steering torque by lateral and longitudinal forces.

$$\alpha_{f2} = -\frac{\partial \alpha_f}{\partial z}\frac{l_f h W}{K_\theta}\ddot{x} + \frac{\partial \alpha_f}{\partial z}\frac{d_f h W}{2K_\phi}\ddot{y} + \frac{\partial \alpha_f}{\partial X}\frac{\alpha_c W}{2}\ddot{x} - \frac{\partial \alpha_f}{\partial T}\left(\xi + \frac{\alpha_c W}{2K_y}\ddot{x}\right)\frac{l_r W}{l}\ddot{y}$$

(7.17)

$$\alpha_{r1} = -\frac{\partial \alpha_r}{\partial z}\frac{l_r h W}{K_\theta}\ddot{x} + \frac{\partial \alpha_r}{\partial z}\frac{d_r h W}{2K_\phi}\ddot{y} - \frac{\partial \alpha_r}{\partial X}\frac{(1-\alpha_c)W}{2}\ddot{x}$$

(7.18)

$$\alpha_{r2} = \frac{\partial \alpha_r}{\partial z}\frac{l_r h W}{K_\theta}\ddot{x} + \frac{\partial \alpha_r}{\partial z}\frac{d_r h W}{2K_\phi}\ddot{y} + \frac{\partial \alpha_r}{\partial X}\frac{(1-\alpha_c)W}{2}\ddot{x}$$

(7.19)

Here, $\partial \alpha_f / \partial X$ and $\partial \alpha_r / \partial X$ are the compliance steers per unit longitudinal force at the front and rear suspension systems. $\partial \alpha_f / \partial T$ is the steering system compliance steer per unit steering torque and α_c is the traction/braking force distribution ratio between the front and rear.

The cornering force due to these toe angle changes at the front wheel is obtained using Eqns (7.5), (7.6), (7.16), and (7.17) as:

$$K_{f1}\alpha_{f1} + K_{f2}\alpha_{f2}$$

$$= 2K_{f0}\left\{1 - \frac{\partial K_f}{\partial W}\frac{\Delta W}{2K_{f0}} - \frac{1}{2}\left(\frac{2X_f}{\mu W_f}\right)^2\right\}$$

$$\times \left\{\frac{\partial \alpha_f}{\partial z}\frac{d_f h W}{2K_\phi}\ddot{y} - \frac{\partial \alpha_f}{\partial T}\left(\xi + \frac{\alpha_c W}{2K_y}\ddot{x}\right)\frac{l_r W}{l}\ddot{y}\right\}$$

$$- 2K_{f0}\left(\frac{\partial \alpha_f}{\partial z}\frac{l_f h W}{K_\theta}\ddot{x} - \frac{\partial \alpha_f}{\partial X}\frac{\alpha_c W}{2}\ddot{x}\right)\frac{\partial K_f}{\partial W}\frac{\Delta W_f}{K_{f0}}$$

$$\approx 2K_f^*\left\{\frac{\partial \alpha_f}{\partial z}\frac{d_f h W}{2K_\phi}\ddot{y} - \frac{\partial \alpha_f}{\partial T}\left(\xi + \frac{\alpha_c W}{2K_y}\ddot{x}\right)\frac{l_r W}{l}\ddot{y}\right.$$

$$\left. - \left(\frac{\partial \alpha_f}{\partial z}\frac{l_f h W}{K_\theta}\ddot{x} - \frac{\partial \alpha_f}{\partial X}\frac{\alpha_c W}{2}\ddot{x}\right)\frac{\partial K_f}{\partial W}\frac{\Delta W_f}{K_{f0}}\right\} = 2K_f^*\alpha_f$$

(7.20)

similarly, for the rear wheel,

$$K_{r1}\alpha_{r1} + K_{r2}\alpha_{r2}$$

$$\approx 2K_r^*\left\{\frac{\partial \alpha_r}{\partial z}\frac{d_r h W}{2K_\phi}\ddot{y} + \left(\frac{\partial \alpha_r}{\partial z}\frac{l_r h W}{K_\theta}\ddot{x} + \frac{\partial \alpha_r}{\partial X}\frac{1-\alpha_c}{2}W\ddot{x}\right)\frac{\partial K_r}{\partial W}\frac{\Delta W_r}{K_{r0}}\right\}$$

$$= 2K_r^*\alpha_r$$

(7.21)

For small longitudinal and lateral accelerations, small values of second order and higher are neglected, as in the previous section.

The above process of introducing Eqns (7.20) and (7.21) is accordingly to replace the toe angle change and compliance steer at the left and right wheels, $(\alpha_{f1}, \alpha_{f2})$ and $(\alpha_{r1}, \alpha_{r2})$, by a single equivalent steer angle, α_f and α_r,

respectively. As the left and right steers due to lateral acceleration are in the same direction, it is possible to consider that a total lateral force produced by the left and right steers acts at the front and rear, respectively. In contrast, as the steers due to longitudinal acceleration are in the opposite direction, the force difference due to left and right wheel load transfer should only be considered to act on the front and the rear. The above is based on using the tire cornering stiffness given by Eqns (7.9) and (7.10).

From Eqns (6.4) and (6.5):

$$\Delta W_f = \frac{hWK_{\phi f}}{d_f K_\phi} \ddot{y}$$

$$\Delta W_r = \frac{hWK_{\phi r}}{d_r K_\phi} \ddot{y}$$

The equivalent front and rear wheel steer angles α_f, α_r, with both roll centers on the ground, take the following forms:

$$\alpha_f = (a_f + b_f \ddot{x})\ddot{y} \tag{7.22}$$

$$\alpha_r = (a_r + b_r \ddot{x})\ddot{y} \tag{7.23}$$

Here,

$$a_f = \frac{\partial \alpha_f}{\partial z} \frac{d_f hW}{2K_\phi} - \frac{\partial \alpha_f}{\partial T} \xi \frac{l_r W}{l} \tag{7.24}$$

$$b_f = \left(\frac{\partial \alpha_f}{\partial X} \frac{\alpha_c W}{2} - \frac{\partial \alpha_f}{\partial z} \frac{l_f hW}{K_\phi} \right) \frac{\partial K_f}{\partial W} \frac{hWK_{\phi f}}{d_f K_\phi K_{f0}} - \frac{\partial \alpha_f}{\partial T} \frac{\alpha_c W}{2K_y} \frac{l_r W}{l} \tag{7.25}$$

$$a_r = \frac{\partial \alpha_r}{\partial z} \frac{d_r hW}{2K_\phi} \tag{7.26}$$

$$b_r = \left(\frac{\partial \alpha_r}{\partial X} \frac{1 - \alpha_c}{2} W + \frac{\partial \alpha_r}{\partial z} \frac{l_r hW}{K_\theta} \right) \frac{\partial K_r}{\partial W} \frac{hWK_{\phi r}}{d_r K_\phi K_{r0}} \tag{7.27}$$

(3) STABILITY FACTOR EXTENSION

Once the front and rear tire side-slip angles and steer angles are given, the relation between front steer angle, δ, and cornering radius, ρ, is

$$\delta = \frac{l}{\rho} + \beta_f - \beta_r + \alpha_f - \alpha_r \tag{6.6'}$$

Substituting Eqns (7.13), (7.14), (7.22), and (7.23) into Eqn (6.6)′ gives:

$$\delta = \frac{l}{\rho} + (A_0 + A_1\ddot{x} + A_2\ddot{x}^2)gl\ddot{y} \tag{7.28}$$

Furthermore, $g\ddot{y} = V^2/\rho$, so

$$\rho = \frac{l}{\delta}\left\{1 + \left(A_0 + A_1\ddot{x} + A_2\ddot{x}^2\right)V^2\right\} \tag{7.29}$$

where

$$A_0 = \frac{W}{2l^2g}\left(\frac{l_rK_{r0} - l_fK_{f0}}{K_{f0}K_{r0}}\right) + \frac{a_r - a_f}{gl} \tag{7.30}$$

$$A_1 = \frac{hW^2}{4l^3g}\left(\frac{l_r}{K_{f0}^2}\frac{\partial K_f}{\partial W} + \frac{l_f}{K_{r0}^2}\frac{\partial K_r}{\partial W}\right) + \frac{b_r - b_f}{gl} \tag{7.31}$$

$$A_2 = \frac{W}{4\mu^2g}\left\{\frac{\alpha_c^2}{l_rK_{f0}} - \frac{(1 - \alpha_c^2)}{l_fK_{r0}}\right\} \tag{7.32}$$

Equation (7.28) gives the front steer angle, δ, necessary for cornering with a radius of ρ at a certain lateral acceleration with traction/braking. While Eqn (7.29) expresses the relation between the cornering radius and the vehicle speed, then,

$$A^* = A_0 + A_1\ddot{x} + A_2\ddot{x}^2 \tag{7.33}$$

could be defined as the stability factor extended for cornering with traction/braking.

The first term A_0 corresponds to the stability factor for steady-state cornering as defined by Eqn (3.43). The second term A_1 is due to load transfer, toe angle change, and compliance steer caused by traction/braking. The third term A_2 is due to tire cornering characteristics changed by traction/braking force and is proportional to the longitudinal acceleration squared, $\ddot{x}^2$.

7.3.2 Effect of traction and braking on cornering

Transforming Eqn (7.28), and assuming $\ddot{x} = \ddot{x}_0$, $\delta = \delta_0$, $\rho_0 = l/\delta_0$ gives:

$$\frac{\rho}{\rho_0} = \frac{1}{1 - \left(A_0 + A_1\ddot{x}_0 + A_2\ddot{x}_0^2\right)\rho_0g\ddot{y}} \tag{7.34}$$

This is the relationship between cornering radius and lateral acceleration during cornering with a constant acceleration and a constant steer angle. Similarly, when $V = V_0$, from Eqn (7.29):

$$\rho = \rho_0\left\{1 + \left(A_0 + A_1\ddot{x} + A_2\ddot{x}^2\right)V_0^2\right\} \tag{7.29)'}$$

This shows how the cornering radius changes in response to longitudinal acceleration when the vehicle undergoes steady-state cornering with a constant steer angle and traction/braking. It assumes the traveling speed is high and the speed change due to traction/braking could be neglected. Here, from Eqn (7.29)$'$

$$\left(\frac{\partial\rho}{\partial\ddot{x}}\right)_{\ddot{x}=0} = \rho_0 V^2 A_1 \tag{7.35}$$

A_1 expressed in Eqn (7.31) is defined as the sensitivity coefficient to longitudinal acceleration during cornering. The primary effect of traction/braking on cornering at small $\ddot{x}$ can be evaluated by A_1.

Figure 7.2 shows the effect of traction/braking by power-off on the cornering radius. Different types of vehicle traction modes are modeled by using Eqn (7.29), neglecting the suspension toe angle change and compliance steer due to longitudinal force. In any case $A_1 > 0$ and near $\ddot{x} = 0$ the cornering radius increases during acceleration and decreases during deceleration. This is prominent in front wheel drive vehicles. For rear wheel drive vehicles the cornering radius decreases as $\ddot{x}$ gets larger.

Figure 7.3 shows the relationship between the cornering radius and longitudinal acceleration. Here, the toe angle change and compliance steer are set so
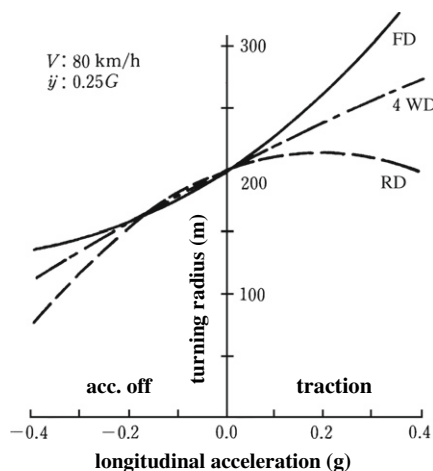
FIGURE 7.2 Effects of longitudinal acceleration on steady cornering.
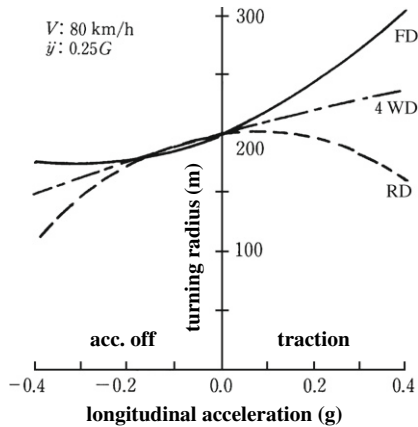
FIGURE 7.3 Turning radius to longitudinal acceleration with toe change and compliance steer.

that A_1 is as small as possible. In a practical sense, the condition of $A_1 \leq 0$ doesn't exist, but near $\ddot{x} = 0$, the effect of longitudinal acceleration becomes negligible. In particular, the effect of traction/braking by power-off for four-wheel-drive vehicles is extremely small.

7.4 VEHICLE TRANSIENT STEER RESPONSE

The previous section extended the definition of stability factor for cornering with traction/braking. Through this, the effect of acceleration or deceleration on cornering has been studied. This extension relied on the assumption that only small accelerations take place. With this assumption, the vehicle equations of motion can be extended to include the effects of traction/braking. This is achieved by assuming that the distance of the front and rear axle from the vehicle center of gravity effectively changes in response to longitudinal acceleration. It is also shown that the analytical study of vehicle transient response to steer input with traction/braking is possible by using these equations of motion.

7.4.1 Equations of motion

Firstly, the equivalent tire cornering stiffness of the vehicle with traction/braking is given by Eqns (7.9)′ and (7.10)′ as in subsection 7.3.1. Similarly, the toe angle change of a vehicle with traction/braking is expressed as:

$$\alpha_f = (p_f + q_f\ddot{x})\ddot{y} \tag{7.36}$$

$$\alpha_r = (p_r + q_r\ddot{x})\ddot{y} \tag{7.37}$$

Here, the toe angle change due to vehicle roll and pitch, and the compliance steer due to the longitudinal force acting at the tires, are taken into consideration, giving

$$p_f = \frac{\partial \alpha_f}{\partial z} \frac{d_f h W}{2K_\phi} \tag{7.38}$$

$$q_f = \left(\frac{\partial \alpha_f}{\partial X} \frac{\alpha_c W}{2} - \frac{\partial \alpha_f}{\partial z} \frac{l_f h W}{K_\phi} \right) \frac{\partial K_f}{\partial W} \frac{h W K_{\phi f}}{d_f K_\phi K_{f0}} \tag{7.39}$$

$$p_r = \frac{\partial \alpha_r}{\partial z} \frac{d_r h W}{2K_\phi} \tag{7.40}$$

$$q_r = \left(\frac{\partial \alpha_r}{\partial X} \frac{1 - \alpha_c}{2} W + \frac{\partial \alpha_r}{\partial z} \frac{l_r h W}{K_\theta} \right) \frac{\partial K_r}{\partial W} \frac{h W K_{\phi r}}{d_r K_\phi K_{r0}} \tag{7.41}$$

Additionally, the torque acting on the steering system produced by the cornering force and the longitudinal force at the front wheels is similar to that in Eqn (7.15):

$$T = 2\left(\xi + \frac{\alpha_c W}{2K_y} \ddot{x} \right) Y_f$$

The front wheel cornering stiffness that accounts for the compliance steer due to the steer torque is expressed in the same manner as in subsection 5.3.1

$$2eK_f^* = \frac{2K_f^*}{1 + 2\frac{\partial \alpha_f}{\partial T}\left(\xi + \frac{\alpha_c W}{2K_y}\ddot{x} \right) K_f^*} \tag{7.42}$$

Assuming the short period of time where longitudinal acceleration $\ddot{x}$ is constant, and the change of the vehicle speed due to this acceleration can be neglected, the vehicle equations of motion for the plane motion in this period becomes as follows:

$$mV\left(\frac{d\beta}{dt} + r \right) = 2eK_f^*\left(\delta - \beta - \frac{l_f}{V}r + \alpha_f \right) + 2K_r^*\left(-\beta + \frac{l_r}{V}r + \alpha_r \right) \tag{7.43}$$

$$I\frac{dr}{dt} = 2l_f eK_f^*\left(\delta - \beta - \frac{l_f}{V}r + \alpha_f \right) - 2l_r K_r^*\left(-\beta + \frac{l_r}{V}r + \alpha_r \right) \tag{7.44}$$

Here, $\ddot{y}$ in α_f, α_r in Eqns (7.36) and (7.37) changes in response to the steer input and could be expressed as $V(d\beta/dt + r)/g$. Consequently, the equations of motion (7.43) and (7.44) become too complicated and the analysis becomes too difficult. For simplicity, the toe angles, α_f and α_r in Eqns (7.36) and (7.37) are assumed to be dependant on the steady-state lateral acceleration only, $\ddot{y} = Vr/g$:

$$\alpha_f = (p_f + q_f \ddot{x})Vr/g \tag{7.36}'$$

$$\alpha_r = (p_r + q_r \ddot{x})Vr/g \tag{7.37}'$$

Substituting these into Eqns (7.43) and (7.44) and rearranging gives:

$$mV\left(\frac{d\beta}{dt} + r\right) = 2eK_f^*\left(\delta - \beta - \frac{l_f^*}{V}r\right) + 2K_r^*\left(-\beta + \frac{l_r^*}{V}r\right) \quad (7.43)'$$

$$I\frac{dr}{dt} = 2l_feK_f^*\left(\delta - \beta - \frac{l_f^*}{V}r\right) - 2l_rK_r^*\left(-\beta + \frac{l_r^*}{V}r\right) \quad (7.44)'$$

whereby

$$l_f^* = l_f\left(1 - \frac{p_f + q_f\ddot{x}}{l_f}V^2\right) \quad (7.45)$$

$$l_r^* = l_r\left(1 - \frac{p_r + q_r\ddot{x}}{l_r}V^2\right) \quad (7.46)$$

Rearranging Eqns (7.43)' and (7.44)' gives:

$$mV\frac{d\beta}{dt} + 2(eK_f^* + K_r^*)\beta + \left\{mV + \frac{2\left(l_f^*eK_f^* - l_r^*K_r^*\right)}{V}\right\}r = 2eK_f^*\delta \quad (7.47)$$

$$2(eK_f^* + K_r^*)\beta + I\frac{dr}{dt} + \frac{2\left(l_fl_f^*eK_f^* - l_rl_r^*K_r^*\right)}{V}r = 2l_feK_f^*\delta \quad (7.48)$$

These equations of motion give us the steer response of the vehicle with traction/braking.

7.4.2 Transient response to steer input

Here, the following equations are obtained as the yaw rate response to steer input by using Eqns (7.47) and (7.48):

$$\frac{r(s)}{\delta(s)} = \frac{G_\delta^r(0)\left(1 + T_rs\right)}{1 + \frac{2\zeta s}{\omega_n} + \frac{s^2}{\omega_n^2}} \quad (7.49)$$

where

$$\omega_n^2 = \frac{4eK_f^*K_r^*l\left(l_f^* + l_r^*\right)}{mIV^2} - \frac{2\left(l_feK_f^* - l_rK_r^*\right)}{I} \quad (7.50)$$

$$2\zeta\omega_n = \frac{2m\left(l_f^*l_feK_f^* + l_r^*l_rK_r^*\right) + 2I\left(eK_f^* + K_r^*\right)}{mIV} \quad (7.51)$$
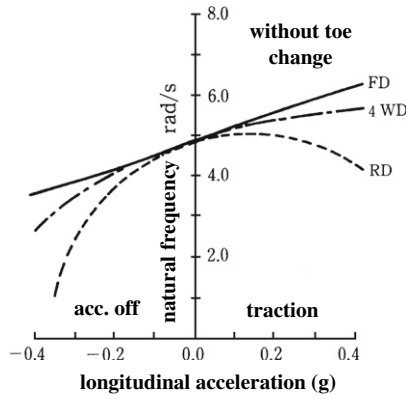
FIGURE 7.4 Effects of longitudinal acceleration on ω_n.

$$T_r = \frac{ml_f V}{2lK_r^*} \tag{7.52}$$

$$G_\delta^r(0) = \frac{V}{(l_f^* + l_r^*)} \frac{1}{1 + A^* V^2} \tag{7.53}$$

and

$$A^* = -\frac{m\left(l_f e K_f^* - l_r K_r^*\right)}{2e K_f^* K_r^* l\left(l_f^* + l_r^*\right)} \tag{7.54}$$

By dealing with the equations under the premise of the small values as in Section 7.3, A^* is the same as the stability factor extended for the vehicle motion with traction/braking, as derived in Section 7.3. Furthermore, using Eqns (7.50)–(7.53), the response parameters to steer input for the vehicle with traction/braking can be obtained. This can be used to evaluate the effects of acceleration or deceleration on the transient steer response.

Figure 7.4 is the relationship of the natural frequency ω_n to the longitudinal acceleration obtained from Eqn (7.50). Figure 7.5 shows the relationship
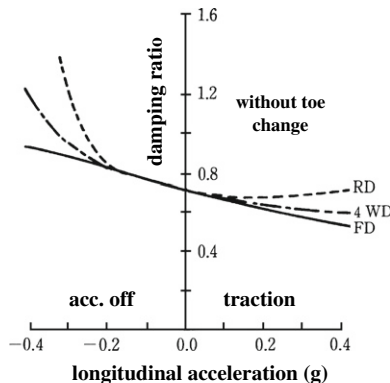
FIGURE 7.5 Effects of longitudinal acceleration on ζ.
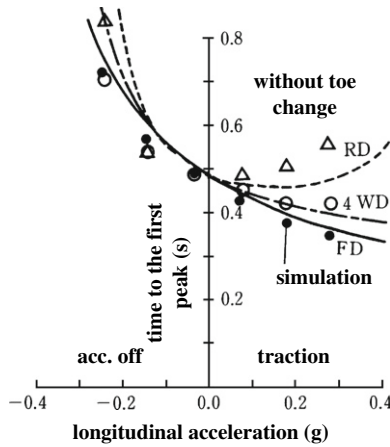
FIGURE 7.6 Effects of longitudinal acceleration on yaw rate response without toe change.

between the damping ratio ζ and the longitudinal acceleration. The natural frequency increases with traction and decreases with braking. In contrast, the damping ratio decreases with traction and increases with braking. In the case of rear wheel drive, the natural frequency decreases with a large longitudinal acceleration.

The time to the first peak, t_p, for the yaw rate response to step steer input is given by Eqn (3.86). Figs 7.6 and 7.7 show how the time to the first peak, t_p, changes with longitudinal acceleration, where Eqns (7.50)–(7.52) are used to obtain t_p. The figures show that t_p becomes smaller with traction and larger with braking. In the case of rear wheel drive, t_p becomes larger during traction. Furthermore, from Fig. 7.7, it is possible to estimate how the effect of traction/braking on t_p can be reduced by using toe angle changes and compliance steer.
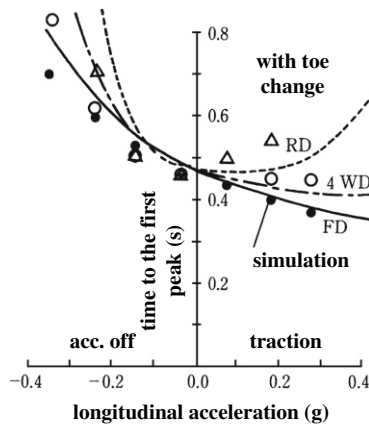
FIGURE 7.7 Effects of longitudinal acceleration on yaw rate response with toe change.
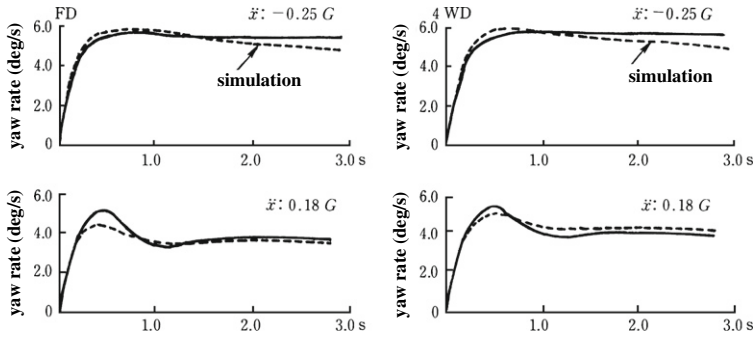
FIGURE 7.8 Effects of longitudinal acceleration on yaw rate response to step steer input, $V = 100$ km/h.

Figure 7.8 shows the yaw rate response to step steer input for the vehicle with traction/braking and is obtained by using Eqns (7.47) and (7.48). In the same figure, the vehicle response is obtained through a numerical solution of the equations of motion (7.1), (7.2), and (3.5)'. The simulated vehicle motions for the vehicle with roll and pitch are also plotted. The two plots agree well with each other. This proves the validity of the simplified method of dealing with the vehicle response to steer input for the vehicle with traction and braking, as carried out under the assumption of quasi-steady state in this chapter.

Chapter | eight

Vehicle Dynamics with Active Motion Controls

8.1 PREFACE

The previous chapters have discussed the motion of a vehicle with only its front wheels being steered in response to the steering wheel operation. In recent years, it has been proved that vehicle dynamic characteristics can be greatly improved by active rear wheel steering in addition to the front wheel steer. Recently, attentions are focused on controlling the vehicle using a direct yaw moment. This is produced by controlling the transverse split of longitudinal forces across the axles. It is called Direct Yaw-moment Control (DYC).

This chapter will look at vehicle motion when rear wheel steering is added to a conventional vehicle with front wheel steer. This will involve studying the vehicle motion and the basic control concept of active front and rear steer in response to the steering wheel. It is assumed that the front wheels have no mechanical connection to the steering wheel. The fundamental concepts of the vehicle motion control using the direct yaw moment will also be considered.

8.2 VEHICLE MOTION WITH ADDITIONAL REAR WHEEL STEER

Assuming that the front and rear wheel steer angles are δ_f, δ_r, then Eqns (3.8) and (3.9), which express the front and rear wheel lateral forces, become:

$$Y_f = -K_f\beta_f = -K_f(\beta + \frac{l_f}{V}r - \delta_f) \tag{8.1}$$

$$Y_r = -K_r\beta_r = -K_r(\beta - \frac{l_r}{V}r - \delta_r) \tag{8.2}$$

215

Substituting these into Eqns (3.4)′and (3.5)′, the vehicle equations of motion in response to front and rear wheel steer are now as follows:

$$mV\frac{d\beta}{dt} + 2(K_f + K_r)\beta + \left\{ mV + \frac{2}{V}(l_fK_f - l_rK_r) \right\}r = 2K_f\delta_f + 2K_r\delta_r$$

(8.3)

$$2(l_fK_f - l_rK_r)\beta + I\frac{dr}{dt} + \frac{2(l_f^2K_f + l_r^2K_r)}{V}r = 2l_fK_f\delta_f - 2l_rK_r\delta_r \qquad (8.4)$$

8.2.1 Rear wheel steer proportional to front wheel steer

There are many possible methods for simultaneous steer of both the front and rear wheels. The simplest method is considered first, where the rear wheel steer is proportional to the front wheel steer.

The front and rear wheel steer angles could be written as:

$$\delta_f = \frac{\delta}{n} \qquad (8.5)$$

$$\delta_r = k\delta_f = \frac{k}{n}\delta \qquad (8.6)$$

Here, in this chapter, δ is not the front wheel steer angle but is used to represent the steering wheel angle, and n is the gear ratio of the front steering system.

Substituting Eqns (8.5) and (8.6) into Eqns (8.3) and (8.4) gives the response of the vehicle to steering wheel angle when the rear wheel steer is proportional to the front wheel steer

$$\frac{\beta(s)}{\delta(s)} = \frac{1}{n} \frac{\begin{vmatrix} 2(K_f + kK_r) & mV + \frac{2}{V}(l_fK_f - l_rK_r) \\ (l_fK_f - kl_rK_r) & Is + \frac{2(l_f^2K_f + l_r^2K_r)}{V} \end{vmatrix}}{\begin{vmatrix} mVs + 2(K_f + K_r) & mV + \frac{2}{V}(l_fK_f - l_rK_r) \\ 2(l_fK_f - l_rK_r) & Is + \frac{2}{V}(l_f^2K_f + l_r^2K_r) \end{vmatrix}} \qquad (8.7)$$

$$\frac{r(s)}{\delta(s)} = \frac{1}{n} \frac{\begin{vmatrix} mVs + 2(K_f + K_r) & 2(K_f + kK_r) \\ 2(l_fK_f - l_rK_r) & 2(l_fK_f - kl_rK_r) \end{vmatrix}}{\begin{vmatrix} mVs + 2(K_f + K_r) & mV + \frac{2}{V}(l_fK_f - l_rK_r) \\ 2(l_fK_f - l_rK_r) & Is + \frac{2(l_f^2K_f + l_r^2K_r)}{V} \end{vmatrix}} \qquad (8.8)$$

Here, using Eqns (8.7) and (8.8), the transfer functions of the lateral acceleration, $V(\dot{\beta} + r)$, and yaw rate responses to steer input can be expressed in

a convenient form that shows how it differs from the usual transfer function with front wheel steer only:

$$\frac{\ddot{y}(s)}{\delta(s)} = \frac{1-k}{n} G_\delta^{\ddot{y}}(0) \frac{1+(1+\lambda_1)T_{y1}s+(1+\lambda_2)T_{y2}s^2}{1+\frac{2\zeta s}{\omega_n}+\frac{s^2}{\omega_n^2}} \qquad (8.9)$$

$$\frac{r(s)}{\delta(s)} = \frac{1-k}{n} G_\delta^{r}(0) \frac{1+(1+\lambda_r)T_r s}{1+\frac{2\zeta s}{\omega_n}+\frac{s^2}{\omega_n^2}} \qquad (8.10)$$

whereby

$$\lambda_1 = \frac{l}{l_r} \frac{k}{1-k}$$

$$\lambda_2 = \frac{K_f+K_r}{K_r} \frac{k}{1-k}$$

$$\lambda_r = \frac{l_f K_f - l_r K_r}{l_f K_f} \frac{k}{1-k}$$

ω_n, ζ, T_{y1}, T_{y2}, T_r, $G_\delta^{\ddot{y}}(0)$, and $G_\delta^{r}(0)$ are the same symbols as used in subsection 3.4.2, for the case of a vehicle with front wheel steer only.

Based on Eqns (8.9) and (8.10), when the rear wheel is steered proportionally to the front wheel, the overall gain is multiplied by $(1-k)$. The coefficients of s and s^2 in the numerator of the transfer function are increased by a ratio of λ_1 and λ_2. If $0 < k < 1$, λ_1 and λ_2 are positive. This means that the phase lag of the lateral acceleration to steer input is reduced when the rear wheel is steered in the same direction as the front wheel, but with a smaller angle than the front steer angle. If the vehicle steer characteristic is near NS, $\lambda_r \approx 0$, and the effect of rear wheel steer on yaw rate response is small.

Figure 8.1 shows the influence of the rear wheel steer on the vehicle lateral acceleration response for a neutral steer vehicle, using Eqn (8.9) [1]. The lateral acceleration response is improved by steering the rear wheel in the same direction as the front wheel.

In particular, ω_n and ζ are unchanged, compared to the case of the front wheel steer vehicle. Using Eqn (8.7), the steady-state value for side-slip angle, β, to a constant steer angle is

$$\beta(s) = \frac{1}{n} \begin{vmatrix} 2(K_f+kK_r) & mV+\frac{2}{V}(l_f K_f - l_r K_r) \\ (l_f K_f - kl_r K_r) & \frac{2(l_f^2 K_f + l_r^2 K_r)}{V} \\ 2(K_f+K_r) & mV+\frac{2}{V}(l_f K_f - l_r K_r) \\ 2(l_f K_f - l_r K_r) & \frac{2(l_f^2 K_f + l_r^2 K_r)}{V} \end{vmatrix} \delta \qquad (8.11)$$
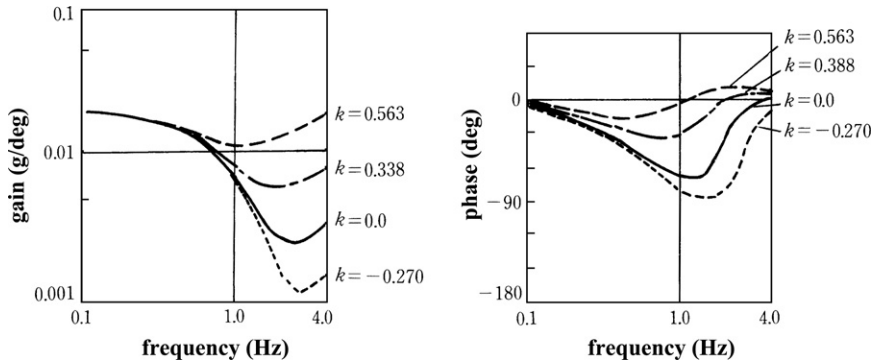
FIGURE 8.1 Effects of front wheel proportional rear wheel steer on lateral acceleration response.

From this a value of k is sought that gives zero steady-state side-slip, $\beta_s = 0$. In other words, the numerator in Eqn (8.11) is zero and

$$k = k_0 = -\frac{l_r\left(1 - \frac{ml_f}{2ll_rK_r}V^2\right)}{l_f\left(1 + \frac{ml_r}{2ll_fK_f}V^2\right)} \tag{8.12}$$

If the proportional constant of the rear to front wheel steer is set as in Eqn (8.12), the side-slip angle during steady-state cornering will be zero. This means that the vehicle traveling direction is the same as its heading direction.

This proportional constant changes with the traveling speed, as shown by Fig. 8.2. When k_0 is negative, the rear wheel and front wheel steer directions are opposite to each other. They are in the same direction if k_0 is positive. If the rear wheel is steered in the opposite direction to the front at low speed, and then in the same direction at high speed, the steady state side-slip angle will be always zero.
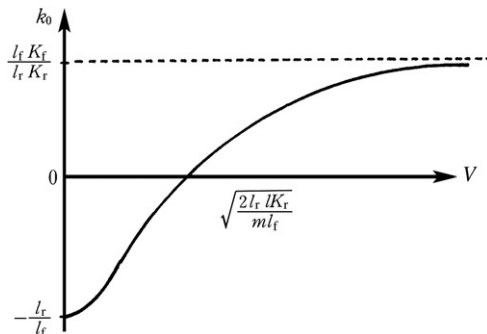
FIGURE 8.2 Rear to front steering ratio for zero side slip.

8.2.2 Rear wheel steer proportional to front wheel steer force

The next case is rear wheel steer proportional to the front wheel steer force. Assuming that the steering force of the front wheel is equal to the moment by the external force acting at the front wheel, where ξ has same meaning as in chapter 5 in this subsection.

$$M = 2\xi K_f\left(\beta + \frac{l_f}{V}r - \delta_f\right) \tag{8.13}$$

The front and rear wheel steering angles can be written as:

$$\delta_f = \frac{\delta}{n} \tag{8.5}$$

$$\delta_r = kM = 2k\xi K_f\left(\beta + \frac{l_f}{V}r - \delta_f\right) \tag{8.14}$$

substituting these into Eqns (8.3) and (8.4), and expressing the side-slip angle and yaw rate responses in the form of a transfer function:
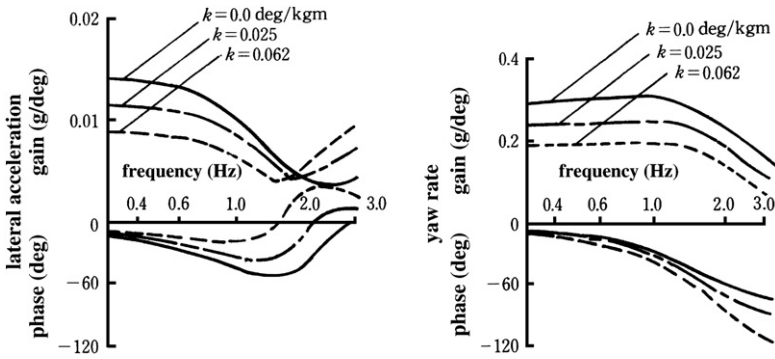
$$\frac{\beta(s)}{\delta(s)} = \frac{1}{n}\frac{\begin{vmatrix} 2(K_f + 2k\xi K_f K_r) & mV + \frac{2}{V}(l_f K_f - l_r K_r) + \frac{4k\xi L_f K_f K_r}{V} \\ (l_f K_f - 2k\xi l_r K_f K_r) & Is + \frac{2(l_f^2 K_f + l_r^2 K_r)}{V} - \frac{4k\xi L_f K_f K_r}{V} \end{vmatrix}}{\begin{vmatrix} mVs + 2(K_f + K_r) + 4k\xi K_f K_r & mV + \frac{2}{V}(l_f K_f - l_r K_r) + \frac{4k\xi L_f K_f K_r}{V} \\ 2(l_f K_f - l_r K_r) - 4k\xi l_r K_f K_r & Is + \frac{2(l_f^2 K_f + l_r^2 K_r)}{V} - \frac{4k\xi L_f K_f K_r}{V} \end{vmatrix}} \tag{8.15}$$

$$\frac{r(s)}{\delta(s)} = \frac{1}{n}\frac{\begin{vmatrix} mVs + 2(K_f + K_r) + 4k\xi K_f K_r & 2(K_f + 2k\xi K_f K_r) \\ 2(l_f K_f - l_r K_r) - 4k\xi l_r K_f K_r & (l_f K_f - 2k\xi l_r K_f K_r) \end{vmatrix}}{\begin{vmatrix} mVs + 2(K_f + K_r) + 4k\xi K_f K_r & mV + \frac{2}{V}(l_f K_f - l_r K_r) + \frac{4k\xi L_f K_f K_r}{V} \\ 2(l_f K_f - l_r K_r) - 4k\xi l_r K_f K_r & Is + \frac{2(l_f^2 K_f + l_r^2 K_r)}{V} - \frac{4k\xi L_f K_f K_r}{V} \end{vmatrix}} \tag{8.16}$$

The transfer function of the lateral acceleration and yaw rate responses to steer input can be derived as in Section 8.2.1,

$$\frac{\ddot{y}(s)}{\delta(s)} = \frac{1}{n}G_\delta^{\ddot{y}}(0)^* \frac{1 + T_{y1}s + (1 + \lambda_2)T_{y2}s^2}{1 + \frac{2\zeta^* s}{\omega_n^*} + \frac{s^2}{\omega_n^{*2}}} \tag{8.17}$$

$$\frac{r(s)}{\delta(s)} = \frac{1}{n}G_\delta^r(0)^* \frac{1 + (1 + \lambda_r)T_r s}{1 + \frac{2\zeta^* s}{\omega_n^*} + \frac{s^2}{\omega_n^{*2}}} \tag{8.18}$$

here, taking

$$A^* = A + \frac{k\xi l_r m}{l^2} \tag{8.19}$$

as the stability factor,

$$G_\delta^{\ddot{y}}(0)^* = VG_\delta^r(0)^* = \frac{1}{1 + A^* V^2} \frac{V^2}{l} \tag{8.20}$$

$$\omega_n^* = \frac{2l}{V} \sqrt{\frac{K_f K_r}{mI}(1 + A^* V^2)} = \sqrt{\omega_n^2 + \frac{4k\xi l_r K_f K_r}{I}} \tag{8.21}$$

$$\zeta^* = \frac{m(l_f^2 K_f + l_r^2 K_r) + I(K_f + K_r) + 2k\xi K_f K_r(I - ml_f l_r)}{2l\sqrt{mIK_f K_r(1 + A^* V^2)}} \tag{8.22}$$

and A is the stability factor defined in Chapter 3 for a front wheel steer vehicle.

$$\lambda_2 = 2k\xi K_r$$

$$\lambda_r = -\frac{2k\xi l_r K_r}{l_f}$$

The time constants (T_{y1}, T_{y2}, and T_r) are the same as the ones used in subsection 3.4.2 for the case of the vehicle with front wheel steer only.

When the rear wheel is steered proportionally to the front wheel steering force, both the numerator and the denominator of transfer functions (8.17) and (8.18) are changed. This gives different natural frequency and damping ratio to the vehicle with only front wheel steer.

If $k > 0$, the stability factor becomes larger, the natural frequency increases, and the coefficient of s^2 in the numerator of lateral acceleration gets bigger, which improves the lateral acceleration response. However, the coefficient of s in the numerator of yaw rate decreases, and this deteriorates the yaw rate response. Figure 8.3 shows the influence of the proportional constant k on the vehicle lateral acceleration and yaw rate frequency responses to steering input by using Eqns (8.17) and (8.18) [2].

8.2.3 Rear wheel steer proportional to yaw rate

The next case is rear wheel steer proportional to the vehicle yaw rate. The front and rear wheel steer angles are written as:

$$\delta_f = \frac{\delta}{n} \tag{8.5}$$

$$\delta_r = kr \tag{8.23}$$

Substituting these into Eqns (8.3) and (8.4), and expressing the side-slip angle and yaw rate response to steer input in the form of transfer functions gives:

FIGURE 8.3 Effects of front steering force proportional to rear steer on frequency responses.

$$\frac{\beta(s)}{\delta(s)} = \frac{1}{n} \frac{\begin{vmatrix} 2K_f & mV + \frac{2}{V}(l_fK_f - l_rK_r) - 2kK_r \\ l_fK_f & Is + \frac{2}{V}(l_f^2K_f + l_r^2K_r) + 2kl_rK_r \end{vmatrix}}{\begin{vmatrix} mVs + 2(K_f + K_r) & mV + \frac{2}{V}(l_fK_f - l_rK_r) - 2kK_r \\ 2(l_fK_f - l_rK_r) & Is + \frac{2}{V}(l_f^2K_f + l_r^2K_r) + 2kl_rK_r \end{vmatrix}} \tag{8.24}$$

$$\frac{r(s)}{\delta(s)} = \frac{1}{n} \frac{\begin{vmatrix} mVs + 2(K_f + K_r) & 2K_f \\ 2(l_fK_f - l_rK_r) & 2l_fK_f \end{vmatrix}}{\begin{vmatrix} mVs + 2(K_f + K_r) & mV + \frac{2}{V}(l_fK_f - l_rK_r) - 2kK_r \\ 2(l_fK_f - l_rK_r) & Is + \frac{2}{V}(l_f^2K_f + l_r^2K_r) + 2kl_rK_r \end{vmatrix}} \tag{8.25}$$

Equations (8.24) and (8.25) can be used to derive the transfer functions of the lateral acceleration and yaw rate responses to a steer input. In these forms, they can be easily compared with the usual transfer functions for front wheel steer only.

$$\frac{\ddot{y}(s)}{\delta(s)} = \frac{1}{n}G_\delta^{\ddot{y}}(0) * \frac{1 + (1 + \lambda_1)T_{y1}s + T_{y2}s^2}{1 + \frac{2\zeta^* s}{\omega_n^*} + \frac{s^2}{\omega_n^{*2}}} \tag{8.26}$$

$$\frac{r(s)}{\delta(s)} = \frac{1}{n}G_\delta^r(0) * \frac{1 + T_r s}{1 + \frac{2\zeta^* s}{\omega_n^*} + \frac{s^2}{\omega_n^{*2}}} \tag{8.27}$$

here, taking

$$A^* = A + \frac{k}{l}\frac{1}{V^2} \tag{8.28}$$

as the stability factor for this case, and

$$G_{\delta}^{\ddot{y}}(0)^* = VG_{\delta}^r(0)^* = \frac{1}{1+A^*V^2}\frac{V^2}{l} \tag{8.29}$$

$$\omega_n^* = \frac{2l}{V}\sqrt{\frac{K_f K_r}{mI}(1+A^*V^2)} = \sqrt{\omega_n^2 + \frac{4kK_f K_r}{mIV}} \tag{8.30}$$

$$\zeta^* = \frac{m(l_f^2 K_f + l_r^2 K_r) + I(K_f + K_r) + kml_r K_r V}{2l\sqrt{mIK_f K_r(1+A^*V^2)}} \tag{8.31}$$

where,

$$\lambda_1 = \frac{kV}{l_r}$$

In this manner, the rear wheel steer proportional to the yaw rate changes the vehicle stability, as in Eqn (8.28), and the natural frequency and damping ratio as well.

If $k > 0$, the natural frequency increases, and the coefficient of s in the numerator of lateral acceleration becomes larger too. Here the vehicle response could be considered to be improved.

8.3　REAR WHEEL STEERING CONTROL FOR ZERO SIDE-SLIP ANGLE

Subsection 8.2.1 shows that a vehicle with zero side-slip angle at the center of gravity, during a steady-state cornering, could be realized by selecting the appropriate proportional constant for the rear to front wheel steer. Further, the study will be extended to the control logic of the rear wheel steering such that the side-slip angle of the center of gravity is always zero in response to any steer input.

8.3.1 Rear wheel steer in response to front wheel steer angle

Consider that the relationship between the rear and front wheel is expressed by a general transfer function, rather than by a simply proportional constant. The rear wheel steer could be written as follows:

$$\delta_r(s) = k(s)\delta_f(s) = \frac{k(s)}{n}\delta(s) \tag{8.6'}$$

Here, $k(s)$ is the transfer function of the rear wheel steer to front wheel steer.

The side-slip angle response to steering wheel steer input is the same as obtained by Eqn (8.7)

$$\frac{\beta(s)}{\delta(s)} = \frac{1}{n}\frac{\begin{vmatrix} 2\{K_f + k(s)K_r\} & mV + \frac{2}{V}(l_f K_f - l_r K_r) \\ 2\{l_f K_f - k(s)l_r K_r\} & Is + \frac{2(l_f^2 K_f + l_r^2 K_r)}{V} \end{vmatrix}}{\begin{vmatrix} mVs + 2(K_f + K_r) & mV + \frac{2}{V}(l_f K_f - l_r K_r) \\ 2(l_f K_f - l_r K_r) & Is + \frac{2}{V}(l_f^2 K_f + l_r^2 K_r) \end{vmatrix}} \tag{8.7'}$$

Consequently, if $k(s)$ is chosen so the numerator of Eqn (8.7)$'$ is zero,

$$\begin{vmatrix} 2\{K_f + k(s)K_r\} & mV + \frac{2}{V}(l_fK_f - l_rK_r) \\ 2\{l_fK_f - k(s)l_rK_r\} & Is + \frac{2(l_f^2K_f + l_r^2K_r)}{V} \end{vmatrix} = 0 \qquad (8.32)$$

then the transfer function of side-slip angle response to steering wheel steer input will become zero.

Expanding Eqn (8.32) gives $k(s)$ as follows:

$$k(s) = -\frac{l_r - \frac{ml_f}{2lK_r}V^2 + \frac{IV}{2lK_r}s}{l_f + \frac{ml_r}{2lK_f}V^2 + \frac{IV}{2lK_f}s} = \frac{k_0}{1 + T_es} - \frac{K_f}{K_r}\frac{T_es}{1 + T_es} \qquad (8.33)$$

here, k_0 is given by Eqn (8.12) and

$$T_e = \frac{IV}{2ll_fK_f + ml_rV^2} \qquad (8.34)$$

In other words, if the rear wheel is steered in response to the front wheel, as described by the transfer function given by Eqn (8.33), the side-slip angle of the center of gravity is always equal to zero. This ensures that the vehicle traveling direction and heading direction are always the same. The yaw rate response to steer input is

$$\frac{r(s)}{\delta(s)} = \frac{1}{n}\frac{1}{1 + \frac{ml_r}{2ll_fK_f}V^2}\frac{V}{l_f}\frac{1}{1 + T_es} \qquad (8.35)$$

8.3.2 Rear wheel steer proportional to front wheel steer and yaw rate

The side slip angle of vehicle centre of gravity can be made equal to zero by steering the rear wheel an amount equal to the sum of the front wheel steer angle and yaw rate proportional terms:

$$\delta_r = k_\delta\delta_f + k_rr = \frac{k_\delta}{n}\delta + k_rr \qquad (8.36)$$

Obtaining the side-slip angle response to steer input gives:

$$\frac{\beta(s)}{\delta(s)} = \frac{1}{n}\frac{\begin{vmatrix} 2(K_f + k_\delta K_r) & mV + \frac{2}{V}(l_fK_f - l_rK_r) - 2k_rK_r \\ (l_fK_f - k_\delta l_rK_r) & Is + \frac{2}{V}(l_f^2K_f + l_r^2K_r) + 2k_rl_rK_r \end{vmatrix}}{\begin{vmatrix} mVs + 2(K_f + K_r) & mV + \frac{2}{V}(l_fK_f - l_rK_r) - 2k_rK_r \\ 2(l_fK_f - l_rK_r) & Is + \frac{2}{V}(l_f^2K_f + l_r^2K_r) + 2k_rl_rK_r \end{vmatrix}} \qquad (8.37)$$

If

$$\begin{vmatrix} 2(K_f + k_\delta K_r) & mV + \frac{2}{V}(l_f K_f - l_r K_r) - 2k_r K_r \\ (l_f K_f - k_\delta l_r K_r) & Is + \frac{2}{V}(l_f^2 K_f + l_r^2 K_r) + 2k_r l_r K_r \end{vmatrix} = 0 \qquad (8.38)$$

is fulfilled, the side-slip angle will be zero. Expanding Eqn (8.38) gives a first order equation in s. Letting the coefficient of s and the constant term equal zero gives k_δ, k_r:

$$k_\delta = -\frac{K_f}{K_r} \qquad (8.39)$$

$$k_r = \frac{mV^2 + 2(l_f K_f - l_r K_r)}{2K_r V} \qquad (8.40)$$

By choosing these proportional constants, $\beta(s)/\delta(s)$ becomes zero, and the vehicle side-slip angle of the center of gravity is always zero. The yaw rate response to steer input is the same as the previous case and is expressed by Eqn (8.35).

8.4 YAW RATE MODEL FOLLOWING REAR WHEEL STEER

There is, in general, a concept of model following control in control engineering. It is possible to realize the intentional vehicle response to the steering wheel input by using the model following rear wheel steering control. One of the easy ways to set an intentional model of vehicle motion is to use a yaw rate model response. The yaw rate model following rear wheel steer will be studied in this section.

8.4.1 Feed-forward model following control

Applying the Laplace transform to the vehicle equations of motion for the steering wheel angle and rear wheel steering angle, Eqns (8.3) and (8.4), and solving for the yaw rate response to the steering angles gives:

$$r(s) = \frac{\frac{1}{n}G_\delta^r(0)(1 + T_r s)\delta(s) + G_{\delta_r}^r(0)(1 + T_{rr}s)\delta_r(s)}{1 + \frac{2\zeta}{\omega_n}s + \frac{1}{\omega_n^2}s^2} = \frac{\omega_n^2 H_r(s)}{s^2 + 2\zeta\omega_n + \omega_n^2} \qquad (8.41)$$

where, $G_\delta^r(0)$ and T_r are already defined in Chapter 3 and

$$H_r(s) = \frac{1}{n}G_\delta^r(0)(1 + T_r s)\delta(s) + G_{\delta_r}^r(0)(1 + T_{rr}s)\delta_r(s) \qquad (8.42)$$

$$G_{\delta_r}^r(0) = -\frac{1}{1 + AV^2}\frac{V}{l} = -G_\delta^r(0)$$

$$T_{rr} = \frac{ml_r V}{2lK_f}$$

The first order lag yaw rate model is used to determine the intentional yaw rate:

$$r_{\mathrm{m}}(s) = \frac{1}{n} \frac{G_{\mathrm{e}}}{1 + T_{\mathrm{e}} s} \delta(s) \tag{8.43}$$

If this response is identical to the response described by Eqn (8.41), the following equation is obtained:

$$\frac{\frac{1}{n} G_{\delta}^r(0)(1 + T_{\mathrm{r}} s) \delta(s) - G_{\delta}^r(0)(1 + T_{\mathrm{rr}} s) \delta_{\mathrm{r}}(s)}{1 + \frac{2\zeta}{\omega_{\mathrm{n}}} s + \frac{1}{\omega_{\mathrm{n}}^2} s^2} = \frac{1}{n} \frac{G_{\mathrm{e}}}{1 + T_{\mathrm{e}} s} \delta(s)$$

It is possible to obtain $\delta_{\mathrm{r}}(s)$ from the above equation as follows:

$$\delta_{\mathrm{r}}(s) = \frac{1}{n} \left\{ -\frac{G_{\mathrm{e}}\left(1 + \frac{2\zeta}{\omega_{\mathrm{n}}} s + \frac{1}{\omega_{\mathrm{n}}^2} s^2\right)}{G_{\delta}^r(0)(1 + T_{\mathrm{e}} s)(1 + T_{\mathrm{r}} s)} + \frac{1 + T_{\mathrm{r}} s}{1 + T_{\mathrm{rr}} s} \right\} \delta(s) \tag{8.44}$$

This is the rear wheel steering control law for the feed-forward yaw rate model following control.

8.4.2 Feed-forward and yaw rate feed-back model following control

The same yaw rate model response is used as in Eqn (8.43). This gives the following expression:

$$\left(s + \frac{1}{T_{\mathrm{e}}}\right) r_{\mathrm{m}}(s) = \frac{1}{n} \frac{G_{\mathrm{e}}}{T_{\mathrm{e}}} \delta(s) \tag{8.43$'$}$$

Here, the error, e, between the model yaw rate, r_{m}, and the vehicle yaw rate with the control, r, is defined as follows:

$$e(s) = \left(s + \frac{1}{T_{\mathrm{e}}}\right)(r(s) - r_{\mathrm{m}}(s))$$

In order to make the error converge to zero in the first order lag response, the following equation must be satisfied:

$$\left(s + \frac{1}{T_{\mathrm{g}}}\right) e(s) = 0$$

From the two equations above, the following expression can be obtained:

$$\left(s + \frac{1}{T_{\mathrm{g}}}\right)\left(s + \frac{1}{T_{\mathrm{e}}}\right)(r(s) - r_{\mathrm{m}}(s)) = 0$$

This equation is rewritten as:

$$\left\{ s^2 + 2\xi\omega_n s + \omega_n^2 + \left(\frac{1}{T_g} + \frac{1}{T_e} - 2\xi\omega_n \right)s + \frac{1}{T_g T_e} - \omega_n^2 \right\}r(s)$$

$$- \left(s + \frac{1}{T_g} \right)\left(s + \frac{1}{T_e} \right)r_m(s)$$

$$= 0$$

Applying Eqns (8.41) and (8.43)$'$ to the above equation gives:

$$\omega_n^2 H_r(s) + (c_1 s + c_0)r(s) - \left(s + \frac{1}{T_g} \right)\frac{G_e}{T_e}\delta(s) = 0$$

where,

$$c_1 = \frac{1}{T_g} + \frac{1}{T_e} - 2\zeta\omega_n$$

$$c_0 = \frac{1}{T_g T_e} - \omega_n^2$$

Substituting Eqn (8.42) into the above equation results in

$$\frac{1}{n}G_\delta^r(0)(1 + T_r s)\delta(s) - G_\delta^r(0)(1 + T_{rr}s)\delta_r(s)$$

$$= -\frac{1}{\omega_n^2}(c_1 s + c_0)r(s) + \frac{1}{n}\frac{G_e}{\omega_n^2 T_e}\left(s + \frac{1}{T_g} \right)\delta(s)$$

The rear wheel steering angle needed to follow the model yaw rate response is obtained from the above equation as follows:

$$\delta_r(s) = \frac{1}{n}\left\{ \frac{1 + T_r s}{1 + T_{rr}s} - \frac{G_e}{\omega_n^2 T_g T_e G_\delta^r(0)}\frac{1 + T_g s}{1 + T_{rr}s} \right\}\delta(s) + \frac{c_0}{\omega_n^2 G_\delta^r(0)}\frac{1 + \frac{c_1}{c_0}s}{1 + T_{rr}s}r(s)$$

(8.45)

This is the rear wheel steering control law for the feed-forward and yaw rate feed-back model following control.

8.5 FRONT AND REAR WHEEL ACTIVE STEER CONTROL

Previously, the vehicle motion has been examined for front wheels that are steered in proportion to the steering wheel angle, as normal, and rear wheels that are steered in response to some control laws. This section will consider both the front and rear wheels being steered according to some control laws. Here, the front wheels are regarded to be disconnected from the steering wheel. This concept is shown in Fig. 8.4.
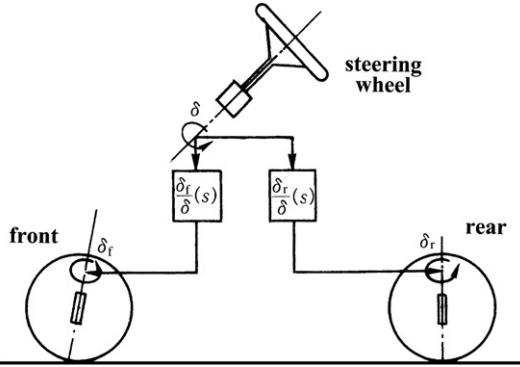
FIGURE 8.4 Front and rear wheel active steer.

Applying Laplace transforms to Eqns (8.3) and (8.4), and expressing the relations among the side-slip angle, the yaw rate, the front wheel steer angle, and the rear wheel steer angle responses to the steering wheel angle input give:

$$\{mVs + 2(K_f + K_r)\}\frac{\beta(s)}{\delta(s)} + \left\{mV + \frac{2}{V}(l_fK_f - l_rK_r)\right\}\frac{r(s)}{\delta(s)}$$

$$= 2K_f\frac{\delta_f(s)}{\delta(s)} + 2K_r\frac{\delta_r(s)}{\delta(s)} \tag{8.46}$$

$$2(l_fK_f - l_rK_r)\frac{\beta(s)}{\delta(s)} + \left\{Is + \frac{2(l_f^2K_f + l_r^2K_r)}{V}\right\}\frac{r(s)}{\delta(s)} = 2l_fK_f\frac{\delta_f(s)}{\delta(s)} - 2l_rK_r\frac{\delta_r(s)}{\delta(s)} \tag{8.47}$$

Usually, the vehicle motion is studied in response to given front and rear wheel steer angles. This is given by the equations of motion (8.3) and (8.4). For control purposes the opposite is required: the front and rear wheel steer angles for a desired vehicle response to steering wheel angle, $\beta(s)/\delta(s)$ and $r(s)/\delta(s)$, are required. This could be achieved by taking $\delta_f(s)/\delta(s)$ and $\delta_r(s)/\delta(s)$ as variables, rewriting Eqns (8.46) and (8.47), and solving the following first order algebraic equations:

$$\begin{bmatrix} 2K_f & 2K_r \\ 2l_fK_f & 2l_rK_r \end{bmatrix} \begin{bmatrix} \frac{\delta_f(s)}{\delta(s)} \\ \frac{\delta_r(s)}{\delta(s)} \end{bmatrix}$$

$$= \begin{bmatrix} \{mVs + 2(K_f + K_r)\}\frac{\beta(s)}{\delta(s)} + \left\{mV + \frac{2}{V}(l_fK_f - l_rK_r)\right\}\frac{r(s)}{\delta(s)} \\ 2(l_fK_f - l_rK_r)\frac{\beta(s)}{\delta(s)} + \left\{Is + \frac{2}{V}\left(l_f^2K_f + l_r^2K_r\right)\right\}\frac{r(s)}{\delta(s)} \end{bmatrix} \tag{8.48}$$

In other words, the front and rear wheels should be steered according to the following steering control laws to have a desired vehicle response of $\beta(s)/\delta(s)$ and $r(s)/\delta(s)$:

$$\frac{\delta_f(s)}{\delta(s)} = \frac{ml_r Vs + 2lK_f}{2lK_f} \frac{\beta(s)}{\delta(s)} + \frac{Is + ml_r V + \frac{2l_f lK_f}{V}}{2lK_f} \frac{r(s)}{\delta(s)} \tag{8.49}$$

$$\frac{\delta_r(s)}{\delta(s)} = \frac{ml_f Vs + 2lK_r}{2lK_r} \frac{\beta(s)}{\delta(s)} - \frac{Is - ml_f V + \frac{2l_r lK_f}{V}}{2lK_r} \frac{r(s)}{\delta(s)} \tag{8.50}$$

The above equation shows that a vehicle's side-slip angle and yaw rate could be set to any arbitrary response using the front and rear wheel steer control laws in Eqns (8.49) and (8.50).

Assuming that the desired responses for the side-slip angle and the yaw rate are a first order lag system with the same time constant:

$$\frac{\beta(s)}{\delta(s)} = \frac{G_\beta}{1 + Ts} \tag{8.51}$$

$$\frac{r(s)}{\delta(s)} = \frac{G_r}{1 + Ts} \tag{8.52}$$

And if $G_\beta = 0$, the side-slip angle is always zero, and the lateral acceleration response is:

$$\frac{\ddot{y}(s)}{\delta(s)} = \frac{G_r V}{1 + Ts} \tag{8.53}$$

Obtaining the front and rear wheel steer control laws by using Eqns (8.49) and (8.50) gives:

$$\frac{\delta_f(s)}{\delta(s)} = \frac{G_r}{2lK_f}\left[\frac{I}{T} + \left(ml_r V + \frac{2ll_f K_f}{V} - \frac{I}{T}\right)\frac{1}{1 + Ts}\right] \tag{8.54}$$

$$\frac{\delta_r(s)}{\delta(s)} = \frac{G_r}{2lK_r}\left[-\frac{I}{T} + \left(ml_f V - \frac{2ll_r K_r}{V} + \frac{I}{T}\right)\frac{1}{1 + Ts}\right] \tag{8.55}$$

These are the front and rear wheel steer control laws in order for the side-slip angle to be always equal to zero, and the yaw rate response to steer input to be a first order lag system.

Moreover, from Eqns (8.51) and (8.52), the lateral acceleration response is described as:

$$\frac{\ddot{y}(s)}{\delta(s)} = V\left\{ s\frac{\beta(s)}{\delta(s)} + \frac{r(s)}{\delta(s)} \right\} = \frac{G_{\mathrm{r}}V\left(1 + \frac{G_\beta}{G_{\mathrm{r}}}s\right)}{1 + Ts}$$

If $G_\beta = G_{\mathrm{r}}T$, then

$$\frac{\ddot{y}(s)}{\delta(s)} = G_{\mathrm{r}}V \tag{8.56}$$

In other words, the lateral acceleration response is completely proportional to the steer input.

The front and rear wheel steer control laws for this case are obtained by assuming $G_\beta = G_{\mathrm{r}}T$ and substituting Eqns (8.51) and (8.52) into Eqns (8.49) and (8.50):

$$\frac{\delta_{\mathrm{f}}(s)}{\delta(s)} = \frac{G_{\mathrm{r}}}{2lK_{\mathrm{f}}}\left[\frac{I}{T} + ml_{\mathrm{r}}V + \left(\frac{2ll_{\mathrm{f}}K_{\mathrm{f}}}{V} + 2lK_{\mathrm{f}}T - \frac{I}{T} \right)\frac{1}{1 + Ts} \right] \tag{8.57}$$

$$\frac{\delta_{\mathrm{r}}(s)}{\delta(s)} = \frac{G_{\mathrm{r}}}{2lK_{\mathrm{r}}}\left[-\frac{I}{T} + ml_{\mathrm{f}}V + \left(-\frac{2ll_{\mathrm{r}}K_{\mathrm{r}}}{V} + 2lK_{\mathrm{r}}T + \frac{I}{T} \right)\frac{1}{1 + Ts} \right] \tag{8.58}$$

Here, by using Eqns (8.54) and (8.55), Fig. 8.5 shows exactly how the front and rear wheel steer angles respond to the steering wheel angle when a ramped step input of the steering wheel angle is given. The frequency response is also shown in Fig. 8.6. If the front and rear wheels are steered like this in response to the steering wheel angle, then the yaw rate responds as in Eqn (8.52). The side-slip angle is always equal to zero and the lateral acceleration response is obtained by Eqn (8.53).

8.6 VEHICLE MOTION WITH DIRECT YAW-MOMENT CONTROL (DYC)

Recently, attention has been focused on the vehicle lateral motion control called DYC. This uses the yaw moment produced by the longitudinal forces of the tires, especially for stabilizing the vehicle motion in critical conditions [3]. Of course, the critical vehicle motions mostly occur in the tire non-linear region. However, in order to understand the fundamental concept of the vehicle motion control by the yaw moment, the linear equations of vehicle motion will be effectively used.

8.6.1 Passive type yaw moment control

The vehicle right and left wheels can normally rotate independently. To achieve this, the traction wheels at the front, rear or both are connected to the driving
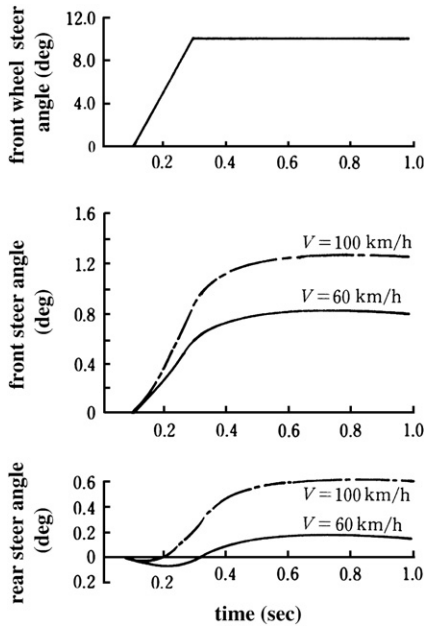
FIGURE 8.5 Front and rear steer angle.
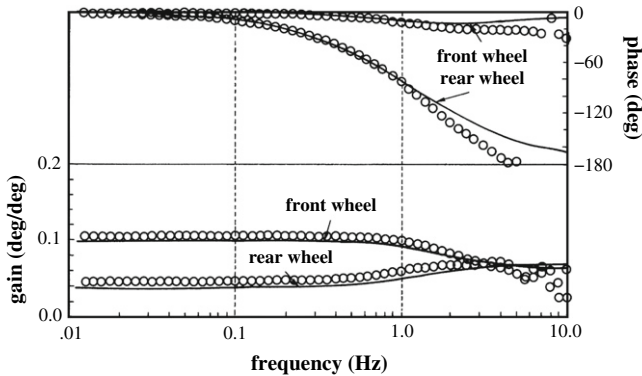
FIGURE 8.6 Front and rear steer frequency responses to steering wheel angle input.

shaft through the differential. If the differential is locked or viscously coupled during cornering, the longitudinal forces arise on the right and left tires in counter directions with each other, which produce the yaw moment to control the lateral motion of the vehicle. This yaw moment and its effect on the vehicle motion will be studied in this subsection.

(1) EFFECTS OF LOCKED DIFFERENTIAL

There is a limited-slip-differential in which the differential gears are locked until the transfer torque through the differential is within a limit. This state is

called the differential lock. Figure 8.7 shows the vehicle plane motion with locked differential.

Depending on the definition by Eqns (2.46) or (2.66), the longitudinal slips of the right and left tires with the locked differential during cornering, s_L and s_R, are expressed by:

$$s_L = \frac{V - \frac{d}{2}r - R_0\omega}{V - \frac{d}{2}r} \approx -\frac{d}{2V}r \tag{8.59}$$

$$s_R = \frac{V + \frac{d}{2}r - R_0\omega}{V + \frac{d}{2}r} \approx \frac{d}{2V}r \tag{8.60}$$

where, ω is axis rotational speed, d is wheel tread, and R_0 is effective tire radius.

Though there is a difference in the definitions of longitudinal slip under braking or traction, the above definition is applied to both under the assumption, $V \approx R_0\omega$.

The longitudinal forces produced by the slip are proportional to the longitudinal slip when it is small. The longitudinal forces exerted on the left and right tires are expressed as:

$$X_L = -K_S s_L = \frac{K_S d}{2V}r$$

$$X_R = -K_S s_R = -\frac{K_S d}{2V}r$$

Here, K_S is the tire longitudinal force per unit slip as defined by Eqn (2.54). Accordingly, the yaw moment, M, produced by the above forces is:

$$M = -\frac{d}{2}X_L + \frac{d}{2}X_R = -\frac{K_S d^2}{2V}r \tag{8.61}$$
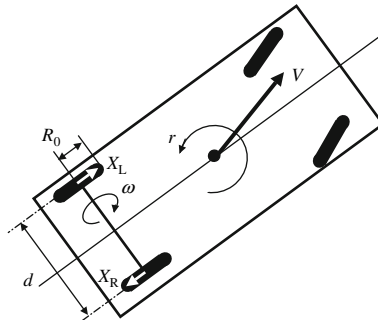
FIGURE 8.7 Vehicle turning with locked differential.

This is a yaw moment in the opposite direction to the yaw rate and is proportional to it. This is called yaw damping. This yaw moment is inversely proportional to the vehicle speed and decreases as the speed increases.

(2) EFFECT OF VISCOUS COUPLING DIFFERENTIAL

There is a differential gear mechanism in which the left and right wheels are viscously connected with each other. This is called a viscous coupling differential.

Figure 8.8 shows the vehicle plane motion with the left and right wheels coupled with a viscous torque. Using the same symbols as in the previous sub-subsection (1), the longitudinal slips of the left and right tires are:

$$s_L = \frac{V - \frac{d}{2}r - R_0(\omega - \frac{\Delta\omega}{2})}{V - \frac{d}{2}r} \approx \frac{-dr + R_0\Delta\omega}{2V} \tag{8.59'}$$

$$s_R = \frac{V + \frac{d}{2}r - R_0(\omega + \frac{\Delta\omega}{2})}{V + \frac{d}{2}r} \approx \frac{dr - R_0\Delta\omega}{2V} \tag{8.60'}$$

where $\Delta\omega$ is rotational speed difference between left and right wheels.

The axle torque due to the longitudinal forces produced by these longitudinal slips is balanced with the viscous coupling torque. This leads to the following equations, where C is the viscous coupling torque coefficient:

$$-R_0 K_S s_L = R_0 K_S s_R = C\Delta\omega \tag{8.61'}$$

Substituting Eqn (8.59)′ or (8.60)′ into Eqn (8.61) gives:

$$R_0 K_S \frac{dr - R_0\Delta\omega}{2V} s_R = C\Delta\omega$$

From this equation, $\Delta\omega$ can be obtained as follows:

$$\Delta\omega = \frac{1}{1 + \frac{2CV}{R_0^2 K_S}} \frac{dr}{R_0} \tag{8.62}$$
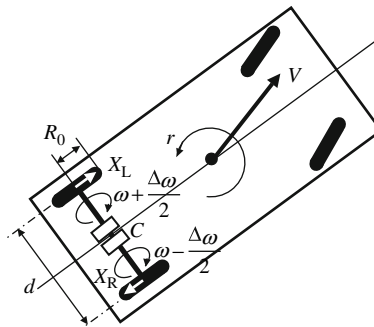
FIGURE 8.8 Vehicle turning with viscous coupling differential.

The longitudinal forces exerted upon the left and right tires are:

$$X_L = -K_S s_L = \frac{C\Delta\omega}{R_0} = \frac{1}{1 + \frac{R_0^2 K_S}{2CV}} \frac{K_S d}{2V} r$$

$$X_R = -K_S s_R = -\frac{C\Delta\omega}{R_0} = -\frac{1}{1 + \frac{R_0^2 K_S}{2CV}} \frac{K_S d}{2V} r$$

and the yaw moment exerted upon the vehicle is:

$$M = -\frac{d}{2} X_L + \frac{d}{2} X_R = -\frac{C}{C + \frac{R_0^2 K_S}{2V}} \frac{K_S d^2}{2V} r \qquad (8.61)''$$

It is understood that the yaw moment is in the opposite direction to the yaw rate and proportional to it, which is the same as the case of the locked differential. Also, it is easy to see from Eqn (8.61)$''$ that the yaw moment can be changed by the viscous torque coefficient. The equation shows that when C is equal to zero, the yaw moment, M, is zero and increases with C until it reaches the same value as in the locked differential case, where C becomes substantially very large. The yaw moment decreases with increasing vehicle speed, which is also the same as the locked differential case.

(3) EFFECT OF YAW MOMENT ON VEHICLE DYNAMICS

The equations of vehicle motion with the additional yaw moment described by:

$$M = -\frac{k_r}{V} r$$

is obtained from Eqns (3.12) and (3.13). Substituting the above yaw moment to the right hand side of Eqn (3.13) gives:

$$mV\frac{d\beta}{dt} + 2(K_f + K_r)\beta + \left\{ mV + \frac{2}{V}(l_f K_f - l_r K_r) \right\} r = 2K_f \frac{\delta}{n} \qquad (8.63)$$

$$2(l_f K_f - l_r K_r)\beta + I\frac{dr}{dt} + \left\{ \frac{2(l_f^2 K_f + l_r^2 K_r) + k_r}{V} \right\} r = 2l_f K_f \frac{\delta}{n} \qquad (8.64)$$

The side-slip response to the steering input in Laplace transform form is obtained as follows:

$$\frac{\beta(s)}{\delta(s)} = \frac{1}{n} \frac{\begin{vmatrix} 2K_f & mV + \frac{2}{V}(l_f K_f - l_r K_r) \\ 2l_f K_f & Is + \frac{2(l_f^2 K_f + l_r^2 K_r) + k_r}{V} \end{vmatrix}}{\begin{vmatrix} mVs + 2(K_f + K_r) & mV + \frac{2}{V}(l_f K_f - l_r K_r) \\ 2(l_f K_f - l_r K_r) & Is + \frac{2(l_f^2 K_f + l_r^2 K_r)}{V} \end{vmatrix}}$$

$$= \frac{1}{n} G_\delta^{*\beta}(0) \frac{1 + T_\beta^* s}{1 + \frac{2\zeta^* s}{\omega_n^*} + \frac{s^2}{\omega_n^{*2}}} \tag{8.65}$$

whereby

$$\omega_n^{*2} = \frac{4K_f K_r l^2}{mIV^2}(1 + AV^2) + \frac{2(K_f + K_r)}{mIV^2} k_r$$

$$\zeta^* = \frac{m(l_f^2 K_f + l_r^2 K_r) + I(K_f + K_r) + \frac{mk_r}{2}}{2l\sqrt{mIK_f K_r(1 + AV^2) + \frac{K_f + K_r}{2l^2 K_f K_r} k_r}}$$

$$G_\delta^{*\beta}(0) = \frac{1 - \frac{m}{2l}\frac{l_f}{l_r K_r}V^2 + \frac{k_r}{2ll_r K_r}}{1 + AV^2 + \frac{K_f + K_r}{2l^2 K_f K_r} k_r} \frac{l_r}{l}$$

$$T_\beta^* = \frac{IV}{2ll_r K_r} \frac{1}{1 - \frac{m}{2l}\frac{l_f}{l_r K_r}V^2 + \frac{k_r}{2ll_r K_r}}$$

The yaw rate response is also obtained as:

$$\frac{r(s)}{\delta(s)} = \frac{1}{n} \frac{\begin{vmatrix} mVs + 2(K_f + K_r) & 2K_f \\ 2(l_f K_f - l_r K_r) & 2l_f K_f \end{vmatrix}}{\begin{vmatrix} mVs + 2(K_f + K_r) & mV + \frac{2}{V}(l_f K_f - l_r K_r) \\ 2(l_f K_f - l_r K_r) & Is + \frac{2(l_f^2 K_f + l_r^2 K_r) + k_r}{V} \end{vmatrix}}$$

$$= \frac{1}{n} G_\delta^{*r}(0) \frac{1 + T_r s}{1 + \frac{2\zeta^* s}{\omega_n^*} + \frac{s^2}{\omega_n^{*2}}} \tag{8.66}$$

whereby,

$$G_\delta^{*r}(0) = \frac{1}{1 + AV^2 + \frac{K_f + K_r}{2l^2 K_f K_r}k_r} \frac{V}{l}$$

It is clear from the above that the vehicle motion with the yaw moment in the opposite direction and proportional to the yaw rate becomes robust to disturbances because the yaw damping and yaw rate gain to steering input are reduced. In other words, the vehicle stability is improved and the handling response is impaired by the yaw moment.

8.6.2 DYC for zero side-slip angle

Next let us look at the active vehicle control using the yaw moment obtained from the tire longitudinal forces. It has already been shown that zero side-slip response is possible by steering the rear wheel in response to the front wheel steering and the yaw rate. The possibility of having zero side-slip motion by DYC is examined in this section.

First, consider the yaw moment proportional to steer angle and yaw rate:

$$M = k_\delta \delta_f + k_r r = \frac{k_\delta}{n}\delta + k_r r \tag{8.67}$$

The vehicle equations of motion are obtained by substituting the above yaw moment into Eqn (3.13).

$$mV\frac{d\beta}{dt} + 2(K_f + K_r)\beta + \left\{mV + \frac{2}{V}(l_f K_f - l_r K_r)\right\}r = 2K_f\delta_f \tag{8.68}$$

$$2(l_f K_f - l_r K_r)\beta + I\frac{dr}{dt} + \left\{\frac{2(l_f^2 K_f + l_r^2 K_r)}{V} - k_r\right\}r = (2l_f K_f + k_\delta)\delta_f \tag{8.69}$$

In order to find the condition for the steady state side-slip angle to be equal to zero, $d\beta/dt$ and dr/dt are set equal to zero in the above equations. The equations are then solved for β:

$$\beta = \frac{\begin{vmatrix} 2K_f & mV + \frac{2}{V}(l_f K_f - l_r K_r) \\ 2l_f K_f + k_\delta & \frac{2(l_f^2 K_f + l_r^2 K_r)}{V} - k_r \end{vmatrix}}{\begin{vmatrix} 2(K_f + K_r) & mV + \frac{2}{V}(l_f K_f - l_r K_r) \\ 2(l_f K_f - l_r K_r) & \frac{2(l_f^2 K_f + l_r^2 K_r)}{V} - k_r \end{vmatrix}}\delta_f$$

Developing the above equation and putting it equal to zero gives the following conditions for steady-state zero side-slip angle:

$$2K_f k_r + \left\{ mV + \frac{2}{V}(l_f K_f - l_r K_r) \right\} k_\delta = \frac{4 l l_r K_f K_r}{V} \left(1 - \frac{m l_f}{2 l l_r K_r} V^2 \right) \quad (8.70)$$

For example, putting $k_r = 0$, in the above equation yields:

$$k_\delta = \frac{4 l l_r K_f K_r (1 - \frac{m l_f}{2 l l_r K_r} V^2)}{mV^2 + 2(l_f K_f - l_r K_r)} \quad (8.71)$$

The yaw rate response to steer input, $r(s)/\delta(s)$, can be obtained by putting $k_r = 0$, substituting Eqn (8.71) into Eqns (8.68) and (8.69) and applying Laplace transforms:

$$\frac{r(s)}{\delta(s)} = \frac{1}{n} \frac{2K_f V}{mV^2 + 2(l_f K_f - l_r K_r)} \left\{ \frac{1 + \frac{m(l_f^2 K_f + l_r^2 K_r)V}{2 l^2 K_f K_r (1 + A V^2)} s}{1 + \frac{2\zeta}{\omega_n} s + \frac{1}{\omega_n^2} s^2} \right\} \quad (8.72)$$

This is the yaw rate response to the steering input for the vehicle with the steady-state zero side slip, which is produced by DYC with the yaw moment proportional to the steering angle.

By putting $k_\delta = 0$ into Eqn (8.70) we obtain:

$$k_r = \frac{2 l l_r K_f K_r}{V} \left(1 - \frac{m l_f}{2 l l_r K_r} V^2 \right) \quad (8.73)$$

and the yaw rate response to steer input can also be found by substituting Eqn (8.73) into Eqns (8.68) and (8.69) and applying the Laplace transforms:

$$\frac{r(s)}{\delta(s)} = \frac{1}{n} \frac{2K_f V}{mV^2 + 2(l_f K_f - l_r K_r)} \left\{ \frac{1 + \frac{m l_f V}{2 l K_r} s}{1 + d_1 s + d_2 s^2} \right\} \quad (8.74)$$

where,

$$d_1 = \frac{m l_f \{ mV^2 + 2(l_f K_f - l_r K_r) \} + 2I(K_f + K_r)}{2 l K_r \{ mV^2 + 2(l_f K_f - l_r K_r) \}} V$$

$$d_2 = \frac{m I V^2}{2 l K_r \{ mV^2 + 2(l_f K_f - l_r K_r) \}}$$

This is the yaw rate response to the steering input for the vehicle with the steady-state zero side-slip by DYC using the yaw moment proportional to the yaw rate algorithm.

By adjusting the parameters, k_δ and k_r, as shown in the above, the steady-state zero side-slip vehicle motion and yaw rate responses described by Eqns (8.72) and (8.74) can be achieved. However, it is important to understand from these equations that if the vehicle speed is low, the denominator in the yaw rate response gain is equal to zero at the speed $V = \sqrt{-(l_f K_f - l_r K_r)/m}$ and changes the sign. Also, if the vehicle speed is less than the above, the constant term in the characteristic equation of the vehicle response becomes negative and the vehicle tends to be unstable. Therefore, it should be understood that the zero side-slip control mentioned above makes sense at vehicle speeds high enough for the conditions to be physically reasonable.

It seems through the above analysis that zero side-slip control by DYC is practical at speeds above that where the steady-state side-slip response to the front wheel steer is changed from positive to negative. This is expressed by the following inequality:

$$1 - \frac{ml_f}{2ll_r K_r} V^2 \le 0$$

Here, the DYC can control the negative side-slip angle to the front steer input and stabilize the vehicle motion at high speed.

Next let us look at the yaw moment that gives the side-slip angle always equal to zero at any time during vehicle motion at high speeds:

$$M(s) = k(s)\delta_f(s) = k(s)\frac{\delta(s)}{n} \tag{8.75}$$

The Laplace transforms of the equations of vehicle motion, with the above yaw moment, are written as follows:

$$mVs\beta(s) + 2(K_f + K_r)\beta(s) + \left\{mV + \frac{2}{V}(l_f K_f - l_r K_r)\right\}r(s) = 2K_f \delta_f(s) \tag{8.76}$$

$$2(l_f K_f - l_r K_r)\beta(s) + Isr(s) + \frac{2\left(l_f^2 K_f + l_r^2 K_r\right)}{V}r(s) = \{2l_f K_f + k(s)\}\delta_f(s) \tag{8.77}$$

Solving the above equation for the side-slip angle and putting it equal to zero gives the following equation:

$$\begin{vmatrix} 2K_f & mV + \frac{2}{V}(l_f K_f - l_r K_r) \\ 2l_f K_f + k(s) & Is + \frac{2}{V}(l_f^2 K_f + l_r^2 K_r) \end{vmatrix} = 0$$

It is possible to solve the above equation for $k(s)$, thereby obtaining the following yaw moment, $M(s)$, to give the side-slip response to steer input always equal to zero:

$$M(s) = k(s)\frac{\delta(s)}{n}$$

$$= \frac{1}{n}\left\{\frac{4ll_rK_fK_r\left(1 - \frac{ml_f}{2ll_rK_r}V^2\right)}{mV^2 + 2(l_fK_f - l_rK_r)} + \frac{2IK_fV}{mV^2 + 2(l_fK_f - l_rK_r)}s\right\}\delta(s) \quad (8.78)$$

The yaw rate response to the steering input is obtained by putting $k(s)$ in the above equation and $\beta(s) = 0$ into Eqn (8.77):

$$\frac{r(s)}{\delta(s)} = \frac{1}{n}\frac{2K_fV}{mV^2 + 2(l_fK_f - l_rK_r)} \quad (8.79)$$

Though it is possible to obtain the yaw moment for zero side-slip response and the desired yaw rate response to the steering input, as in Eqns (8.78) and (8.79), attention must be given to the fact that these equations are reasonable at the high vehicle speeds. Even so, it is clear that the yaw rate response gain of the vehicle with the zero side-slip DYC control is fairly small compared to that of the normal front wheel steer vehicle and decreases with the increasing vehicle speed significantly.

8.6.3 Yaw rate model following DYC

Here, the yaw rate model following control by DYC will be investigated in Section 8.4.

The vehicle responses to the steering wheel and the yaw moment, M, produced by the longitudinal forces of the right and left tires are:

$$mV\frac{d\beta}{dt} + 2(K_f + K_r)\beta + \left\{mV + \frac{2}{V}\left(l_fK_f - l_rK_r\right)\right\}r = 2K_f\frac{\delta}{n} \quad (8.80)$$

$$2(l_fK_f - l_rK_r)\beta + I\frac{dr}{dt} + \frac{2\left(l_f^2K_f + l_r^2K_r\right)}{V}r = 2l_fK_f\frac{\delta}{n} + M \quad (8.81)$$

Applying Laplace transforms to the above equations and solving the equations for the yaw rate response, $r(s)$, to the steering and yaw moment input, gives the following equations:

$$r(s) = \frac{\frac{1}{n}G_\delta^r(0)(1 + T_rs)\delta(s) + G_M^r(0)(1 + T_Ms)M(s)}{1 + \frac{2\zeta}{\omega_n}s + \frac{1}{\omega_n^2}s^2} = \frac{\omega_n^2 H_M(s)}{s^2 + 2\zeta\omega_n + \omega_n^2}$$

$$(8.82)$$

Where,

$$H_M(s) = \frac{1}{n}G_\delta^r(0)(1 + T_r s)\delta(s) + G_M^r(0)(1 + T_M s)M(s) \qquad (8.83)$$

$$G_M^r(0) = \frac{(K_f + K_r)V}{2l^2 K_f K_r(1 + AV^2)}$$

$$T_M = \frac{mV}{2(K_f + K_r)}$$

(1) FEED-FORWARD YAW RATE MODEL FOLLOWING DYC

Here, the same yaw rate model response is adopted as in the rear wheel steer:

$$r_m(s) = \frac{1}{n}\frac{G_e}{1 + T_e s}\delta(s) \qquad (8.43)''$$

If this response is identical with the response described by Eqn (8.82), the following equation is obtained:

$$\frac{\frac{1}{n}G_\delta^r(0)(1 + T_r s)\delta(s) + G_M^r(0)(1 + T_M s)M(s)}{1 + \frac{2\zeta}{\omega_n}s + \frac{1}{\omega_n^2}s^2} = \frac{1}{n}\frac{G_e}{1 + T_e s}\delta(s)$$

It is possible to obtain $M(s)$ from the above equation as follows:

$$M(s) = \frac{1}{n}\left\{\frac{G_e\left(1 + \frac{2\zeta}{\omega_n}s + \frac{1}{\omega_n^2}s^2\right)}{G_M^r(0)(1 + T_M s)(1 + T_e s)} - \frac{G_\delta^r(0)}{G_M^r(0)}\frac{1 + T_r s}{1 + T_M s}\right\}\delta(s) \qquad (8.84)$$

This is the required direct yaw-moment control law for the feed-forward control to follow the first order lag yaw rate model response.

(2) FEED-FORWARD AND YAW RATE FEED-BACK MODEL FOLLOWING DYC

The same yaw rate model response as in sub-subsection (1) is adopted again. Using Eqn (8.43), Eqn (8.43)$'$ is obtained as:

$$\left(s + \frac{1}{T_e}\right)r_m(s) = \frac{1}{n}\frac{G_e}{T_e}\delta(s) \qquad (8.43)''$$

Again, the error, e, between the model yaw rate, r_m, and the vehicle yaw rate response to the steering and yaw moment input, r, is as follows:

$$e(s) = \left(s + \frac{1}{T_e}\right)(r(s) - r_m(s))$$

In order to make the error converge to zero in the first order lag response:

$$\left(s + \frac{1}{T_g}\right)e(s) = 0$$

From the above two equations, the following expression can be obtained:

$$\left(s + \frac{1}{T_g}\right)\left(s + \frac{1}{T_e}\right)(r(s) - r_m(s)) = 0$$

This equation is rewritten as:

$$\left\{s^2 + 2\zeta\omega_n s + \omega_n^2 + \left(\frac{1}{T_g} + \frac{1}{T_e} - 2\zeta\omega_n\right)s + \frac{1}{T_g T_e} - \omega_n^2\right\}r(s)$$
$$- \left(s + \frac{1}{T_g}\right)\left(s + \frac{1}{T_e}\right)r_m(s)$$
$$= 0$$

Applying Eqns (8.80) and (8.43)′, the above equation becomes:

$$\omega_n^2 H_M(s) + (c_1 s + c_0)r(s) - \left(s + \frac{1}{T_g}\right)\frac{G_e}{T_e}\delta(s) = 0$$

where, c_1 and c_0 are the same as defined in Section 8.4:

$$c_1 = \frac{1}{T_g} + \frac{1}{T_e} - 2\zeta\omega_n$$

$$c_0 = \frac{1}{T_g T_e} - \omega_n^2$$

Substituting Eqn (8.81) into the above equation gives the following relationship:

$$\frac{1}{n}G_\delta^r(0)(1 + T_r s)\delta(s) + G_M^r(0)(1 + T_M s)M(s)$$
$$= -\frac{1}{\omega_n^2}(c_1 s + c_0)r(s) + \frac{1}{n}\frac{G_e}{\omega_n^2 T_e}\left(s + \frac{1}{T_g}\right)\delta(s)$$

Thereby the yaw moment needed for the DYC to follow the model yaw rate response is obtained from the above equation as follows:

$$M(s) = \frac{1}{n} \left\{ -\frac{G_\delta^r(0)}{G_M^r(0)} \frac{1 + T_r s}{1 + T_M s} + \frac{G_e}{\omega_n^2 T_g T_e G_M^r(0)} \frac{1 + T_g s}{1 + T_M s} \right\} \delta(s)$$
$$- \frac{c_0}{\omega_n^2 G_M^r(0)} \frac{1 + \frac{c_1}{c_0} s}{1 + T_M s} r(s) \tag{8.85}$$

This is the direct yaw-moment control law for the feed-forward and yaw rate feed-back control to follow the first order lag yaw rate model response to the steering input.

REFERENCES

[1] Y. Furukawa, Improvement of vehicle handling by 4 wheel steering system, JSAE Journal, Vol. 40, No. 3, 1986 (In Japanese).

[2] N. Irie, et al., Improving vehicle stability and controllability through active rear wheel steering, JSAE Journal, Vol. 40, No. 3, 1986 (In Japanese).

[3] M. Abe, Vehicle dynamics and control for improving handling and active safety – from 4WS to DYC, Proceedings of the IMechE Part K, Vol. 213, 1999.

Vehicle Motion with Human Driver

9.1 PREFACE

The vehicle dealt with in this book is that capable of moving freely, in a plane, by the forces generated from the motion of the vehicle body itself, similar to aircraft and ships.

The vehicle lateral motion, yaw motion, and roll motion, arise through steering action or by disturbances and external forces. The vehicle motion is controlled through the actions of the driver who observes the vehicle motion and carries out a suitable steer to achieve his intended path.

The previous chapters have studied the inherent motion characteristics of the vehicle in considerable detail, focusing on the vehicle's response to steer and disturbances. However, the previous chapters are based on the assumption that the driver is not actively steering to control the vehicle motion intentionally.

The vehicle motion response to steer and disturbances, based on a ground fixed coordinate frame, is expressed by the transfer functions given in Eqns $(3.87)'$, $(3.88)'$, (4.11), and (4.12). These transfer functions include $1/s^2$ and $1/s$ forms of integration of the vehicle lateral displacement and yaw angle response to steer and disturbances. This shows that these responses to the steer input will increase their value over time if suitable control isn't added. By this analysis, the vehicle motion relative to the coordinate axis fixed onto the absolute space could be said to be 'unstable' by nature. This is why the vehicle can move freely in the plane when a suitable steer is given, i.e., the vehicle has freedom of motion that is unrestricted and 'unstable'.

Until now, the 'unstable' vehicle motion characteristics have not been treated as a major factor. However, this kind of treatment is incomplete in the discussion of vehicle dynamics. The vehicle is capable of meaningful motion that follows the driver's intention through a suitable steer action. It is important

to understand the vehicle motion in the absolute space when steer is given intentionally by the driver in response to the vehicle motion.

9.2 HUMAN CONTROL ACTION

In situations where a human controls the machine, the human controller plays an important role in deciding the motion. In such situations, examination of the moving body will always have the problem of how to describe the human as the controller.

From this point of view, pioneering researches concerning the functions of human operators have been carried out by several researchers, from which valuable results have been obtained. However, even when concerned with the above human controller function only, humans are not consistent, and the same treatment may not be able to describe every condition. Moreover, the vehicle motion that is dealt with in the previous chapters, could well be derived by theoretical expansion of the basic equations of motion based on Newton's Law, even if the secondary factors that govern the motion are omitted. In other words, there is a theoretical guarantee to the nature of the motion, which could be expressed by mathematical equations. On the contrary to this, with regards to humans, there is no certain guarantee that the human control action can be described completely using mathematical equations.

Nevertheless, if observed carefully, a human operator exhibits some regular behavior from the viewpoint of machine control. A model that simulates the human's regularity can be derived and made to represent the human functions as the controller. This is the basic way of thinking when dealing with the human control function.

This is similar to the concept of the black box used in control engineering. The fact that automatic control theory can now be applied easily to human control behavior allows researchers to understand the human control function and develop effective designs of machines controlled by a human operator. One popular method is treating the human control behavior as a linear continuous feedback control, and expressing it as a transfer function. Various transfer functions have then been proposed to suit different conditions.

Table 9.1 shows the proposed transfer functions of a human controller. All these transfer functions have almost the same characteristics. Here, the following transfer function is used as the example:

Table 9.1 Transfer Functions of a Human Controller

1	$K \frac{(1 + Ts)}{s} e^{-\tau s}$	by Tustin
2	$K \frac{(T_1 s + 1) e^{-\tau s}}{(T_2 s + 1)(T_3 s + 1)}$	by McRuer & Krendel
3	$K(T_1 s + 1 + \frac{1}{T_2 s}) e^{-\tau s}$	by Ragazzini
4	$K \frac{(A_n s^n + \cdots + A_0)}{s^l (B_m s^m + \cdots + B_0)} e^{-\tau s}$	by Jackson

$$H(s) = h\left(\tau_D s + 1 + \frac{1}{\tau_I s}\right)e^{-\tau_L s} \tag{9.1}$$

The physical meaning of human control can now be studied in more detail.

Firstly, a human operator will have a time lag to make an action (output) under a given stimulus (input). This is represented by $e^{-\tau_L s}$, and the time lag is expressed by τ_L. The control action that the human operator can do at ease and with the least workload is the kind of action that gives an output signal proportional to the input signal, in other words, proportional action. This is represented by the proportional constant, h. The human operator is also capable of the control action that predicts a change in the input. Here the output signal is normally proportional to the input rate or the differential value of the input. In other words, this is called the derivative control action. This is represented by the derivative time, τ_D. The human operator is also capable of making integral action where the output signal is proportional to the integrated value of the input signal. This shows that the human operator is able to relocate point when it is deviated away from the original. This is represented by the integral time, τ_I.

Combining all the control actions mentioned above, the human transfer function $H(s)$ can be represented by Eqn (9.1).

The human operator is different from normal control systems. The distinctive characteristics of the human controller lie in the fact that the transfer function constants, h, τ_D, τ_I, can be changed for appropriate control within a possible range. This characteristic is generally called the control action adaptability of the control system. Among h, τ_D, and τ_I, the human operator is able to change the constant of the proportional action, h, substantially without workload, while the other constants have some limitations. In particular, the increase of derivative action could give considerable workload to the human operator. If the control target needs intense derivative control action up to a certain level, the human may not be able to carry out the control anymore.

The control action that the human controller is capable of without much workload and continuously for a long time is considered to be the proportional action, with very weak derivative action or an integral one.

9.3 VEHICLE MOTION UNDER DRIVER CONTROL

9.3.1 Driver model

Using the previous ideas for general human control behavior, the control behavior of a human driver controlling the vehicle motion through the steer angle will be considered.

Expressing the transfer function of the vehicle lateral motion to the steer angle in absolute space will give something like Eqn (3.87) or (3.87)'. The equation shows that the vehicle path, the control target of the human driver, has characteristics near to the double integration of the steer angle. Generally, for a control target with transfer function of $1/s^2$, differential action is needed, in addition to proportional action, to stabilize the system.
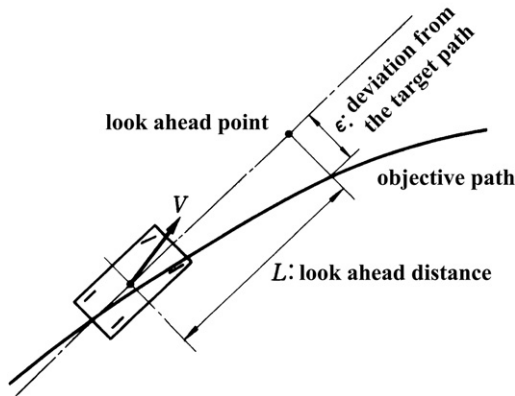
FIGURE 9.1 Course error at $L(m)$ ahead point.

A driver could also sense the vehicle attitude, i.e., yaw angle, as well as the lateral displacement. The transfer function of the vehicle yaw angle response to steer angle in the absolute space is given by Eqns (3.88) or (3.88)$'$ and has characteristics near to the single integration of the steer angle. If the driver makes the control action by sensing the yaw angle, rather than the lateral displacement, it is expected that the driver will be able to control the vehicle more easily, even without the differential action, but through some actions equivalent to the differential action.

Based on this argument, the driver inside the vehicle is assumed to look forward to $L(m)$ ahead of the vehicle and estimate the deviation of the vehicle lateral displacement relative to the target course. The estimated lateral displacement is a lateral component of the vehicle traveling distance in a time of L/V at the current attitude. The driver makes the feedback control based on this deviation. The scenario is shown in Fig. 9.1. This approach now becomes the most fundamental understanding of the human driver's control model for dealing with the vehicle motion. Figure 9.2 shows the block diagram of such an approach. Here, L is called the looking ahead distance, and the $L(m)$ point is called the look ahead point.

At this time, since the vehicle has strong integration characteristics, some differential control element is included in the transfer function of the human driver's control behavior. Consequently, the human driver's transfer function becomes:

$$H(s) = h(1 + \tau_D s)e^{-\tau_L s} \tag{9.2}$$
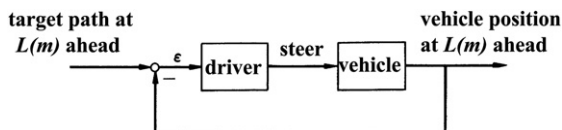
FIGURE 9.2 Closed loop driver–vehicle system.
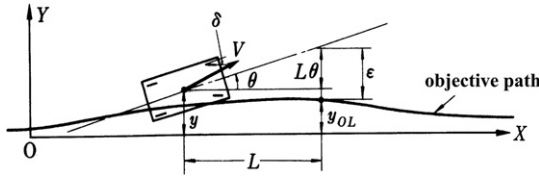
FIGURE 9.3 Vehicle motion controlled by driver with nearly straight objective path.

9.3.2 Vehicle motion following a course

To study the vehicle motion under the control, a target course is defined that consists of gentle curves, and is almost a straight line, as shown in Fig. 9.3. The vehicle receives the control action from the driver and moves along this target course. If the X-axis is the direction along the target course, and the Y-axis is the direction perpendicular to it, then the vehicle state of motion will be as shown in Fig. 9.3.

Here, y is the vehicle lateral displacement, θ is the yaw angle, and y_{OL} is the lateral displacement of the target course at the look ahead point. Since $|\theta| \ll 1$, the supposed lateral deviation of the vehicle from the target course at the look ahead point is:

$$\varepsilon = y + L\theta - y_{OL} \tag{9.3}$$

Furthermore, if the vehicle motion is expressed in terms of the steer angle δ, the transfer function of y and θ to δ, $G_y(s)$, and $G_\theta(s)$, is given by Eqns (3.87)′and (3.88)′.

$$G_y(s) = \frac{y(s)}{\delta(s)} = G_\delta^y(0)\frac{1 + T_{y1}s + T_{y2}s^2}{s^2\left(1 + \frac{2\zeta s}{\omega_n} + \frac{s^2}{\omega_n^2}\right)} \tag{9.4}$$

$$G_\theta(s) = \frac{\theta(s)}{\delta(s)} = G_\delta^r(0)\frac{1 + T_r s}{s\left(1 + \frac{2\zeta s}{\omega_n} + \frac{s^2}{\omega_n^2}\right)} \tag{9.5}$$

The vehicle motion, y, in relation to the given target course, y_{OL}, is expressed in block diagram form as in Fig. 9.4. The vehicle under driver
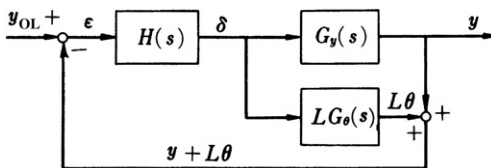
FIGURE 9.4 Block diagram of driver–vehicle system.

control, even when deviating away from the target, will eventually converge to and follow the target course if the system as shown in the figure is stable. At this instance, the vehicle motion is also affected by the vehicle's inherent dynamic characteristics, expressed by $G_y(s)$ and $G_\theta(s)$, and by the human driver's control characteristics expressed by the form of $H(s)$ and the value of $L(m)$.

Figure 9.5 shows a computer simulation of vehicle motion based on the above approach. The driver's transfer function, $H(s) = h/(1 + \tau_L s)$, instead of Eqn (9.2) is used to investigate the basic motion of the vehicle under the control by the human driver. The figure indicates that the vehicle motion is greatly affected by how the human controls the vehicle and the vehicle's inherent motion characteristics.

These results are for vehicle motion when acted on by a sudden external force in the lateral direction. The force acts for a short period of time at the center of gravity of the vehicle traveling in straight line. Figure 9.5a is the vehicle motion when the driver look ahead distance, L, is changed, while Fig. 9.5b is the vehicle motion when the vehicle steer characteristics are changed. Here, y_{OL} is always 0.

It is shown that if the look ahead distance, L, is too short, the vehicle motion oscillates and becomes unstable. If L is big, the vehicle is stable and could return to the course. For the vehicle motion to be stable enough, L must increase with speed. The oscillation with poor damping occurs for the OS characteristic vehicle, while in the case of US characteristics, the motion is damped and stable. However, vehicles, which exhibit a strong US characteristic have large lateral displacements and deteriorated damping. Furthermore, with concern to the controlled vehicle tracking the target course, it is also shown that if the look ahead distance is too large, or the vehicle exhibits too much US characteristic, the target course tracking will be impaired too.

9.3.3 Motion stability

Here, the stability of the vehicle motion, under the human driver's control, described in subsection 9.3.2 is studied.

The transfer function of y to y_{OL} is derived from the block diagram of Fig. 9.4, giving:

$$\frac{y(s)}{y_{OL}(s)} = \frac{G_y(s)H(s)}{1 + H(s)[G_y(s) + LG_\theta(s)]} \tag{9.6}$$

Therefore, the characteristic equation for the controlled vehicle is:

$$1 + H(s)[G_y(s) + LG_\theta(s)] = 0 \tag{9.7}$$

Substituting Eqns (9.2), (9.4), and (9.5) into Eqn (9.7) results in the final characteristic equation. However, the characteristic equation is again too complicated. The vehicle characteristics must be first simplified before

FIGURE 9.5 Vehicle motion controlled by modeled driver.

understanding the basic characteristics of vehicle stability under a driver's control.

The yaw rate response to the front wheel steer input is approximated from Eqn (3.78) under the assumptions of $K_f = K_r = K$, $l_f = l_r = l/2$:

$$\frac{r(s)}{\delta(s)} = \frac{V}{l} \frac{1}{1 + t_r s} \tag{9.8}$$

where,

$$t_r = \frac{mV}{4K} \tag{9.9}$$

The yaw angle response to steer input is described as:

$$G_\theta(s) = \frac{\theta(s)}{\delta(s)} = \frac{V}{l} \frac{1}{1 + t_r s} \frac{1}{s} \tag{9.10}$$

Assuming that the side-slip angle is very small, the lateral acceleration is expressed as:

$$d^2 y / dt^2 = Vr = V \, d\theta / dt$$

and so the lateral displacement to steer input is described by:

$$G_y(s) = \frac{y(s)}{\delta(s)} = \frac{V^2}{l} \frac{1}{1 + t_r s} \frac{1}{s^2} \tag{9.11}$$

Here, substituting Eqns (9.2), (9.10), and (9.11) into Eqn (9.7), gives the following characteristic equation:

$$s^2 + \frac{V^2}{l}\left(\frac{L}{V}s + 1\right)\frac{h(1 + \tau_D s)e^{-\tau_L s}}{1 + t_r s} = 0 \tag{9.12}$$

For further simplifications, the driver is considered without derivative control action, which means $\tau_D = 0.0$, under the long time continuous control task. Furthermore, the driver time lag is approximated as:

$$e^{-\tau_L s} \approx \frac{1}{1 + \tau_L s} \tag{9.13}$$

Now, the characteristic equation becomes:

$$s^2 + \frac{V^2}{l}\left(\frac{L}{V}s + 1\right)\frac{h}{(1 + t_r s)(1 + \tau_L s)} = 0 \tag{9.14}$$

The development of the above Eqn (9.13) leads to:

$$A_4 s^4 + A_3 s^3 + A_2 s^2 + A_1 s + A_0 = 0 \qquad (9.14)'$$

where

$$
\begin{aligned}
A_4 &= \tau_{\mathrm{L}} t_{\mathrm{r}} \\
A_3 &= \tau_{\mathrm{L}} + t_{\mathrm{r}} \\
A_2 &= 1 \\
A_1 &= \frac{hL}{l} V \\
A_0 &= \frac{h}{l} V^2
\end{aligned}
\qquad (9.15)
$$

As all the coefficients A_i ($i = 1$–4) are positive and the stability conditions of the driver–vehicle system is:

$$
\begin{vmatrix}
A_1 & A_0 & 0 \\
A_3 & A_2 & A_1 \\
0 & A_4 & A_3
\end{vmatrix}
= A_1 A_2 A_3 - A_0 A_3^2 - A_1^2 A_4 > 0 \qquad (9.16)
$$

Substituting Eqn (9.15) into the inequality (9.16) gives:

$$\frac{h}{l} V \left\{ (\tau_{\mathrm{L}} + t_{\mathrm{r}}) L - (\tau_{\mathrm{L}} + t_{\mathrm{r}})^2 V - \frac{hL^2 V}{l} \tau_{\mathrm{L}} t_{\mathrm{r}} \right\} \geq 0 \qquad (9.16)'$$

As all, h, l, and V, are positive:

$$h \leq \frac{\tau_{\mathrm{L}} + t_{\mathrm{r}}}{\tau_{\mathrm{L}} t_{\mathrm{r}}} \frac{l}{LV} \left\{ 1 - \frac{V(\tau_{\mathrm{L}} + t_{\mathrm{r}})}{L} \right\} \qquad (9.17)$$

This inequality gives us the stable region of the driver parameters, on an h–L plane, for given values of τ_{L}, t_{r}, l, and V.

If it is possible that both τ_{L} and t_{r} are small enough to be neglected, the following characteristic equation can be used instead of Eqn (9.14)':

$$s^2 + \frac{hL}{l} Vs + \frac{h}{l} V^2 = 0 \qquad (9.14)''$$

As all the coefficients of this equation are positive, the driver–vehicle is stable at any positive h and L. This means that the driver–vehicle system becomes unstable only when there is a response delay in either the driver or the vehicle response.

The driver time lag, τ_{L}, cannot be completely equal to zero. Also, the mechanical system from the driver's hands to the front wheels must lead to some response delay of the front steer angle responding to the driver's input to the steering wheel. Thus, it is not reasonable to set $\tau_{\mathrm{L}} = 0$.

On the other hand, the vehicle response delay, t_r, as expressed by Eqn (9.9), can be regarded as zero when V is low and m is small with respect to K. Under this condition, the characteristic equation changes to the following form:

$$A_3 s^3 + A_2 s^2 + A_1 s + A_0 = 0 \qquad (9.14)'''$$

where,

$$
\begin{aligned}
A_3 &= \tau_L \\
A_2 &= 1 \\
A_1 &= \frac{hL}{l} V \\
A_0 &= \frac{h}{l} V^2
\end{aligned}
\qquad (9.15)'
$$

The stability condition of the above is:

$$A_1 A_2 - A_0 A_3 \geq 0$$

Substituting Eqn (9.15)' into the above gives:

$$\frac{hV}{l}(L - V\tau_L) \geq 0$$

Namely, the driver–vehicle system is stable when L is greater than $V\tau_L$.

It is clear that for a stable system, there is a lower limit of the driver's look ahead distance (preview distance). This limit is due to the response delay of the driver and the critical preview distance is equal to the distance the vehicle moves, with speed V, during the delay time, τ_L. In another word, L/V can be called the preview time of the driver and if the preview time is greater than the delay time, τ_L, the system is stable.
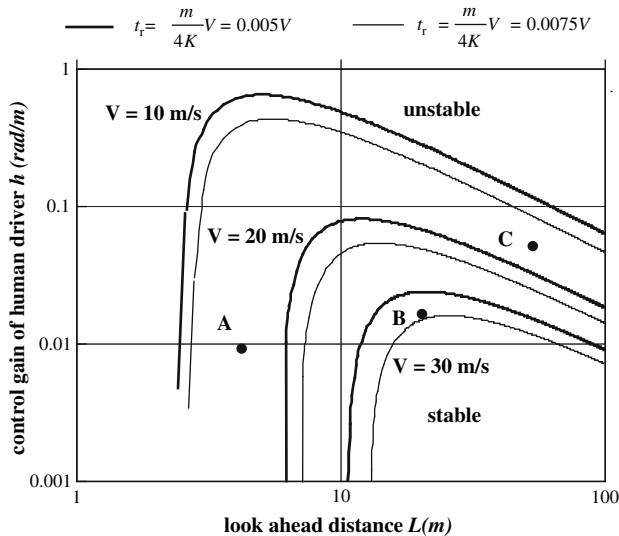
FIGURE 9.6 Stable region on h–L plane.

The driver–vehicle system is always stable if the vehicle response delay is negligible and either (a) the look ahead distance is longer than the distance moved during his (or her) delay time, or (b) the preview time is larger than the delay. If either case is true, there is no limit of the gain constant, h, for assuring stability.

When both the driver and vehicle response delays are not negligible, the stability condition is described by Eqn (9.17), which gives us the stability region shown previously. Figure 9.6 shows the calculation results of the stability region on the h–L plane. It is understandable that the upper limit of the driver control gain, h, arises for the first time when the response delay of the vehicle becomes significant, especially with regards to vehicle speed. The upper limit of h rapidly decreases with the increase of the vehicle speed.

Figure 9.7 is the calculation results for $y_0 = 3.5$ m width lane change behavior at the vehicle speed 20 (m/s), $t_r = 0.1$(s), and $\tau_L = 0.1$(s) using Eqns (9.6), (9.10), and (9.11) for the driver–vehicle system. The following equation is used as the
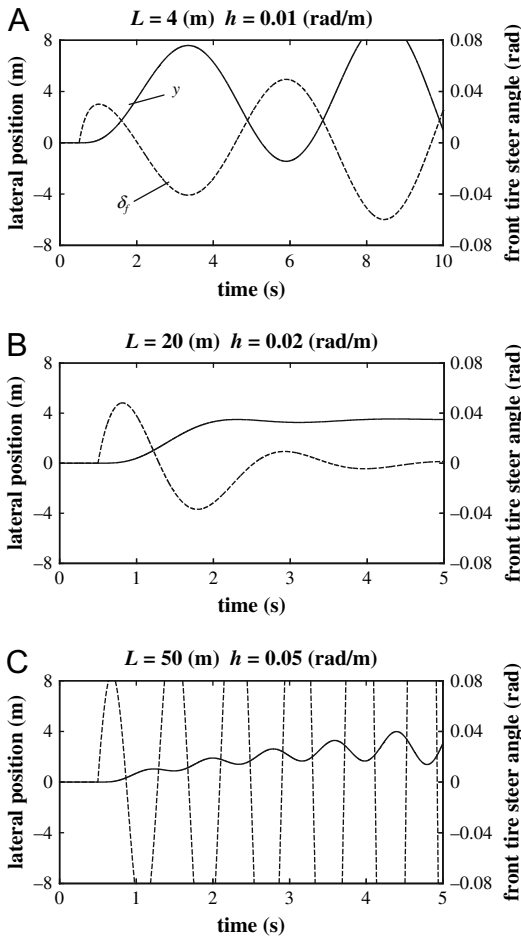
FIGURE 9.7 Simplified driver–vehicle system lane change response.

driver transfer function, with the parameters corresponding to the points A, B, and C, respectively, in Fig. 9.6.

$$H(s) \approx \frac{h}{1 + \tau_L s} \tag{9.18}$$

It is interesting to see that the driver–vehicle system with driver parameters located out of the stable region (points A and C) is oscillatory and unstable.

Example 9.1

Investigate how the derivative control action of the driver contributes to stabilize the driver–vehicle system.

Solution
Adopting Eqns (9.10) and (9.11) as the vehicle response to the steering input and using $e^{-\tau_L s} = 1/(1 + \tau_L s)$, the characteristic equation of the driver–vehicle system becomes:

$$s^2 + \frac{V^2}{I}\left(\frac{L}{V}s + 1\right)\frac{h(1 + \tau_D s)}{(1 + t_r s)(1 + \tau_L s)} = 0 \tag{E9.1}$$

Here, if the driver controls the vehicle with the derivative time constant, τ_D, almost the same as the lag time, τ_L, then the characteristic equation becomes:

$$t_r s^3 + s^2 + \frac{hLV}{I}s + \frac{hV^2}{I} = 0$$

and the stability condition is:

$$\frac{hV}{I}(L - Vt_r) \geq 0 \text{ or } L \geq Vt_r \tag{E9.2}$$

Or if the driver's derivative time is almost equal to the response time of the vehicle, t_r, then the characteristic equation is:

$$\tau_L s^3 + s^2 + \frac{hLV}{I}s + \frac{hV^2}{I} = 0$$

and the stability condition becomes:

$$\frac{hV}{I}(L - V\tau_L) \geq 0 \quad \text{or} \quad L \geq V\tau_L \tag{E9.3}$$

It is understood that if the driver uses a derivative time almost equal to their lag time or the vehicle response time, the stability limit in the *h–L* plane can be widened and the upper limit of the gain, *h*, is eliminated.

So far, the region for the proportional constant, *h*, and the look ahead distance, *L*, has been chosen in order for the vehicle motion under human control to be stable. However, while this can distinguish whether the motion is stable or not, it cannot determine the level of stability.
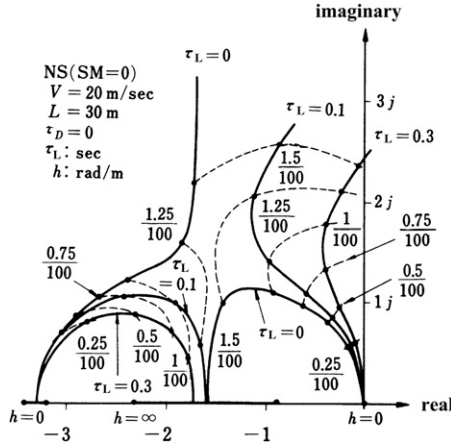
FIGURE 9.8 Root locus of driver–vehicle system for various τ_L.

Yamakawa, took the human driver's transfer function as $H(s) = h(1 + \tau_D s)e^{-\tau_L s}$, and using equations equivalent to Eqns (9.4) and (9.5) determined the roots of the characteristic equation of a vehicle under the control of a human driver [1]. Two of the results are shown in Figs 9.8 and 9.9.

Figure 9.8 is the root locus when the human time lag, τ_L, and proportional constant, *h*, are changed. From the figure, it can be seen that the existence of
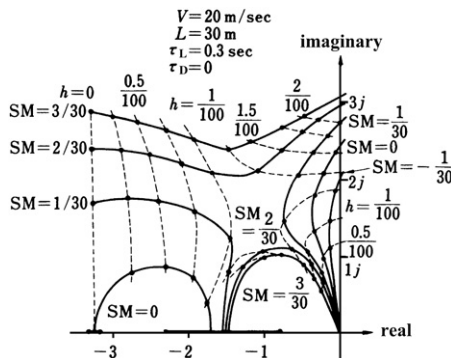
FIGURE 9.9 Root locus of driver–vehicle system for various SM.

time lag, τ_L, is the basic cause for the vehicle motion to become unstable. If the proportional constant, h, is too large, the vehicle motion will become unstable. Figure 9.9 is the root locus when the vehicle SM and the proportional constant, h, are changed. From the figure, it can be seen that if the vehicle has an US characteristic, the larger the SM, the more stable the vehicle motion will become.

9.4 HUMAN ADAPTATION TO VEHICLE CHARACTERISTICS AND LANE CHANGE BEHAVIOR

Until here, the characteristics of vehicle motion and human control behavior have been regarded as independent of each other. However, unlike mechanical controllers, a human's distinctive characteristic is the ability to change control behavior to produce an appropriate control that suits the control objective.

For simplicity, the following characteristic equation can be found by substituting $t_r = 0$ in Eqn (9.12):

$$s^2 + \frac{V^2}{l}\left(\frac{L}{V}s + 1\right)h(\tau_D s + 1)e^{-\tau_L s} = 0 \qquad (9.12)'$$

If the human driver changes h proportionally to the inverse of vehicle speed squared, V^2, and the look ahead distance, L, proportionally to V, then the above equation will not change even if the vehicle speed changes. In this condition, the vehicle motion will not differ greatly with the traveling speed. The human driver is not independent of the vehicle motion characteristics and behaves as a controller that skillfully changes the control characteristics to suit the vehicle characteristics.

A generic way of understanding the adaptive behavior of the human controllers has been proposed. McRuer has modeled the human control behavior and shows it adapts fully to the machine characteristics. This is done by assuming that the human controller is a continuous linear feedback controller as described in Section 9.2 [2]. As shown in Fig. 9.10, the human controller adapts to the changes of control objective, $G(j\omega)$, by adjusting human control
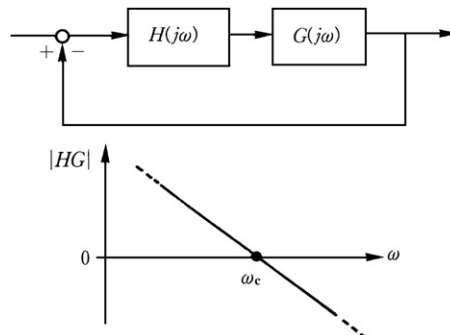
FIGURE 9.10 Crossover model.
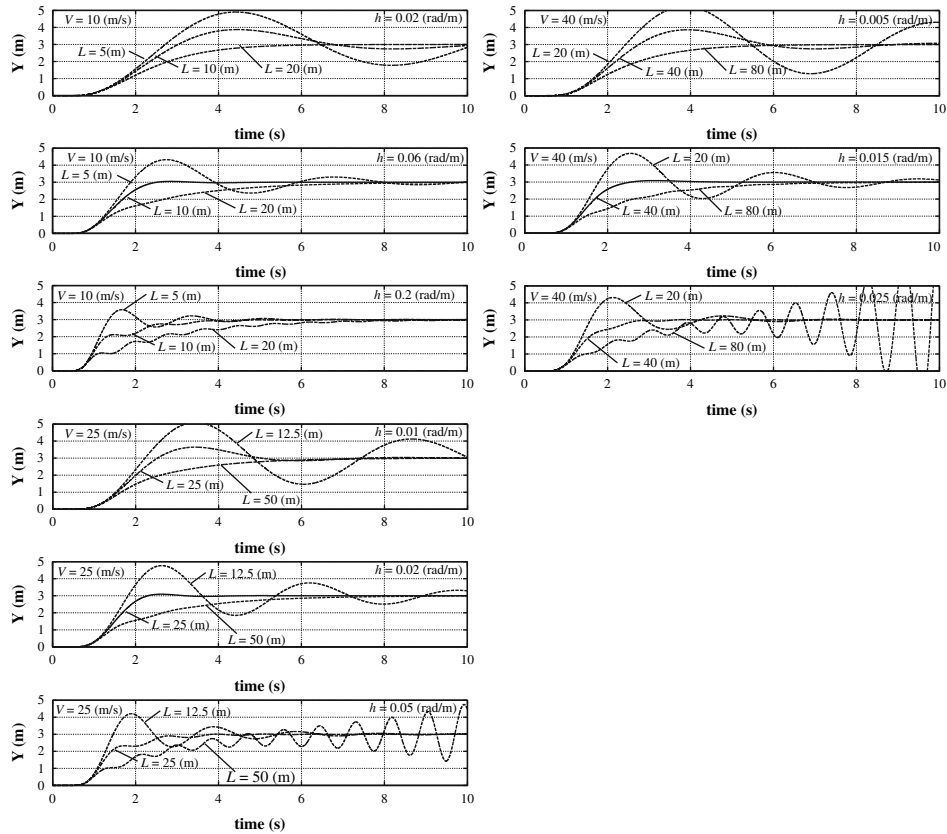
FIGURE 9.11 Effects of driver parameters on vehicle motion under various running speed.

behavior, $H(j\omega)$, such that near the crossover frequency, ω_c, where the open loop frequency response gain $|H(j\omega)G(j\omega)|$ is 1, then

$$H(j\omega)G(j\omega) \approx \frac{\omega_c e^{j\omega\tau}}{j\omega} \tag{9.19}$$

here, τ is the time lag of the human muscles. This is called the crossover model. By applying this method, it might be possible to consider the human adaptation to the vehicle characteristic changes.

Figure 9.11 shows the simulated results of a vehicle lane change for several combinations of the driver parameters h–L and various vehicle speeds. Here, the feasibility that a human driver changes their parameters for different vehicle speeds is seen. As is predicted at the beginning in this section, it is obvious that the parameters, h and L, should be adapted to the change of vehicle speed in order to maintain consistent, ordinary driving behavior during the lane change.

Example 9.2

Execute the Matlab-Simulink simulation of the vehicle lane change behaviors, as in Fig. 9.11, to compare the results of the high US and OS vehicles with the normal vehicle. Investigate how the driver should adapt to the vehicles in order to keep consistent lane change behaviors under variations of the steer characteristics.

FIGURE E9.2(a).

```
1      % Simulation parameters
2 -    dt = 0.001; % simulation rate (s)
3 -    tf = 10.;   % simulation time (s)
4 -     V = 25;    % velocity (m/s)
5      % Vehicle parameters
6 -     m = 1500;  % mass (kg)
7 -     I = 2500;  % moment of inertia about z-axis:I (kgm^2)
8 -    lf = 1.1;   % distance from C.O.G to front axle (m)
9 -    lr = 1.6;   % distance from C.O.G to front axle (m)
10 -    l = lf+lr; % wheel base (m)
11 -   Kf = 55000; % front cornering stiffness (N/rad)
12 -   Kr = 60000; % rear cornering stiffness (N/rad)
13     % Steering characteristics
14 -   tL = 0.2;   % 1st order delay time (s)
15 -   y0 = 3.0;   % target path (m)
16 -    L = 1.0*V; % look ahead distance (m)
17 -    h = 0.02;  % propotional gain (rad/s)
```

FIGURE E9.2(b).

FIGURE E9.2(c).

FIGURE E9.2(d).

FIGURE E9.2(e).

Solution

It is convenient to use Eqns (3.21) and (3.22) to simulate the vehicle motion during a lane change on a straight road. Eqn (9.2) is used to find the course error, $L(m)$ ahead, during the lane change. Equation (9.18) acts as the driver transfer function. The above equations are rewritten for the integral type of block diagram required for simulation:

$$\frac{dv}{dt} = -\frac{2(K_f + K_r)}{mV}v - \frac{2(l_f K_f - l_r K_r)}{mV}r + \frac{2(K_f + K_r)}{m}\theta + \frac{2K_f}{m}\delta \qquad \text{(E9.4)}$$

$$\frac{dr}{dt} = -\frac{2(l_f K_f - l_r K_r)}{IV}\frac{dy}{dt} - \frac{2(l_f^2 K_f + l_r^2 K_r)}{IV}\frac{d\theta}{dt} + \frac{2(l_f K_f - l_r K)}{I}\theta + \frac{2l_f K_f}{I}\delta$$

$$\text{(E9.5)}$$

$$\frac{dy}{dt} = v \qquad \text{(E9.6)}$$

$$\frac{d\theta}{dt} = r \qquad \text{(E9.7)}$$

$$\frac{d\delta}{dt} = -\frac{1}{\tau_L}\delta - \frac{h}{\tau_L}(y + L\theta - y_{OL}) \qquad \text{(E9.8)}$$

From the above equations, the block diagram for simulation is obtained as shown in Fig. E9.2(a). The driver–vehicle system parameters for the simulation are as in Fig. E9.2(b). The simulation program is shown in Fig. E9.2(c) and Fig. E9.2(d) is a result of the simulation.

The results are summarized in Fig. E9.2(e). It is found from this figure that if the vehicle is highly US, the driver should increase the gain, h, and decrease the preview distance, L. On the other hand, if the vehicle becomes OS, then the driver should decrease the gain, h, and increase the preview distance, L, compared with the case of the normal steer characteristic vehicle.

9.5 DRIVER PARAMETER IDENTIFICATION [3]

This section intends to show how the driver adapts his (or her) parameters to the vehicle motion characteristics by driver parameter identification using experimental data.

As the transfer function of the driver steering behavior is described by Eqn (9.2) and the course error detected by the driver is expressed by Eqn (9.3), the steer angle of the driver is described as follows:

$$\delta(s) = -h(1 + \tau_D s)e^{-\tau_L s}\{y(s) + L\theta(s) - y_{OL}(s)\} \qquad \text{(9.20)}$$

In order to simplify the model and reduce the number of parameters in the driver model, it is assumed that $dy/dt \approx V\theta$, as shown in Subsection 9.3.3, and the driver does the equivalent derivative control action by looking ahead, preview behavior. As a result, the driver derivative time, τ_D, is almost zero, and Eqn (9.20) can be rewritten as follows:

$$\delta(s) = -he^{-\tau_{LS}}\left\{\left(1 + \frac{L}{V}s\right)y(s) - y_{OL}(s)\right\}$$

Moreover, assuming that τ_L is small and $e^{-\tau_{LS}} \approx 1/(1 + \tau_L s)$, a simplified driver model is used that describes the steering angle determined by the driver:

$$\delta(s) = -\frac{h}{1 + \tau_L s}\left\{(1 + \tau_h s)y(s) - y_{OL}(s)\right\} \tag{9.21}$$

Assuming that τ_h represents the effects of the look ahead (preview) behavior and includes the effect of the derivative control action of the driver, if any derivative control action is negligible, this is regarded to be the preview time, *L/V*. The block diagram of the simplified driver–vehicle model is shown in Fig. 9.12 and the driver steering characteristics can be represented by the three parameters h, τ_h, and τ_L.

Next is to study the experimental identification of the three parameters. The behavior of a typical driver–vehicle system can be observed during a lane change on a straight road. The parameters can be identified from an experimentally measured time history of the driver steering angle, δ^*, and lateral displacement, y^*, during the lane change.

The error is defined between the measured steering angle, δ^*, and the driver steering angle response to the lateral displacement, y^*, and the lane change width, y_{OL}, estimated by the driver model, Eqn (9.21):

$$
\begin{aligned}
e(s) &= (1 + \tau_L s)\left[\delta^*(s) + \frac{h}{1 + \tau_L s}\left\{(1 + \tau_h s)y^*(s) - y_{OL}(s)\right\}\right] \\
&= (1 + \tau_L s)\delta^*(s) + h\{(1 + \tau_h s)y^*(s) - y_{OL}(s)\}
\end{aligned}
\tag{9.22}
$$

The square integral of the weighted sum of the error and error rate is defined as the evaluation function:
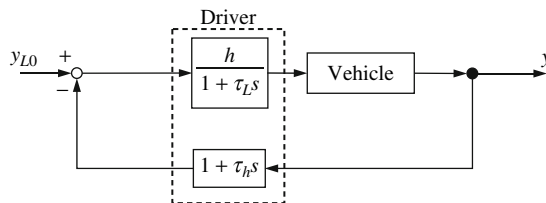
FIGURE 9.12 Block diagram of simplified driver–vehicle model.
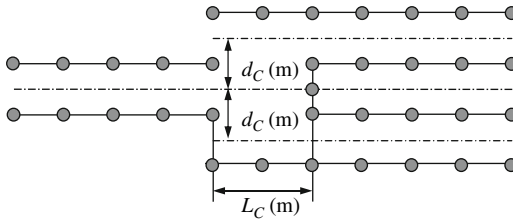
FIGURE 9.13 Lane change test course.

$$J = \int_0^T e^2 \, dt = \int_0^T \left[\delta^* + \tau_L \frac{d\delta^*}{dt} + h \left\{ y^* + \tau_h \frac{dy^*}{dt} - y_{OL} \right\} \right]^2 dt \quad (9.23)$$

where T is the time period long enough for the driver to finish the lane change. It is possible for the parameters, h, τ_h, and τ_L to be found, which minimize J, by solving the following equations:

$$\frac{\partial J}{\partial h} = 0, \quad \frac{\partial J}{\partial \tau_L} = 0, \quad \frac{\partial J}{\partial (h\tau_h)} = 0 \quad (9.24)$$

The above equations are first order linear algebraic equations of h, τ_L, and $h\tau_h$ and easy to be solved for h, τ_L, and τ_h. The solved parameters are the identified driver parameters. With these, the driver steering angle can be
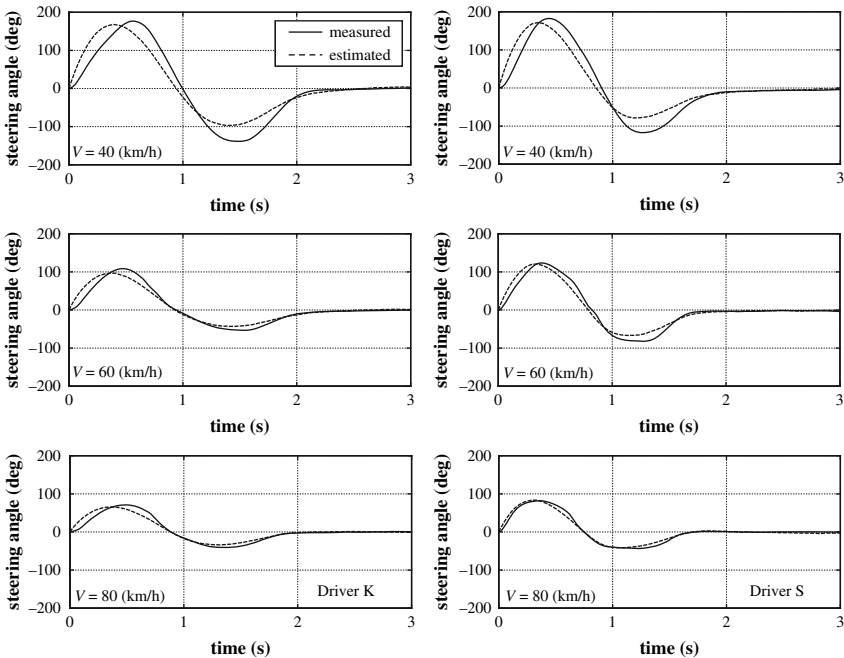
FIGURE 9.14 Comparison of measured and estimated driver steering angle.

described by the identified model and is as close as possible to the real driver steering angle measured.

Next is to look at the results of applying the above identification method to the experimental data obtained in the lane change test on a proving ground. The lane change test course is shown in Fig. 9.13. The lane change width, d_C, is 3.0 m
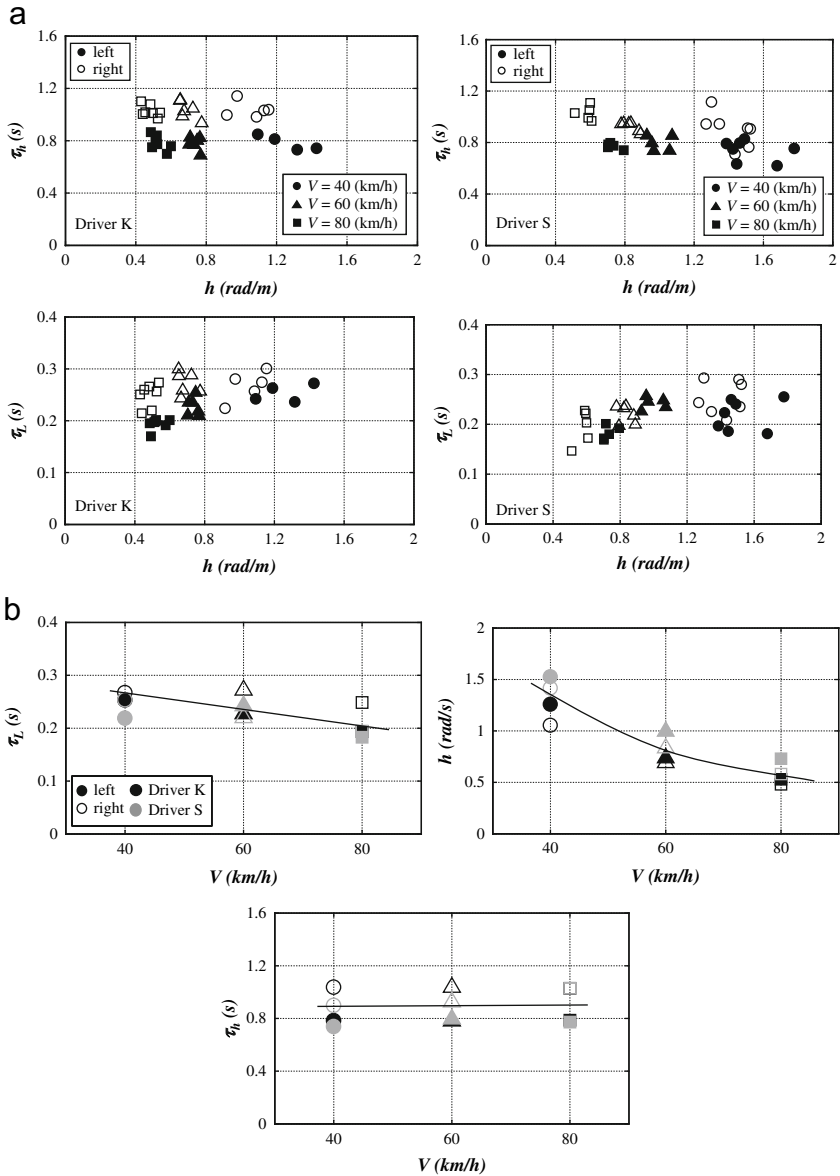
FIGURE 9.15 (a) Driver parameters with change of vehicle speed on parameter plane. (b) Change of driver parameters with increase of vehicle speed.

and the lane change lengths, L_C, are 15 m, 22.5 m, and 30 m for vehicle speeds 40 km/h, 60 km/h, and 80 km/h, respectively.

In Fig. 9.14, the estimated steering angle is compared with the real driver steering angle. They agree well with each other, which means that the driver steering behavior is adequately described by Eqn (9.21). It is possible to characterize the driver with the parameters identified.

The parameters identified are shown in Fig. 9.15(a)–(b), which show how the driver parameters change according to the increase in vehicle speed. It is understood that the proportional gain, h, significantly decreases with the increase of vehicle speed. In contrast, τ_h is always around 0.8–1.0 (s) and does not change with increasing vehicle speed. So, if τ_h is to be approximated as the preview time, L/V, the preview distance (look ahead distance) is almost proportional to the vehicle speed and equal to 0.8 V–1.0 V. The above view corresponds with the driver adaptation to vehicle characteristics discussed in Section 9.4. The response delay, τ_L, decreases with the vehicle speed, which suggests that the increasing vehicle speed pushes the driver to achieve more stressful work loads on the steering control.

PROBLEMS

9.1 Even though the transient characteristics are neglected, the response of the lateral displacement of the vehicle to the steering input is basically a second order integral and is described as $y(s)/\delta(s) = V^2/(ls^2)$. So, confirm that a proportional control action is not enough and some kind of derivative control action is essential for the driver to stabilize the lateral motion of the vehicle.

9.2 The yaw rate response is approximated by Eqn (9.8) in subsection 9.3.3. Try to calculate the time constant of this first order lag response for a normal passenger vehicle at vehicle speeds 10 km/h–100 km/h. Find the vehicle speed range at which the response time constant becomes significant compared with the response time of the human driver.

9.3 Try to calculate the range of the parameter L for the driver–vehicle system to be stable, use Eqn (9.17) with some specific values of h, τ_L, t_r, l, and V.

9.4 Execute the Matlab-Simulink simulation of the driver–vehicle system behavior subjected to the gust wind force with the same conditions as in Example 4.3 under the fixed driver parameters. Refer to Example 9.2 for the driver parameters to be used in the simulation.

9.5 Try to mention possible driver models to simulate steering behaviors of the drivers other than a linear continues PD control model.

REFERENCES

[1] S. Yamakawa, An investigation of vehicle under-steer/over-steer characteristics with a driver steering control, JSAE Journal, Vol. 18, No. 11, 1964 (In Japanese).

[2] D. T. McRuer, A review of quasi-linear pilot models, IEEE Trans, On human factors in electronics, Vol. HFE-8, No. 3, 1969.

[3] J. Ishio et al., Vehicle handling quality evaluation through model based driver steering behavior, Vehicle System Dynamics, Vol. 46 supplement, 2008.

FURTHER READING

[1] A. Tustin, The nature of the human operators response in manual control and its implication for controller design, J. Instn. Elect. Engrs, 94, 190, 1947.

[2] D.T. Mcruer, E.S. Krendel, The human operator as a servo system element, J. Franklin Inst., 267, 381–403, 511–536, 1959.

[3] J.R. Ragazzini, ''Engineering Aspects of the Human Being as a Servo-Mechanism'', Meeting of the American Psychological Associations, 1948.

[4] G.A. Jackson, Measuring human performance with a parameter tracking version of the cross-over model, NASA CR-910, 1967.

Vehicle Handling Quality

10.1 PREFACE

Previously, the study has focused on the motion characteristics of the vehicle itself, the kind of motion the vehicle exhibits, and the vehicle's motions when it is controlled by the human driver. Not only is it important to characterize such motion so that it can be estimated theoretically and observed objectively, but it is also important, to evaluate how easy it is for a driver to control the vehicle, in another word, handling quality evaluation. This is important both objectively and subjectively.

For normal machines, a human operator, as a third party, observes and also estimates theoretically the machine performance and function to evaluate the machine objectively. However, in the case of airplane and also the vehicle, where the machine function is only fulfilled with the direct control of the human operator, the subjective rating of the pilot/driver himself toward the controllability is very important.

This chapter will investigate the relationship of the fundamental motion characteristics of the vehicle with the driver's subjective rating of the vehicle handling quality. Nevertheless, at this stage now, a theoretical methodology that could express the vehicle controllability analytically is not yet established. For that reason, only a methodology based on actual practical facts and experiences can be applied. Here, the vehicle's controllability is concluded by the driver's evaluation when the vehicle motion characteristics are changed.

10.2 VEHICLE CONTROLLABILITY

As mentioned above, the theoretical methodology that could express the vehicle's controllability analytically is not yet established. At this moment, there is also no general methodology to deal with the subjective evaluation of the driver or any relationship between the vehicle motion characteristics and the vehicle's

controllability. Various methodologies are applied, and each corresponds and suits different cases.

In contrast, in the field of aerospace, pilot rating (written below as PR) has been used for a long time as the method of expressing qualitatively the pilot's subjective evaluation of handling and stability. The PR has been continuously modified, and is now relied on as the general assessment method to evaluate the airplane handling and stability, in the design of easy-to-control airplane.

In a similar way to PR, trials have been done to measure the subjective evaluation of the vehicle's controllability based on the driver's evaluation. By changing the vehicle motion characteristics and examining systematically the driver's evaluation of the vehicle's controllability when he actually drives the vehicle, the relation between vehicle characteristics and the controllability becomes clear to a certain extent. Since the vehicle's controllability is ultimately the subjective evaluation of the driver himself, this method is practical and straightforward. However, on the other hand, this method is also easily subjected to individual differences in drivers who make the evaluation. Hence, the objectiveness and generality of the results become weak. Persisting with this method will bring difficulties in deriving the theoretical relation between the vehicle motion characteristics and the vehicle's controllability. The prior estimation of the vehicle's controllability to new changes in the vehicle motion characteristic will be difficult too.

The task performance is another method to evaluate the vehicle's controllability. This is a method where a target course is set and an actual experiment is carried out, for example, to see how well the vehicle could pass through this course in a certain amount of time at a certain speed without error. This method has an advantage of objective results, but questions remain on how to set the target course and evaluate the result, and whether this corresponds fully to the driver's subjective evaluation or not. Of course, the theoretical study of the relationship between the vehicle motion characteristics and the vehicle's controllability is not necessarily easy.

There is also a method to evaluate the vehicle's controllability by measuring the biological reaction of the driver, for example, heart beat, metabolism, perspiration rate (skin current) etc., which depend on the driver's workload. By changing the vehicle motion characteristics systematically, and investigating the changes in driver's biological reaction, it is possible to find the vehicle characteristics that make the vehicle easier to control. Although this method gives us the objective measurement results, the results themselves are easily affected by various causes and hence, the definite relation between biological reactions and vehicle's controllability is difficult to establish.

The above are simple methods of looking at the driver's evaluation of controllability through experiments, when the vehicle motion characteristics are being changed. Of course, by changing the vehicle motion characteristic and investigating the vehicle's controllability, it is possible to establish a general form of the relationship between vehicle motion characteristics and controllability to a certain degree. It still doesn't provide us a method for estimating the vehicle's controllability when subjected to changes in the vehicle motion characteristics.

Even though the general methodology to deal with the vehicle's controllability isn't established yet, the relation between vehicle motion characteristic and controllability is becoming clearer with the different evaluation methods as described above. The following sections will introduce and expand on these results.

10.3 VEHICLE MOTION CHARACTERISTICS AND CONTROLLABILITY

10.3.1 Steer characteristics and controllability

Chapters 3 and 4 have shown that the vehicle steer characteristic is an important factor, which influences the vehicle motion characteristics. Firstly, the relationship between the vehicle steer characteristic and the vehicle's controllability will be considered.

Fig. 10.1 shows the frequency distribution of the steering angle correction for US characteristic vehicle and OS characteristic vehicle [1]. This is based on the actual measurement of the driver's steering angle correction during high speed traveling. The vehicle is a normal passenger car with the aerodynamic center coincided with the center of gravity that is subjected to random lateral wind. From the figure, it can be seen that an US characteristic vehicle, with a large steer angle has a small correction frequency; while an OS characteristic vehicle has a smaller steering angle and the correction frequency is large. This is because the more US the vehicle is, the smaller the gain of the vehicle motion to steer input. This is also seen in Chapter 4, particularly in subsection 4.2.3, concerning the difference in vehicle motion caused by disturbances due to steer characteristics.

Furthermore, Fig. 10.2 shows the measurement data of the driver's heart beat during the same test. The heart beat of the driver when driving an US characteristic vehicle is at an average of 120; whereby in relation to that, the heart beat of the driver when driving an OS characteristic vehicle is at around 130–140. It is implied that an OS characteristic vehicle requires a larger control workload to the driver compared to an US characteristic vehicle.
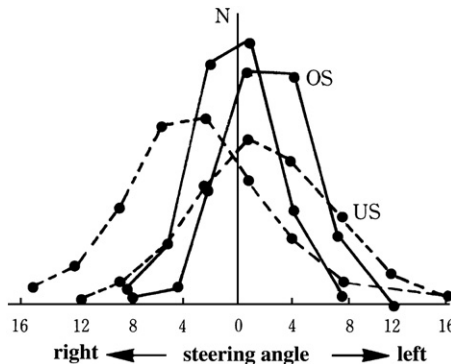
FIGURE 10.1 Steering correction distribution.
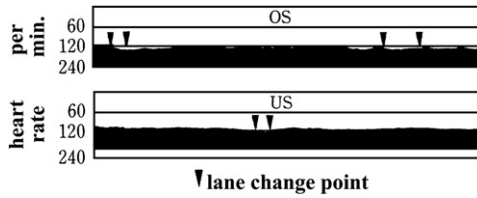
FIGURE 10.2 Driver heart rate change at $V = 140$ km/h.

From the above, it is assumed that the US characteristic vehicle is easier for the driver to control compared to the OS characteristic vehicle.

The extent of the US, OS characteristic of the vehicle is determined and shown by the stability factor, A.

$$A = -\frac{m}{2l^2}\frac{l_f K_f - l_r K_r}{K_f K_r} \tag{3.43$''$}$$

There is an example to examine the relation between the derivative control action and this stability factor, A. In this example, the driver's steering angle when driving a vehicle along a given course is measured, and the equivalent derivative action that should be included in the driver's control action is calculated [2]. The result is shown in Fig. 10.3. As explained in Chapter 9, derivative control action is one of the causes of the workload to the driver, and thus, the vehicle that could be controlled with less derivative control action is considered to be easier to control. The horizontal axis shows the stability factor, A, which is larger than 0 and expresses the extent of the US characteristic. Based on the above, it is considered that Fig. 10.3 shows the relationship between the vehicle US characteristic and the vehicle controllability.
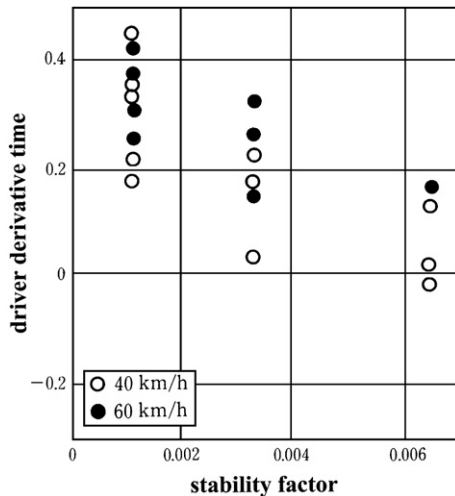
FIGURE 10.3 Effect of stability factor on derivative control action.

The figure shows that an US characteristic vehicle is easier to control. However, there is no guarantee at all that the driver will evaluate the vehicle's controllability based only on the amount of differential action required in his control action. Moreover, the stability factor, A, or SM etc. shows the vehicle steer characteristic and are the only factors directly affecting the vehicle steady-state characteristic. However, if the vehicle steer characteristic changes, the vehicle inherent dynamic characteristic will also change. Besides the steer characteristic, there are other factors, which determine the vehicle dynamic characteristics. Therefore, it is unsuitable for us to judge the vehicle's controllability based only on the steer characteristics and to draw the conclusion that an US characteristic vehicle is easier to control.

10.3.2 Dynamic characteristics and controllability

If a driver gives a sudden steer of a fixed angle to a vehicle originally traveling in a straight line, and then removes his hands (free control), a stable vehicle will reach a steady state while making some oscillatory yaw motion. One of the indices that determine the vehicle motion characteristic in such conditions is the yaw damping. The yaw damping is affected by and changes with the vehicle steer characteristics, the steering system characteristics, and the vehicle body roll etc. Bergman has investigated the relation of the measured actual vehicle yaw damping with the subjective rating of the driver, based on the 10-point rating system [3]. The result is shown in Fig. 10.4. From the figure, it could be considered that a vehicle with larger yaw damping is easier to control.

Fig. 10.5 shows the relation of the controllability with the vehicle under-steer rate U_R for the same vehicle. From this figure, it is clear that it isn't always the vehicle with a strong US characteristic which is easier for the driver to control.

One of the common methods for studying the vehicle dynamic characteristics is to observe the vehicle response to periodical steer, as described in
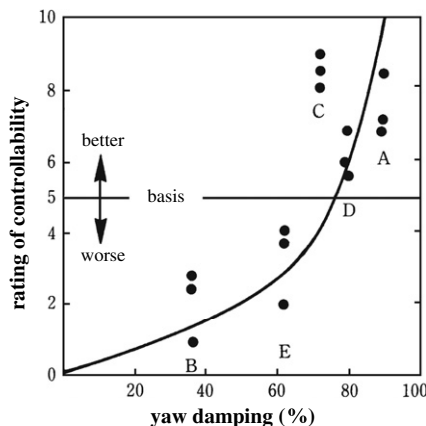
FIGURE 10.4 Relation of controllability to yaw damping.
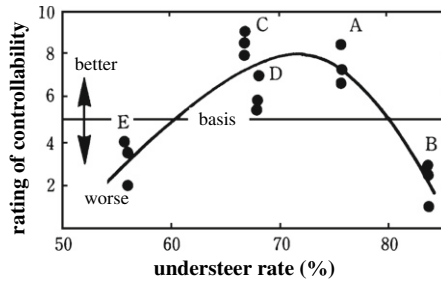
FIGURE 10.5 Relation of controllability to understeer rate.

subsection 3.4.3. In particular, the driver is sensitive to the yaw rate changes in relation to the steer angle. Some examples study the vehicle's relation between controllability and yaw rate gain for a periodical steer input.

When the parameters that govern the vehicle motion characteristics are changed, the shape of the yaw rate gain, for example, the one shown in Fig. 3.30 in subsection 3.4.3, will change. Sugimoto uses the ratio of the peak gain value to the gain value at low frequency ($f = 0.2$ Hz), $|G_{(peak)}|/|G_{(0.2)}|$, to represent such changes in the shape of the gain, as shown in Fig. 10.6. The relation between this ratio and the rating on the vehicle's controllability is examined by measuring the above ratio for different normal passenger cars [4].

The result is shown in Fig. 10.7. Looking at the figure, the controllability is rated best at a $|G_{(peak)}|/|G_{(0.2)}|$ ratio of around 1.2. At the ratio above this, the controllability of the vehicle becomes rather poor. This is because with $|G_{(peak)}|/|G_{(0.2)}|$ ratio larger than 1, the vehicle damping is insufficient, while oppositely, with ratio smaller than 1, delay is large and the responsiveness becomes poor, which could be presumed from the general knowledge concerning the yaw rate frequency response. From the above, it is somehow confirmed that the $|G_{(peak)}|/|G_{(0.2)}|$ ratio is an important index for the vehicle motion characteristics that relates to the vehicle's controllability.

However, even if the $|G_{(peak)}|/|G_{(0.2)}|$ ratio value remains virtually unchanged with the change of the dynamic parameters, it is possible that there will be changes in the frequency of the peak gain, the reduction ratio of the gain at the high frequency region, and the phase lag. Consequently, the
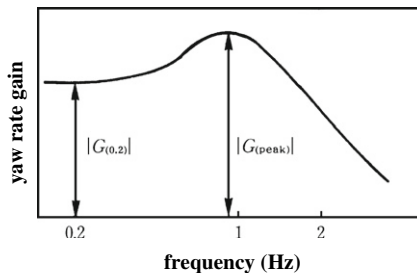
FIGURE 10.6 Frequency response gain ratio.
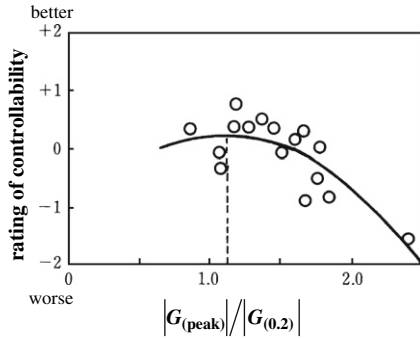
FIGURE 10.7 Relation of controllability to frequency response gain ratio.

vehicle's controllability, for example, even under a fixed task, cannot be considered to depend only on the $|G_{(peak)}|/|G_{(0.2)}|$ ratio, and be judged by the value of the gain itself only.

The result obtained by Lincke is a good example that proves this [5]. Figure 10.8 shows the gain of the yaw rate response to periodical steer inputs for four vehicles with different motion characteristics. Lincke then rates the controllability for the four vehicles based on the driver's rating with a four-point system by setting the course as shown in Fig. 10.9, and the vehicle speed at 60 mph. The result is shown in Fig. 10.10. As could be seen from the figure, the vehicle's controllability coincides well with the frequency which gives the yaw rate gain peak, or in other words, the natural frequency of the vehicle motion. If the vehicle Q is compared with the vehicle W, W has a small $|G_{(peak)}|$, with large yaw damping, but the two vehicles have the same natural frequency, and similar rating of controllability. If vehicles T and W are compared, the yaw damping of the two vehicles is about the same, but T has a smaller natural frequency, and thus, a poor rating of controllability. Consequently, in this kind of situation, the
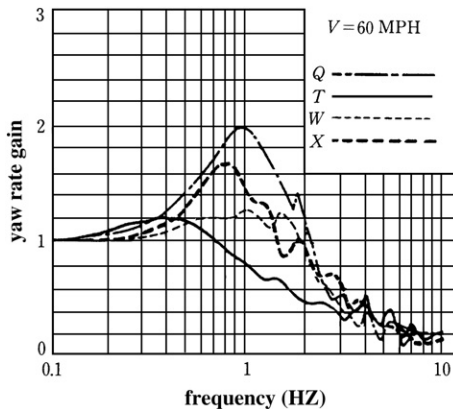
FIGURE 10.8 Four kinds of yaw rate gain.
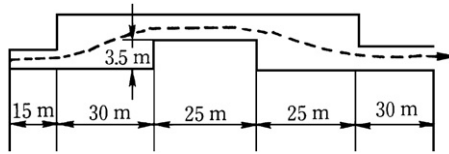
FIGURE 10.9 Evaluation test course.

natural frequency is the vehicle motion characteristic which is more strongly related to the vehicle's controllability rather than the damping ratio.

As described in Chapter 3, expressing the vehicle lateral motion by the two degrees of freedom vehicle model, i.e., by the side-slip angle, β, and yaw rate, r, the theoretical system natural frequency, ω_n, and damping ratio, ζ, could be written as the following approximated equations:

$$\omega_n = \frac{2(K_f + K_r)}{mV}\sqrt{\frac{l_f l_r}{k^2}}\sqrt{1 + AV^2} \qquad (3.67)''$$

$$\zeta = \frac{1 + k^2/l_f l_r}{2\sqrt{k^2/l_f l_r}}\frac{1}{\sqrt{1 + AV^2}} \qquad (3.68)''$$

In particular, this ω_n becomes the important characteristic expression that relates to the vehicle controllability.

Nevertheless, from Figs 10.4 and 10.7, it cannot be said that the damping ratio is not related to the vehicle's controllability at all. For the same reason as mentioned previously, the vehicle's controllability cannot be considered to depend only on the natural frequency, and the conclusion that a vehicle with a higher natural frequency has a better controllability cannot be drawn.

The vehicle dynamic characteristics could be examined by the time lag of the motion response to a steer input. In other words, the responsiveness expressed by the response time. Previous researches on general manual control systems show that the control objective with a large delay is more difficult to control. The vehicle yaw rate response to steer input is given by
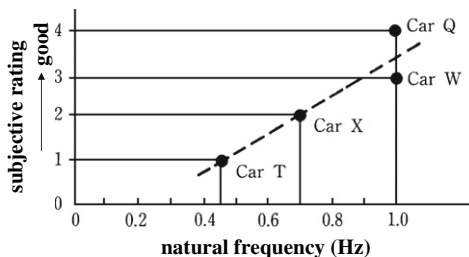
FIGURE 10.10 Controllability and natural frequency (Hz).

Eqn (3.78)′. If $l_f \approx l_r$, $K_f \approx K_r$, from Eqn (3.78), this could be approximated by the following equation:

$$\frac{r(s)}{\delta(s)} = \frac{G_\delta^r(0)}{1 + t_r s}$$

(3.78)″

where

$$t_r = \frac{mV}{2(K_f + K_r)}\left(\frac{k^2}{l_f l_r}\right)$$

(10.1)

Hoffmann et al. measured the equivalent yaw velocity response time, t_r, for different cars and investigated the relationship between this and the actual error (the vehicle touches the cone and tumbles it) rate when the vehicle is required to pass through a course marked by cones without error (without touching the cones) [6]. The result is shown in Fig. 10.11. From the figure, it can be noticed that at the response time of around 0.2 s, the error rate is the lowest, and for response time larger than this, the error rate increases tremendously. It is assumed that with the increase of the response time, t_r, the vehicle becomes more difficult to control.

The side-slip response time is defined as the side-slip angle response delay to yaw rate. If $l_f K_f \approx l_r K_r$, the side-slip angle, β, response to the yaw rate, r, when the steer angle δ is fixed at 0, could be expressed as follows from Eqn (3.12):

$$mV\frac{d\beta}{dt} + 2(K_f + K_r)\beta = -mVr$$

(3.12)′

Hence, the side-slip angle response time, t_β, is expressed as:

$$t_\beta = \frac{mV}{2(K_f + K_r)}$$

(10.2)
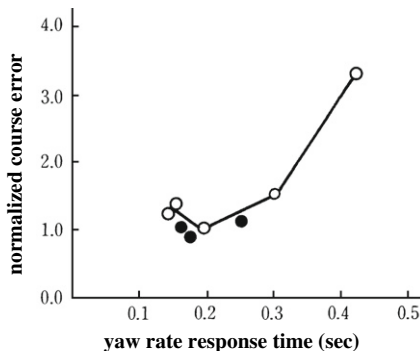
FIGURE 10.11 Course error and yaw rate response time.

Bergman measured the equivalent side-slip response time, t_β, for different cars and investigated the relation of this with the driver's rating on controllability based on a 10-point rating system [7]. The result is shown in Fig. 10.12.

The result shows that with the increase in the side-slip response time, the vehicle becomes less easy to control.

From Eqns (10.1), (10.2), (3.73), and (3.74), if $k^2 \approx l_f l_r$, then t_β and t_r are about the same, and equal to the response time, t_R, described in subsection 3.4.1 (3).

$$t_r \approx t_\beta \approx t_R \approx \frac{mV}{2(K_f + K_r)} \tag{10.3}$$

In this manner, it is now understood that the vehicle motion response time is an important index for the expression of the vehicle motion characteristic that affects the vehicle's controllability. The response time is mainly dependant on the vehicle front and rear cornering stiffness, the vehicle mass, and the traveling speed.

The yaw rate responsiveness as described in subsection 3.4.2 could be expressed also by:

$$t_p = \frac{1}{\omega_n \sqrt{1 - \zeta^2}} \left\{ \pi - \tan^{-1} \left(\frac{\sqrt{1 - \zeta^2} \omega_n T_r}{1 - \zeta \omega_n T_r} \right) \right\} \tag{3.86'}$$

Lincke et al. call the product of the steady-state value of the side-slip angle with respect to the unit lateral acceleration with a constant steer input:

$$\frac{G_\delta^\beta(0)}{G_\delta^{\ddot{y}}(0)} = \frac{l_r}{V^2} \left(1 - \frac{m}{2l} \frac{l_f}{l_r K_r} V^2 \right)$$
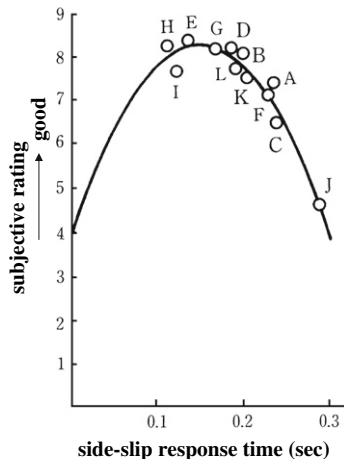
FIGURE 10.12 Relation of controllability to side-slip response time.
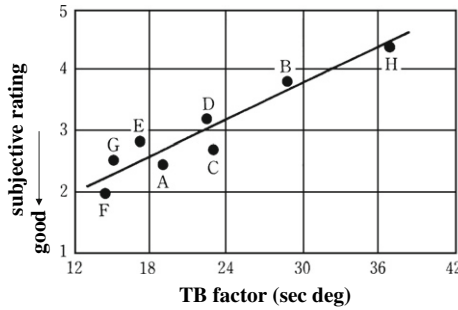
FIGURE 10.13 Relation of controllability to TB factor.

and the equivalent t_p, in other words,

$$\text{TB} = t_p G_\delta^\beta(0) / G_\delta^{\ddot{y}}(0) \tag{10.4}$$

as the TB factor, and show the strong relation of this value with the vehicle's controllability [5]. The result is shown in Fig. 10.13.

Based on the figure, when t_p is small, and $G_\delta^\beta(0)$ value is small, the yaw rate responsiveness is good and the side slip at that instant is small: the vehicle is easier to control.

10.3.3 Response time and gain constant and controllability

As is seen from the above, it is difficult to express the vehicle's controllability by just representing the vehicle motion characteristic expression. Furthermore, there is also no guarantee that the driver evaluates the vehicle's controllability by just that particular motion characteristic. Consequently, it isn't always suitable to judge the vehicle's controllability based on merely a single motion characteristic.

The vehicle yaw rate response to steer input given by Eqn $(3.78)''$ is dependant not only on the response time, t_r, but also the gain constant $G_\delta^r(0)$. Here, Weir et al. measured the actual vehicle equivalent t_r and $G_\delta^r(0)$, and investigated the relation of these two values with the vehicle's controllability [8]. The result is shown in Fig. 10.14. From this figure, it is understood that the t_r and $G_\delta^r(0)$ of the vehicle that are easy to control, occupy a certain region within the $t_r - G_\delta^r(0)$ plane. The region enclosed by the solid line is the region that is considered by experienced drivers as easy to control; while the region enclosed by the dotted line is the region considered by normal drivers as easy to control. If these two regions are compared for experienced drivers and normal drivers, the experienced drivers prefer a larger $G_\delta^r(0)$ even though t_r is a little large; while the normal drivers prefer a smaller t_r even though $G_\delta^r(0)$ is relatively small. The upper limit of $G_\delta^r(0)$ for both types of driver is virtually the same, which is precisely near the point where the vehicle exhibits the NS characteristic.
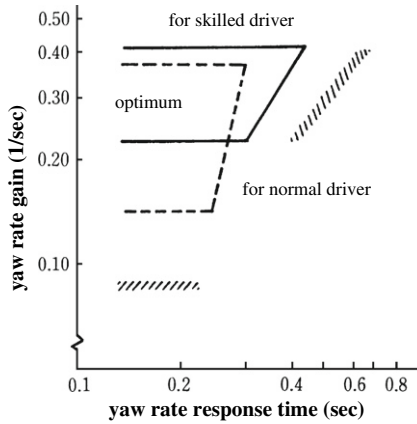
FIGURE 10.14 Relation of controllability to yaw rate gain and response time.

The above is an example, which focuses on the vehicle yaw rate response to steer input. Bergman puts his focus on the vehicle lateral motion and tries to investigate the relationship between controllability and the vehicle lateral acceleration gain constant, $G_\delta^{\ddot{y}}(0)$, and the side-slip response time, t_β [7].

From Eqn (10.3), it is found that t_β and t_r are two quantities that have about the same characteristics. $G_\delta^r(0)$ is expressed as:

$$G_\delta^r(0) = \frac{1}{1+AV^2}\frac{V}{l} \tag{3.81$'$}$$

and $G_\delta^{\ddot{y}}(0)$ is:

$$G_\delta^{\ddot{y}}(0) = \frac{1}{1+AV^2}\frac{V^2}{l} \tag{3.89$'$}$$

Therefore, it could be seen that $G_\delta^{\ddot{y}}(0)$ and $G_\delta^r(0)$ also have the same characteristic. Consequently, the combination of t_β and $G_\delta^{\ddot{y}}(0)$ could be seen as nearly the same as the combination of t_r and $G_\delta^r(0)$.

Bergman measured the equivalent t_β and $G_\delta^{\ddot{y}}(0)$ for a few vehicles, and evaluated the vehicle controllability based on the driver's rating by a 10-point system. Then, he studied the relation of these two quantities with the vehicle's controllability. The result is shown in Fig. 10.15. Looking at the figure, it is understood that the t_β and $G_\delta^{\ddot{y}}(0)$ of the vehicle that are easy to control, occupy a certain region in the $t_\beta - G_\delta^{\ddot{y}}(0)$ plane, as in Fig. 10.14. From the same figure, it is understood that the effect of the changes of t_β on the vehicle's controllability is more prominent than the effect of the changes of $G_\delta^{\ddot{y}}(0)$. In other words, the side-slip response time is a vehicle motion characteristic that is more sensitive to the vehicle's controllability compared to the lateral acceleration gain constant.

Looking at the vehicle controllability related to the two vehicle motion characteristics leads to a relatively well understanding of the relationship of
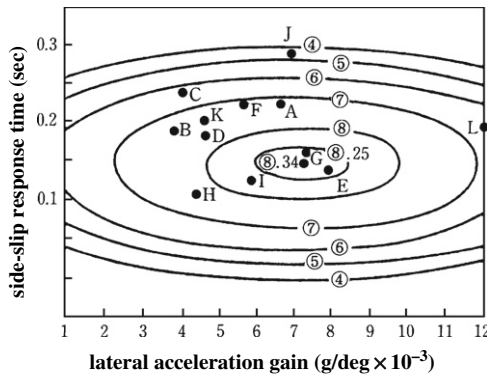
FIGURE 10.15 Relation of controllability to lateral acceleration gain and side-slip response time.

vehicle controllability with the vehicle motion characteristics. However, there is no theoretical background on which the two vehicle motion characteristics should be considered in order to be able to express the vehicle controllability. Although in the above examples, the response time and the steady-state gain have been selected. Consequently, when the parameters that govern the motion characteristics are changed, or when a new vehicle specification is given, it is impossible to judge that the vehicle is easy to control just because the vehicle $t_r - G_\delta^r(0)$ or $t_\beta - G_\delta^{\ddot{y}}(0)$ falls in the region shown in the example.

The vehicle has to also fulfill many other functional requirements other than controllability and various considerations are needed. When other requirements are put at a higher priority than the controllability, then, little importance may be laid on the vehicle controllability. Nevertheless, even if the problem is limited to the controllability of the vehicle motion presented in this book, a general theoretical method has not been provided for estimating the vehicle's controllability.

On the other hand, there is still no general method to measure qualitatively the actual driver's evaluation of the vehicle handling quality that is as accurate and comprehensive as the PR is for aircraft. The vehicle controllability evaluation obtained in practice lacks accuracy and comprehensiveness. Consequently, it is not sufficient enough to just try to theoretically understand the relation between vehicle motion characteristics and the vehicle controllability. While trying to establish the methodology to measure the controllability of the actual vehicle evaluated by human drivers, a theoretical progress and development for the investigation of the controllability is highly needed.

10.4 POSSIBILITY OF HANDLING QUALITY EVALUATION BASED ON DRIVER MODEL

As is mentioned above there is so far no established method to estimate the driver handling quality evaluation related to the vehicle handling characteristics, however, since the drivers adapt his/her parameters to the vehicle different characteristics during maneuvering as is discussed in Chapter 9, the driver
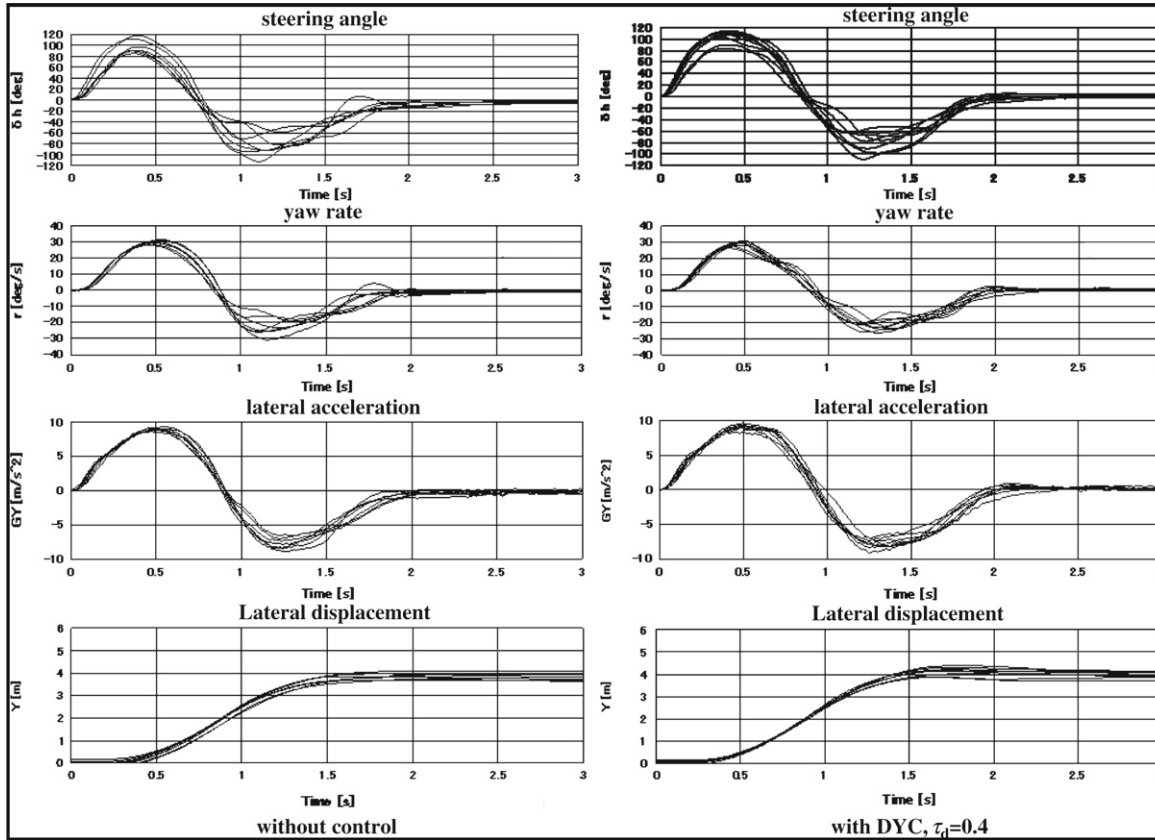
FIGURE 10.16 Vehicle responses during lane change for driver A.
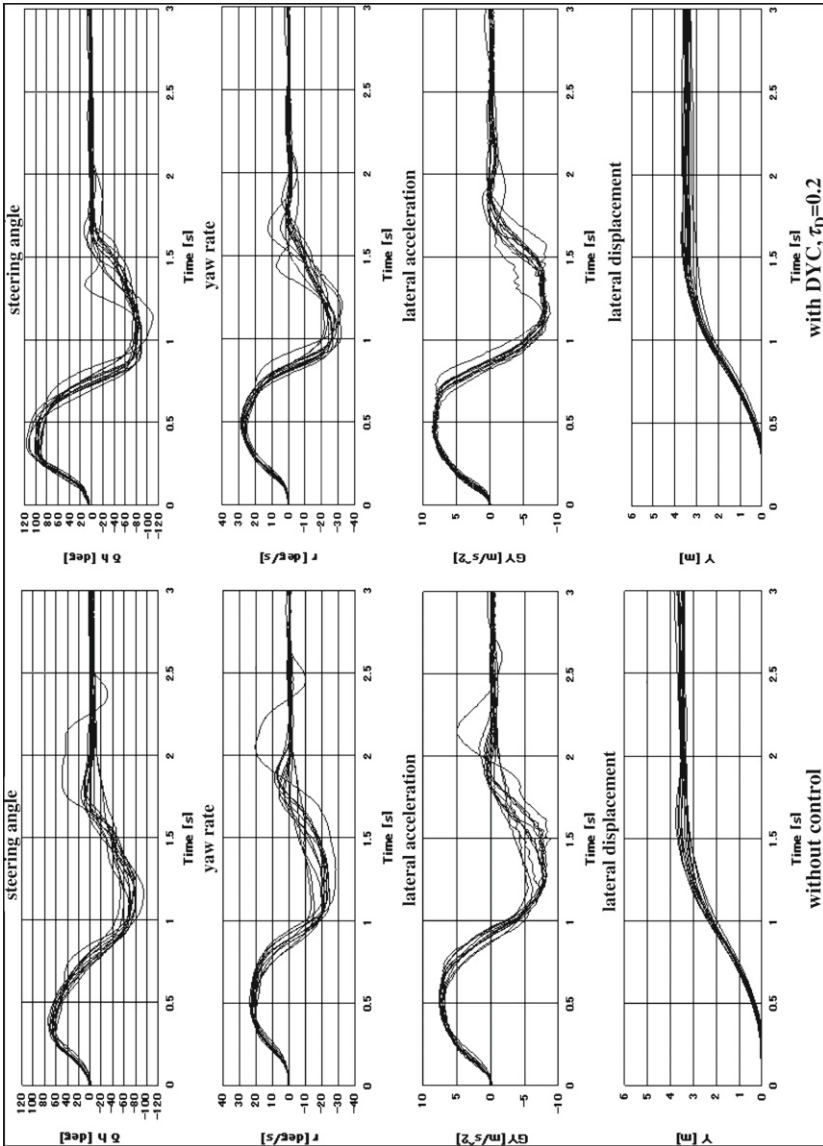
FIGURE 10.17 Vehicle responses during lane change for driver B.

parameters are supposed to reflect the vehicle handling characteristics. Thus, it can be envisaged that there is a possibility to estimate the handling quality evaluation focusing on the driver's adaptive behavior to the vehicle based on a driver steering model.

Therefore, it seems that the crossover model introduced in Section 9.4 is applicable to estimate them; however, it has not necessarily been applied successfully to theoretically estimating the relation of handling quality evaluation to the vehicle specific handling parameters. As supposed, reason is that as the crossover model itself has been developed for analyzing a pilot–aircraft system, it is not necessarily a sufficient tool to generally estimate and determine the specific driver handling parameters related to the specific road-vehicle handling characteristics. Instead, the experimental identification of the driver model parameters as described in Section 9.5 seems effective to analyze and predict vehicle controllability evaluation by the drivers [9].

If the same driver model as described by Eqn (9.21) during a lane change is supposed, then, the parameters h and τ_L represent responsiveness of the driver. If a vehicle stationary gain is small, the driver is required to increase h to compensate for smaller stationary gain. If a vehicle is dynamically responsive, larger τ_L is allowable for the driver to control the vehicle. Also the larger the time constant, τ_L, is, the more relaxed driver behavior during his (or her) maneuvering is expected. The derivative time, τ_h represents a level of the differential control to stabilize the less stable vehicle motion or to compensate for the delay of the driver response due to larger τ_L. The smaller the required derivative time for the driver, the easier the driver feels to control the vehicle.

Based upon the above view, once the driver parameters are identified for a specific vehicle during a lane change, the handling quality of the vehicle to be evaluated by the driver is extrapolated through the parameters identified.
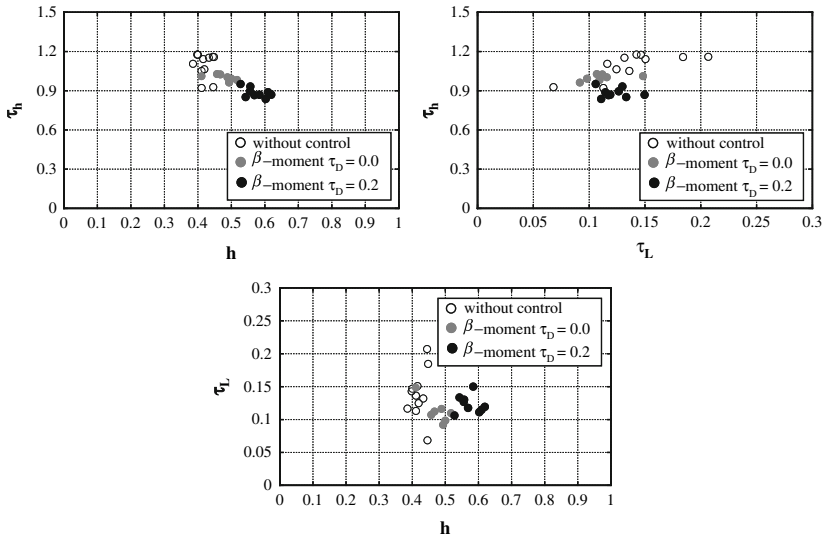
FIGURE 10.18 Identified handling parameters for driver A.
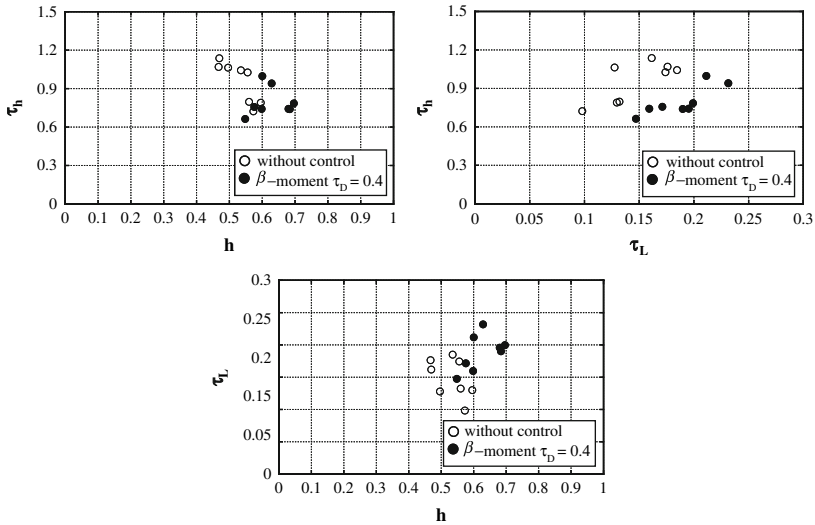
FIGURE 10.19 Identified handling parameters for driver B.

Figures 10.16 and 10.17 show the measured time histories of the driver–vehicle system behavior during lane changes on a proving ground for different vehicles with and without active side-slip control by DYC. Here, DYC controls the tire longitudinal forces to give the vehicle as much as possible the same yaw moment as linear tires can generate even when the vehicle has fallen into tire non-linear ranges to stabilize the vehicle. Though drivers feel easy to control the vehicle with DYC and give better subjective handling evaluations, almost no significant differences, which support the drivers' opinion are found between the measured time histories of the vehicles with and without DYC.

On the other hand, there are significant differences in the driver parameters identified by the same method as described in Section 9.5 using the time histories of a driver–vehicle system during the lane changes. Figures 10.18 and 10.19 show the identified driver parameters for drivers A and B, respectively. It is found in the figures that the vehicle with DYC allows larger time delay of the drivers, τ_L, and smaller derivative time, τ_h, compared with the vehicle without control, which supports the drivers' opinion on the vehicle handling quality [10].

REFERENCES

[1] T. Nakatsuka, Vehicle safety in high speed driving and human characteristics, The Japanese Journal of Ergonomics, Vol. 4, No. 4, 1968 (In Japanese).

[2] Y. Saito, et al., Effects of US and OS characteristics on driver handling behavior, JARI Report, No. 4, 1971 (In Japanese).

[3] W. Bergman, Bergman gives new meaning to understeer and oversteer, SAE Journal, Vol. 73, No. 12, 1965.

[4] Sugimoto et al., Analysis on vehicle running stability subjected to side wind on highway, Proceedings of Annual Meeting of JSAE, No. 761, 1976 (In Japanese).

[5] W. Linke et al., Simulation and measurement of driver vehicle handling performance, SAE Paper 730489.

[6] E. R. Hoffman, et al., The effect of change in some vehicle handling variable on driver steering performance, human factors, June, 1996.

[7] W. Bergman. Relationships of certain vehicle handling parameters to subjective ratings of ease of vehicle control, Proceedings of the 16th FISITA Congress, Tokyo, May, 1976.

[8] D. H. Weir et al., Correlation and evaluation of driver/vehicle directional handling data, SAE Paper 780010.

[9] J. Ishio et al., Vehicle handling quality evaluation through model based driver steering behavior, Vehicle System Dynamics, Vol., No., 2008.

[10] M. Abe et al., A study on vehicle handling evaluation by model based driver steering behavior, Proceedings of FISITA 2008, Munich, September 2008, in CD.

Index